

INVESTIGATION OF DRUG-RELATED CHANGES ON BONE TISSUES OF
RAT ANIMAL MODELS IN HEALTHY AND DISEASE STATES

A THESIS SUBMITTED TO
THE GRADUATE SCHOOL OF NATURAL AND APPLIED SCIENCES
OF
MIDDLE EAST TECHNICAL UNIVERSITY

BY

ŞEBNEM GARİP

IN PARTIAL FULFILLMENT OF THE REQUIREMENTS
FOR
THE DEGREE OF DOCTOR OF PHILOSOPHY
IN
BIOCHEMISTRY

SEPTEMBER 2012

Approval of the Thesis

**INVESTIGATION OF DRUG-RELATED CHANGES ON BONE TISSUES
OF RAT ANIMAL MODELS IN HEALTHY AND DISEASE STATES**

submitted by **ŞEBNEM GARİP** in partial fulfillment of the requirements for the degree of **Doctor of Philosophy in Biochemistry Department, Middle East Technical University** by,

Prof. Dr. Canan Özgen
Dean, Graduate School of **Natural and Applied Sciences**

Prof. Dr. Candan Gürakan
Head of Department, **Biochemistry**

Prof. Dr. Feride Severcan
Supervisor, **Biological Sciences Dept., METU**

Assist. Prof. Dr. Sreeparna Banerjee
Co-Supervisor, **Biological Sciences Dept., METU**

Examining Committee Members:

Prof. Dr. Sezer Komsuoğlu
Neurology Dept., Kocaeli University

Prof. Dr. Feride Severcan
Biological Sciences Dept., METU

Prof. Dr. Mesude İşcan
Biological Sciences Dept., METU

Assoc. Prof. Dr. Zafer Evis
Engineering Sciences Dept., METU

Assist. Prof. Dr. Çağdaş Son
Biological Sciences Dept., METU

Date: 14.09.2012

I hereby declare that all information in this document has been obtained and presented in accordance with academic rules and ethical conduct. I also declare that, as required by these rules and conduct, I have fully cited and referenced all material and results that are not original to this work.

Name, Last name: Şebnem Garip

Signature :

ABSTRACT

INVESTIGATION OF DRUG-RELATED CHANGES ON BONE TISSUES OF RAT ANIMAL MODELS IN HEALTHY AND DISEASE STATES

Garip, Şebnem

PhD, Department of Biochemistry

Supervisor: Prof. Dr. Feride Severcan

Co-Supervisor: Assist. Prof. Dr. Sreeparna Banerjee

September 2012, 204 pages

Disease- and drug-related bone disorders are rapidly increasing in the population. The drugs which are used for the treatment of neurodegenerative diseases and metabolic derangements, may have negative or positive effects on bone tissues.

In the first study, the possible side-effects of Carbamazepine and epileptic seizures on bone structure and composition were investigated by FTIR and synchrotron-FTIR microspectroscopy, AFM and micro- and nano-hardness analysis. The effects on the blood parameters, bone turnover and vitamin D metabolism were also investigated by ELISA and western blot analysis. The current study provides the first report on differentiation of the effects of both epileptic seizures and AED therapy on bones. Besides Carbamazepine treatment, seizures also caused a decrease in the strength of bone. The biochemical data showed that both the epileptic and drug-treated groups decreased vitamin D levels by increasing the vitamin D catabolism enzyme; 25-hydroxyvitamin D-24-hydroxylase.

In the second study, the possible pleiotropic (positive) effects of cholesterol lowering drug; Simvastatin on bones were investigated by ATR-FTIR spectroscopy. The current study provides the first report on dose-dependent effects of simvastatin on protein structure and lipid conformation of bones. ATR-FTIR studies showed that although both high and low dose simvastatin strengthen bones, low dose simvastatin treatment is much more effective in increasing bone strength. Neural network analysis revealed an increased antiparallel and aggregated beta sheet and random coil in the protein secondary structure of high dose group implying a protein denaturation. Moreover, high dose may induce lipid peroxidation which limit the pleiotropic effects of high dose treatment on bones. This study clearly demonstrated that using low dose simvastatin is safer and more effective for bone health than high dose simvastatin treatment.

Key words: Bone, anti-epileptic drug (AED) Carbamazepine, cholesterol lowering drug Simvastatin, CYP enzymes, Fourier transform infrared (FTIR) microspectroscopy, Synchrotron-FTIR (SR-FTIR) microspectroscopy, attenuated total reflection- FTIR (ATR-FTIR) spectroscopy, atomic force microscopy (AFM), biomechanical tests.

ÖZ

SIÇAN HAYVAN MODELLERİNDE KEMİK DOKUSUNDAKİ İLACA BAĞLI DEĞİŞİMLERİN SAĞLIK VE HASTALIK DURUMLARINDA ARAŞTIRILMASI

Garip, Şebnem

Doktora, Biyokimya Bölümü

Tez Yürütücüsü: Prof. Dr. Feride Severcan

Ortak Tez Yürütücüsü: Yrd. Doç. Dr. Sreeparna Banerjee

Eylül 2012, 204 sayfa

Hastalık ve ilaç alakalı kemik bozuklukları toplumda hızla artış göstermektedir. Sinir dokusunun bozulumu ile ilgili hastalıkların ve metabolik dengesizliklerin tedavisinde kullanılan ilaçlar, kemik dokusu üzerinde negatif etki veya pozitif etki gösterebilirler.

İlk çalışmada, Karbamazepin ve epileptik nöbetlerin kemik dokusu üzerindeki olası yan etkileri, FTIR, sinkrotron-FTIR mikrospektroskopisi, AFM ve mikro- ve nano-sertlik ölçüm analizleri ile incelenmiştir. Mevcut çalışma ile hem epileptik nöbetlerin hem de ilaç tedavisinin kemik dokusu üzerindeki etkileri ayırt edilerek, ilk kez rapor edilmektedir. Karbamazepin'in yanısıra, epilepsi ve epileptik nöbetler de kemik güçlülüğünde azalmaya neden olmaktadır. Biyokimya çalışmalarında, hem epileptik hem de ilaç verilmiş sıçanların, vitamin D katabolizmasını sağlayan

25-hidroksivitamin D-1 α -hidroksilaz enziminde artışa neden olarak, vitamin D yetersizliğine neden olduğu görülmüştür.

İkinci çalışmada, sıklıkla kullanılan bir kolesterol düşürücü ilaç olan Simvastatin'in olası pleiotropik (pozitif) etkileri (ATR)-Fourier kızılötesi dönüşüm (FTIR) spektroskopisi ile incelendi. Mevcut çalışma Simvastatin'in kemik protein yapısı ve lipit konformasyonu üzerindeki doza bağlı etkilerini inceleyen ilk çalışmadır. ATR-FTIR çalışması, hem düşük hem de yüksek dozun kemik dokularını güçlendirmesine rağmen düşük dozun kemiği güçlendirmede daha etkili olduğunu göstermiştir. Yapay sinir ağları analizi, yüksek doz da tibia kemik dokusunun protein ikincil yapılarında, antiparalel ve agrega beta plaka tabakasında ve düzensiz sargıda bir artma olduğunu ve buna bağlı olarak protein yapı bozukluğunu göstermiştir. Ayrıca, yüksek doz Simvastatin tedavisi lipit peroksidasyonuna ve lipit membranı düzensizliğine neden olabilmektedir. Lipit peroksidasyonu yüksek doz Simvastatin'in kemik dokusu üzerindeki pleiotropik etkilerini kısıtlayabilmektedir. Bu çalışma sonuçları göstermektedir ki, düşük doz Simvastatin kullanımı kemik dokusu üzerinde hem daha etkili sonuçlar vermektedir, hem de yüksek doz kullanımına nazaran daha güvenlidir.

Anahtar Kelimeler: Kemik, antiepileptik ilaç Karbamazepin, kolesterol düşürücü ilaç Simvastatin, CYP enzimleri, Fourier kızılötesi dönüşüm (FTIR) mikrospektroskopisi, sinkotron-FTIR (SR-FTIR) mikrospektroskopisi, Hafifletilmiş toplam yansıtma (ATR)-Fourier kızılötesi dönüşüm spektroskopisi, atomik güç mikroskobu, biyomekanik testleri.

To my mother Sevil Garip,

ACKNOWLEDGEMENTS

I wish to express my sincere thanks to Prof. Dr. Feride Severcan for her valuable guidance, supervision, patience and understanding throughout the research.

I would like to thank to Assist. Prof. Dr. Sreeparna Banerjee for her invaluable help and support during my study.

I wish to extend my thanks to Dr. Boskey, Dr. Lisa Miller and Dr. Mann for their valuable suggestions and support during my stay in their laboratory in USA. I would also like to thank to TÜBİTAK for supporting me for research studies in abroad as a scholar of Abroad Research Fellowship Programme.

I would like to also thank to Assist. Prof. Dr. Gül İlbay and Assoc. Prof. Dr. Deniz Şahin (Kocaeli University, Faculty of Medicine) for carrying out the animal studies in carbamazepine research.

I would like to extend my thanks to Prof. Dr. Mesude İşcan and Assoc. Prof. Dr. Zafer Evis for their constructive contribution as members of my thesis follow-up committee. I would like to thank Assoc. Prof. Dr. Zafer Evis for also assisting me throughout the biomechanical studies.

I would like to also thank to Prof. Dr. Mete Severcan for performing the bioinformatic studies in simvastatin research.

I am also indebted to my beloved friends and labmates; İlke Şen, Ebru Aras, Damla Güldağ, Gülgün Çakmak, Nihal Şimşek Özek, Özlem Bozkurt, Ceren

Aksoy and Seza Ergün, for their patience, support and friendship throughout my Ph.D. studies.

I would like to also thank the many other people who have assisted me in some way or another. Randy Smith, Beda Mohanty, Hayat Taleb, Mila Spevak, İdil Uysal and Asli Sade Memişoğlu.

I want to express my deepest gratitude to my mother Sevil Garip, my brother Baha Garip, my aunt Göksel Satır and my beloved grandmother Neriman Altunel for their love and support and instilling the values of hard work and respect. I would also like to thank my other family members for supporting and believing in me even when the times were stressful.

I would like to send my ultimate appreciation to my father, Yusuf Garip for the freedom to follow my own path, and stipulating that I do my best in anything I should undertake. I believe that he is watching me and so proud of me.

TABLE OF CONTENTS

ABSTRACT.....	iv
ÖZ.....	vi
ACKNOWLEDGEMENTS.....	ix
TABLE OF CONTENTS.....	xi
LIST OF TABLES.....	xvi
LIST OF FIGURES.....	xviii
LIST OF ABBREVIATIONS.....	xxvii
CHAPTERS	
1. INTRODUCTION	1
1.1 Bone Composition and Structure.....	1
1.1.1 Molecular Structure.....	3
1.1.1.1 Type I Collagen Structure and Collagen Cross-Linking.....	3
1.1.2. Cellular Structure.....	4
1.1.2.1 Osteoclasts.....	4
1.1.2.2 Osteoblasts.....	5
1.2 Bone Remodeling (Bone Turnover).....	6
1.3 Vitamin D and Bone Metabolism.....	7
1.3.1 The role of Vitamin D and PTH in Bone Metabolism.....	8
1.4 Epilepsy, Seizures and Anti-epileptic Drugs (AEDs).....	9
1.4.1 Treatment of Epilepsy.....	12
1.4.1.1 Anti-epileptic Drugs (AEDs).....	12
1.4.1.1.1 Mechanism of Bone Loss with AED Use.....	14
1.4.1.1.2 Carbamazepine.....	16
1.4.1.1.3 Carbamazepine and Bone Disorders.....	17
1.5 Hypercholesterolemia and Statins.....	19
1.5.1 Treatment of Hypercholesterolemia.....	19

1.5.1.1	Statins (HMG-CoA Reductase Inhibitors).....	19
1.5.1.1.1	Mevalonate Pathway and Statins.....	20
1.5.1.1.2	Pleiotropic Effects of Statins on Bone.....	21
1.5.1.1.3	Simvastatin.....	23
1.5.1.1.4	Simvastatin and Bone.....	23
1.6	The Importance of Animal Studies in Bone Research.....	25
1.6.1	Animal Models Used in The Present Study.....	26
1.7	Biophysical and Biomechanical Techniques Used in The Current Study....	27
1.7.1	Spectroscopic and Microspectroscopic Techniques.....	28
1.7.1.1	Basis of Spectroscopy.....	28
1.7.1.2	Infrared Spectroscopy.....	31
1.7.1.3	Fourier Transform Infrared (FTIR) Spectroscopy.....	32
1.7.1.4	Attenuated Total Reflectance Fourier Transform Infrared (ATR- FTIR) Spectroscopy.....	35
1.7.1.5	Fourier Transform Infrared Microspectroscopy.....	37
1.7.1.6	Synchrotron Fourier Transform Infrared (SR-FTIR) Microspectroscopy.....	37
1.7.1.6.1	Advantages of Synchrotron Fourier Transform Infrared (SR- FTIR) Microspectroscopy.....	39
1.7.1.7	FTIR Spectroscopy and Microspectroscopy in Bone Research.....	40
1.7.2	Atomic Force Microscopy (AFM).....	41
1.7.2.1	Atomic Force Microscopy (AFM) in Bone Research.....	43
1.7.3	Biomechanical Indentation Tests.....	44
1.8	Aim of the Study.....	45
2.	MATERIALS and METHODS.....	47
2.1.	Study 1: Carbamazepine Study.....	47
2.1.1	Chemicals.....	48
2.1.2.1	Electroencephalographic (EEG) Recording.....	49
2.1.3	Methods.....	50

2.1.3.1 Fourier Transform Infrared (FTIR) and Synchrotron-Fourier Transform Infrared (SR-FTIR) Microspectroscopic Studies.....	50
2.1.3.1.1 Sample Preparation.....	50
2.1.3.1.2 Data Acquisition and Spectroscopic Measurements.....	53
2.1.3.1.3 Data Analysis.....	56
2.1.3.2 Indentation Studies.....	57
2.1.3.2.1 Vickers Microhardness Study.....	57
2.1.3.2.2 Nano-Indentation Study.....	59
2.1.3.3 Atomic Force Microscopy Studies.....	62
2.1.3.4 Measurement of Serum Parameters.....	63
2.1.3.5 Measurement of CYP Enzymes Protein Levels.....	64
2.1.3.5.1 Liver and Kidney Lysate Preparation.....	64
2.1.3.5.2 Protein Quantification.....	64
2.1.3.5.3 Preparation of Gels.....	64
2.1.3.5.4 SDS-polyacrylamide Gel Electrophoresis.....	66
2.1.3.5.5 Western Blot Analysis.....	67
2.1.3.6 Statistical Analysis.....	68
2.2. Study 2: Simvastatin Study.....	70
2.2.1 Chemicals.....	70
2.2.2 Animal Studies.....	70
2.2.3 Attenuated Total Reflectance (ATR-FTIR) Spectroscopy Study.....	71
2.2.3.1 Sample Preparation.....	71
2.2.3.2 Data Acquisition and Spectroscopic Measurements.....	71
2.2.3.2.1 Neural Network (NN) Analysis.....	74
2.2.3.2.2 Cluster Analysis.....	74
2.2.3 Vickers Microhardness Study.....	75
2.2.4 Statistical Analysis.....	75
3. RESULTS.	76
3.1. Study 1: Carbamazepine Study.....	76

3.1.1 FTIR Microspectroscopy Studies.....	77
3.1.1.1 The Effects of Carbamazepine and Epileptic Seizures on Bone Mineral.....	79
3.1.1.1.1 Mineral Content.....	79
3.1.1.1.2 Carbonate Substitution.....	86
3.1.1.1.3 Crystallinity.....	94
3.1.1.2 The Effects of Carbamazepine and Epileptic Seizures on Bone Matrix.....	99
3.1.2 Hardness Studies.....	104
3.1.2.1 Vickers Microhardness Studies.....	105
3.1.2.2 Nanohardness Studies.....	107
3.1.3 SR-FTIR Microspectroscopy Studies.....	111
3.1.4 Atomic Force Microscopy Studies.....	118
3.1.5 Biochemical Studies.....	121
3.1.5.1 Measurement of Bone Turnover Markers.....	121
3.1.5.2 Protein Level Measurement of Vitamin D Metabolism Enzymes.....	124
3.2 Study 2: Simvastatin Study.....	126
3.2.1 ATR-FTIR Spectroscopy Study.....	127
3.2.1.1 The Effects of Low and High Dose Simvastatin on Bone Mineral.....	132
3.2.1.2 The Effects of Low and High Dose Simvastatin on Bone Lipids.....	135
3.2.1.3 The Effects of Low and High Dose Simvastatin on Bone Proteins.....	138
3.2.1.3.1 Protein Secondary Structure.....	138
3.2.2 Vickers Microhardness Study.....	143
4. DISCUSSIONS	144
4.1 Study 1: The Effects of Carbamazepine on Bone Tissues.....	144

4.1.1 Carbamazepine and Epileptic Seizures Change Bone Mineral and Matrix Composition.....	145
4.1.2 Carbamazepine and Epileptic Seizures Decrease Bone Mechanical Strength.....	150
4.1.3 Carbamazepine and Epileptic Seizures Affect PTH Levels and Bone Turnover Differently.....	152
4.1.4 Carbamazepine and Epileptic Seizures Increase the Protein Levels of Vitamin D Catabolism Enzyme.....	155
4.2 Study 2: The Dose-dependent Effects of Simvastatin on Bone Tissues.....	159
4.2.1 Simvastatin Effects Bone Mineral and Matrix Composition.....	161
4.2.2 High and Low Dose Simvastatin Have Opposite Effects on Bone Lipids and Membrane.....	163
4.2.3 High Dose Simvastatin Induce Lipid Peroxidation.....	164
4.2.4 The effects of Simvastatin on Protein Secondary Structure.....	165
5. CONCLUSION.....	167
REFERENCES.....	172
APPENDICES	
A. CHEMICALS.....	200
CURRICULUM VITAE.....	201

LIST OF TABLES

TABLES

Table 1.1 Summary of AED development according to years.....	14
Table 1.2 Proposed mechanisms contributing to AED induced bone disease (Valsamis et al., 2006).....	15
Table 2.1 The integrated spectral regions.....	66
Table 3.1 General band assignment of a bone tissue between 1800-800 cm ⁻¹ wavenumber region.....	88
Table 3.2 Calculated mineral/matrix parameter in cortical, trabecular and growth plate parts of bone tissues for control (n=7), control + CBZ (n=7), epileptic (n=7) and epileptic + CBZ groups. (*) represents the significancy compared to control group and (+) represents the significancy compared to epileptic group.....	91
Table 3.3 Calculated carbonate/mineral parameter in cortical, trabecular and growth plate parts of bone tissues for control (n=7), control + CBZ (n=7), epileptic (n=7) and epileptic + CBZ groups. (*) represents the significancy compared to control group and (+) represents the significancy compared to epileptic group.....	99
Table 3.4 A-type, B-type and labile (L type) carbonate ratios calculated by taking carbonate/Amide I intensity ratio in cortical, trabecular and growth plate parts of bone tissues for control (n=7), control + CBZ (n=7), epileptic (n=7) and epileptic + CBZ groups. (*) represents the significancy compared to control group and (+) represents the significancy compared to epileptic group.....	103
Table 3.5 Calculated crystallinity parameter in cortical, trabecular and growth plate parts of bone tissues for control (n=7), control + CBZ (n=7), epileptic (n=7) and epileptic + CBZ groups. (*) represents the significancy compared to control group and (+) represents the significancy compared to epileptic group.....	105

Table 3.6 Calculated crosslinks parameter in cortical, trabecular and growth plate parts of bone tissues for control (n=7), control + CBZ (n=7), epileptic (n=7) and epileptic + CBZ groups. (*) represents the significancy compared to control group and (+) represents the significancy compared to epileptic group.....	111
Table 3.7 Calculated SR-FTIRM parameters in periosteum, mid-cortical and endosteum parts of spine cortical for control (n=7), control + CBZ (n=7), epileptic (n=7) and epileptic + CBZ groups. (*) represents the significancy compared to control group and (+) represents the significancy compared to epileptic group.....	129
Table 3.8 The root mean square (RMS) and arithmetic average height (Ra) values obtained from 3 μm^2 AFM images of spine tissue for control (n=7), control + CBZ (n=7), epileptic (n=7) and epileptic + CBZ groups. (*) represents the significancy compared to control group and (+) represents the significancy compared to epileptic group.....	131
Table 3.9 General band assignment of bone tissue between 3030-750 cm^{-1} wavenumber region.....	142
Table 3.10 The band area ratios of some functional groups in control (n=10), 20mg and 50mg simvastatin-treated groups.....	145
Table 3.11 The band frequency, area and half-bandwidth values of some functional groups in control, 20mg and 50mg simvastatin-treated groups.....	149
Table 3.12 The results of the neural network predictions based on FTIR data in 1600–1700 cm^{-1} spectral region (Amide I band) for control, 20mg and 50mg simvastatin-treated groups.....	151
Table 3.13 The results of the changes in the intensities of main protein secondary structures for control, 20mg and 50mg simvastatin-treated groups.....	152

LIST OF FIGURES

FIGURES

Figure 1.1 Organization in a long bone (A). B, C, and D: cancellous bone; B', C', and D': cortical bone (Adopted from Kelly, P.J., 2011 with permission).....	2
Figure 1.2 Vitamin D metabolism and function.....	9
Figure 1.3 Types of seizures according to the localization. A) Primary Generalized Seizure, B) Partial Seizure, C) Partial Seizure with Secondary Generalization.....	12
Figure 1.4 Representation of pregnane X receptor (PXR) mediated vitamin D catabolism. PXR is activated by various antiepileptic medications and other pharmaceutical agents and induces CYP 24, the enzyme which metabolises active vitamin D3 to inactive form. Abbreviations: PXR: Pregnane X receptor, DPH: phenytoin, CBZ: carbamazepine, PB: phenobarbital, VDR: vitamin D receptor, PTH: parathyroid hormone, CYP 24: 24-hydroxylase (Adopted from Valsamis et al., 2006 with permission).....	17
Figure 1.5 Mevalonate pathway.....	24
Figure 1.6 A mechanism by which simvastatin antagonizes TNF- α inhibition on BMP-2-induced osteoblastic differentiation. Simvastatin supports BMP-2-induced osteoblast differentiation shown as Runx2 expression and ALP activation through antagonizing TNF- α -to-MAPK pathway and augmenting Smad1,5,8 signaling. Activation of mevalonate pathway leads to post-translational modification of Ras Rho such as farnesylation and geranylgeranylation. Activated Ras/Rho proteins are key components for signaltransducing kinase cascades including ERK1/2 and SAPK/JNK. Simvastatin prevents TNF- α -induced membrane localization of Ras/Rho (Adopted from Yamashita et al., 2008 with permission).....	28
Figure 1.7 The electromagnetic spectrum.....	33
Figure 1.8 Energy level diagram illustrating the ground and first excited electronic energy level. Vibrational energy levels are represented as parallel lines	

superimposed on the electronic levels. The long arrows show a possible electronic transition from the ground state to the first excited state while the short arrow represents a vibrational transition within the ground electronic state34

Figure 1.9 The vibrational modes associated to a molecular dipole moment change detectable in an IR absorption spectrum (Adopted from Marcelli et al., 2012 with permission).....36

Figure 1.10 Typical setup of a Fourier transform infrared (FTIR) spectrometer (Reproduced from Gerwert and Kötting, 2010 with permission).....38

Figure 1.11 Schematic representation of ATR attachment top plate (Reproduced from Ellis and Goodacre, 2001 with permission).....41

Figure 1.12 Diagram of National Synchrotron Light Source (A: electron source, B: linear accelerator, C: booster accelerator ring, VUV: Vacuum ultraviolet storage ring with associated beamlines). Electrons are accelerated from with a linear accelerator and produce an energy of 75 million electron milivolts (meV), and enter a booster ring, and are accelerated more and enter vacuum ultraviolet (VUV) storage ring.....45

Figure 1.13 Schematic representation of AFM Principle.....48

Figure 2.1 A summary of experiments carried out in the first study.....55

Figure 2.2 Schematic representation of femur, tibia and spine bone tissues.....59

Figure 2.3 The selected area (rectangular shape) in a visible FTIR image (A) of the sample is scanned spot by spot (B) across the surface and collecting at each spot a complete infrared spectrum (C, F). The different spots are recorded sequentially, and the image is reconstituted by matching the spectral information of each single spot to construct a larger image. The imaging results were expressed as histograms (G) describing the pixel distribution of the parameters interested, mean values, standard deviations of the pixel distributions, and representative color-coded images (D, E).....61

Figure 2.4 Cortical (blue), trabecular (green) and growth plate (red) parts of bone.....	62
Figure 2.5 Schematic representation of cortical cross-section showing periosteum (outer bone membrane), mid-cortical and endosteum (inner bone membrane).....	63
Figure 2.6 FTIRM (A) and SR-FTIRM (B) spectra of a bone tissue.....	64
Figure 2.7 Spectrum from the embedding medium; PMMA.	65
Figure 2.8 Representative Vickers indentation images of cortical, trabecular and spine regions of control bone tissue.....	67
Figure 2.9 The representative image of (a) femur tissue and (b) cross-section obtained from distal femur. Dots on the cortical bone shows the place of (i) 7 x 7= 49 indents and (ii) 30 x 1= 30 indents across the radial of cortical bone, obtained for each sample.....	69
Figure 2.10 Representative displacement curves for (A) 1000 μ N and (B) 5000 μ N loads.....	70
Figure 2.11 Representative phase (A) and height (B) 3x3 μ m ² AFM images of a bone tissue.	72
Figure 2.12 A summary of experiments carried out in the second study.....	79
Figure 2.13 Infrared spectrum of air.....	81
Figure 3.1 The averaged spectra of control (pink), epileptic (blue) and their drug-treated groups (orange and black, respectively) in 1800-800 cm^{-1} region (The spectra were normalized to Amide I).....	87
Figure 3.2 The averaged band area of ν_1 , ν_3 phosphate at 1200-900 cm^{-1} of control, epileptic and drug-treated groups. One way ANOVA with Bonferroni post-hoc test was used for statistical analysis. (*) represents the significancy compared to control group and (+) represents the significancy compared to epileptic group (* ⁺ p \leq 0.05; ** ⁺ p \leq 0.01; *** ⁺ p \leq 0.001).....	89
Figure 3.3 Typical FTIR images of mineral/matrix ratios in cortical (A), trabecular (B) and growth plate (C) sites of spine bone for control, epileptic and drug-treated	

groups. Color bars represent the scales for each of the parameters. Axes are in pixels, where one pixel is 6.5 μm . The pixel histograms for these images are shown in (D) cortical, (E) trabecular and (F) growth plate.....92

Figure 3.4 Typical FTIR images of mineral/matrix ratios in cortical (A), trabecular (B) and growth plate (C) sites of tibia bone for control, epileptic and drug-treated groups. Color bars represent the scales for each of the parameters. The pixel histograms for these images are shown in (D) cortical, (E) trabecular and (F) growth plate.....94

Figure 3.5 Typical FTIR images of mineral/matrix ratios in cortical (A) and trabecular (B) sites of femur bone for control, epileptic and drug-treated groups. Color bars represent the scales for each of the parameters. Axes are in pixels, where one pixel is 6.5 μm . The pixel histograms for these images are shown in (D) cortical, and (E) trabecular.....95

Figure 3.6 Typical FTIR images of carbonate/phosphate ratios in cortical (A), trabecular (B) and growth plate (C) sites of spine bone for control, epileptic and drug-treated groups. Color bars represent the scales for each of the parameters. The pixel histograms for these images are shown in (D) cortical, (E) trabecular and (F) growth plate.....97

Figure 3.7 The averaged band area of ν_2 carbonate at 890-850 cm^{-1} in spine tissue control, epileptic and drug-treated groups. One way ANOVA with Bonferroni post-hoc test was used for statistical analysis. (*) represents the significancy compared to control group and (+) represents the significancy compared to epileptic group (*,+ p \leq 0.05; **,++ p \leq 0.01; ***,+++ p \leq 0.001).....98

Figure 3.8 Typical FTIR images of carbonate/phosphate ratios in cortical (A), trabecular (B) and growth plate (C) sites of tibia bone for control, epileptic and drug-treated groups. Color bars represent the scales for each of the parameters. The pixel histograms for these images are shown in (D) cortical, (E) trabecular and (F) growth plate.....100

Figure 3.9 Typical FTIR images of carbonate/phosphate ratios in cortical (A) and trabecular (B) sites of femur bone for control, epileptic and drug-treated groups. Color bars represent the scales for each of the parameters. Axes are in pixels, where one pixel is 6.5 μm . The pixel histograms for these images are shown in (D) cortical, and (E) trabecular.....101

Figure 3.10 Typical FTIR images of crystallinity ratio in cortical (A), trabecular (B) and growth plate (C) sites of spine bone for control, epileptic and drug-treated groups. Color bars represent the scales for each of the parameters. The pixel histograms for these images are shown in (D) cortical, (E) trabecular and (F) growth plate.....106

Figure 3.11 Typical FTIR images of crystallinity ratio in cortical (A), trabecular (B) and growth plate (C) sites of tibia bone for control, epileptic and drug-treated groups. Color bars represent the scales for each of the parameters. The pixel histograms for these images are shown in (D) cortical, (E) trabecular and (F) growth plate.....107

Figure 3.12 Typical FTIR images of crystallinity ratio in cortical (A) and trabecular (B) sites of tibia bone for control, epileptic and drug-treated groups. Color bars represent the scales for each of the parameters. Axes are in pixels, where one pixel is 6.5 μm . The pixel histograms for these images are shown in (D) cortical, and (E) trabecular.....108

Figure 3.14 Typical FTIR images of collagen crosslinks ratio in cortical (A) and trabecular (B) and growth plate (C) sites of spine bone for control, epileptic and drug-treated groups. Color bars represent the scales for each of the parameters. The pixel histograms for these images are shown in (D) cortical, (E) trabecular and (F) growth plate.....110

Figure 3.15 Typical FTIR images of collagen crosslinks ratio in cortical (A), trabecular (B) and growth plate (C) sites of tibia bone for control, epileptic and drug-treated groups. Color bars represent the scales for each of the parameters. The

pixel histograms for these images are shown in (D) cortical, (E) trabecular and (F) growth plate.....	113
Figure 3.16 Typical FTIR images of collagen crosslinks ratio in cortical (A) and trabecular (B) sites of femur bone for control, epileptic and drug-treated groups. Color bars represent the scales for each of the parameters. Axes are in pixels, where one pixel is 6.5 μm . The pixel histograms for these images are shown in (D) cortical, and (E) trabecular.....	114
Figure 3.17 Microhardness values of control, epileptic and drug-treated groups in cortical (A), trabecular (B) and growth plate (C) sites of spine, tibia and femur bone tissues. (*) represents the significancy compared to control group and (+) represents the significancy compared to epileptic group (* ⁺ p \leq 0.05; ** ⁺⁺ p \leq 0.01; *** ⁺⁺⁺ p \leq 0.001).....	117
Figure 3.18 Hardness (H) and elastic modulus (E) values obtained from 7x7=49 indents on cortical bone of spine tissues using 1000 μN and 5000 μN loads. (*) represents the significancy compared to control group and (+) represents the significancy compared to epileptic group (* ⁺ p \leq 0.05; ** ⁺⁺ p \leq 0.01; *** ⁺⁺⁺ p \leq 0.001).....	120
Figure 3.19 Hardness (H) and elastic modulus (E) values from 30x1=30 indents across the cortical radial of spine tissues using 5000 μN load. (*) represents the significancy compared to control group and (+) represents the significancy compared to epileptic group (* ⁺ p \leq 0.05; ** ⁺⁺ p \leq 0.01; *** ⁺⁺⁺ p \leq 0.001).....	122
Figure 3.20 Typical FTIR images of mineral/matrix ratio in periosteum, mid-cortical and endosteum parts of spine cortical for control, epileptic and drug-treated groups. Color bars represent the scales for each of the parameters. Axes are in pixels, where one pixel is 1.0 μm	125
Figure 3.21 Typical FTIR images of carbonate/mineral ratio in periosteum, mid-cortical and endosteum parts of spine cortical for control, epileptic and drug-treated	

groups. Color bars represent the scales for each of the parameters. Axes are in pixels, where one pixel is 1.0 μm126

Figure 3.22 Typical FTIR images of crosslink ratio in periosteum, mid-cortical and endosteum parts of spine cortical for control, epileptic and drug-treated groups. Color bars represent the scales for each of the parameters. Axes are in pixels, where one pixel is 1.0 μm127

Figure 3.23 Typical FTIR images of crystallinity ratio in periosteum, mid-cortical and endosteum parts of spine cortical for control, epileptic and drug-treated groups. Color bars represent the scales for each of the parameters. Axes are in pixels, where one pixel is 1.0 μm128

Figure 3.24 3 μm^2 AFM height and phase images of spine bone tissues of control, epileptic and drug-treated groups.132

Figure 3.25 Serum calcium, 25(OH)D, 1,25(OH)D and PTH levels of control, epileptic and drug-treated groups. One way ANOVA with Tukey's post-hoc test was used for statistical analysis. (*) represents the significancy compared to control group and (+) represents the significancy compared to epileptic group. The *p* values less than or equal to 0.05 were considered as statistically significant (*⁺*p* \leq 0.05; **⁺*p* \leq 0.01; ***⁺*p* \leq 0.001).....135

Figure 3.26 Serum bone formation (ALP and osteocalcin) and resorption (C-telopeptide) of control, epileptic and drug-treated groups. (*) represents the significancy compared to control group and (+) represents the significancy compared to epileptic group (*⁺*p* \leq 0.05; **⁺*p* \leq 0.01; ***⁺*p* \leq 0.001).....136

Figure 3.27 Protein levels of CYP27a1, CYP27b1 and CYP24 enzymes in liver and kidney tissues of epileptic and drug-treated groups are shown in representative western blot images (A) and histograms (B). 6 μg of total proteins from each sample was loaded and transferred on PVDF membrane at 100V for 1 hour 30 minutes, 5% Skim milk in PBST was used as blocking agent. Antibody Dilutions: CYP27a1 1:750; CYP27b1 1:750; CYP24 1:750; Anti-Rabbit-HRP 1:2000; All

primary antibody incubations were carried out at 4°C overnight in the presence of blocking agent except secondary antibodies (room temperature 1h with gentle shaking). β -Actin protein was probed as loading control. One way ANOVA with Tukey's post-hoc test was used for statistical analysis. (*) represents the significancy compared to control group and (+) represents the significancy compared to epileptic group. The p values less than or equal to 0.05 were considered as statistically significant (*⁺ $p \leq 0.05$; **⁺⁺ $p \leq 0.01$; ***⁺⁺⁺ $p \leq 0.001$).....137

Figure 3.28 A typical FTIR spectrum of a rat tibia in the 4000-750 cm^{-1} region..140

Figure 3.29 The average spectra of control (n=10), 20 mg simvastatin treated (n=10) and 50 mg simvastatin treated (n=6) groups in (A) 3030-2840 cm^{-1} , (B) 1700-750 cm^{-1} region (The spectra were normalized with respect to the CH_2 asymmetric stretching band)..... 143

Figure 3.30 Curve-fitting analysis of the ν_1, ν_3 phosphate stretching band (1200-900 cm^{-1}) of A) control, B) 20 mg simvastatin treated, C) 50 mg simvastatin treated groups.146

Figure 3.31 The average spectra of control (n=10), 20 mg simvastatin treated (n=10) and 50 mg simvastatin treated (n=6) groups in 3030-2840 cm^{-1} region (The spectra were normalized with respect to the CH_2 asymmetric stretching band). The frequency shift in CH_2 asymmetric stretching band and area difference in CH_2 symmetric stretching band were shown in seperate windows for better representation.....148

Figure 3.32 The second derivative average spectra of control (dotted spectrum), 20 mg simvastatin treated (solid spectrum) and 50 mg simvastatin treated (dashed spectrum) groups in 1700-1600 cm^{-1} region.....153

Figure 3.33 The dendrogram of a hierarchical cluster analysis of control (C), 20mg simvastatin-treated (T) and 50mg simvastatin-treated (F) groups performed on the first derivative spectra of tissue samples and resulting from Ward's algorithm.

Study was conducted in the 3050–2800cm⁻¹ and 1800–450cm⁻¹ spectral regions.....154

Figure 3.34 The hardness values of control, 20 mg and 50 mg simvastatin-treated groups. P values less than or equal to 0.05 were considered as statistically significant (**p ≤ 0,01; ***p ≤ 0,001).....155

LIST OF ABBREVIATIONS

ATR-FTIR	Attenuated Total Reflectance Fourier Transform Infrared
SR-FTIR	Synchrotron Fourier Transform Infrared
AFM	Atomic Force Microscopy
BaF ₂	Barium Fluoride
ELISA	Enzyme Linked-Immunosorbent Assay
FTIR	Fourier Transform Infrared
IR	Infrared
MSC	Mesenchymal stem cell
PBS	Phosphate buffered saline
25OHD	25-hydroxyvitamin D ₃
[1,25(OH) ₂ D]	1,25-dihydroxyvitamin D
[24,25(OH) ₂ D]	24,25-dihydroxyvitamin D
PXR	Pregnane X receptor
VDR	Vitamin D receptor
PTH	Parathyroid hormone
RANK	Receptor activator of nuclear factor κ B
OPG	Osteoprotegerin

CHAPTER 1

INTRODUCTION

In this chapter, firstly a brief information about the structure and composition of the bone tissue and the factors that affect bone metabolism and turnover were given. The vitamin D metabolism was also summarized. Moreover, Carbamazepine and Simvastatin drugs used in this study, were described with their disease states; epilepsy and hypercholesterolemia, respectively. Besides the importance of the animal studies, the features of the rat groups used in the present study were also explained in this chapter. The last section presents the biophysical and biomechanical techniques applied in the current study.

1.1 Bone Composition and Structure

Bones are stiff organs as a part of the skeletal system of vertebrates. They are multifunctional in that they provide countenance and protect the diverse organs of the body, endow the body with the capability of movement, store minerals, and function in hematopoiesis. Bones are formed in a diversity of shapes and have a complicated external and internal structure. There are 206 separate bones in an adult (Gentry and Bramblett, 1988).

The connection between the structure and mechanics of bones are very important for medical research, since the bone strength relies on bone mass, composition, microarchitecture and material features. Understanding of the pathophysiology of

bone disease and enhance the diagnosis and cure of the bone diseases, understanding the structure and composition of bones is necessary.

There are two different regions in the mature bone called the cortical (compact) and trabecular (cancellous) bones. Cortical bone which counts ~80% of the total bone mass, is found in the shafts of long bone tissues including femur and tibia and radius and outer surfaces of the flat bone tissues including skull, mandible and scapula. Its porosity is 5–30% (Hall, 2007). Trabecular bone is found primarily at the end of long bone tissues and the inner parts of flat bone tissues. Trabecular bone constitutes the remaining 20% of the skeleton and its porosity is 30–90% (Hall, 2007). The microscopic difference between cortical and trabecular bone is that cortical is composed of haversian sites and osteons, while the latter does not (Figure 1.1).

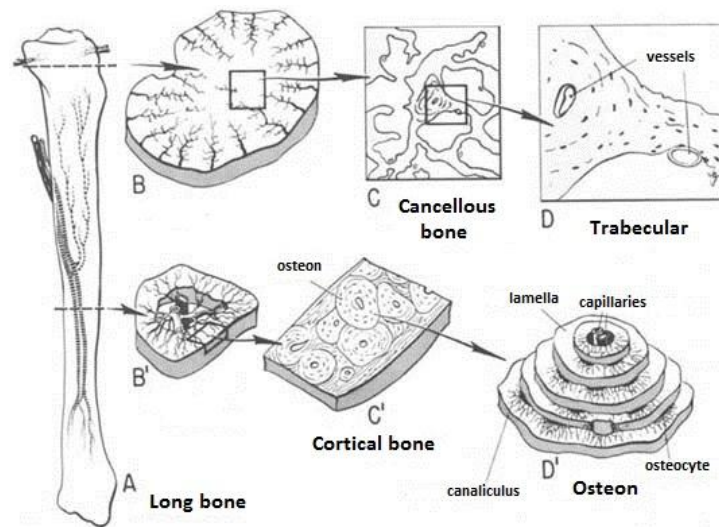


Figure 1.1 Organization in a long bone (A). B, C, and D: cancellous bone; B', C', and D': cortical bone (Adopted from Kelly, P.J., 2011 with permission).

1.1.1 Molecular Structure

Bone is consisted of 50-70% mineral, 20-40% organic matrix, 5-10% water, and <3% lipids. Mineral part of bone contributes mechanical stiffness and load-bearing strength to bone, while the matrix part contributes elasticity and flexibility. The bone mineral is mainly hydroxyapatite [$\text{Ca}_{10}(\text{PO}_4)_6(\text{OH})_2$], with lower amounts of carbonate which substitutes for both phosphate and hydroxyl ions in the crystals (Bazin *et al.*, 2009). Bone matrix is mainly consist of collagenous proteins in which 85 to 90% of them is type I collagen with small amounts of other type collagens including types III, V and FACIT (Fibril-Associated Collagens with Interrupted Triple Helices). The triple-helix structure of type I collagen is essential for the unity and function of bones. The structure of type I collagen and the cross-links are discussed in the next subsection of this part.

The remained bone proteins are noncollagenous proteins which have role in regulating matrix mineralization and proliferation and activity of bone cells. These noncollagenous proteins are proteoglycans, glycoproteins and γ -glutamic acid-containing proteins (Zu *et al.*, 2007). Although they are not as abundant as the collagenous proteins, their importance cannot be under valued in bone physiology.

1.1.1.1 Type I Collagen Structure and Collagen Cross-Linking

The confirmed definition of collagen is: “ structural proteins of the extracellular matrix which contain one or more domains harboring the conformation of a collagen triple helix ” (Bou-Gharios and de Crombrughe, 2008). The triple-helix structure is consist of 3 polypeptide chains consisting of Gly-X-Y repeats of amino acid sequence (van der Rest and Garrone, 1991).

In fibrils, collagen molecules are parallel to each other. Hydroxyapatite crystals are found in these gaps between collagens. A lysine oxidase enzyme deaminates some of the lysyl and hydroxylysyl residues which results in an increase in aldehyde derivatives in fibrillogenesis. These aldehydes correlate with a lysyl or hydroxylysyl residue of neighbor molecules, constructing interchain cross-links. They are necessary for the elasticity of the fibrils (van der Rest and Garrone, 1991).

Among the major cross links, pyrrolic cross links are reducible with NaBH_4 and named reducible cross links and pyridinium cross links; pyridinoline (PYD) and deoxypyridinoline (DPD) are non-reducible and named non-reducible cross links (Paschalis et al., 2004). The reducible cross links are known as intermediates since they convert to non-reducible cross-links during maturation of the tissue.

1.1.2. Cellular Structure

There are two types of bone cells. Osteoclasts which resorb (dissolve) the bone. Osteoblast family that includes bone forming cells; osteoblasts, osteocytes which has role in maintaining bone, and lining cells which cover the surface of the bone.

1.1.2.1 Osteoclasts

Osteoclasts grow up (osteoclastogenesis) from hematopoietic cells of the monocyte/macrophage lineage cells. The osteoblasts/stromal cells are essentially included in osteoclastogenesis. Cell-to-cell contact of osteoclast progenitors with osteoblasts/stromal cells is necessary for stimulating differentiation of osteoclasts (Suda *et al.*, 1997b). Macrophage colony stimulating factor (M-CSF) produced by osteoblasts/stromal cells is a crucial factor for stimulating the differentiation of osteoclasts from monocyte/macrophage lineage cells. Another crucial factor for

osteoclast development is receptor activator of nuclear factor κ B ligand (RANKL). RANKL which is a membrane associated protein, is expressed in osteoblasts/stromal cells as a response to several factors; $1\alpha,25$ -dihydroxyvitamin D_3 [$1\alpha,25(OH)_2 D_3$], parathyroid hormone (PTH), and interleukin 11 (IL-11). In the presence of M-CSF, osteoclast precursors which have RANK (receptor activator of nuclear factor κ B), recognize RANKL and differentiate into osteoclasts. RANKL enhances bone resorption activity of mature osteoclasts which also have RANK. Osteoprotegerin (OPG) produced by osteoblasts/stromal cells, is a lure receptor for RANKL. OPG functions as an inhibitory factor for osteoclastogenesis.

1.1.2.2 Osteoblasts

Osteoblasts are derived from mesenchymal stem cells (MSCs). When an osteoblast is in its terminal differentiation stage and resides entrapped in its self produced bone matrix it is called an osteocyte. Osteocytes are the most abundant cells in bone and are believed to maintain the bone by sensing mechanical strains and bone damage (Seeman and Delmas, 2006). Another bone cell that is derived from osteoblasts is the lining cell; lining cells cover the bone surfaces and thereby separate the bone surface from the bone marrow. However, the exact function of bone lining cells remains unclear (Parfitt, 2001).

PTH is an important external factor, since it increases bone mineral density and improves bone mechanical strength, when administered intermittently (Ejersted et al., 1993). As an anabolic effect on bone formation, PTH increases differentiation of skeletal progenitor cells, osteoblast activity, and osteoblast maintenance (Schmidt et al., 1995). PTH which binds to the PTH/PTHrP receptor, induces the interaction of the receptor with G proteins resulting in the production of cAMP, activation of protein kinase A (PKA) (Jouishomme et al., 1994) and protein kinase

C (PKC) via phospholipase D (PLD) (Radeff et al., 2004). However, a recent study (Tian et al., 2011) reported that PTH effects osteoblasts not only via the cAMP/PKA pathway but also via Wnt/ β -catenin-dependent pathways.

1.2 Bone Remodeling (Bone Turnover)

The aim of bone turnover is to maintain bone strength by removing damaged bone and to regulate calcium homeostasis (Parfitt, 2002; Seeman, 2008). The two main steps of remodeling which are osteoclast bone resorption and osteoblast bone formation, occur consecutively (Seeman, 2008). The resorption step removes damaged bone and is important bone health. It is an also essential process for calcium regulation since it releases stored calcium into the blood circulation. The formation step restores bone's structure by replacing the same volume of removed bone with normal bone.

Measurement of the bone turnover markers in the serum, gives information about the bone formation and resorption which affect bone mass and bone quality. In the in vivo resorption models, measurement of C-telopeptide gives the information about the total activity of osteoclastic resorption (Henriksen et al. 2004). Measuring C-telopeptide release under antiresorptive treatment including bisphosphonates, will reflect the activity of osteoclastic resorption (Schaller et al. 2004, Karsdal et al. 2005). In vivo measurements of bone formation are mainly limited to measuring alkaline phosphatase (ALP) in the serum (Rawadi et al. 2003). Measurement of osteocalcin is also present in the studies (Torricelli et al. 2002, Eghbali-Fatourehchi et al. 2005).

1.3 Vitamin D and Bone Metabolism

Vitamin D has a crucial role for bone health since calcium homeostasis is maintained by increased calcium absorption in intestines by vitamin D. Cholecalciferol (D₃) which is either found in foods of animal origin, or produced endogenously by sun-light from 7-dehydrocholesterol present in the skin epidermis, is the main form of vitamin D. Vitamin D₃ is biologically inactive but after liver and kidney hydroxylations, it becomes biologically active.

After absorption or production from precursor, the production of 25-hydroxyvitamin D (25OHD) takes place in the liver by the regulation of the enzyme 25-hydroxylase (CYP27B1). The level of 25-hydroxyvitamin D in serum is the main parameter for vitamin D status (De Luca 1979). 25OHD is converted to 1,25-dihydroxyvitamin D (active form of vit. D) by 1- α -hydroxylase (CYP27A1) in the kidney (Horst and Reinhardt 1997). 25OHD is also converted to the biologically inactive form; 24,25-dihydroxyvitamin D by 24-hydroxylase (CYP24) in the kidneys (Figure 1.2).

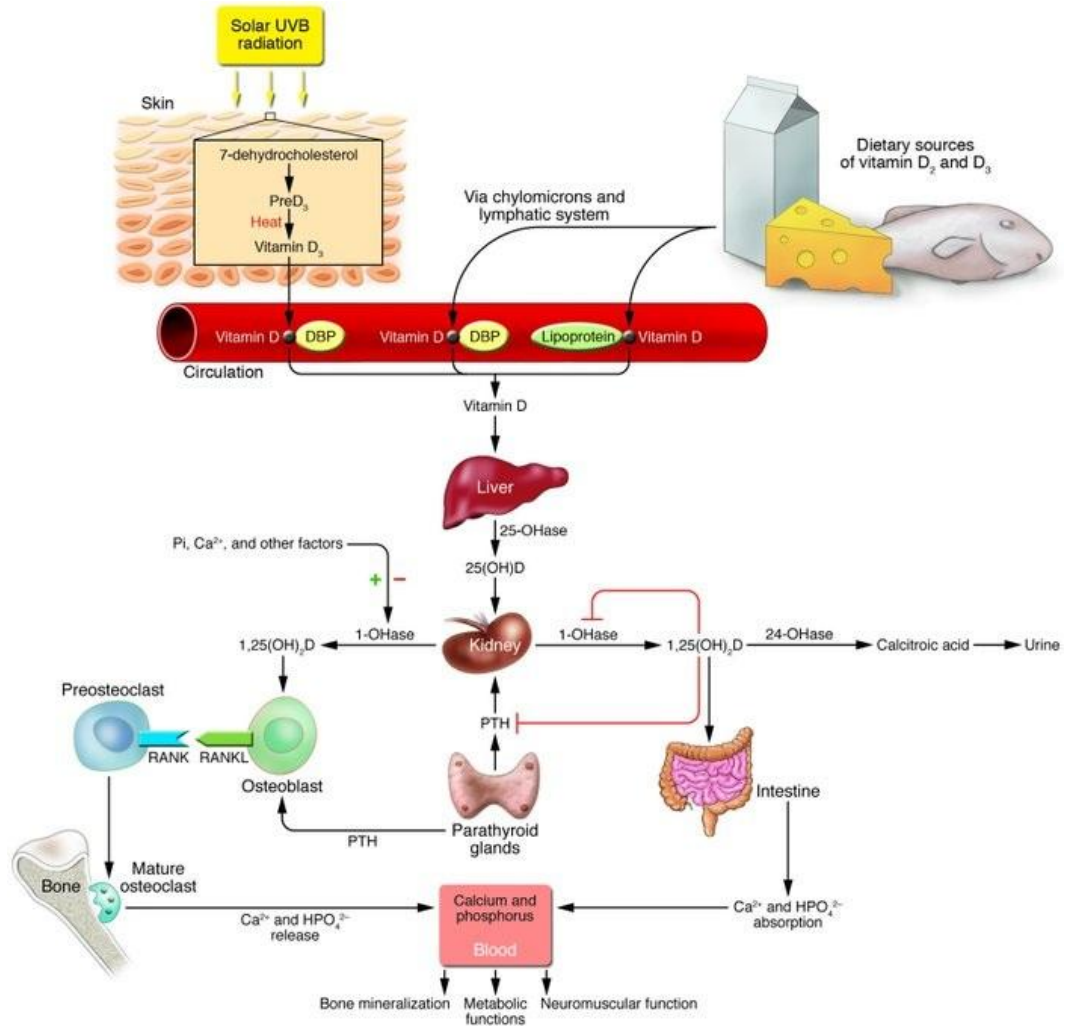


Figure 1.2 Vitamin D metabolism and function.

1.3.1 The role of Vitamin D and PTH in Bone Metabolism

$1\alpha,25(\text{OH})_2\text{D}_3$ which regulates the development and function of osteoblasts, also has a role in the alkaline phosphatase expression, collagen, and osteocalcin in

osteoblasts (Colvard et al 1989). It also induces bone resorption by activating osteoclasts (Merke et al 1986).

Besides 1-alpha-dihydroxy vitamin D, PTH increases bone resorption by increasing the osteoclast amount and activity (Bingham et al 1969). However only osteoblasts have got VDR which replies to 1-alpha-dihydroxy vitamin D, and PTH/PTHrP receptors for PTH. Thus, it can be a proof for mediating the resorption process through osteoblasts (McSheely and Bibby 1985). As mentioned in "Osteoclasts" section (Section 1.1.2.1), it has been reported that PTH and 1-alpha-dihydroxy vitamin D enhance the RANKL expression in osteoblasts, which bolster osteoclast development and bone resorption.

PTH and 1-alpha-dihydroxy vitamin D together retains calcium homeostasis in serum. Reduced serum calcium concentration and elevated serum phosphate concentration result in elevated levels of PTH (Fine et al 1993), which stimulates the production of 1-alpha-dihydroxy vitamin D. Increasing in serum calcium level inhibits the production of PTH (Herfarth et al 1992a). In addition, 1-alpha-dihydroxy vitamin D blocks the PTH gene transcription (Holick 1994).

Some medications including anticonvulsants, decrease serum 25OHD concentration. Taking medication may also affect the vit. D metabolism in kidneys and liver (Mosekilde et al 1977).

1.4 Epilepsy, Seizures and Anti-epileptic Drugs (AEDs)

Epilepsy (Greek word means "attack") is the most common serious neurological disorder of the nervous system, affecting ~1–2% of the population worldwide (McHugh et al., 2008). Recurring seizures because of immoderate discharge of cerebral neurons are the characteristic of epilepsy. "Seizure occurs when cell may

fire as many as 500 times a second, much faster than the normal rate of about 80 times a second in the brain" (DeLorenzo et al., 2005). This excessive neuronal activity can cause strange emotions, sensations, and behavior, or sometimes muscle spasms, convulsions, and loss of consciousness (McNamara, 1994; de Sousa et al., 2006). The incidence of epilepsy is 6 per 1000 people a year in developed countries according to the records of WHO (Hauser et al., 1993; McNamara, 1999) while it is 7 per 1000 people a year in Turkey (Aziz et al., 1997).

The classification of epileptic seizures based on seizure type, etiology, provoking factors and age of onset was proposed by the International League Against Epilepsy (ILAE) in 1981. ILAE has been working on a recent classification based on seizure type, syndrome, etiology and impairment (Blume et al., 2001). Epileptic seizures are categorized mainly into two groups due to the origin of the epileptic seizure in the brain is either localized (partial seizures) or distributed (generalized seizures). In partial seizures, awareness can be affected (complex partial seizure) or not (simple partial seizure). Moreover, a partial seizure may spread in the brain which is called secondary generalization (Figure 1.3).

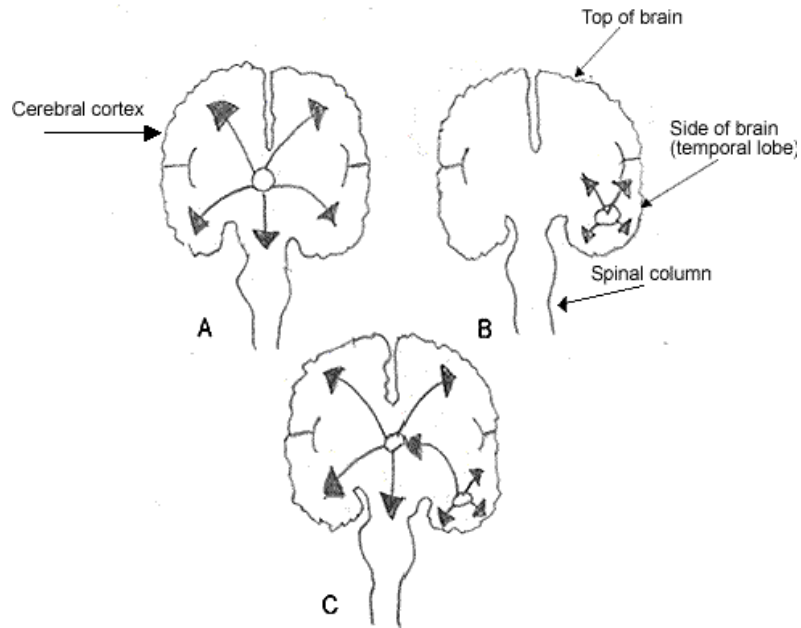


Figure 1.3 Types of seizures according to the localization. A) Primary Generalized Seizure, B) Partial Seizure, C) Partial Seizure with Secondary Generalization.

Generalized seizures are divided into subgroups based on their effects on the system. All subgroups include consciousness loss. They are absence (petit mal), myoclonic, clonic, tonic, tonic-clonic (grand mal) and atonic seizures (Lothman *et al.*, 1991; McNamara, 1999). This classification is important since each seizure type responds differently to medication (Engel, 1992; Dam, 1996). Among generalized seizures, absence seizures will be discussed in this study.

Absence epileptic seizures are obvious as short episodes such as 1 to 10 seconds of staring and unresponsiveness. Mostly there are not other evidents (Shneker and Fountain, 2003).

In a convulsion, first body muscles contract and then relax rapidly and continuously, inducing an uncontrolled shaking of the body. Although convulsion is often a symptom of an epileptic seizure (convulsive seizures), not all epileptic seizures lead to convulsions (non-convulsive seizures). Absence seizures are non-convulsive seizures with minimal or no body movement. There are also mixed form of epilepsies which are absence epilepsies with both non-convulsive and convulsive seizures. Mixed form epilepsies are frequently resistant to AED treatment (refractory) (Midyanovzkaya et al., 2004). This kind of epilepsy is in the scope of the current thesis, since genetically induced absence epileptic rats with convulsive seizures (mixed form of epilepsy) were used in the first study of the thesis.

1.4.1 Treatment of Epilepsy

There is no known cure for epilepsy. The aim of the treatment for epilepsy is to prevent epileptic seizures and abstain side effects.

1.4.1.1 Anti-epileptic Drugs (AEDs)

The first treatment is always the seizure therapy with medicines (also called anti-epileptic drug (AED)). There have been approved drugs for the treatment of epilepsy since 19th century.

By using anti-epileptic drugs, many individuals with epilepsy are exposed to the side-effects of drug treatment (Matsuda et al., 1989). According to previous studies, anti-epileptic drug treatment can induce disorders of bone, mineral and vitamin D metabolism (Cohen et al., 1997; Tsukahara et al., 2002; Nowińska et al., 2012). There are numerous reports of anti-epileptic-associated osteopenia or osteoporosis in adults (Weinstein et al., 1984; Valimaki et al., 1994; Okishi et al.,

1996; Verotti et al., 2000; Feldkamp et al., 2000; Tsukahara et al., 2002; Mintzer et al., 2006; Chou et al., 2007; Kim et al., 2007; Menon and Harinarayan, 2010) and in children (Barden et al., 1982; Nishiyama et al., 1986; Ala-Houhala et al., 1986; Timperlake et al., 1988; Takeshita et al., 1989; Chung et al., 1994; Sheth et al., 1995; Akin et al., 1998; Kafali et al., 1999; Erbayat et al., 2000; Gniatkowska-Nowakowska, A., 2010; Shellhaas and Joshi, 2010). However, the exact mechanism of bone disorders is still not clarified.

Table 1.1 Summary of AED development according to years.

Year	Generic Name	Brand Name
1912	Phenobarbital	Phenobarb
1938	Diphenylhydantoin	Phenytoin
1945	Trimethadione	Tridione
1960s	Diazepam	Valium
1974	Carbamazepine	Tegretol
1978	Valproic acid	Depakene
1985+	Vigabatrin	Sabril
	Lamotrigine	Lamictal
	Topiramate	Topamax
	Oxcarbazepine	Trileptal
	Levetiracetam	Keppra

Antiepileptic drugs are classified as either enzyme inducing or non-enzyme inducing. Although, CYP450 enzyme inducing anti epileptic drugs (carbamazepine, phenobarbital, and phenytoin) are mostly correlated with vitamin D and bone disorders (Hoikka et al., 1981; Valimaki et al., 1994; Verotti et al., 2000; 2002), it was reported that a cytochrome P450 enzyme inhibitor; valproate

may also induce disorders in bone metabolism (Sheth et al., 1995; Sato et al., 2001; Guo et al., 2001; Pack et al., 2005).

1.4.1.1.1 Mechanism of Bone Loss with AED Use

Although a number of factors are reported to induce adverse effects on bone, the exact mechanisms for AED-related bone disorders have not been clarified, yet (Table 1.2).

Table 1.2 Proposed factors related to AED-induced bone disorders (Valsamis et al., 2006).

- Vitamin D Inactivation
 - Hepatic enzyme induction
 - PXR activation
- Altered calcium metabolism (DPH)
 - ↓ Intestinal absorption
 - ↓ vitamin D mediated absorption
 - ↓ intestinal cation transport
- ↑ PTH
 - Vitamin D insufficiency
 - ↓ cellular response to PTH
- Vitamin K deficiency
- ↓ Calcitonin
- Osteoblast Inhibition

Abbreviations: **PXR:** Pregnane X receptor, **DPH:** phenytoin, **PTH:** parathyroid hormone

Vitamin D levels have been shown to be decreased due to enzyme-inducing AED treatment such as Phenytoin and Carbamazepine. Low vitamin D levels may result

in bone loss by inducing low calcium levels (hypocalcemia), low phosphate levels (hypophosphatemia) and secondary hyperparathyroidism (Valsamis et al., 2006).

It was hypothesized that vitamin D deficiency related to AED-use is regulated via the pregnane X receptor (PXR) (Pascussi et al., 2005) (Figure 1.4). DNA binding domain of the vit. D receptor has the sixty percent homology with the domain of pregnane X receptor which is also secreted in intestine, kidneys and liver. Pregnane X receptor was reported to induce the expression of CYP450 enzymes which have roles in the metabolism of drugs. Moreover, pregnane X receptor can be induced by various drugs such as phenytoin, and carbamazepine (Valsamis et al., 2006). It was shown that PXR activators can stimulate the expression of VDR target gene; CYP24. As mentioned before, CYP24 is an CYP450 enzyme which converts the 25-hydroxy vitamin D and 1-alpha-dihydroxy vitamin D to inactive vitamin D form resulting in a vit. D deficiency, hypocalcemia and secondary hyperparathyroidism. It may also result in increasing bone turnover and loss of bone. However, these factors are not enough to explain the reduced vit. D levels in VPA therapy since this drug is an inhibitor of CYP450 enzymes, and not a pregnane X receptor activator (Valsamis et al., 2006).

Through the homology between VDR and PXR, PXR activation by AEDs may also affect osteoblast function and growth and maturation of osteoclasts resulting in adverse bone effects (Valsamis et al., 2006).

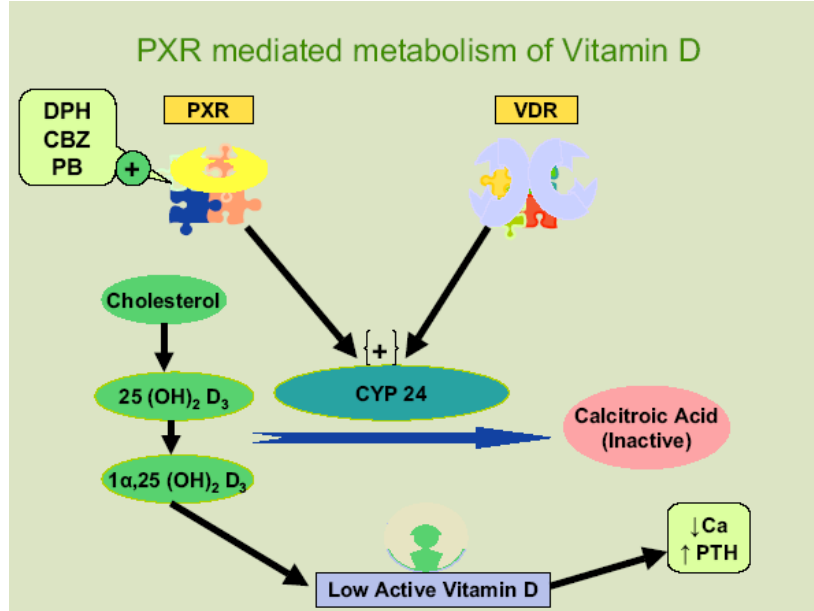


Figure 1.4 Representation of PXR-induced vitamin D catabolism. Diverse AEDs and other pharmaceutical agents activate PXR which results in the induction of CYP 24 enzyme which metabolises the active vitamin D to inactive form (Adopted from Valsamis et al., 2006 with permission).

1.4.1.1.2 Carbamazepine

Carbamazepine which has been one of the most widely used and effective antiepileptic drugs for epilepsy treatment since 30 years (Landmark et al., 2007), can be used alone or with other seizure medicines to control complex partial seizures and generalized seizures. Besides epilepsy, it is also used for the treatment of neuropsychiatric disorders (Edgar et al., 2007), neuropathy (Colvin et al., 2008) and depression (Soares et al., 2007) in recent years.

Carbamazepine inhibits the seizures by blocking the presynaptic Na⁺ channels (Sitges et al., 2007). Voltage-gated Na⁺ channels are crucial for action potentials, and the mutants in these sodium channels are the reason for generalised epilepsies (Armijo et al., 2005). Na⁺ channels have three states which are resting, active and inactive states. In resting state, sodium channels enable the sodium transport into cells. In active state, sodium channels enable the excess transport of sodium into cells during an action potential. In inactive state, sodium channels do not enable the transport of any ion into cells. After the action potential is terminated, channels favor the inactive state for a limited time which is called refractory period (Ochoa et al., 2012). Carbamazepine prevents the continuous firing of the axons by stabilizing the inactive form of channels (Granger et al., 1995).

Carbamazepine undergoes enzyme biotransformation through epoxidation with the formation of its nearly 30 metabolites as detected in human or rat urine (Lertratanangkoon and Horning, 1982; Schnabel et al., 1996). One main metabolic pathway is oxidation to carbamazepine-10,11-epoxide (carbamazepine epoxide) which is the drug's active anticonvulsive metabolite for epilepsy treatment. Other major pathways are the oxidations to 2-hydroxycarbamazepine and 3-hydroxycarbamazepine which may play as precursors to the formation of protein-reactive metabolites. It was suggested that these metabolites may be responsible for the drug's adverse effects such as anticonvulsant hypersensitivity syndrome (Lu et al., 2008).

1.4.1.1.3 Carbamazepine and Bone Disorders

In literature, there are controversial results about the effects of Carbamazepine on bone tissues of epilepsy patients. Some of the clinical studies (Verrotti et al., 2000; 2002; Andress et al., 2002; Farhat et al., 2002; Vestergaard et al., 2004; Crawford et al., 2005; Song et al., 2005; Kumandas et al., 2006; Mintzer et al., 2006; Chou et

al., 2007; Kim et al., 2007; Mintzer, S., 2010; Beerhorst et al., 2011; Nowińska et al., 2012) reported that Carbamazepine therapy decrease the bone mineral density (BMD) and causes the disorders in bone metabolism. However, some other clinical studies (Hoikka et al., 1984; Ala-houhala et al., 1986; Sheth et al., 1995; Akin et al., 1998; Kafali et al., 1999; Erbayat et al., 2000; Ecevit et al., 2004; Tekgul et al., 2006; Gissel et al., 2007; Suzuki et al., 2007; Pack AM, 2008; Misra et al., 2010; Pack et al., 2011) showed no significant differences in the BMD of epileptic patients treated with Carbamazepine. All these studies reported the effects of the drug only in epileptic patients. There is no study which investigates the effect of Carbamazepine on bone tissues of healthy animal models or patients without interfering with any disease. Moreover, in the studies mentioned above, epileptic patients had epileptic seizures besides the anti-epileptic drug treatment, thus it was not clarified that the effects on bone metabolism in epileptic patients are due to anti-epileptic drug treatment or also from epileptic seizures. Only the effect of epilepsy and epileptic seizures on bone tissues haven't been studied yet. Thus, up to now the effects of epileptic seizures and the effects of Carbamazepine on bone tissues, can not be differentiated from each other.

The certain mechanisms for possible side-effects of CBZ on bone tissues have not been clarified yet. The possible mechanisms by which Carbamazepine determines alterations of bone metabolism may be multiple: (1) increased catabolism or decreased anabolism of active vitamin D by inhibiting or stimulating CYP enzymes, (2) effect on vitamin D metabolism without alteration on CYP enzymes, and (3) a direct effect on bone turnover dependent or independent of vitamin D and/or PTH (Feldkamp et al., 2000; von Borstel et al., 2007). For this reason, we aimed to clarify and differentiate the effects of Carbamazepine and epileptic seizures on bone tissues and clarify the action mechanism of anti-epileptic drug and seizures on vitamin D and bone metabolism.

1.5 Hypercholesterolemia and Statins

The high levels of cholesterol in blood is called hypercholesterolemia (Biggerstaff and Wooten, 2004). Cholesterol is a sterol which is found in the structure of membranes and also is the precursor of vitamin D.

Cholesterol is transported in the blood within lipoproteins, since it is insoluble in water. Lipoproteins are grouped based on the density of lipids in their structure which are namely; very low density (VLDL), intermediate density (IDL), low density (VLD) and high density (HDL) lipoproteins (Kontush and Chapman, 2006). All lipoproteins carry cholesterol, but very high concentration of LDL cholesterol is related with an increased risk of atherosclerosis and coronary heart diseases (Hooper et al., 2012).

1.5.1 Treatment of Hypercholesterolemia

In adults to decrease total blood cholesterol and LDL, reducing dietary fat is commonly advised (Sweetman S.C., 2009). However diet is not often sufficient to lower LDL in people with very high cholesterol and cholesterol-lowering drugs are usually required (Reamy and Stephens, 2007).

1.5.1.1 Statins (HMG-CoA Reductase Inhibitors)

Statins which are called HMG-CoA reductase inhibitors due to their inhibiting ability of HMG-CoA reductase enzyme, are taken for decreasing cholesterol concentration. In liver, this enzyme plays an essential role in the production of cholesterol. In recent years, statin drugs are also taken in patients with a high risk of cardiovascular diseases (Kontush and Chapman, 2006).

Atorvastatin (brand name; Lipitor) was chosen as the best selling pharmaceutical in US history with 12.4 billion, according to Pfizer records in 2008. Since 2010, several statins have been marketed including atorvastatin, fluvastatin, lovastatin, pitavastatin, pravastatin, rosuvastatin and simvastatin.

Statins work by competitive inhibiting of HMG-CoA reductase which has a role in rate limiting step in the mevalonate pathway. Since statins have a quite similar homology with HMG-CoA in molecular structure, they steal the place of HMG-CoA in the enzyme and decrease the rate of the pathway in which mevalonate, cholesterol and a number of other compounds are produced (Bonetti et al., 2003).

1.5.1.1.1 Mevalonate Pathway and Statins

Cholesterol is supplied into cells via the mevalonate pathway in endoplasmic reticulum by the synthesis from acetyl coenzyme A (CoA) with the rate limiting step of HMG-CoA reductase (Tsuchiya et al., 2010) (Figure 1.5).

Through the main pathway, FPP separates into 2 ways in which GTP coupling G proteins including Ras are farnesylated and small G proteins including Rac, Rab, and Rho are geranylgeranylated (Takai et al., 2001; Kowluru A., 2003) (Figure 1.17).

The overall benefits of statins seem to be more than alterations in only lipid levels (Sorrentino and Landmesser, 2005). Recent studies show that there are cholesterol independent or “pleiotropic” effects of statin drugs on the immune system, central nervous system, and bone (Garip et al., 2010a; 2010b; Li et al., 2011). Most of these effects are regulated by the isoprenoid inhibition. Especially, inhibiting the isoprenylation of small GTP-binding proteins play an essential role in the positive

effects of statin drugs (Stüve et al., 2003; Chen et al., 2010). Herein, among the pleiotropic effects of statins, we focus on their effects on bone tissues.

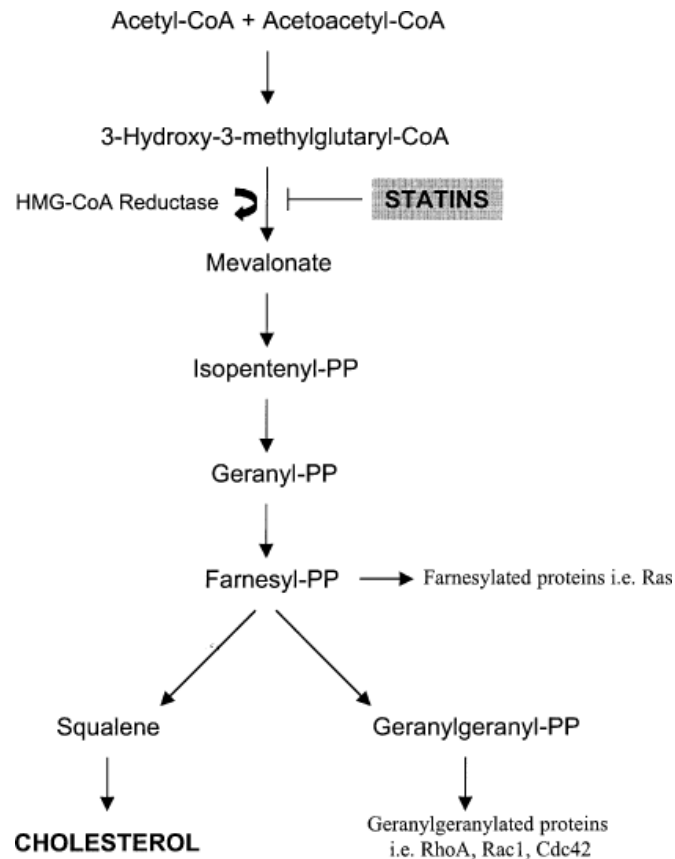


Figure 1.5 Mevalonate pathway.

1.5.1.1.2 Pleiotropic Effects of Statins on Bone

It was firstly reported in a study in late 1999 that statin drugs might directly affect bones (Mundy et al., 1999). In this study, it was shown that two compounds,

lovastatin and simvastatin, stimulate the promoter of a bone morphogenetic protein-2 (BMP-2) in an osteoblast cell line. Since those findings and epidemiological studies have produced mixed results about the effects of statins on bone mineral density and fracture risk in humans. Some of them reported an increased BMD related with statin therapy (Chan et al., 2001; Maeda et al., 2001; Stein et al., 2001; Garrett and Mundy, 2002; Bauer et al., 2004; Luppattelli et al., 2004; Rosenson et al., 2005; Wong et al., 2005; Lee et al., 2008; Fukui et al., 2012), others reported no effect (Maritz et al., 2001; Van staa et al., 2001; Hsia et al., 2002; Yao et al., 2006; Anbinder et al., 2007; Rejnmark et al., 2010).

The possibility that pleiotropic effects on bone are through reduced cholesterol concentration appears unlikely, since the studies with nonstatin cholesterol-lowering drugs showed no effect on bone. Statins may affect bone directly via osteoblastic cells (Chen et al., 2010; Wadagaki et al., 2011; Liu et al., 2012). Besides the stimulation of bone formation, statin drugs might also inhibit bone resorption as bisphosphonates by reducing the prenylation of GTP binding proteins, which blocks osteoclast activity (Fisher et al., 1999) and inhibits osteoblast apoptosis (Plotkin et al., 1999). "Further work is need to demonstrate if manipulating the cholesterol and mevalonate synthetic pathways can be used to increase bone formation and reduce the risk of fracture" (Edwards and Spector, 2002).

Up to now, mostly simvastatin, but also lovastatin and pravastatin have been reported as stimulating the bone formation (Mundy et al., 1999). Moreover, both simvastatin (Maeda et al., 2001) and pravastatin (Ohnaka et al., 2001) induced respectively, BMP-2 expression and osteocalcin to increase osteoblast differentiation in humans. Pravastatin, differently from other statins, is largely absorbed to liver by active transport (Hatanaka T., 2000) which results in a limitation of its availability on another site. This might explain some of the mixed

results due to ineffectiveness on bone, reported in the studies with pravastatin. All the other epidemiological studies were carried out with a less amount of patients taking pravastatin.

Since just less than the 5% oral dose of a statin drug arrives the circulation, among the statins, simvastatin was shown to have highest doses in circulation after metabolized (Bellosa et al., 2000).

1.5.1.1.3 Simvastatin

Simvastatin (trade name; Zocor) is a synthetic derivative of a fermentation product of *Aspergillus terreus*. With its high performance in lowering cholesterol concentration, its tolerability and success in reducing the cardiovascular risk, simvastatin is one of the most commonly used statins (Collins et al., 2003; Szendroedi et al., 2009).

1.5.1.1.4 Simvastatin and Bone

Similar to anti-resorptive agents including bisphosphonates, simvastatin inhibits osteoclast generation by inhibiting the prenylation of certain GTP binding proteins (Rho, Rac, Rab etc.) (Cruz and Gruber, 2002; Jadhav and Jain, 2006). However, the relationship between the use of simvastatin and improvement of bone quality reported in the literature is still controversial. Some clinical and animal studies have reported positive effects of orally applied low dose (10-25 mg/kg/day) (Mundy et al., 1999; Chan et al., 2001; Maeda et al., 2001; Garrett and Mundy, 2002; Bauer et al., 2004; Garip et al., 2010a; 2010b; Li et al., 2011; Du et al., 2012) and high dose (40-80 mg/kg/day) (Mundy et al., 1999; Stein et al., 2001; Bauer et al., 2004; Luppattelli et al., 2004; Rosenson et al., 2005; Garip et al., 2010a; 2010b) simvastatin on bone tissue by increasing bone formation through

induction of BMP-2. In addition, some earlier animal studies supported that simvastatin (0,1-5 mg/kg/day) has positive effects on bone defect healing when applied locally to the site of injury (Mundy et al., 1999; Wong and Rabie, 2005; Lee et al., 2008; Fukui et al., 2012). In a recent dose-dependent study (Ma et al., 2008), it was reported that high and low dose simvastatin treatment is effective to repair of bone defects when applied locally but ineffective to promote bone formation when applied orally. In another study (Anbinder et al., 2006), it was showed that low dose simvastatin treatment has no effect on tibial defects when applied both locally and orally. There are also clinical and animal studies that supported low dose (Maritz et al., 2001; Van staa et al., 2001; Hsia et al., 2002; Yao et al., 2006; Anbinder et al., 2007) and high dose (Hsia et al., 2002) simvastatin therapy has no effect on bone tissues.

The exact mechanism for pleiotropic effects of simvastatin on bone, has not been clarified yet. In a recent study, it was hypothesized that "simvastatin may support BMP-induced osteoblast differentiation through antagonizing TNF- α -to-Ras/Rho/MAPK pathway and amplifying BMP-Smad signaling" (Yamashita et al., 2008). In this study, cDNAarray analyses of BMP/TGF- β -signaling molecules showed stimulated expression of Smad-1,2,3 proteins in simvastatin-treated C2C12 cells. Thus, simvastatin-related increased in Smad expression may have a role in amplifying BMP-induced Smad-1,5,8 activation in the differentiation of osteoblasts (Figure 1.6). Yamashita et al. (2008) reported that in osteoblast differentiation simvastatin inhibits the phosphorylation of SAPK/JNK and ERK1/2 pathways by preventing the Ras/Rho proteins. Prenylation is the essential process for the anchoring of Ras/Rho G-proteins to cell membrane. Statin drugs decrease membrane levels besides the Ras/Rho protein activation through inhibiting isoprenylation (Auer et al., 2002). It was suggested that this process is the cause of simvastatin effect for antagonizing TNF- α -to-MAPK pathway in cells (Yamashita et al., 2008) (Figure 1.6).

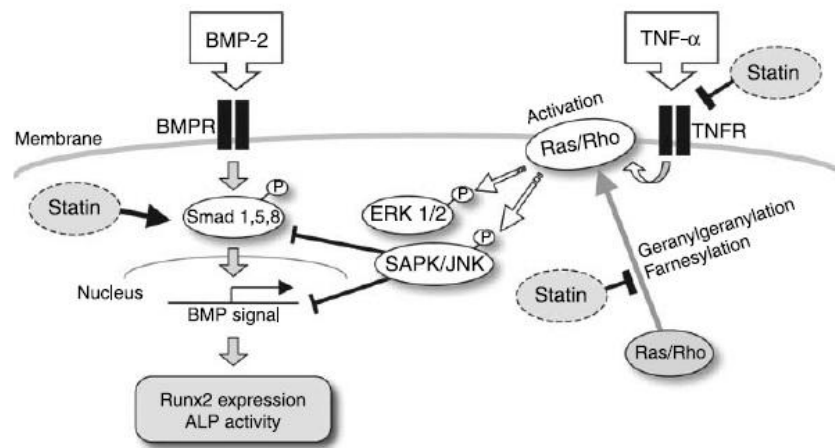


Figure 1.6 A proposed mechanism of simvastatin in osteoblastic differentiation. (Adopted from Yamashita et al., 2008 with permission).

1.6 The Importance of Animal Studies in Bone Research

The mechanisms in charge of drug-induced bone diseases are numerous and can not be clarified, yet. Animal studies enable us to get rid of the all diversities due to life style, individual diseases, and conformity (Nissen-Meyer L.S.H., 2008). Whereas measurement of BMD is commonly used in the diagnosis of bone diseases, there are other factors which increase the fracture risk, independently from BMD (Pack and Morrell, 2004; Raisz L.G., 2005). Bone turnover which is measured via biochemical markers of bone formation and resorption, reflects the alterations in the rate of bone remodelling. Structural and material features including microarchitecture, geometry and mineral and matrix composition (Turner, C.H., 2002) which are determined by imaging and biomechanical techniques, also reflect bone strength. However, these bone quality evaluation techniques cannot be used in human studies *in vivo*. Thus, the fracture risk and bone mineral density measurement are the primary clinical endpoint. In contrast,

in animal studies both the imaging and biomechanical strength tests (bending and hardness tests) can be applied to get information about bone quality.

Accumulating evidence that drug treatment may not only affect bone mass, but may also affect bone quality and strength (Pack, A., 2008) underline the need for animal model studies to estimate the positive and negative effects and mechanisms of action for drugs in bone tissue. Bone quality investigation in human is troubling, however studies with animals supply a system in which the effects of drugs on bone structural features can be studied without interfering with any disease state or lifestyle (Nissen-Meyer L.S.H., 2008).

1.6.1 Animal Models Used in The Present Study

In the first study of the thesis, we used a genetically induced epileptic model; Wistar Albino Glaxo from Rijswijk (WAG/Rij rats) which closely resemble the model of genetically induced absence epilepsy in humans (Luijtelaar and Sitnikova, 2006) among the other models. The main advantage of studying with genetically induced epileptic model, is the elimination of the effects of epileptic agents like PTZ. WAG/Rij strain is an inbred strain with homozygous individuals. The seizure reply between human and rat is in close accordance according to the pharmacological studies with effective antiepileptic drugs. The subgroup of WAG/Rij rats, is genetically sloped to non-convulsive seizures with audiogenic convulsive seizures and it is called mixed epileptic form (Midzyanovskaya et al., 2004). Mixed epileptic forms in patients are often resistant to drug therapy (refractory). Thus, animal systems for convulsive and nonconvulsive epileptic seizures are necessary for experimental research (Midzyanovskaya et al., 2004). The comparison of this epileptic group with a control group, gives the advantage of getting information about the effects of epileptic seizures alone. As a control group, Wistar healthy rats can be used since there are no baseline differences

between these two groups except an unknown inherited mutation which induces absence epilepsy with audogenic susceptibility (Naquet and Meldrum, 1972; Coenen et al., 1992). In the current study, 6-month rats were used since the absence epilepsy is mostly seen in early adults. These rats have still growth plates besides the complete mineralization of primary spongiosa.

In the both first and second studies of the thesis, drugs were also administered to healthy Wistar rats. Thus, only the effects of the drugs were clarified without interfering with any disease state.

1.7 Biophysical and Biomechanical Techniques Used in The Current Study

Early diagnosis of bone diseases is crucial for the protection from disorders in tissues. BMD has been widely used as an agent marker of bone strength. Besides the BMD values, for the strength and quality of the bone tissue, structural and mechanical features of bone, are also important (Raisz et al., 2005). Thus, studies with measuring BMD by Dual Energy X-ray Absorptiometry (DXA), cannot give much information about bone quality (Paschalis et al., 1997; Verotti et al., 2010). One of the most important features of bone that defines its mechanical strength is its material features (Bouxsein M.L, 2004). Material features including mineral content, matrix composition, and crystal sizes can be defined by vibrational infrared spectroscopy and microspectroscopy. Vibrational spectroscopy and microspectroscopy points out composition, physical and chemical structure of important bone components. Since most of the bone diseases will result in abnormalities in composition, vibrational techniques may have an essential role as either in diagnosis or in monitoring the development of therapy (Carden and Morris, 2000). To understand the relationship between the structure and the mechanical characteristics of a bone at a micro- and nanostructural scale, is also another important parameter for the early diagnosis of bone disorders (Paschalis et

al., 2011). Moreover, along with the clinical methods and imaging techniques, biochemical tests including measurement of bone turnover markers, play a crucial role in the evaluation and diagnosis of metabolic bone disorders (Seibel M.J., 2005).

Consequently, a combination of biophysical, biomechanical and biochemical studies is needed for understanding an overall pathology and early diagnosis of disorders in bone research.

1.7.1 Spectroscopic and Microspectroscopic Techniques

1.7.1.1 Basis of Spectroscopy

Electromagnetic radiation is categorized due to the frequency of its wave. The electromagnetic spectrum, is composed of radio waves, microwaves, infrared radiation, visible light, ultraviolet radiation, X-rays and gamma rays which are in respective of increased frequency and decreased wavelength (Figure 1.7).

The behavior of electromagnetic radiation alters qualitatively like its frequency when it interacts with a matter. Spectroscopy which is the study of the interaction between a matter and an electromagnetic radiation, gives a data called spectrum. "A spectrum is a plot of the intensity of energy detected versus the wavelength or frequency of the energy" (Freifelder et al., 1982). Spectra can be used for both qualitative and quantitative analysis.

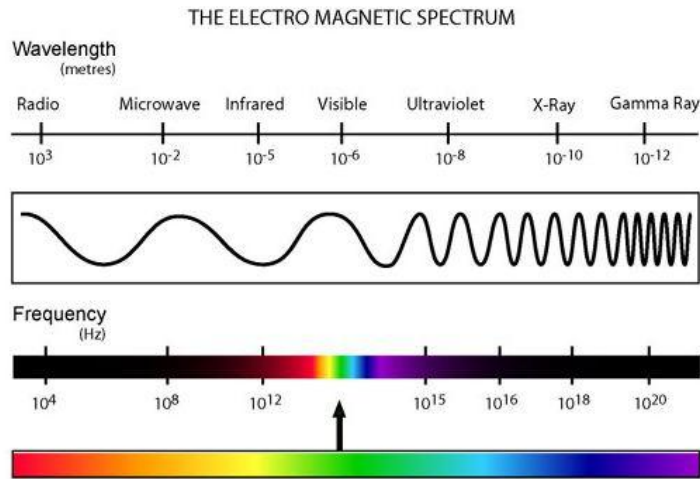


Figure 1.7 The electromagnetic spectrum.

Radiation is redirected between the energy levels of the atoms or molecules when an EM radiation and matter interact. In this phenomenon, an excitation of a molecule to higher energy levels takes place (Freifelder et al., 1982). An energy level diagram shows the energy levels as shown in Figure 1.8.

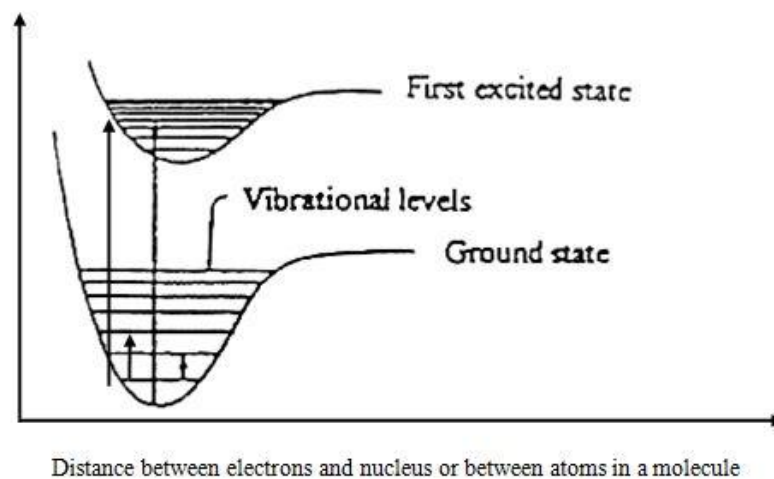


Figure 1.8 Diagram of an energy level representing the ground and first excited states of energy levels (Adopted from Freifelder et al., 1982 with permission).

The frequency dependence of absorption arises since energy is absorbed by transitions stimulated in different energy states of a molecule in a sample. The transitions occur only if there is a strong interaction between the incident radiation and the molecule. Absorption is most probable when the energy level separation matches the energy of the incident radiation as indicated below,

$$\Delta E = h\nu$$

where ΔE is the separation between the energy states of interest, ν is the frequency of the applied radiation and h is Planck's constant ($h = 6.6 \times 10^{-34}$ joule second).

$$c = \lambda \nu$$

where c is the speed of light ($3.0 \times 10^8 \text{ ms}^{-1}$) and λ is the wavelength of light. Above equations might be used to determine a spectroscopic unit namely wavenumber that is denoted by $\bar{\nu}$. Wavenumber is defined as the reciprocal of the wavelength as follows;

$$\bar{\nu} = \text{wavenumber} = (1/\lambda) \text{ [has a unit of } \text{cm}^{-1} \text{]}$$

$$\text{Thus, } E = h \cdot \nu = h c \bar{\nu},$$

It is shown with these equations that both wavenumber and frequency are directly proportional to energy.

1.7.1.2 Infrared Spectroscopy

Infrared energy reveals vibration modes in a molecule at the atomic level through changing the dipole moment. Infrared vibrational spectroscopy investigates photon absorption and transmission depend on frequencies and intensities in the IR energy range. In a molecule, each chemical bond vibrates at a frequency that is only belonged to that bond. Atoms of a molecule (e.g. CH₂) might have several modes of vibration due to the stretching and bending vibrations of the groups. If a vibration causes a change in the dipole moment of a molecule, then it will absorb a photon with the same frequency. There are three regions namely the near-, mid- and far- infrared, in the IR region of the EM spectrum (Smith, 1999).

Region	Wavenumber range (cm ⁻¹)	Wavelength (μm)
Near	14000-4000	0.8–2.5
Middle	4000-400	2.5–25
Far	400-4	25–1000

The IR spectra of complex molecules are also complex since they have numerous bonds. Thus, they have much more bands in their infrared spectra. A complex molecule might have six different vibration modes including symmetric and asymmetric stretch., scissoring, rocking, wagging and twisting, as represented in Figure 1.9.

Fourier transform infrared (FTIR) spectroscopy is an infrared vibrational spectroscopy technique.

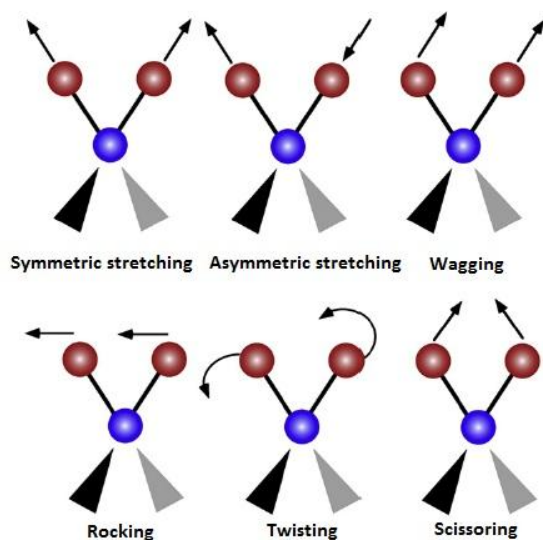


Figure 1.9 The vibrational modes associated to a molecular dipole moment change detectable in an IR absorption spectrum (Adopted from Marcelli et al., 2012 with permission).

1.7.1.3 Fourier Transform Infrared (FTIR) Spectroscopy

FTIR spectrometer is based on an important parameter called Michelson Interferometer. The interferometer has a beamsplitter that accepts the incoming IR beam, then divides it to 2 different beams. One of the beams goes to a fixed flat mirror while the other one goes to a moving flat mirror. The 2 beams meet back and recombine at the beamsplitter. The final signal which is the result of the two beams which come from different paths, is called an "interferogram" (Gerwert and Kötting, 2010). Data points that compose the signal in an interferogram, has

information about each infrared frequency from the origin. In other words, when an interferogram is measured, all the frequencies are simultaneously measured, too. Thus, using the interferometer causes fast measurements. Fourier transform which is a mathematical function, enables to convert an interferogram into an intensity-versus-frequency spectrum. This conversion is performed by a computer and a plot of intensity against frequency (cm^{-1}) is presented for further analysis (Figure 1.10).

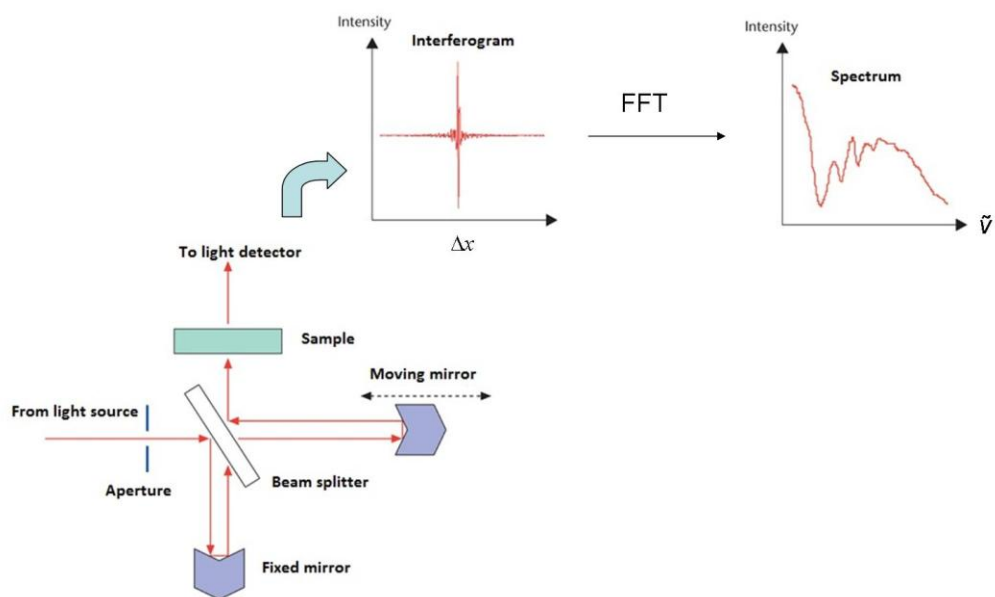


Figure 1.10 Typical setup of a Fourier transform infrared (FTIR) spectrometer (Reproduced from Gerwert and Kötting, 2010 with permission).

Some of the major advantages of FTIR spectroscopy include:

- Speed: FTIR measurements are made in seconds instead of minutes because of the simultaneous measurements of the all frequencies (known as " Fellgett Advantage") (Diem, 1999).
- Sensitivity: FTIR has an improved sensitivity since the higher sensitivity of the detectors and the higher optical throughput (known as "Jacquinot Advantage") that results in lower noise levels (Stuart, 1997). The higher sensitivity allows getting infrared spectra in a high quality from as low as few micrograms sample amounts (Dighton *et al.*, 2001). Moreover, samples can be investigated in diverse physical states; solids, liquids and gases.
- Non-disturbing: It is a non-disturbing technique which provides structural and functional information about the sample (Dogan *et al.*, 2007).
- Mechanical simplicity: Mechanical breakdown is a very small possibility since the only moving part of the instrument is the moving mirror.
- Internally calibrated: FTIR spectrometer is self-calibrating and uses a HeNe laser which is called as "Connes Advantage".

These advantages, along with several others, make FTIR measurements extremely accurate and reproducible. FTIR spectroscopy is a precious technique with higher sensitivity in determining the alterations of functional groups belonged to the various components of tissues including lipids, nucleic acids, carbohydrates and proteins (Dogan *et al.*, 2007). From the shifts in band frequencies, intensities and bandwidths, precious structural and compositional informations that might have diagnostic value, can be obtained (Ci *et al.* 1999; Toyran *et al.*, 2004; 2007; Bozkurt *et al.*, 2010; Garip *et al.*, 2010a; Severcan *et al.*, 2010; Cakmak *et al.*, 2011).

In recent years, FTIR spectroscopy has become a hopeful tool in biomedicine for diagnosis and discrimination of characteristic molecular changes between normal and disease states, including bone diseases (Paschalis et al., 1997; Boyar et al., 2004; Misof et al., 2005; Boskey et al., 2009a; 2009b; Garip et al., 2010a; 2010b). This technique is also used in our laboratory for the investigation of the effects of diseases and drugs on different tissues, the cytotoxic effects of radiation on rat liver microsomal membranes (Cakmak et al., 2011) and foods (Dogan et al., 2007), effects of diabetes on different tissues (Bozkurt et al., 2010; Severcan et al., 2010), for the characterization of microorganisms (Garip *et al.*, 2007; Garip et al., 2009) and plants (Gorgulu et.al., 2007), also for the discrimination of cancer cells (Ozek et al., 2010) and for the determination of stem cell differentiation (Aksoy et.al., 2012).

1.7.1.4 Attenuated Total Reflectance Fourier Transform Infrared (ATR-FTIR) Spectroscopy

An ATR is depend on the alterations in an internally reflected IR beam caused by a contact with a sample. The internal reflectance forms an evanescent wave extending over the surface of the crystal into a contacted sample. The evanescent wave exceeds just a few microns ($0.5 \mu - 5 \mu$) over both surface of the crystal and into a sample. When the sample absorbs energy in the target spectrum region, the evanescent wave will be attenuated. The attenuated energy then goes to the detector in the infrared spectrometer (Figure 1.11). An IR spectrum is formed after that. The most important requirements for the technique are; the sample has to be in contact directly with the crystal and the refractive index of the crystal has to be higher than the refractive index of the sample. If the latter requirement is not met, the light would be transmitted instead of reflected in the crystal. Among many kinds of materials used for ATR crystal including diamond, amorphous material

transmitting infrared (AMTIR), germanium and silicon, zinc selenide (ZnSe) is the most common one (Perkin Elmer Life Sciences, 2005; Kazarian *et al.*, 2006).

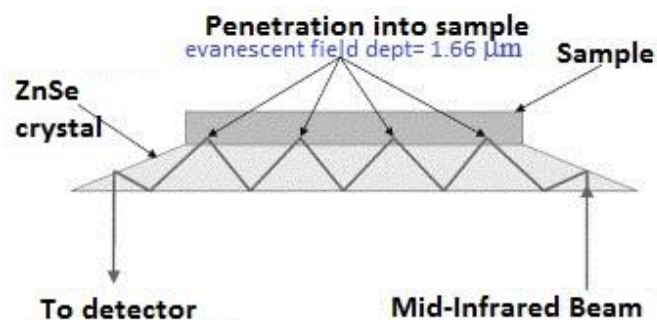


Figure 1.11 Schematic representation of ATR attachment top plate (Reproduced from Ellis and Goodacre, 2001 with permission).

In traditionally IR spectrometers, the infrared radiation is transmitted across the sample which is in solid, liquid or gas form. The thickness is very important for the spectral features of a sample in liquid or solid form. Thus, a pathlength should be constant during quantitative analyses. ATR technique provides a constant pathlength for the samples since the wave can protrude a limited distance over the surface of the crystal into the sample (Cocciardi *et al.*, 2005). Another advantage of the technique is the easier sample preparation for both solid and liquid samples when compared to the sample preparation for transmission mode. Moreover, sample preparation might be messy and take too much time and is difficult to get the true sample/matrix ratios and homogenous samples in traditional IR spectrometers with transmission mode. The ATR technique addresses these issues.

1.7.1.5 Fourier Transform Infrared Microspectroscopy

The infrared spectrometer coupled to an optical microscope (Figure 1.26) enables studying biological samples and getting molecular information with a high spatial resolution (Levin and Bhargawa, 2005). It allows investigating the molecular chemistry of biological materials by enabling the connection to morphology. FTIR imaging techniques are non-invasive technique differently from fluorescence imaging spectroscopy because staining is not required to produce the image contrast (Hof et al., 2005). Using infrared microspectroscopy enables to monitor the intrinsic spectroscopic properties of the sample itself.

The spectral data is collected by scanning the sample spot-by-spot through the surface and getting an IR spectrum from each spot. The size of the spot or pixel is determined by the size of the microscope aperture which might be between 10 μm x 10 μm to 200 μm x 200 μm . The mapping enables recording the high quality IR spectra with the information about the chemical distribution of each molecule in a sample. Every spot which is recorded sequentially, is collected together to form a larger image. The recorded information by IR microscopy is commonly represented by false-colour images, that look like the images of histological-stained samples (Marcelli et al., 2012).

1.7.1.6 Synchrotron Fourier Transform Infrared (SR-FTIR) Microspectroscopy

"Synchrotron radiation produced by relativistic electrons in high-energy accelerators, extends from x-rays down through the infrared spectral range, and serves as a source for a number of biologically relevant measurement techniques" (Miller et al., 2001). Synchrotron radiation-based FTIR microspectroscopy which uses the synchrotron radiation as a light source, generates spectroscopic

information with a higher spatial resolution and a higher signal to noise ratio from a given sample. FTIR microscopes with a conventional infrared source meet a S/N limitation in 20 to 30 μm area in diameters. This limits the analysis of biological samples only to the tissue level. These FTIR microscopes can not probe cells which are 5 to 30 μm in diameter. The synchrotron source enables probing very small regions with its higher brightness and acceptable S/N (Reffner et al., 1995). Thus, synchrotron radiation-based FT-IR microscopy is a novel microscopic technique in the field of cellular biology. Applications are served for comparison of different types of cancer cells and cancerous tissues as well as for the study of drug-induced biochemical alterations in tissues.

The first IR microspectroscopy coupled with synchrotron beamline was built at Brookhaven National Laboratory (New York, USA) in 1993. Figure 1.12 shows the synchrotron diagram at the NSLS of Brookhaven National Laboratory.

"A synchrotron infrared source is 100–1000 times brighter than a conventional thermal (e.g., global) source" (Cakmak et al., 2012). Synchrotron infrared light which enables to focus on a small spot, allows studying samples which are smaller and in more diluted concentrations. With its 1000-fold increased brightness, data collection takes ~30 times less duration than the global source (Miller and Dumas, 2006). SR-FTIR microspectroscopy with more brightness and 1000 times greater signal-to-noise ratio than the thermal source, allows us to investigate the alterations in the microstructures with a high spatial resolution (Holman et al., 2003). It also allows to monitor the biochemical alterations in samples successfully in a non-invasive and non-destructive manner without any dyes, fluorescent labels, or stains.

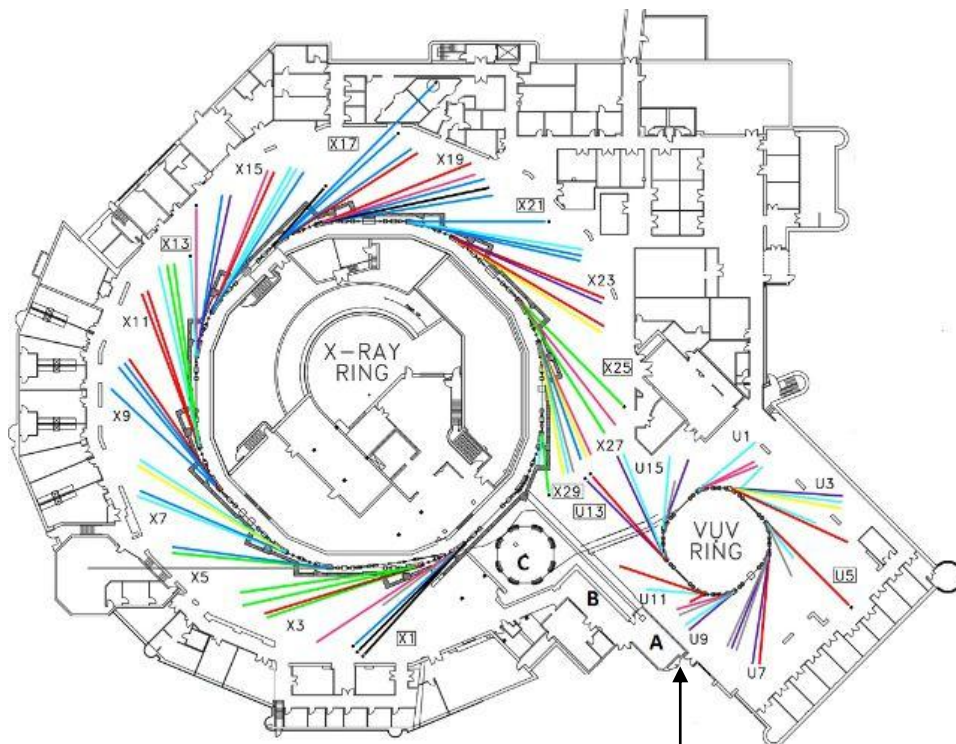


Figure 1.12 "Diagram of National Synchrotron Light Source (A: electron source, B: linear accelerator, C: booster accelerator ring, VUV: Vacuum ultraviolet storage ring with associated beamlines). Electrons are accelerated from with a linear accelerator and produce an energy of 75 million electron milivolts (meV), and enter a booster ring, and are accelerated more and enter vacuum ultraviolet (VUV) storage ring" (Cakmak G., 2010).

1.7.1.6.1 Advantages of Synchrotron Fourier Transform Infrared (SR-FTIR) Microspectroscopy

An advantage of SR-FTIRM for bone research is enabling the collection of data in between $4000\text{-}400\text{ cm}^{-1}$ infrared range while the global FTIRM can only collect data between $4000\text{-}700\text{ cm}^{-1}$. The mercury-cadmiumtelluride detectors in commercial infrared microscopes cannot monitor the $700\text{-}400\text{ cm}^{-1}$ frequency

region which is below the cutoff of these detectors (Miller et al., 2001). Mineral properties including crystallinity, can also be obtained from the ν_4 PO_4^{3-} band (500-650 cm^{-1}) other than ν_1, ν_3 PO_4^{3-} band (1200-900 cm^{-1}). Studying with the former phosphate band gives more accurate data since this band is affected from other absorptions less than the latter phosphate band. Thus, it can be fit to fewer components (Rey et al., 1990) than the ν_1, ν_3 contour, and simplify curve-fitting analysis.

1.7.1.7 FTIR Spectroscopy and Microspectroscopy in Bone Research

"The ability to diagnose the early onset of disease, rapidly and non-invasively has multiple benefits. These include the early intervention of therapeutic strategies leading to a reduction in morbidity and mortality, and the releasing of economic resources within overburdened health care systems" (Ellis and Goodacre, 2006). Vibrational spectroscopy has been widely preferred with the advantages above to get information about molecular structure of mineralized tissues including bone (Paschalis et al., 1997; Boyar et al., 2004; Misof et al., 2005; Severcan et al., 2008; Boskey et al., 2009a; 2009b; Garip et al., 2010a; 2010b). Since the different anatomical bone regions such as cortical and trabecular, react to both diseases and drugs differently, bone chemistry studies are complex (Jerome et al., 1994; Carlson et al., 1997). To determine these site-specific variations, microscopic examination of bone tissue is crucial (Huang et al., 2003). "With the use of multichannel array detectors, FTIR microspectroscopy enables investigators to examine spectra at discrete points within tissue sections in short periods of time" (Lewis et al., 1995; Marcott et al., 1998). To diagnose pathological regions in bones, this "point-by-point mapping" has also been applied (Boskey and Camacho, 2007). The spatial resolution in FTIR imaging is $\sim 10 \mu\text{m}$ while it is much improved (1-2 μm) with using synchrotron light source (Boskey and Camacho, 2007).

With the advantages mentioned above, FTIR and ATR-FTIR spectroscopy and microspectroscopy techniques have been applied to determine changes in bone development and to detect disease and drug-induced modifications in bone biopsies from patients and animals with bone disorders and drug-treated vs non-treated bones (Huang et al., 2003; Faibish et al., 2005; Boskey and Camacho, 2007; Youn and Milner, 2008; Boskey et al., 2009a; Dooley et al., 2009; Rieppo et al., 2009; Garip et al., 2010a; Garip et al., 2010b). For more detailed information, applications of vibrational spectroscopic and microspectroscopic techniques to describe bone diseases and treatment has been reviewed elsewhere (Boskey and Camacho, 2005; Garip and Boskey, 2012).

1.7.2 Atomic Force Microscopy (AFM)

The atomic force microscope (AFM) measures the forces between a tip and a sample. The tip which is fixed to a cantilever, is adjusted close to sample surface. "Attractive or repulsive forces resulting from interactions between the tip and the surface will cause a positive or negative bending of the cantilever. The bending is detected by means of a laser beam, which is reflected from the back side of the cantilever" (Blanchard, C.H., 1996). Figure 1.13 shows the basic concepts of AFM.

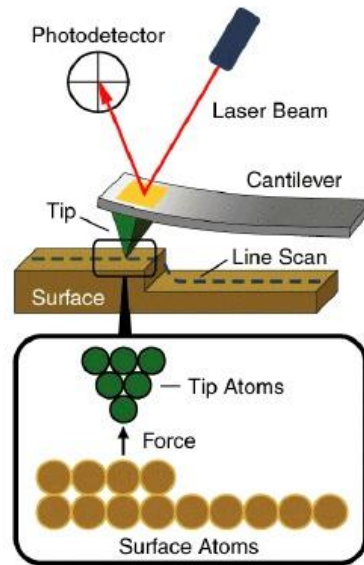


Figure 1.13 Schematic representation of AFM Principle.

There are mainly three modes of AFM:

In contact mode, the tip has physical contact continuously with the surface of the sample. The deflection of the cantilever Δx is proportional to the force acting on the tip, via Hook's law, $F = -k \cdot \Delta x$, where k is the spring constant of the cantilever. In contact mode, either the constant height between the tip and the surface or a constant force conditions can be used. In the constant height, the tip is fixed to a target height while in the constant force, the deflection of the cantilever is fixed and the motion of the piezo scanner in z -direction is monitored. The possible damage of the surface is a disadvantage while the fast scan and high resolution are the advantages of this mode.

In non-contact mode, scanning is done with the forces between the tip and the sample without interfering the shape of the sample. This eliminates the disadvantage of contact mode, however recording needs to be carried out very slowly when there are significant features on the surface. Moreover, it is just useful for only extremely hydrophobic samples.

In tapping mode, the tip is tapped rapidly against the surface as it scans over the area to be imaged. Elimination of the shearing forces and the less damage to the sample surface are the most important advantages of the tapping mode. Due to these advantages, tapping mode is the most useful mode for biological samples including bone (Vilalta-Clemente et al., 2008).

1.7.2.1 Atomic Force Microscopy (AFM) in Bone Research

Atomic force microscopy (AFM) is an important technique to monitor the bone ultrastructure in a condition which is very close to bone physiological state (Turner et al., 2007). AFM has similar spatial resolution with TEM with the advantage of elimination of the excessive sample dehydration and preparation. "Detailed knowledge about bone ultrastructure below macro level and its relation to bone material properties is essential for the complementary diagnostic tools and therapies for bone diseases" (Turner et al., 2007).

Bone surfaces can be examined by AFM with the possible quantification of hydroxyapatite crystal sizes or collagen fibril diameters (Hassenkam et al., 2004; Avci et al., 2005). Moreover, AFM imaging allows to study bone structure in 3D in the presence of drug treatments. Thus it enables to determine mechanisms resulted in drug-related disorders and loss of bone at the nano scale. "In the future AFM will surely become one of the most important tools in the medical research

for imaging, mechanical probing and manipulation of bone and other tissue constructs at the nano scale in a real-time fashion" (Turner et al., 2007).

1.7.3 Biomechanical Indentation Tests

Hardness measurement is applied by an indentation machine in which a selected mass is loaded to the sample for a limited time (dwell time), and then removed automatically. The dimensions of the indentation are measured to get hardness values. The tests can be categorized based on the geometry and/or the size of the indenter employed. There are Brinell, Rockwell, Vickers, and Knoop indenters with different geometries. Based on the size of the indenter; macroindentation, microhardness and nanoindentation are defined. All of these tests can be used for biomechanical studies of bone (Kavukcuoglu et al., 2009; Isaksson et al., 2010). Each of these methods assesses bone structures at different scales. Since it is not possible to extrapolate the mechanical properties of the bone from a single indentation test, it is ideal to perform different tests at various levels of the bone structure. The size of an osteon is about 200 to 300 μm , and each lamella in bone is 3 to 7 μm wide. Microhardness indentations range from 20 to 150 μm in length, while in nanoindentations it can be as low as 1 μm .

Indentation methods at different scales are often used and effective tools in materials research (Lum and Duncan-Hewitt, 1996; Amitay-Sadovsky and Wagner, 1998). Hardness, elastic modulus, and fracture toughness of samples can also be calculated (Meredith et al., 1996; Xu et al., 1998). Hardness and elastic modulus of bones are in correlation with the microarchitecture and composition of the tissues (Currey and Brear, 1990). Significant correlations between hardness, and degree of mineralization of bone (DMB) and Young's modulus in human bone are reported in previous studies (Follet et al., 2004; Boivin et al., 2008). Thus, a

relationship between hardness, stiffness and strength was clearly supported in bone samples.

1.8 Aim of the Study

A number of drugs may have metabolic effects on the skeletal system, and may result in either bone loss or increased bone strength. Among these drugs, anti-epileptic drug; Carbamazepine and a cholesterol lowering drug; Simvastatin were used to determine their possible effects on bone tissues in the current thesis. The main aim of the present thesis study is to investigate the effects of antiepileptic drug; Carbamazepine on bone tissues of healthy and epileptic rats. To compare the drug-bone interactions we have chosen another well-known cholesterol reducing drug, Simvastatin and studies its the dose-dependent effects on healthy bone tissues. These studies will provide new strategies to prevent the side-effects of drugs on bone metabolism and to support new treatments against bone disorders.

Study 1; Epilepsy is a common serious neurological disorder of the nervous system. Carbamazepine is one of the most widely used and effective antiepileptic drugs for epilepsy treatment. However the reported results about its side-effects on bones are contradictory. Moreover, there is not any study in the literature, investigating the independent effect of epileptic seizures on bone tissues. Thus, the side-effects of AED; Carbamazepine therapy on bone tissues could not be differentiated from the effects of the epileptic seizures. The exact mechanisms for possible adverse bone effects of Carbamazepine have not been determined yet. These mechanisms may be multiple.

Within this context, in the first study, we aimed to clarify and differentiate the effects of Carbamazepine and epileptic seizures on bone tissues and clarify the

action mechanism of anti-epileptic drug and seizures on vitamin D and bone metabolism. We hypothesized that besides Carbamazepine therapy, epileptic seizures have also adverse effects on bone and both the drug and seizures cause bone disorders through inhibiting and/or stimulating vitamin D anabolism and catabolism enzymes, respectively.

Study 2; As a comparative study, we used one of the common and well-known cholesterol reducing drug; Simvastatin, to determine its possible dose dependent effects on healthy bone tissues. It is used to reduce high cholesterol levels and to prevent cardiovascular diseases. Moreover, by inhibiting HMG-CoA reductase, simvastatin not only inhibit cholesterol synthesis but also show various other beneficial effects called pleiotropic effect. In recent years, among the pleiotropic effects, there has been a growing interest in the effect of simvastatin on bone tissue and osteoporosis. However, the relationship between the use of simvastatin and improvement of bone quality reported in the literature is still controversial. Moreover, it was shown that high and low dose simvastatin therapy might cause lipid peroxidation in soft tissues. There is not any report about the effects of simvastatin on bone lipids.

Considering an urgent need for the more effective drugs that are able to induce new bone formation with less negative side effect, the current study aimed to investigate dose-dependent effects of simvastatin treatment on bone tissues and to clarify whether it causes lipid peroxidation on bones. We hypothesized that both low and high dose simvastatin increase the bone strength however, their possible adverse effects on bone lipids, may limit their pleiotropic effects on bone tissues. Moreover, FTIR spectroscopy with multivariate and neural network analyses can be used to clarify drug-related pleiotropic and/or adverse effects on bones.

2.1.1 Chemicals

The list of used chemicals and their suppliers are given in Appendix A.

2.1.2 Animal Studies

Animal studies were performed at Kocaeli University. Genetically absence epileptic rats (WAG/Rij) and as a control healthy rats (Wistar rats) weighted 250-350 g, are used. 6-month male rats represent early adults (Brzoska and Moniuszko-Jakoniuk, 2004 and refs in Jayo et al., 2000). Standard pellet diet was given to rats. Regulation of the degree of temperature, humidity, and rate of air exchange was done with 12 hours night & day cycle. Carbamazepine was administered by gavage: 50 mg/kg/day for 5 weeks according to the previous studies (Onodera et al., 2001; 2002).

The WAG/Rij rats were primarily screened for the audiogenic susceptibility and animals having sound-induced convulsions (susceptible to audiogenic kindling) are grouped (N=7 for each group).

The animal groups are;

Group 1: Wistar healthy control + Physiological serum

Group 2: Wistar control + Carbamazepine (50 mg/kg/day)

Group 3: WAG/Rij epileptic (absence epilepsy + convulsive seizures) + Physiological serum

Group 4: WAG/Rij epileptic + Carbamazepine (50 mg/kg/day)

Comparing epileptic rats (WAG/Rij) with healthy Wistar rats, gives information about the effects of epilepsy and convulsive epileptic seizures alone. Giving Carbamazepine to the healthy Wistar rats and comparing this group with non-

treated healthy Wistar control group gives information about the effects of Carbamazepine on bone without interfering with any disease state.

2.1.2.1 Electroencephalographic (EEG) Recording

To test audiogenic susceptibility each animal was put into a box (60x60x60 cm³) and a standard complex sound (“keys ringing”) (Krushinski et al., 1974) produced by a vibro device, with a frequency range of 13–85kHz and mean intensity of 50–60 dB was administered to the rat for 1.5 minutes. The spikewave discharges (SWDs), were monitored in rats which are susceptible and not susceptible to audiogenic convulsions to diagnose the absence epilepsy in WAG/Rij rats. For this purpose, EEG tripolar record electrodes were placed on cortex surface under anesthetic conditions with ketamine and chlorpromazin. Cortical electrodes were located on frontal regions and parietal regions. Reference electrodes were placed on the cerebellum. After a week the rats were taken into pleksiglas cage and the EEG records were done during seizures and after seizures for 30 minutes.

All rats were exposed to the sound stimulation once a day for 5 weeks and EEG records were taken during seizures and after seizures. At the end of the 5 weeks, rats were decapitated and the bone tissues (femur, tibia and lumbar spine), liver and kidney tissues were removed and stored at -80°C until performing biophysical and biomechanical experiments. The blood samples were taken from the same animals and processed to get serum samples. Soft tissues and serum samples were also stored at -80°C for biochemical studies.

2.1.3 Methods

2.1.3.1 Fourier Transform Infrared (FTIR) and Synchrotron-Fourier Transform Infrared (SR-FTIR) Microspectroscopic Studies

2.1.3.1.1 Sample Preparation

Bone tissues; distal femur, proximal tibia (close parts to knee) and lumbar spine (L1-L5) will be used for the studies with FTIR microspectroscopy (Figure 2.2). These are the most affected parts from osteoporosis according to previous studies. The seven tibia, femur and spine bone samples per group were cleaned of soft tissue and were partially fixed in different percentages of ethanol, dehydrated with different percentage of ethanol and acetone solutions, and then embedded in polymethylmethacrylate (PMMA).

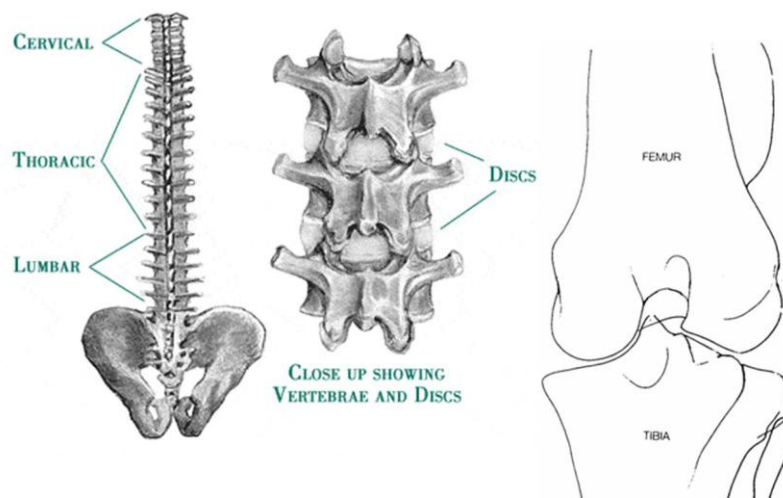


Figure 2.2 Schematic representation of femur, tibia and spine bone tissues.

Preparation of embedding medium PMMA will be done according to Methacrylate Method (R.G Erben, 1997).

- **Fixation in EtOH**, tissues kept in:

70% EtOH for 2 times 2 days each

95% EtOH 2 times 2 days each

100% 2-propanol 2 times 1 day each

Xylene solution for 2 times 1 day each

- **Infiltration of PMMA**, tissues kept in:

Solution I (60 ml methylmethacrylate, 25 ml buthylmethacrylate, 5 ml methylbenzoate, 1.2 ml polyethylene glycol 200) for 4 days

Solution II (100 ml methylmethacrylate, 0.4 gr benzoyl peroxide) for 4 days

Solution III (100 ml methylmethacrylate, 0.8 gr benzoyl peroxide) for 4 days

- **Embedding in PMMA**

Tissues embedded in Solution III added with 400 μ l N,N-dimethyl-p-toluidine (accelerator of polymerization, for 100 ml of Sol III).

Solution III mixed on ice for 1 hour prior to usage.

Embedded tissues kept at 4°C for 3 days and put in oven at 60°C for 1 day.

After trimming, the bones in embedding blocks will be ready for sectioning. Longitudinal nondecalcified sections of the bone tissues (4 sections per bone) were cut by a microtome at 2 μ m thickness and mounted on IR-transparent, 1 mm thick x 13 mm diameter BaF₂ infrared windows for FTIRM and SR-FTIRM studies.

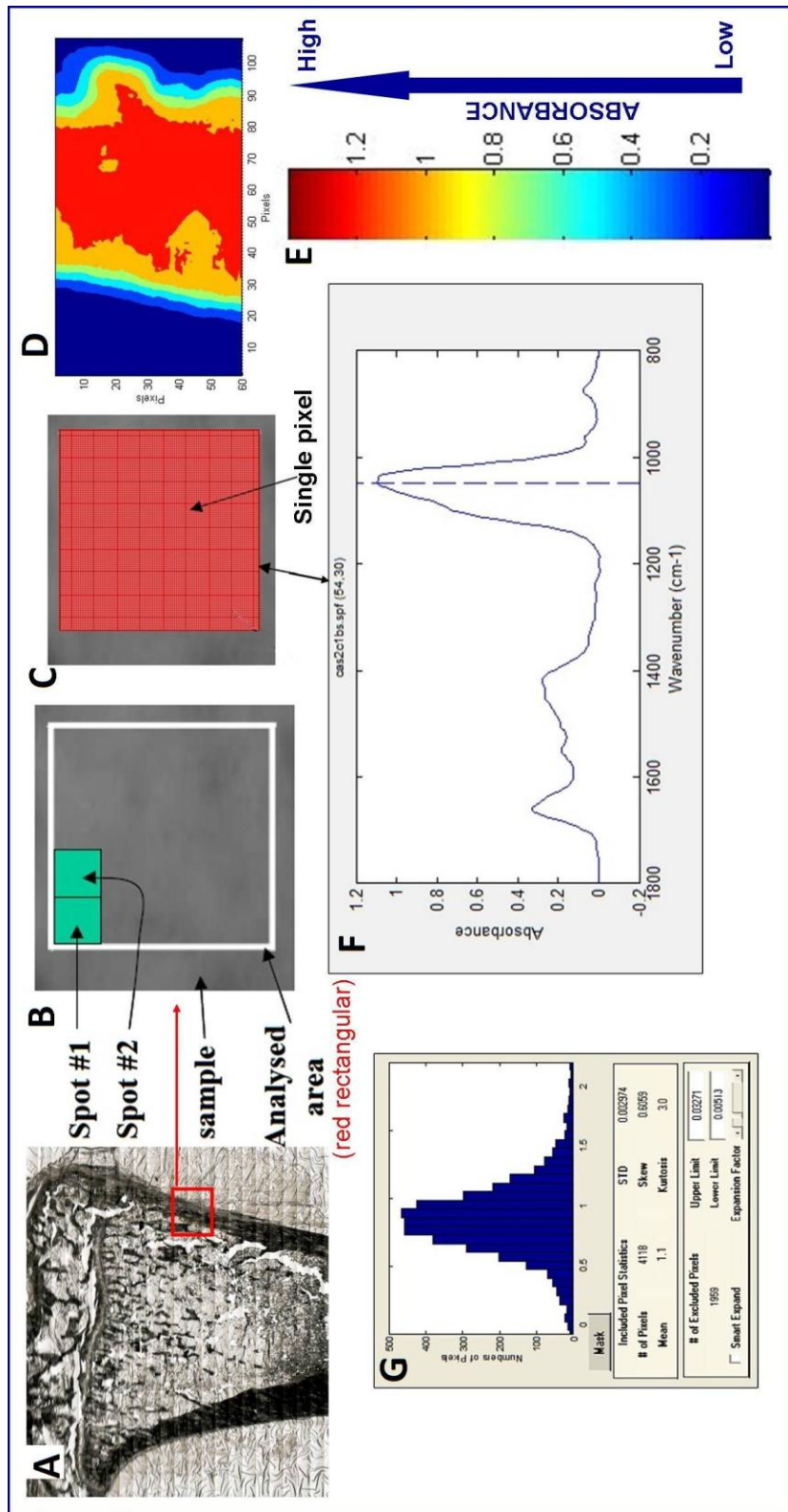


Figure 2.3 The selected area (rectangular shape) in a visible FTIR image (A) of the sample is scanned spot by spot (B) across the surface and collecting at each spot a complete infrared spectrum (C, F). The different spots are recorded sequentially, and the image is reconstructed by matching the spectral information of each single spot to construct a larger image. The imaging results were expressed as histograms (G) describing the pixel distribution of the parameters interested, mean values, standard deviations of the pixel distributions, and representative color-coded images (D, E).

2.1.3.1.2 Data Acquisition and Spectroscopic Measurements

In FTIR Microspectroscopy studies, Perkin Elmer Spectrum One/Spotlight 400 Fourier Transform Infrared Microspectrometer (Perkin Elmer Corp., Sheldon, Connecticut) was used to map bone sections. For each tissue section, an IR image was obtained with a $6.25\ \mu\text{m} \times 6.25\ \mu\text{m}$ pixel size. Infrared spectra were collected in transmission mode between $2000\text{-}800\ \text{cm}^{-1}$ wavenumber region with $4\ \text{cm}^{-1}$ resolution and 100 numbers of scans. A spectrum from an area not belonged to bone, was recorded as background. IR data from different anatomical bone sites; namely cortical, trabecular, and growth plate were collected (Figure 2.4). For each animal, totally 9 maps were recorded from randomly chosen, different regions of cortical, trabecular and growth plate parts of bone (3 maps from cortical, 3 maps from trabecular and 3 maps from growth plate). Since we have 7 animals for each group, 63 different maps were used to calculate the IR parameters for each control, epileptic and drug-treated groups.

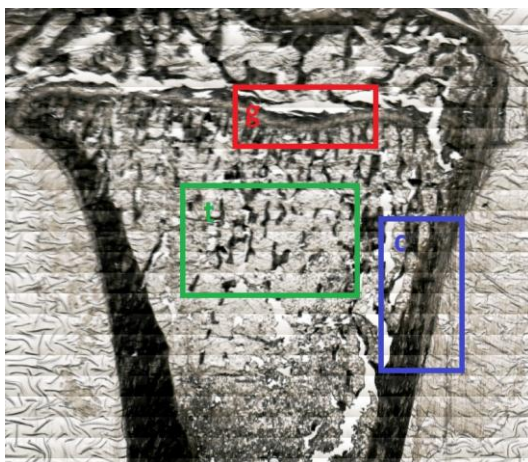


Figure 2.4 Cortical (blue), trabecular (green) and growth plate (red) parts of bone.

Spine bone samples which was determined as the most affected bone tissue according to FTIR imaging studies, were examined detailly by Synchrotron-FTIR Microspectroscopy. SR-FTIR data of 15 different areas from cortical bone (5 maps from endosteum, 5 maps from mid-cortical, 5 maps from periosteum) for each animal were collected (Figure 2.5).

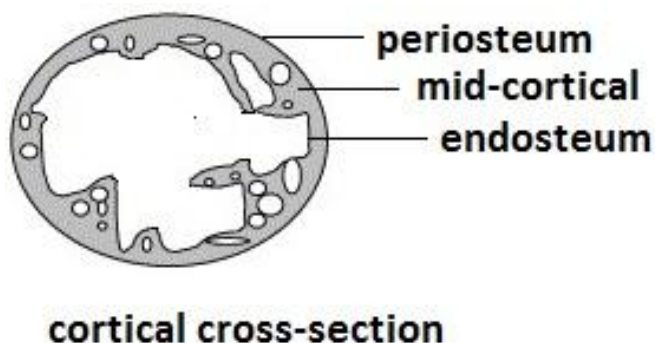


Figure 2.5 Schematic representation of cortical cross-section showing periosteum (outer bone membrane), mid-cortical and endosteum (inner bone membrane).

The Synchrotron-FTIR Microspectroscopy studies were performed at NSLS, Brookhaven National Laboratory (Upton, NY). A Thermo Nicolet Magna 860 FTIR spectrometer equipped with a Continuum infrared microscope (ThermoNicolet, Madison, WI), was used with synchrotron light as the infrared source. The spectra were recorded in transmission mode in 2000-500 cm^{-1} wavenumber range at a spectral resolution of 4 cm^{-1} with 500 scan number and 10 $\mu\text{m} \times 10 \mu\text{m}$ aperture size with 1 $\mu\text{m} \times 1 \mu\text{m}$ pixel resolution.

In FTIRM data collection was done between 4000-700 cm^{-1} , where in SR-FTIRM collection of data was done in between 4000-400 cm^{-1} infrared range. In the latter technique, $\nu_4 \text{PO}_4^{3-}$ band (500-650 cm^{-1}) can also be monitored besides $\nu_1, \nu_3 \text{PO}_4^{3-}$ band (1200-900 cm^{-1}) (Figure 2.6).

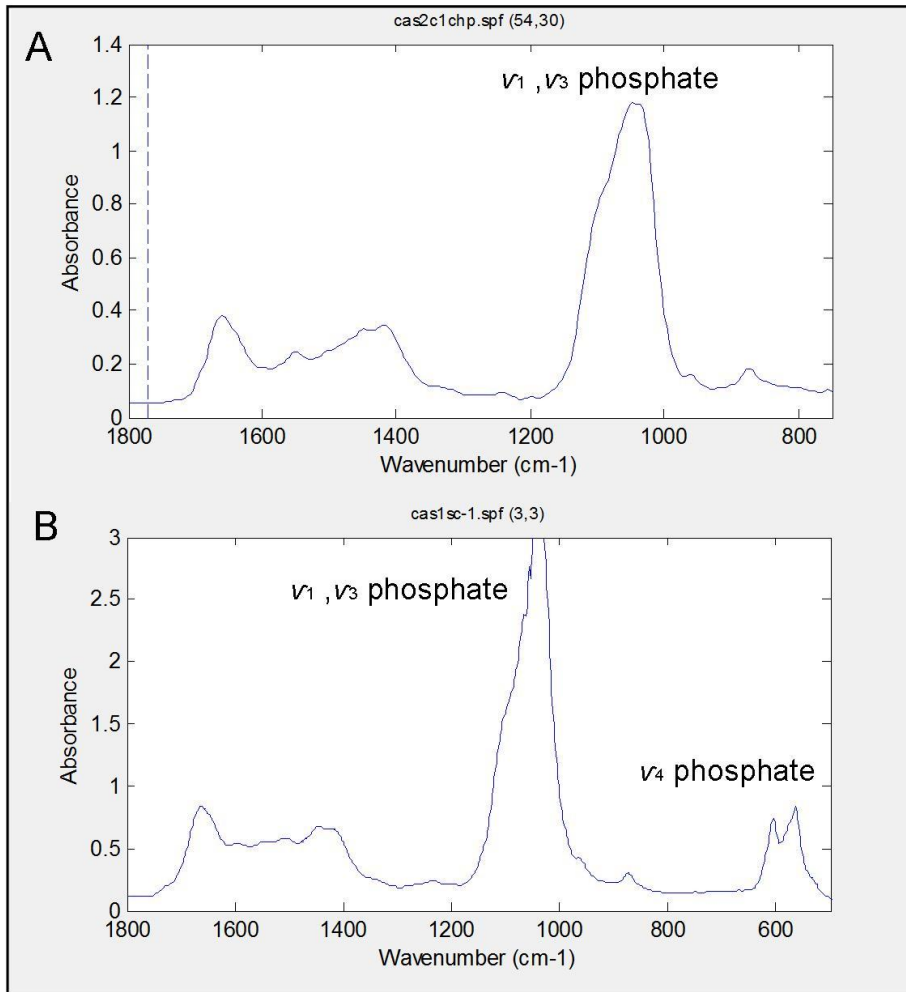


Figure 2.6 FTIRM (A) and SR-FTIRM (B) spectra of a bone tissue.

2.1.3.1.3 Data Analysis

ISys software (Spectral Dimensions, Olney, MD, USA) was used to analyze the FTIR and SR-FTIR microspectroscopic data. Whole baseline correction were performed between 2000-800 cm^{-1} region in FTIRM studies and between 2000-500 cm^{-1} region in SR-FTIRM studies. After spectral subtraction of embedding medium (PMMA), spectral masking was applied to get rid of the contributions from the nonbone parts on the sections by marking the bone samples. Figure 2.7 shows a PMMA spectrum.

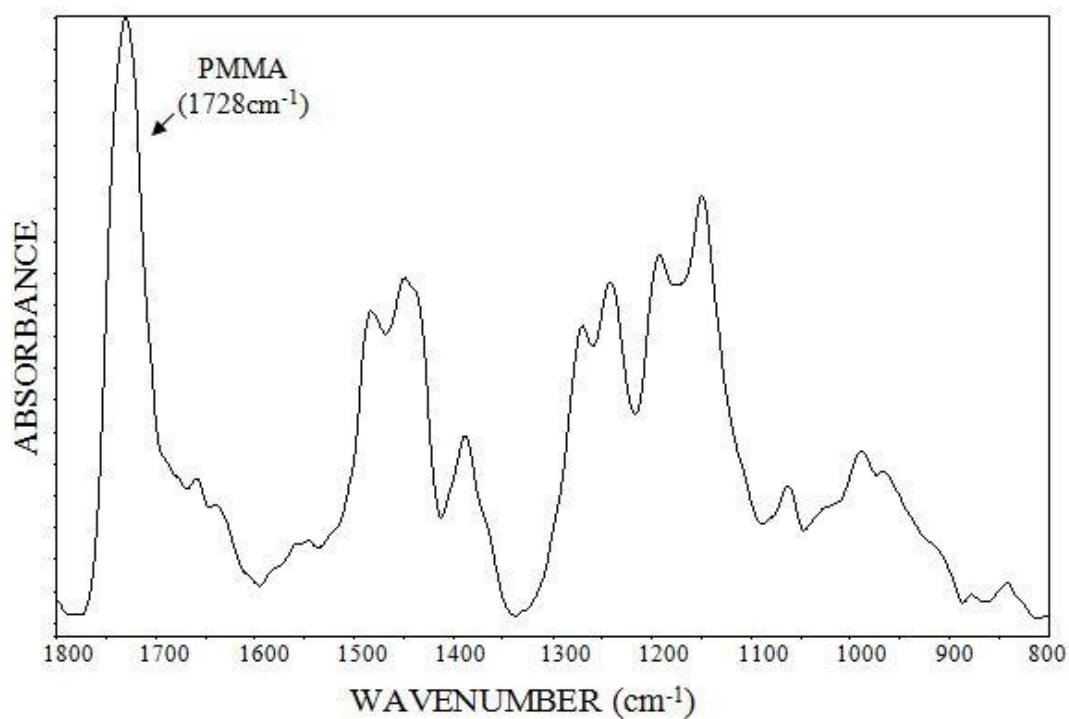


Figure 2.7 Spectrum from the embedding medium; PMMA.

The chemical maps were constructed for each group by taking the ratio of the area and intensity values of specifically selected spectral bands arisen from mineral, matrix, collagen and carbonate. Ratios of various bands were used for the analysis to get rid of the effects of section thickness. The spectral regions for the IR bands that were used to determine distribution of functional groups were presented in Table 2.1.

Table 2.1 The integrated spectral regions

Infrared Band	Integrated Spectral Range (cm⁻¹)
Amide I	1712-1534
Amide II	1534-1480
$\nu_1, \nu_3 \text{PO}_4^{3-}$	1200-900
$\nu_2 \text{CO}_3^{2-}$	890-850
$\nu_4 \text{PO}_4^{3-}$ (only monitored in SR-FTIRM)	650-500

2.1.3.2 Indentation Studies

2.1.3.2.1 Vickers Microhardness Study

The microhardness values of the tibia, femur and spine bone samples were measured by a Vickers microhardness tester (HMV-2, Shimadzu, Japan). The PMMA embedded bone tissue blocks which were used in FTIR microscopic studies, were also used to measure the microhardness values of the bones. A diamond indenter was used with a load of 25 g for 10 seconds on the surface of the

blocks (Boivin et al., 2008). The diagonal-shaped indent which was formed after the indentation, was measured to get the microhardness values of the bones. 15 measurements were carried out for each sample (5 in the cortical, 5 in the trabecular bone and 5 in the growth plate) (Figure 2.8).

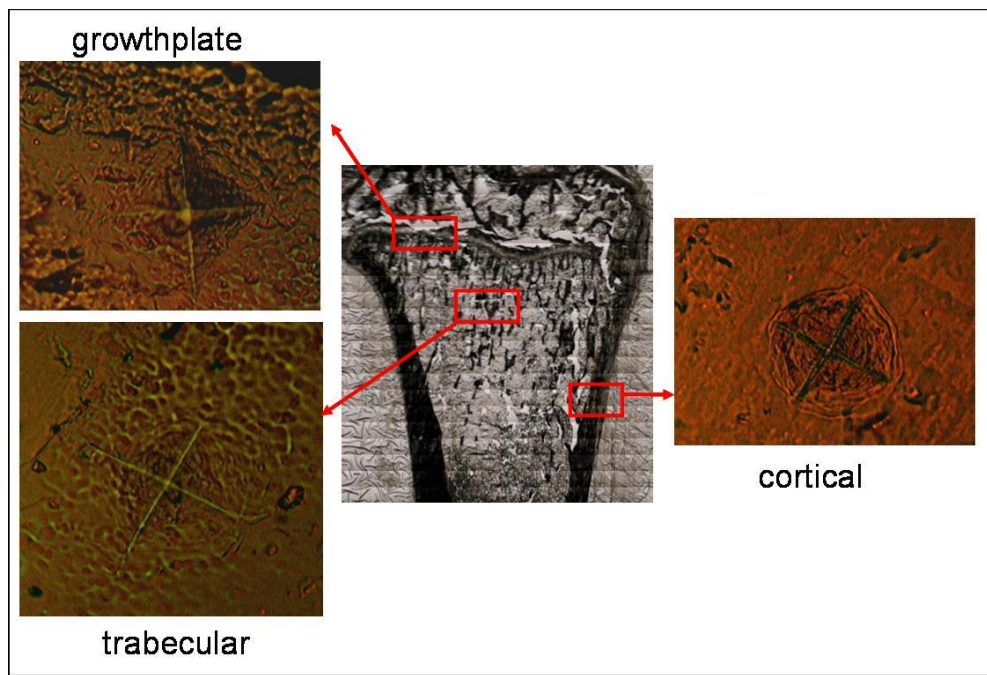


Figure 2.8 Representative Vickers indentation images of cortical, trabecular and spine regions of control bone tissue.

For the calculation, formula below was used:

$$HV = 0.001854 \frac{P}{d^2}$$

where;

HV: Vickers hardness (GPa); P: Applied load (N); d: diagonal indent length (mm). The results of the vickers microhardness were given as GPa by multiplying the Hv values with 0.009807 for converting it to GPa.

2.1.3.2.2 Nano-Indentation Study

After soft tissues were removed from bones, cross-sections were cut from distal femur, proximal tibia and lumbar spine. Then the bone tissues were embedded to epoxy (Buehler SampL-Kwick Powder & Liquid). After embedded tissues were waited for 24 hours at room temperature, bone-embedded epoxy blocks were trimmed with flat silicone carbide sanding 400-, 600-, 800- and 1200-grit discs respectively and then polished. Figure 2.9 shows the location of the nano-indentation measurements on cortical bone.

The nanoindentation tests were carried out with a Triboindenter™ (Hysitron Inc., MN) and a diamond Berkovich pyramid tip. For indentation two different maximum loads of 1000 ve 5000 μN were applied with a 5 s hold time at peak load. First, a grid pattern of totally 98 indents were performed as seen in Figure 2.9 and then nearly 300 indents were carried ou across the cortical radial sections of each bone to get information about the endosteum, mid-cortical and prosteum parts of cortical (Figure 2.9). For first nanoindentations, indents were spaced every $5\mu\text{m}$ in both x- (radial) and y- (tangential) directions. The Oliver & Pharr method (Oliver and Pharr, 1992) was used to determine the mechanical properties. This method uses the following equations to find the bone's elastic modulus, E, and hardness, H:

$$E_r = \frac{\sqrt{\pi}}{2} \frac{S}{\sqrt{A_c}} \quad E = \frac{1 - \nu_s^2}{\frac{1}{E_r} - \frac{1 - \nu_i^2}{E_i}} \quad H = \frac{P_{\max}}{A_c}$$

where, E_r : elastic modulus, S : contact stiffness, P_{max} : maximum load, A_c : contact area. ν_i and ν_s : Poisson's ratio for the indenter and sample, respectively. $E_i = 1140$ GPa, $\nu_i = 0.07$, Poisson's ratio for the bone; $\nu_s = 0.3$ (Kavukcuoglu et al., 2009). The average displacement for $1000\mu\text{N}$ load was $\approx 150\text{nm}$ and for $5000\mu\text{N}$ load was $\approx 400\text{nm}$ (Figure 2.10).

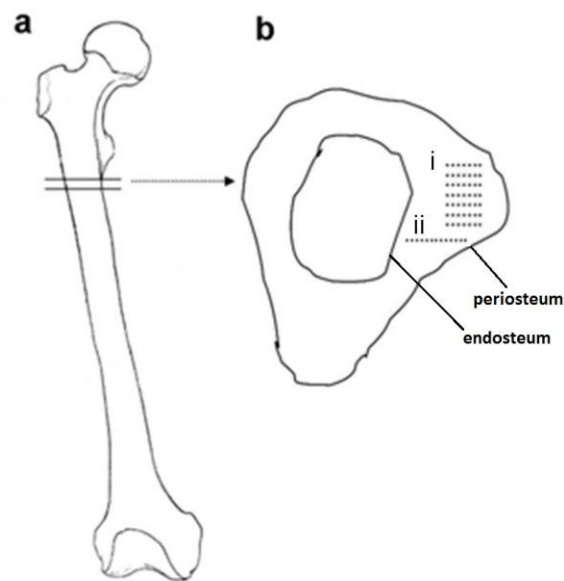


Figure 2.9 The representative image of (a) femur tissue and (b) cross-section obtained from distal femur. Dots on the cortical bone shows the place of (i) $7 \times 7 = 49$ indents and (ii) $30 \times 1 = 30$ indents across the radial of cortical bone, obtained for each sample.

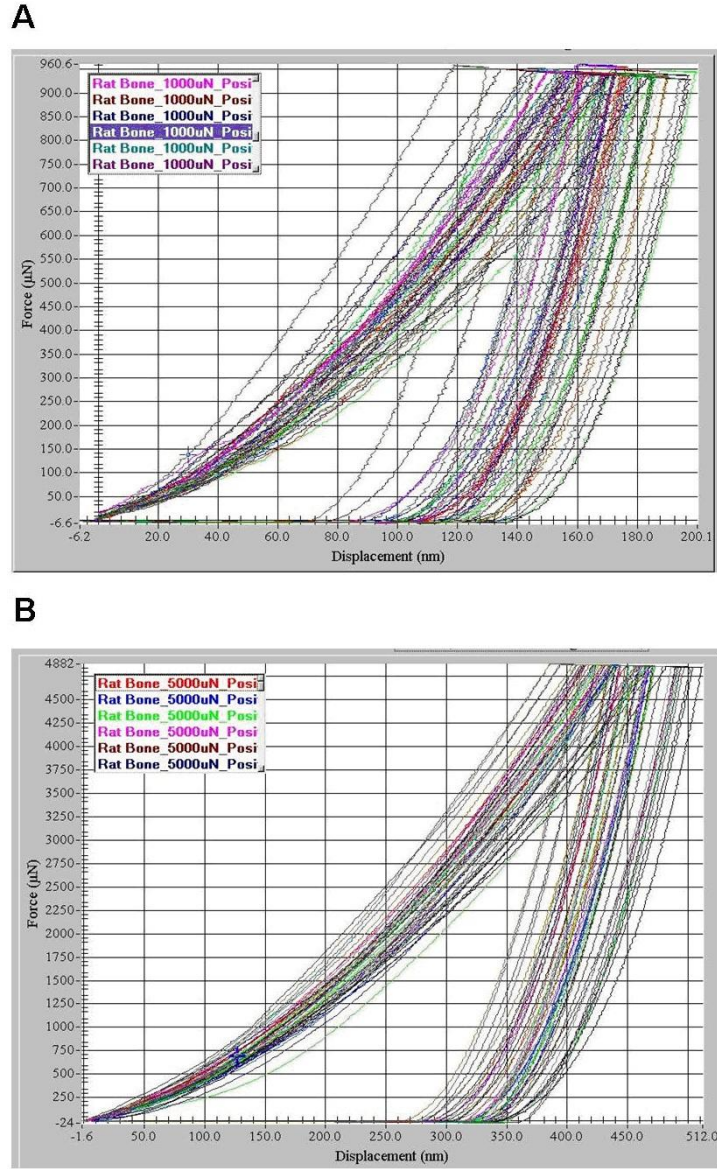


Figure 2.10 Representative displacement curves for (A) 1000 µN and (B) 5000 µN loads.

2.1.3.3 Atomic Force Microscopy Studies

According to the FTIR imaging and indentation studies, the most affected bone tissue from seizures and drug treatment, spine tissue, was further examined by AFM to get information about the surface topography and features of bone tissues. Raw spine bone cross-sections were used for AFM studies without any embedding or trimming processes. The AFM images were recorded with Nanoscope IV Scanning Probe Microscope (Nanoscope IV Scanning Probe Microscope, Digital Instruments, Veeco Metrology Group) in tapping mode using standard silicon cantilevers, at room temperature, under atmospheric pressure. The AFM images given in the current study are the representative images of about five $3 \times 3 \mu\text{m}^2$ AFM images for each sample which were recorded from random positions on cortical part of bone tissues. $3 \mu\text{m}^2$ scanning area was used to get more accurate information about morphology of the surface and surface defects (Dinc Y., 2007). After scanning the target areas, a phase image and a height image of that area were obtained (Figure 2.11). In AFM height images, the light color represents the higher height as mineral crystals while the dark color represents the lower height as matrix collagens (Bozec et al., 2005). Root mean square (RMS) and arithmetic average height (Ra) which were measured from AFM data, give information about surface roughness of the samples (Gomes et al., 2011).

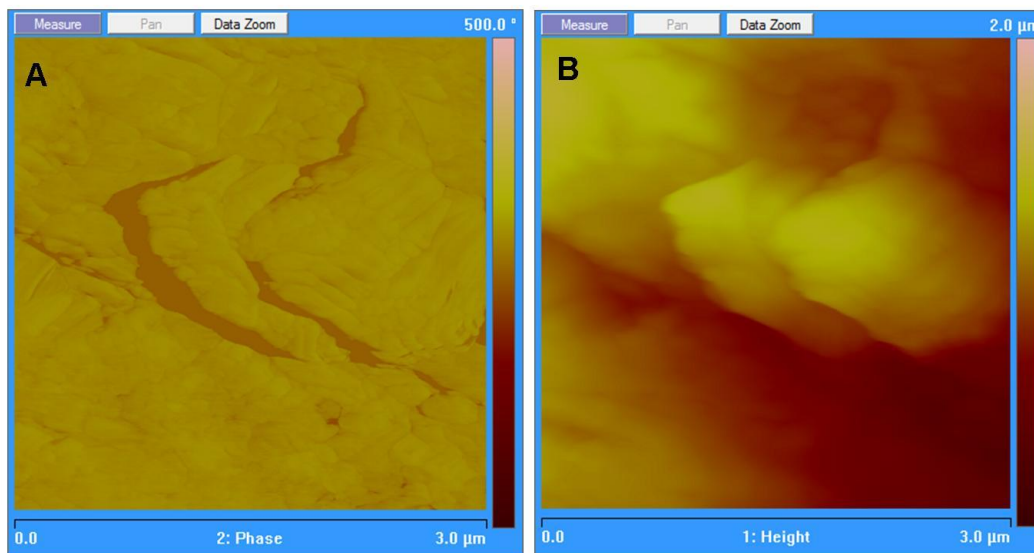


Figure 2.11 Representative phase (A) and height (B) $3 \times 3 \mu\text{m}^2$ AFM images of a bone tissue.

2.1.3.4 Measurement of Serum Parameters

Blood samples were centrifuged at $1000 \times g$ (3000 rpm) for 30 minutes at $+4^\circ\text{C}$, and then the supernatants were immediately frozen at -80°C until assay. Serum calcium levels were measured with Abbot Aeroset autoanalyser using Aeroset kit (Abbot Lab. Abbot Park, IL 60064, USA). Serum osteocalcin, parathormone, C-telopeptide, BAP and 25-hydroxy vitamin D levels were measured with ELISA method using microarray device. OC and PTH levels were measured with DRG ELISA kit (DRG International, Inc. USA), BAP and 25-OH vitamin D levels were measured with IDS ELISA kit (IDS Ltd. Fountain Hills, USA), whereas CTX levels were measured with Uscn ELISA kit (Uscn Life Science Inc. Wuhan). Analyses of all the samples, standards, and controls were run in duplicate. The measurements were carried out according to the directions of the manufacturer.

2.1.3.5 Measurement of CYP Enzymes Protein Levels

2.1.3.5.1 Liver and Kidney Lysate Preparation

Lysates were prepared for the determination of CYP enzyme protein levels in liver and kidneys of healthy, epileptic and drug-treated rats by western blot analysis. The tissue samples were digested in lysis buffer (2,5µl lysis buffer for 1 mg of tissue). Lysates were centrifuged at 14000xg for 10 minutes. Supernatants were kept in -20°C for the experiments.

2.1.3.5.2 Protein Quantification

The amount of protein in liver and kidney was quantified to ensure equal loading in western blot gels. Protein amount was measured by Bradford assay. Briefly, the 5x dye reagent concentrate was diluted 1 in 5 with distilled water. The standard samples were prepared as a 1:250, 1:500, 1:750, and 1:1000 dilution of 2 mg/ml stock solutions of BSA. Samples were prepared by 1:100 diluting the lysates distilled water and then adding 5 µl of diluted lysate sample to 245 µl of 1x protein assay solution in 98-well plates. Both samples and BSA controls were read at absorbance 595 nm and a standard curve was drawn. Protein concentrations in unknown samples were estimated from the linear part of this curve.

2.1.3.5.3 Preparation of Gels

All gels were prepared freshly according to the Laemmli method in which separating and stacking gels were prepared, separately (Laemmli U.K., 1970). Gels were waited at 4°C for two hours before use. The same vertical electrophoresis apparatus (Hoefler Inc., San Francisco, USA) was used for electrophoresis and protein blotting.

Glass plates (8.5 cm) were assembled onto a setting rig with spacers. A 12% separating gel was made first as follows:

- 6.08 ml distilled water
- 3.5 ml Tris (1.5 M pH 8.8)
- 140 μ l SDS (10%)
- 4.2 ml acrylamide:bisacrylamide (40%)
- 70 μ l ammonium persulphate (APS) (10%)
- 7 μ l N,N,N',N'-tetramethylethylenediamine (TEMED)

The tube containing the above 'ingredients' was mixed thoroughly and 7 ml added to the setting rig between the glass plates, covered with 1 ml isopropanol (20%) and left to set for about 45 minutes. Once set, the alcohol was poured off and the 4% stacking gel was prepared as follows:

- 4.44 ml distilled water
- 1.75 ml Tris (0.5 M pH 6.8)
- 70 μ l SDS (10%)
- 700 μ l acrylamide:bisacrylamide (40%)
- 35 μ l APS (10%)
- 7 μ l TEMED.

Again all ingredients were mixed by inversion and then 1-2 ml applied on top of the already set resolving gel and a comb put in. Once the gel was set, it was waited at 4°C for two hours before using for SDS-polyacrylamide gel electrophoresis (PAGE).

2.1.3.5.4 SDS-polyacrylamide Gel Electrophoresis

The 10x running buffer was prepared as follows for 500 mL:

- 15.1 g Tris (25 mM)
- 72 g glycine (192 mM)
- 5 g SDS (0.1%)
- pH 8.56.

1x running buffer was made up to 1 L with 100 ml 10x stock and 900 ml distilled water mixed well. The set gels were placed in the running rig. The comb was taken out and the wells cleaned out to ensure the removal of all acrylamide. 1x running buffer was poured into the rig ensuring the plates were covered.

Approximately 6 µg of samples were run mixed with 6x loading dye. The volume of the sample to be added to the gel to get 6 µg of protein was determined from the protein concentration (See section 2.1.3.5.2). The mixture of sample and 6x loading dye was denatured at 95°C for 6 minutes.

6 µl of prestained broad range protein marker (10-250 kDa) ladder (Thermo Scientific, USA) was added to the first well and samples were added to the other wells. The gel was run in 1x running buffer in a Hoefer miniVE electrophoresis and electrotransfer unit (Hoefer, Inc., San Francisco, USA) at 100 V for the first 30 minutes with a BioRad PowerPac 300 (BioRad Laboratories Ltd., Hemel Hemstead, UK) and then at 150 V until the dye had run to the bottom of the gel (approximately another hour).

2.1.3.5.5 Western Blot Analysis

500 mL of 10x blotting buffer was prepared as follows:

- 15.15g Tris (25 mM)
- 72 g glycine (192 mM)
- pH 8.48.

100 ml 10x blotting buffer was mixed with 200 ml methanol and made up to 1 L with distilled water and kept in +4 °C.

Polyvinylidene difluoride (PVDF) membrane (Roche Applied Sciences, Germany), was waited in methanol for few minutes with shaking. Once the gel had finished running it was removed from the running rig and glass plates. Both the gel and membrane were put in 1x blotting buffer for 10 minutes with shaking. Meanwhile, sponges and watman paper were soaked in 1x blotting buffer. The order of layers in the transfer cassette were arranged as follows:

- black cassette
- sponge
- filter paper
- gel
- nitrocellulose membrane
- filter paper
- sponge
- red cassette

This blot 'sandwich' was slotted into the rig with the black cassette facing the back. Blotting buffer was poured into the electrophoresis rig (Hoefer, Inc., San

Francisco, USA) and proteins were transferred at 100 V for 1 hour in the refrigerator.

After protein transfer was done, membranes were washed with PBS/Tween (0.1%) for 10 minutes for three times. Membranes were blocked with 5% skim milk powder in PBS/Tween for 1 hour with shaking at room temperature. Membranes were further incubated for overnight at 4°C in one of the rabbit antibodies CYP27a1 (1:600) (Abcam, Cambridge, USA), CYP27b1 (1:750) (Santa Cruz, USA) and CYP24 (1:750) (Santa Cruz, USA) in 5 ml 5% skim milk. After being washed three times for 10 minutes in PBS/Tween, membranes were incubated in horse-radish peroxidase-conjugated (HRP) anti-rabbit secondary antibody (1:2000) for 1 hour with shaking. Membranes were then washed three times as before. Actin (1:1000) (Santa Cruz, USA) served as a loading control for each blot. Immuno-reactivity was visualized with the Enhanced chemiluminescent (ECL) reagents (Pierce). Under red light, 1 piece of film (Medical X-ray film, Kodak USA) was exposed to the membrane for 30 seconds. The film images were scanned to obtain a digital image and protein amounts in samples were determined by using Image J analysis software.

2.1.3.6 Statistical Analysis

Mean values and standard deviation were calculated for each parameter in all animals and the data shown as the mean and standard deviations for each animal group. Statistical analysis was performed by using the SPSS for windows (version 13.0) statistical package (SPSS Inc., Chicago, IL, USA). After testing data for normal distribution and homogeneity of the variance, the FTIRM and AFM results and micro- and nano-hardness values for each group were compared with the one-way ANOVA with a Bonferroni post-hoc test to highlight significant differences between the groups. Comparisons of serum parameters between the different

animal groups were made by one-way ANOVA with Tukey's post-hoc test to estimate statistical differences between specific groups. The values were expressed as mean \pm standard deviation (SD). The p values less than or equal to 0.05 were considered as statistically significant (*⁺ $p \leq 0,05$; **⁺⁺ $p \leq 0,01$; ***⁺⁺⁺ $p \leq 0,001$).

2.2. Study 2: Simvastatin Study

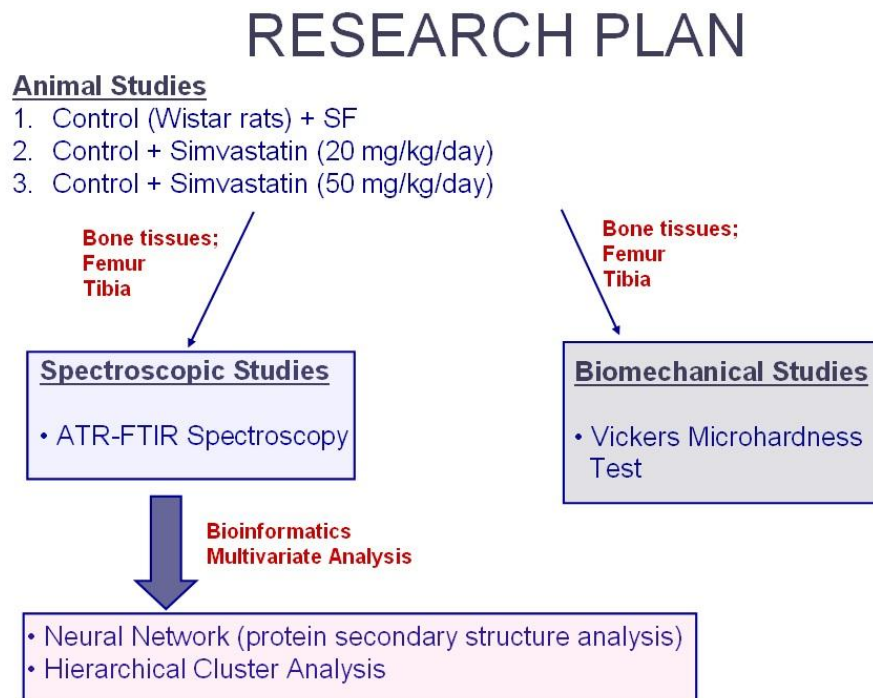


Figure 2.12 A summary of experiments carried out in the second study.

2.2.1 Chemicals

The list of used chemicals and their suppliers are given in Appendix A.

2.2.2 Animal Studies

Adult male Wistar rats (12-14 weeks) weighing 250-300g were taken from Experimental Animal Center, Hacettepe University, Ankara. Approval for the

study was obtained from the Animal Ethical Committee of Hacettepe University. A standard diet was given to rats and they were kept in 12 hours /12 hours, dark & light, controlled temperature and humidity (40-50%) with a controlled ventilation.

The rats were randomly separated as;

Group 1: Wistar healthy control + Physiological serum (n=10)

Group 2: Wistar control + simvastatin (20 mg/kg/day) (n=10)

Group 3: Wistar control + simvastatin (50 mg/kg/day) (n=10)

Simvastatin, dissolved in physiologic saline (20mg/kg or 50 mg/kg), were given to the simvastatin treatment groups daily through gavage feeding for 30 days. The rats in the three groups were then decapitated and the tibia bone tissues were taken and cleared from soft tissues, then frozen at -80°C for ATR-FTIR studies.

2.2.3 Attenuated Total Reflectance (ATR-FTIR) Spectroscopy Study

2.2.3.1 Sample Preparation

In ATR-FTIR spectroscopy measurements, tibia and femur bone powders were used. After the removal of soft tissues from bones, the cortices of bone samples first were ground in liquid nitrogen in a colloid mill (Retsch MM200) to get powdered tissue and then bone powder placed on the ATR crystal of the FTIR spectrometer.

2.2.3.2 Data Acquisition and Spectroscopic Measurements

Homogenous powdered bone samples were scanned by Spectrum 100 FTIR spectrometer (Perkin-Elmer Inc., Norwalk, CT, USA) with ATR unit to get infrared spectra between 4000-650 cm^{-1} wavenumber region. 100 scans at 4 cm^{-1}

resolution were recorded. The spectrum of air was recorded as a background and subtracted automatically by the software. Figure 2.13 shows the infrared spectrum of air. Spectrum One Software (Perkin Elmer Inc., Norwalk, CT, USA) was used to record and analyze spectral data.

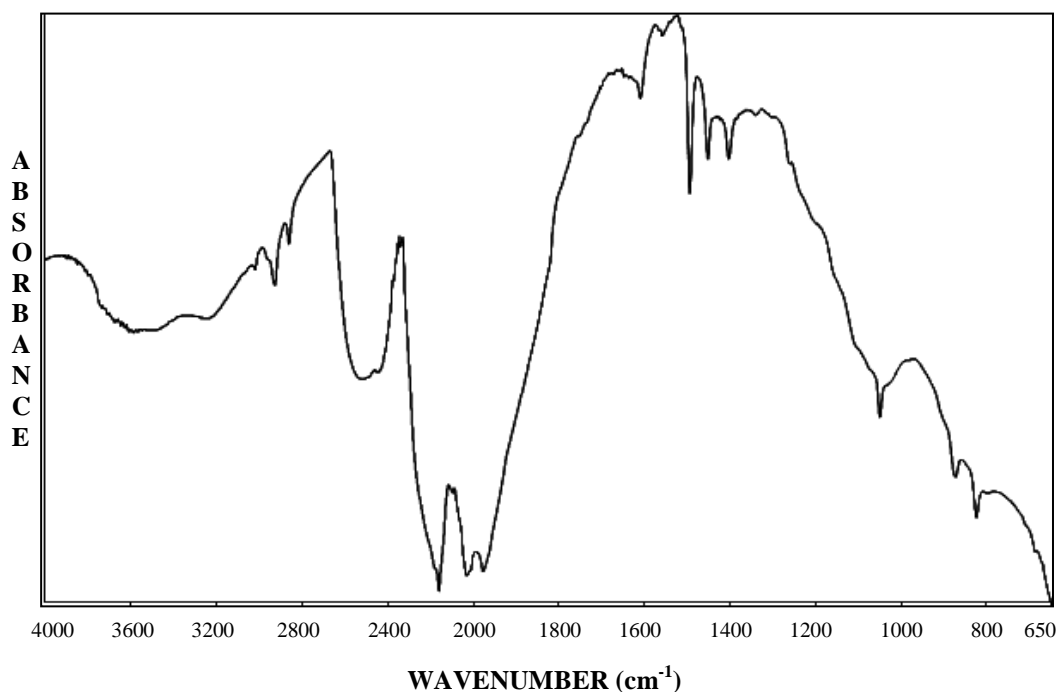


Figure 2.13 Infrared spectrum of air.

Before the spectral analysis are performed, according to the requirements of analysis technique, some preprocessing steps are applied to the spectral data sets to make the spectra comparable. By these preprocessing approaches the number of variables can either be reduced to prevent overfitting. Baseline correction, which is mainly used to get rid of a sloping and curving baseline, is a wavelength-dependent intercept and unique for each sample spectrum (Franke, 2006). For the data analysis in detail and evaluation of the alterations in band area values, original

base-line corrected spectrum was used, while the band positions (frequency values) were measured according to the center of weight of the bands from raw spectral data. All these mentioned quantitative analysis were performed on non-normalized but pre-processed average spectra. However, by the purpose of visual presentation of the differences, the average spectra of sampling groups were normalized with respect to the specific bands and information about the intensity of the spectrum is completely eliminated (Kramer, 1998).

In the ν_1 , ν_3 phosphate (1200-900 cm^{-1}) and ν_2 carbonate (890-850 cm^{-1}) region curve fitting analysis was performed to get information about the alterations in the crystallinity of the hydroxyapatite phase and the carbonate substitution, respectively in bone tissues. GRAMS/32 (Galactic Industries Corporation, Salem, NH, USA) software was used for curve-fitting analysis. Sub-bands were determined by taking the second derivative analysis. The iterations were re-performed until the correlation was lower than 0.995 (Garip et al., 2010). Then the ratio of the areas of the interested bands were calculated to get information about crystallinity and carbonate substitution.

Amide I band between 1700 and 1600 cm^{-1} resulted from proteins was evaluated for the analysis of secondary structure of proteins. For the determination of simvastatin-induced protein secondary structure variations, two methods; vector normalization and neural network analysis were used. For vector normalization method, intensity calculations from second derivative spectra using the amide I band were performed. For this procedure, OPUS software (Bruker Optics, Reinstetten, Germany) was used. First the second derivative of the spectra was taken by using Savitzky–Golay algorithm with 9 smooth points. Then second derivatives were vector normalized between 1700-1600 cm^{-1} wavenumber region. The intensities of the bands were calculated after that (Toyran et al., 2006; Ozek et al., 2009).

2.2.3.2.1 Neural Network (NN) Analysis

The neural networks were first trained using a data set, which contains FTIR spectra of 18 water soluble proteins recorded in water applying the method described in reference (Severcan, Severcan and Haris, 2004). The secondary structures of these proteins were known from X-ray crystallographic analysis. Amide I band was preprocessed before applying to the neural networks. Preprocessing involves normalization and discrete cosine transformation (DCT) of this band. Interpolation of the available FTIR spectra was done to increase the size of the data set resulted in improving the training of NNs. Bayesian regularization was used for neural network training. The trained neural networks have standard error of prediction values which were 4.19 % for α -helix, 3.49 % for β -sheet and 3.15 % for turns. The training and testing algorithms were explained in detail in Severcan and Haris, 2004.

2.2.3.2.2 Cluster Analysis

For the comparison of control and simvastatin-treated groups, hierarchical cluster analysis were performed with using 9 smooth points and Savitzky-Golay algorithm. It was performed to determine spectral differences among control and treated groups using frequency range between 3030-2800 cm^{-1} and 1800-450 cm^{-1} . The spectra were first vector normalized over the investigated frequency range and then Ward's algorithm was used to obtain dendograms by OPUS 5.5 (Bruker Optic, GmbH). Spectral distance was calculated between pairs of spectra as Pearson's product moment correlation coefficient. Cluster analysis offers the opportunity to evaluate experimental results and differentiate between control and treated samples without any training of the spectral data. The result of the analysis are represented in the form a dendrogram. The change in variances between the spectra of samples is represented by heterogeneity values. Higher variations

between groups are represented by higher heterogeneity values. Calculations and algorithms were explained in detail in Severcan et al., 2010.

2.2.3 Vickers Microhardness Study

After soft tissues were removed from bones, longitudinal-sections were cut from distal femur and proximal tibia. Then the bone tissues were embedded to epoxy (Claritine Epoxy Powder & Liquid). After embedded tissues were waited for 20 minutes at room temperature, bone-embedded epoxy blocks were trimmed with flat silicone carbide sanding 400, 600, 800 and 1200-grit discs respectively and then polished.

The microhardness of the tibia and femur bone samples were determined as described detailly in Section 2.1.3.2.1 in "Materials and Methods" part of the thesis. A diamond indenter was used with a load of 25 g for 10 seconds on the surfaces of the blocks (Boivin et al., 2008). 15 measurements were applied on each sample (5 in the cortical, 5 in the trabecular bone and 5 in the growth plate).

2.2.4 Statistical Analysis

Statistical analysis was performed by using the SPSS for windows (version 13.0) statistical package (SPSS Inc., Chicago, IL, USA). The results were expressed as mean \pm standard deviation (SD). Spectroscopic and microhardness data were analyzed statistically by using Mann–Whitney U test and the p values less than or equal to 0.05 were considered as statistically significant (* $p \leq 0.05$; ** $p \leq 0.01$; *** $p \leq 0.001$).

CHAPTER 3

RESULTS

In the first study of the thesis, the effects of anti-epileptic drug; Carbamazepine on bone tissues of epileptic and healthy rats were investigated. The effects of epileptic seizures on bones of epileptic rats were also studied in this part. In the second study of the thesis, to see the effect of other kind of drug on bone tissues, the dose-dependent effects of widely used cholesterol reducing agent, Simvastatin, on bone tissues of healthy rats were investigated.

3.1. Study 1: Carbamazepine Study

First study of the thesis is addressed to investigate the possible side-effects of Carbamazepine and epileptic seizures on bone tissues of genetically epileptic and healthy rats and clarify the mechanism of action of the drug and seizures on bone and vitamin D metabolism by FTIR and SR-FTIR microspectroscopy, AFM, micro- and nano-hardness tests, ELISA and western blot analysis. The comparison of epileptic rats (WAG/Rij) with control healthy rats (Wistar) gives information about the effects of epileptic seizures alone. The comparison of epileptic rats (WAG/Rij) with control healthy rats (Wistar) gives information about the effects of epileptic seizures alone. Comparison of the epileptic rats treated with carbamazepine with the non-treated epileptic group, gives information about the effects of carbamazepine alone on epileptic bones. Moreover, comparison of the carbamazepine administered to healthy rats with

non-treated healthy control rats gives information about the effects of the drug in a non-diseased state.

3.1.1 FTIR Microspectroscopy Studies

The averaged infrared spectra of the spine tissues of healthy control, epileptic and drug-treated rat groups in 1800-800 cm^{-1} region, is shown in Figure 3.1. The wavenumber (frequency) values of the bands at peak positions were used to assign the bands. The main bands are labelled in the figure and specific assignments of these spectral bands for bones are listed in Table 3.1.

Table 3.1 General band assignment of a bone tissue between 1800-800 cm^{-1} wavenumber region.

Wavenumber (cm^{-1})	Definition of the spectral assignments
1720-1590	Amide I: C=O stretching vibrations of proteins (matrix)
3065	Amide II: N-H bending and C-N stretching vibrations of proteins (matrix)
1200-900	$\nu_1, \nu_3 \text{ PO}_4^{-3}$: symmetric and antisymmetric stretching vibrations of phosphate (mineral)
890-850	$\nu_2 \text{ CO}_2^{-3}$: bending vibration of carbonate (mineral)

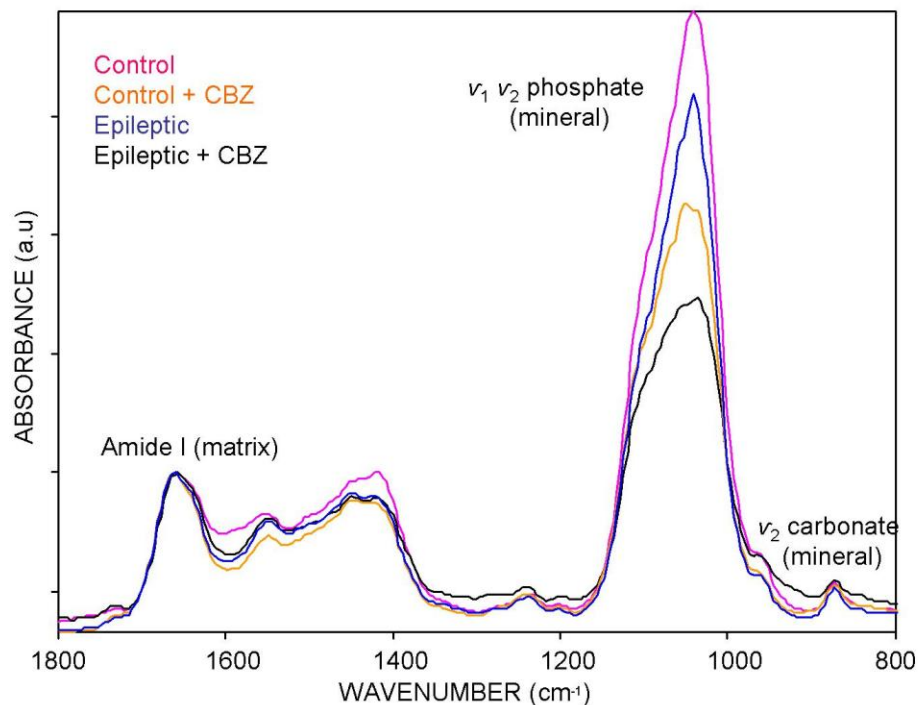


Figure 3.1 The averaged spectra of control (pink), epileptic (blue) and their drud-treated groups (orange and black, respectively) in 1800-800 cm^{-1} region (Amide I band was used for the normalization process).

The band areas reflect the concentration of the related molecules (Freifelder, 1982; Garip et al., 2010a; Aksoy, 2012). IR band areas, intensity ratios, and area ratios were calculated to determine parameters such as mineral/matrix ratio, carbonate/phosphate ratio, crystallinity, and collagen-crosslinks ratio. The FTIRM parameter results were expressed as representative color-coded images for each parameter and histograms which describe the pixel distribution, mean values and standard deviations of these parameters. Each parameter value was calculated from 21 different maps for each animal group and the mean values of these calculated parameters were given in tables, while one of the 21 maps was given as representative image for that parameter. Pixel histograms show the average value

and heterogeneity of each of the measured parameter. As the parameter values decrease, the pixel distribution in the histograms of these parameters slide to the left side. Moreover, differences in the uniformity (narrowing of the bands) of the pixel distributions in histograms show a lower heterogeneity of the calculated parameters in the tissues. All bone tissues were investigated in three parts; cortical, trabecular and growth plate.

3.1.1.1 The Effects of Carbamazepine and Epileptic Seizures on Bone Mineral

3.1.1.1.1 Mineral Content

As seen from the Figure 3.1, there was a decrease in the total area of ν_{1,ν_3} phosphate band at $1200-900\text{ cm}^{-1}$ and a change in the ν_{1,ν_3} phosphate band contour between groups. The decrease in phosphate in epileptic and carbamazepine-treated groups is visible from the band area of ν_{1,ν_3} phosphate band in all parts of the spine bone tissues (Figure 3.2).

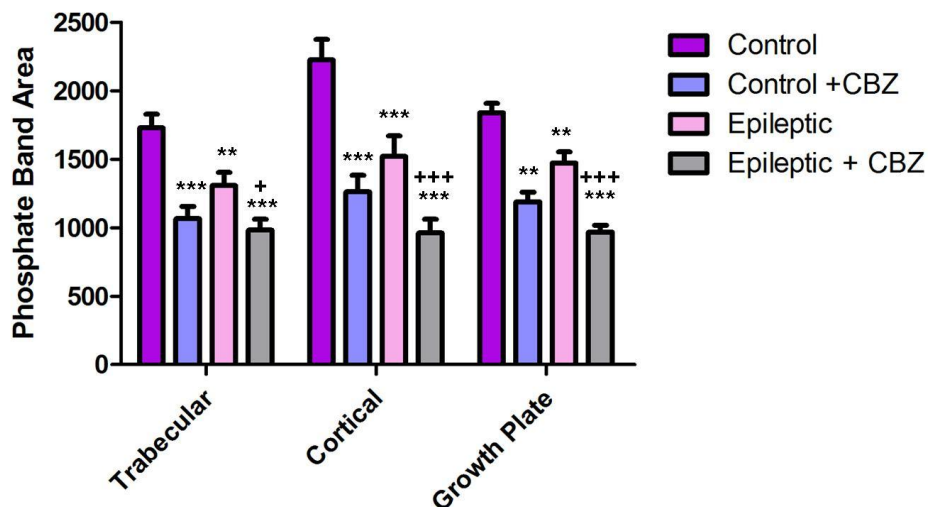


Figure 3.2 The averaged band area of ν_1, ν_3 phosphate at $1200-900\text{ cm}^{-1}$ of control, epileptic and drug-treated groups. (*) represents the significancy compared to control group and (+) represents the significancy compared to epileptic group (*⁺ $p \leq 0.05$; **⁺ $p \leq 0.01$; ***⁺ $p \leq 0.001$).

The mineralization level can be determined by taking the ratio of the ν_1, ν_3 phosphate band ($1200-900\text{ cm}^{-1}$) area to the Amide I ($1720-1590\text{ cm}^{-1}$) band area which is called mineral-to-matrix ratio (Boyar et al., 2004; Gourion-Arsiquaud et al., 2012). Representative images for mineral-to-matrix ratio and typical pixel histograms of respective images for spine, tibia and femur bone tissues are presented in Figure 3.3; Figure 3.4 and Figure 3.5, respectively. Mineral/matrix ratio is related to chemically determined mineral content (ash weight) (Boskey and Mendelsohn, 2005). It was visually apparent from the Figure 3.3 that the mineral-to-matrix ratio (ν_1, ν_3 phosphate / Amide I) was significantly decreased in both epileptic and carbamazepine-treated groups compared to the healthy control in the

cortical parts of spine bone tissues (Table 3.2). This significant decrease in mineral-to-matrix ratio was also shown in the trabecular and growth plate parts of the spines (Figure 3.3 and Table 3.2). This decrease was also seen from the pixel distributions of mineral-to-matrix parameter in the histograms which were slided to the left side when compared with the control groups (Figure 3.3).

Table 3.2 Calculated mineral/matrix parameter in cortical, trabecular and growth plate parts of bone tissues for control (n=7), control + CBZ (n=7), epileptic (n=7) and epileptic + CBZ groups. (*) represents the significancy compared to control group and (+) represents the significancy compared to epileptic group.

	BONE PART	CONTROL	CONTROL + CBZ	EPILEPTIC	EPILEPTIC + CBZ
Spine	Cortical	7.7 ± 0.5	5.6 ± 0.4**	5.2 ± 0.3**	3.8 ± 0.4*** +++
	Trabecular	6.5 ± 0.3	5.0 ± 0.5**	4.0 ± 0.5**	3.1 ± 0.7*** +
	Growth Plate	7.5 ± 0.2	6.2 ± 0.5**	4.9 ± 0.2***	3.4 ± 0.8*** +
Tibia	Cortical	10.0 ± 0.7	8.3 ± 0.5**	8.0 ± 0.4**	6.0 ± 0.4*** ++
	Trabecular	9.0 ± 0.5	6.5 ± 1.0**	8.0 ± 0.5	4.1 ± 1.2*** +++
	Growth Plate	8.9 ± 0.5	4.5 ± 1.0	8.7 ± 0.5	4.3 ± 0.8*** +++
Femur	Cortical	6.3 ± 0.3	5.2 ± 0.2*	4.9 ± 0.2*	4.0 ± 0.1** +
	Trabecular	6.8 ± 0.2	5.5 ± 0.3	4.5 ± 0.1	3.9 ± 0.2*** +

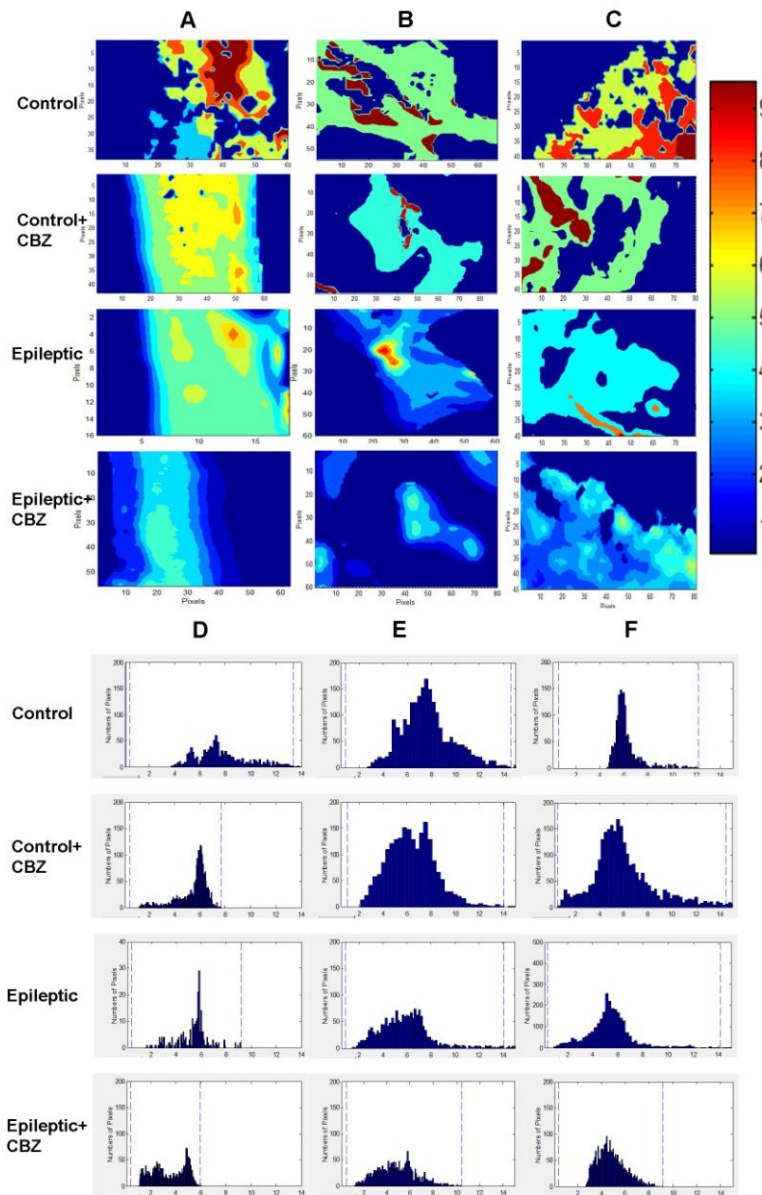


Figure 3.3 Typical FTIR images of mineral/matrix ratios in cortical (A), trabecular (B) and growth plate (C) sites of spine bone for control, epileptic and drug-treated groups. The scales of each parameter are represented by color bars. Axes are in pixels (one pixel is $6.5 \mu\text{m}$). The pixel histograms for these images are shown in (D) cortical, (E) trabecular and (F) growth plate.

In the tibia tissues, the significant decreases occurred in epileptic and drug-treated groups compared to control as in the spine tissues (Figure 3.4 and Table 3.2). In the tibia, this parameter significantly decreased in carbamazepine-treated groups for all bone parts, while significant variations were obtained only in the cortical bone of the epileptic group. The significant decrease in mineral content in cortical bone but not significant in trabecular and growth plate bone, shows a higher variation in spatial distribution of trabecular and growth plate mineral content (Boskey et al., 2009a). This variation was also seen from the histograms in which the pixel distributions were more broad implying an increased heterogeneity of mineral content in these bone parts.

Representative FTIRM images of femur bone and typical histograms of respective images for mineral/matrix ratio were shown in Figure 3.5. Although the variations of the measured parameters were parallel in both femur parts, they were much more significant in the cortical part than the trabecular part of the tissue. Mineral to matrix ratio significantly decreased in both epileptic and carbamazepine-treated groups (Table 3.2).

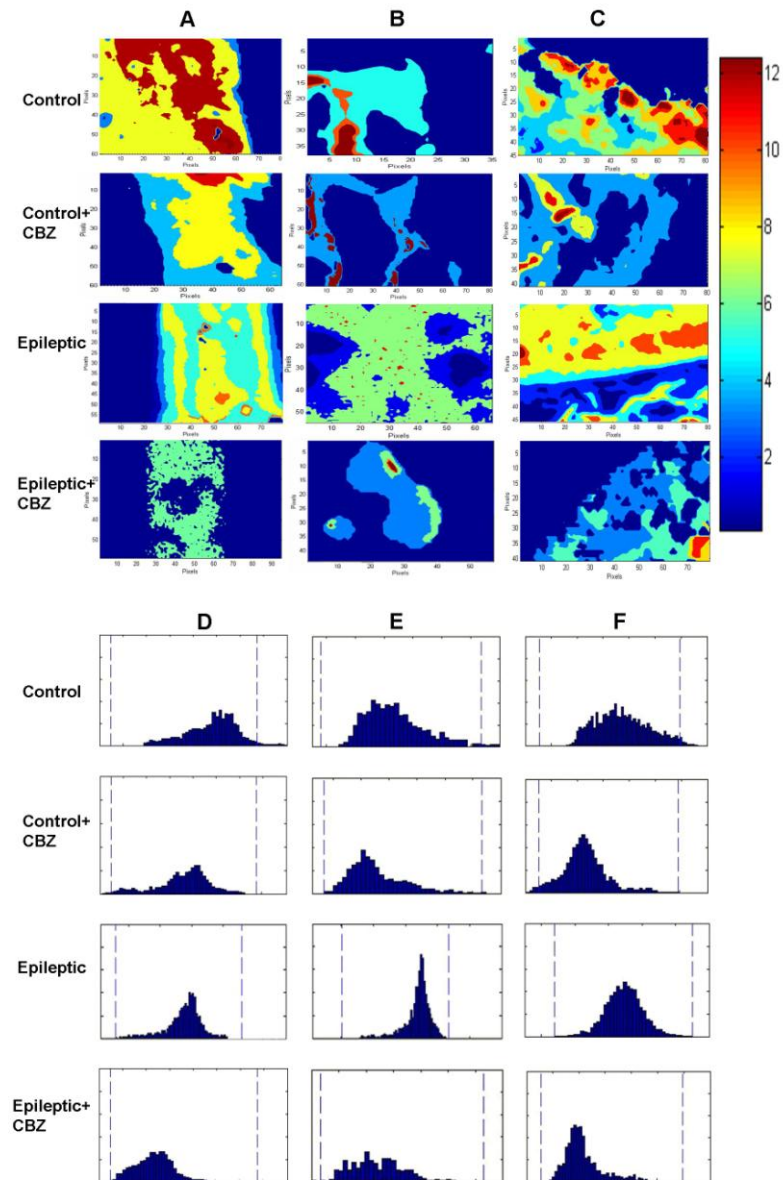


Figure 3.4 Typical FTIR images of mineral/matrix ratios in cortical (A), trabecular (B) and growth plate (C) sites of tibia bone for control, epileptic and drug-treated groups. The scales of each parameter are represented by color bars. The pixel histograms for these images are shown in (D) cortical, (E) trabecular and (F) growth plate.

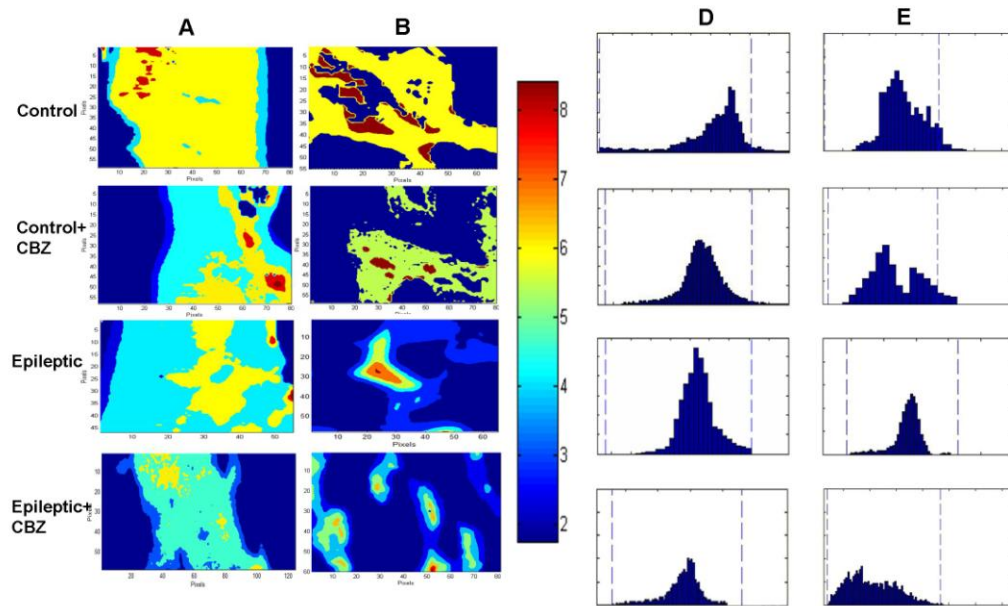


Figure 3.5 Typical FTIR images of mineral/matrix ratios in cortical (**A**) and trabecular (**B**) sites of femur bone for control, epileptic and drug-treated groups. The scales of each parameter are represented by color bars. The pixel histograms for these images are shown in (**D**) cortical, and (**E**) trabecular.

As a summary, mineral content was found to be decreased in epileptic group compared to the healthy control. This change in mineral content was due to the effect of epilepsy and epileptic seizures alone. The mineral content of drug-treated bones, especially drug-treated epileptic bones, were also found to be decreased. In fact drug administration decreased mineral content of bones more severely than epileptic seizures.

3.1.1.1.2 Carbonate Substitution

Another calculated parameter is carbonate/phosphate ratio which was obtained by taking the ratio of the integrated areas of carbonate (890-850 cm^{-1}) to ν_1, ν_3 phosphate (1200-900 cm^{-1}) band. This parameter is related to the chemically determined extent of carbonate substitution for phosphate or hydroxide in the mineral crystals (Krushinski et al., 1974; Calton et al., 2012). Carbonate/phosphate band area ratio was significantly decreased compared to healthy control in all parts of spine tissues of epileptic group (Figure 3.6 and Table 3.3). As seen from the figure and table, there was a significant decrease in this ratio in all parts of spine tissues of carbamazepine-treated groups relative to the epileptic and healthy control group. The calculated band areas of carbonate band at 890-850 cm^{-1} also supported this result by a decrease in carbonate band area in epileptic and carbamazepine-treated groups (Figure 3.7). The decrease in relative carbonate value was also seen from the pixel distributions in the histograms which were slided to the left side of the histogram.

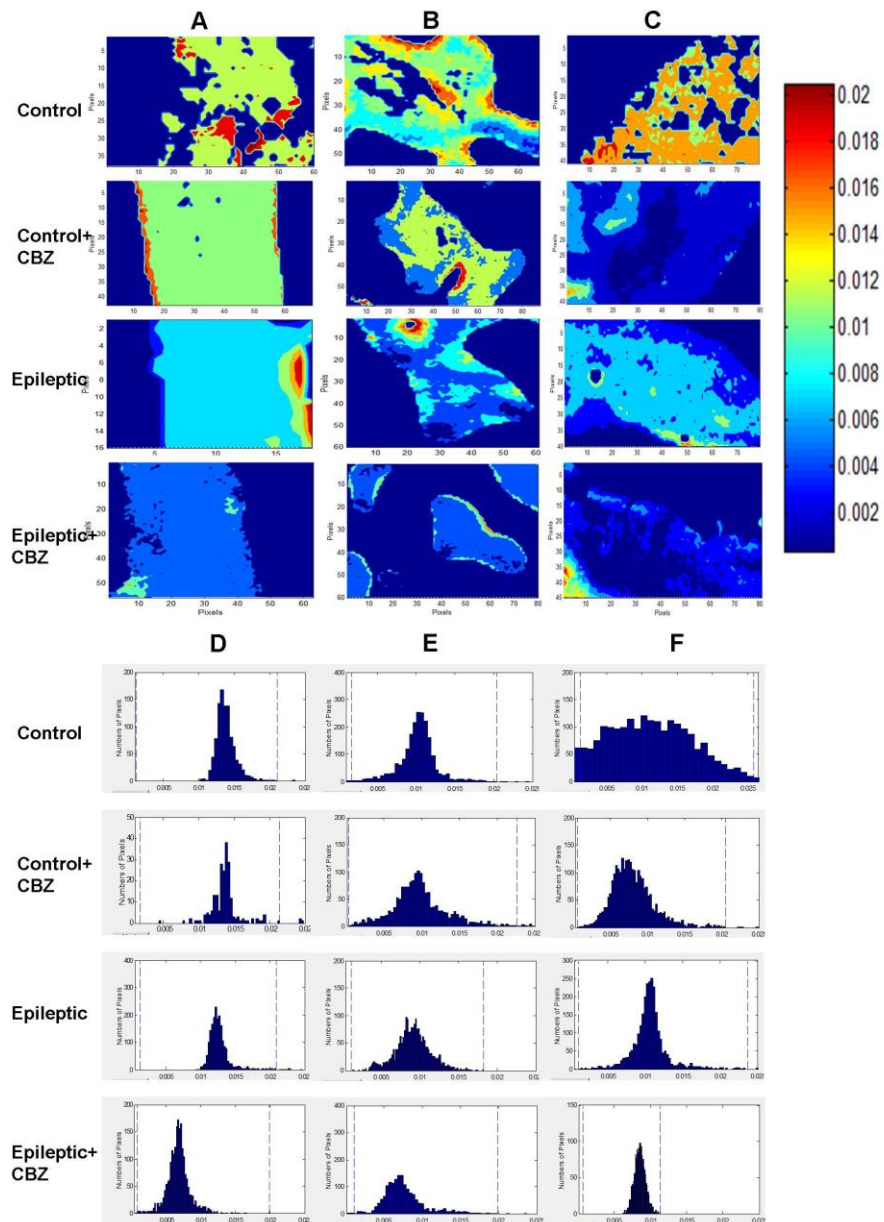


Figure 3.6 Typical FTIR images of carbonate/phosphate ratios in cortical (A), trabecular (B) and growth plate (C) sites of spine bone for control, epileptic and drug-treated groups. The scales of each parameter are represented by color bars. The pixel histograms for these images are shown in (D) cortical, (E) trabecular and (F) growth plate.

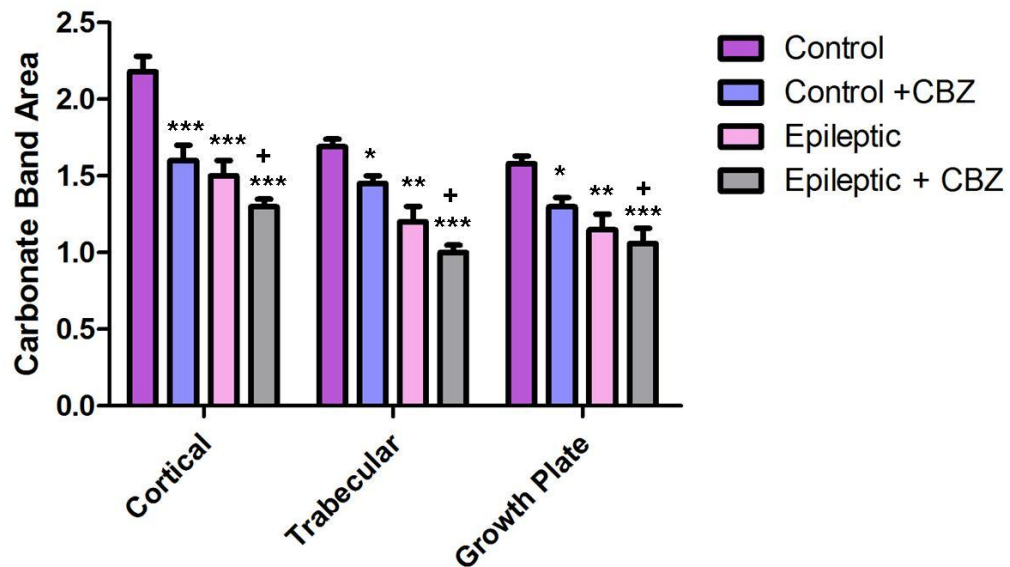


Figure 3.7 The averaged band area of ν_2 carbonate at $890\text{-}850\text{ cm}^{-1}$ in spine tissue control, epileptic and drug-treated groups. (*) represents the significance compared to control group and (+) represents the significance compared to epileptic group (*,+ $p \leq 0.05$; **,++ $p \leq 0.01$; ***,+++ $p \leq 0.001$).

In tibia bone tissues, there was a significant decrease in carbonate/phosphate ratio in all parts of carbamazepine-treated groups relative to the epileptic and healthy control groups. As can be seen from Table 3.3, this ratio was also significantly decreased relative to healthy control in cortical and growth plate of epileptic group of the tibia (Figure 3.8). However there was no significant change in trabecular of the epileptic group compared to the healthy group. The degree of the effect of the drug on bone tissue which was more severe than the effect of the epileptic seizures, could also be seen from the pixel distributions in the histograms of these groups. The pixel distributions were slid more to the left side (more decreased

parameter value) in drug-treated groups than the epileptic group compared to the control.

In femur bones, this parameter was significantly decreased for both epileptic and drug-treated groups in cortical and trabecular part compared to the epileptic and healthy control groups (Figure 3.9 and Table 3.3).

Table 3.3 Calculated carbonate/mineral parameter in cortical, trabecular and growth plate parts of bone tissues for control (n=7), control + CBZ (n=7), epileptic (n=7) and epileptic + CBZ groups. (*) represents the significancy compared to control group and (+) represents the significancy compared to epileptic group.

	BONE PART	CONTROL	CONTROL + CBZ	EPILEPTIC	EPILEPTIC + CBZ
Spine	Cortical	0.014 ± 0.000	0.012 ± 0.000*	0.010 ± 0.000**	0.007 ± 0.000*** +++
	Trabecular	0.015 ± 0.000	0.013 ± 0.000*	0.009 ± 0.000**	0.007 ± 0.000*** +
	Growth Plate	0.016 ± 0.000	0.007 ± 0.000***	0.009 ± 0.000***	0.07 ± 0.000*** +
Tibia	Cortical	0.021 ± 0.000	0.019 ± 0.000*	0.018 ± 0.000**	0.013 ± 0.000*** ++
	Trabecular	0.020 ± 0.000	0.012 ± 0.000***	0.020 ± 0.000	0.018 ± 0.000* +
	Growth Plate	0.018 ± 0.000	0.015 ± 0.000**	0.016 ± 0.000*	0.014 ± 0.000** +
Femur	Cortical	0.014 ± 0.000	0.013 ± 0.000*	0.012 ± 0.000*	0.010 ± 0.000** +
	Trabecular	0.015 ± 0.000	0.014 ± 0.000*	0.013 ± 0.000*	0.011 ± 0.000** +

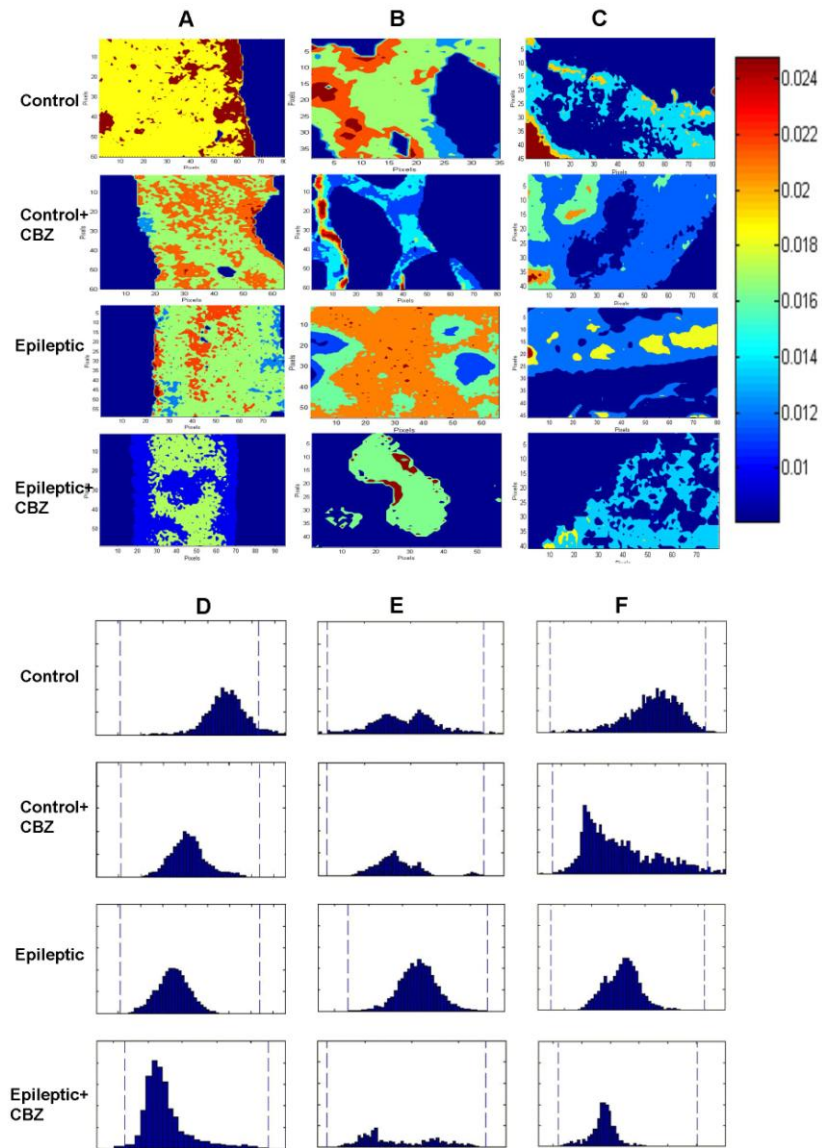


Figure 3.8 Typical FTIR images of carbonate/phosphate ratios in cortical (A), trabecular (B) and growth plate (C) sites of tibia bone for control, epileptic and drug-treated groups. The scales of each parameter are represented by color bars. The pixel histograms for these images are shown in (D) cortical, (E) trabecular and (F) growth plate.

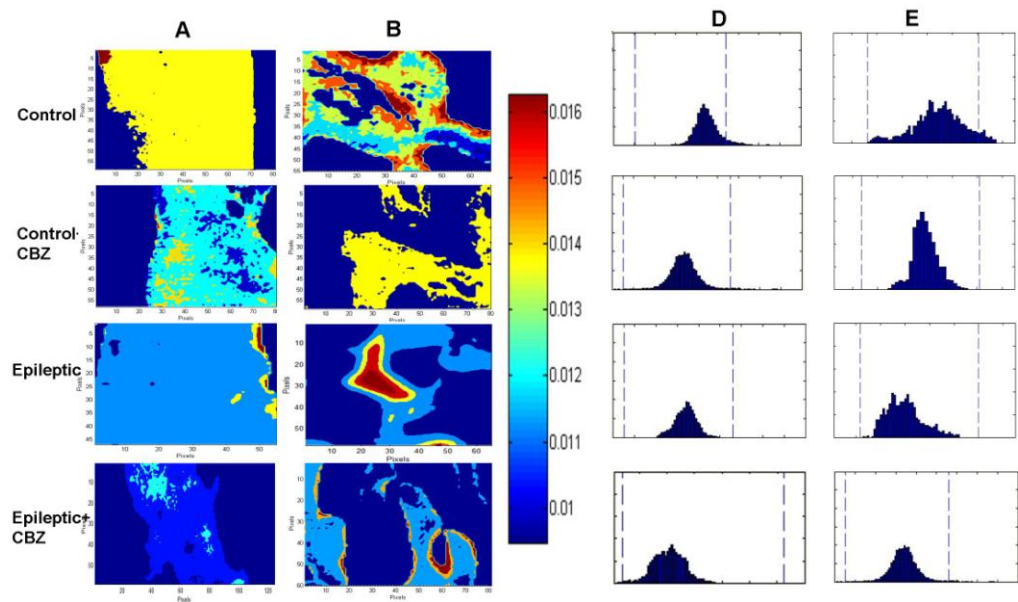


Figure 3.9 Typical FTIR images of carbonate/phosphate ratios in cortical (**A**) and trabecular (**B**) sites of femur bone for control, epileptic and drug-treated groups. The scales of each parameter are represented by color bars. The pixel histograms for these images are shown in (**D**) cortical and (**E**) trabecular.

While there is a decrease in phosphate content in hydroxyapatite crystals, it is expected that the carbonate content which substitutes for phosphate or hydroxide in the mineral crystals would increase. However, in current results according to the carbonate/phosphate ratio and carbonate band area, there was a decrease in carbonate content. This controversial finding about carbonate content was further studied by determining its substitutions in bones. In the ν_2 CO_3^{2-} region ($890\text{-}850\text{ cm}^{-1}$) curve-fitting analysis was performed to get information about alterations in the relative ratios of different carbonate types in hydroxyapatites. There were 3 sub-bands in this region. A band at 866 cm^{-1} is assigned to labile (L type)

carbonate, and two bands at 872 cm^{-1} and 878 cm^{-1} are assigned to type B and type A carbonates, respectively (Huang et al., 2003). In bone tissues, carbonate substitutes for the hydroxyl group called A type carbonate and/or the phosphate group called B type carbonate, or it exists on the surface of the bone apatite crystals called labile- L type carbonate (Jerome et al., 1997; Camacho et al., 1999; Huang et al., 2003). To monitor the alterations in these 3 types of carbonate, we estimated the ratio of the intensity of each component to the intensity of Amide I band (Table 3.4). In all three bone tissues, B type carbonate which substitutes for phosphate group in the crystals, significantly increased in epileptic and carbamazepine-treated groups (Table 3.4). Since the B type carbonate which substitutes for phosphate in the mineral crystals, increased, while the A type and L type carbonate significantly decreased in all groups relative to the control group, this may be the explanation for the decrease in total carbonate content in the bones.

Table 3.4 A-type, B-type and labile (L. type) carbonate ratios calculated by taking carbonate/Amide I intensity ratio in cortical, trabecular and growth plate parts of bone tissues for control (n=7), control + CBZ (n=7), epileptic (n=7) and epileptic + CBZ groups. (*) represents the significance compared to control group and (+) represents the significance compared to epileptic group.

	BONE PART	CARBONATE TYPE	CONTROL	CONTROL+ CBZ	EPILEPTIC	EPILEPTIC+CBZ
Spine	Cortical	A Type	2.54 ± 0.04	2.40 ± 0.04**	2.45 ± 0.03*	2.33 ± 0.01** +
		B Type	2.51 ± 0.02	2.58 ± 0.01**	2.56 ± 0.01*	2.60 ± 0.03*+
		L Type	2.88 ± 0.03	2.85 ± 0.03	2.86 ± 0.02	2.80 ± 0.02*+
	Trabecular	A Type	3.33 ± 0.02	3.28 ± 0.02*	3.30 ± 0.02	3.20 ± 0.04***+
		B Type	3.30 ± 0.03	3.35 ± 0.03	3.34 ± 0.01	3.42 ± 0.03***++
		L Type	3.48 ± 0.04	3.40 ± 0.02*	3.45 ± 0.02	3.33 ± 0.04***++
Tibia	Growth Plate	A Type	3.46 ± 0.02	3.35 ± 0.03**	3.40 ± 0.03*	3.29 ± 0.1***++
		B Type	3.53 ± 0.01	3.63 ± 0.02**	3.60 ± 0.04*	3.71 ± 0.04***+
		L Type	0.87 ± 0.03	0.70 ± 0.05***	0.75 ± 0.05*	0.65 ± 0.03***+
	Cortical	A Type	3.23 ± 0.04	3.19 ± 0.02	3.20 ± 0.02	3.15 ± 0.02*+
		B Type	3.22 ± 0.03	3.30 ± 0.01**	3.28 ± 0.01*	3.40 ± 0.03***++
		L Type	3.88 ± 0.02	3.72 ± 0.05**	3.76 ± 0.03*	3.65 ± 0.01***++
Femur	Trabecular	A Type	3.73 ± 0.04	3.60 ± 0.03**	3.65 ± 0.02*	3.51 ± 0.04***++
		B Type	3.78 ± 0.04	3.83 ± 0.03	3.70 ± 0.04	3.90 ± 0.01*++
		L Type	4.25 ± 0.02	4.19 ± 0.01*	4.23 ± 0.01	3.90 ± 0.1***++
	Growth Plate	A Type	2.68 ± 0.03	2.60 ± 0.03*	2.65 ± 0.03	2.51 ± 0.04***++
		B Type	2.66 ± 0.03	2.70 ± 0.03	2.70 ± 0.04	2.83 ± 0.03***+
		L Type	2.85 ± 0.04	2.81 ± 0.04	2.84 ± 0.04	2.70 ± 0.03***++
Cortical	A Type	2.89 ± 0.02	2.80 ± 0.03*	2.84 ± 0.03	2.81 ± 0.02*	
	B Type	2.83 ± 0.02	2.93 ± 0.02**	2.90 ± 0.02*	3.01 ± 0.02***++	
	L Type	3.17 ± 0.05	3.00 ± 0.07**	3.07 ± 0.03*	2.91 ± 0.2***++	
Trabecular	A Type	2.63 ± 0.03	2.62 ± 0.02	2.62 ± 0.02	2.52 ± 0.03*+	
	B Type	2.56 ± 0.02	2.58 ± 0.01	2.59 ± 0.01	2.63 ± 0.02*+	
	L Type	2.72 ± 0.01	2.70 ± 0.03	2.71 ± 0.02	2.36 ± 0.01***++	

As a summary, although total carbonate content was found to be decreased, B-type carbonate content which substitutes for phosphate groups in the mineral part of bone, was shown to be increased in both epileptic and drug-treated groups compared to the control in all bone tissues.

3.1.1.1.3 Crystallinity

Mineral crystallinity gives the information about the crystallite size and perfection as measured by X-ray diffraction, and was estimated by taking the intensity ratios of subbands at 1030 (stoichiometric apatite) and 1020 cm^{-1} (nonstoichiometric apatite) (Boskey et al., 2005; Severcan et al., 2008; Garip et al., 2010a; Gourion-Arsiquaud et al., 2012). This parameter significantly increased in all different parts of spine tissue for carbamazepine-treated groups compared to the epileptic and healthy control, while the crystallinity ratio increased significantly only for cortical and growth plate in the epileptic group relative to the healthy control group (Figure 3.10 and Table 3.4). The pixel distribution of the crystallinity parameter in the drug-treated groups was skewed to the right, showing the presence of relatively more large crystals than smaller ones (Figure 3.10).

For tibia tissues, significantly increased crystallinity value was observed for both epileptic and carbamazepine-treated groups in all parts of tibia (Figure 3.12, Table 3.5). In the pixel distributions of the trabecular bone of the tibia tissues, all groups had bimodal peaks indicating a heterogeneity in crystal size/perfection while the pixel histograms of the FTIR images in cortical and growth plate bone showed a more uniform distribution of crystallinity in all groups (Faibish et al., 2006).

In femur tissues, this ratio was significantly increased for epileptic and carbamazepin-treated groups in cortical bone while a slight increase was observed for these groups in trabecular bone (Figure 3.13, Table 3.5).

Table 3.5 Calculated crystallinity parameter in cortical, trabecular and growth plate parts of bone tissues for control (n=7), control + CBZ (n=7), epileptic (n=7) and epileptic + CBZ groups. (*) represents the significancy compared to control group and (+) represents the significancy compared to epileptic group.

	BONE PART	CONTROL	CONTROL + CBZ	EPILEPTIC	EPILEPTIC + CBZ
Spine	Cortical	0.45 ± 0.05	0.70 ± 0.04***	0.80 ± 0.05***	1.00 ± 0.03*** +++
	Trabecular	0.65 ± 0.03	0.70 ± 0.01*	0.82 ± 0.03**	0.95 ± 0.05*** +
	Growth Plate	0.60 ± 0.04	0.93 ± 0.02***	1.00 ± 0.02*	1.10 ± 0.03*** +
Tibia	Cortical	0.19 ± 0.02	0.23 ± 0.01*	0.24 ± 0.03	0.28 ± 0.03**
	Trabecular	0.15 ± 0.02	0.25 ± 0.04**	0.21 ± 0.01*	0.30 ± 0.02*** ++
	Growth Plate	0.13 ± 0.04	0.17 ± 0.03	0.23 ± 0.04*	0.26 ± 0.03***
Femur	Cortical	0.14 ± 0.03	0.20 ± 0.02*	0.24 ± 0.01**	0.27 ± 0.01*** +
	Trabecular	0.16 ± 0.02	0.19 ± 0.01	0.17 ± 0.01	0.19 ± 0.01

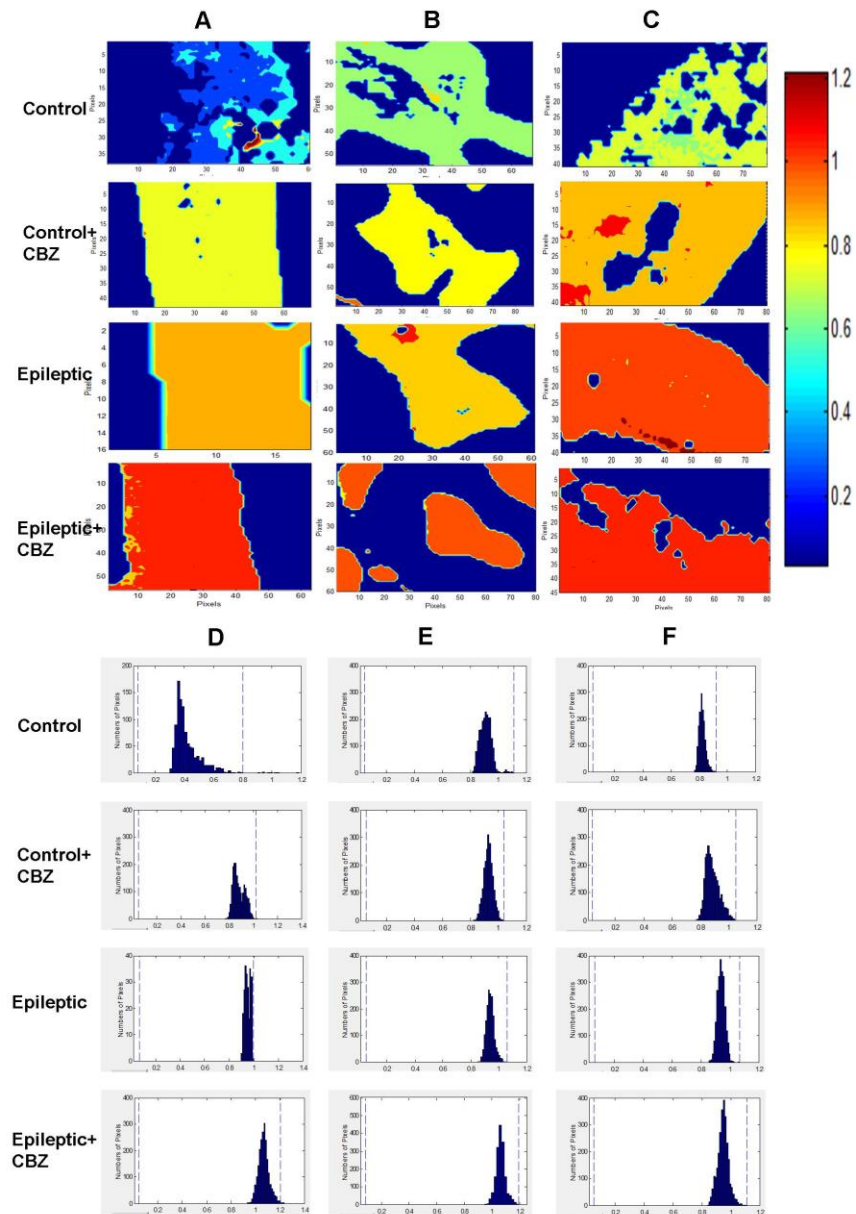


Figure 3.10 Typical FTIR images of crystallinity ratio in cortical (A), trabecular (B) and growth plate (C) sites of spine bone for control, epileptic and drug-treated groups. The scales of each parameter are represented by color bars. The pixel histograms for these images are shown in (D) cortical, (E) trabecular and (F) growth plate.

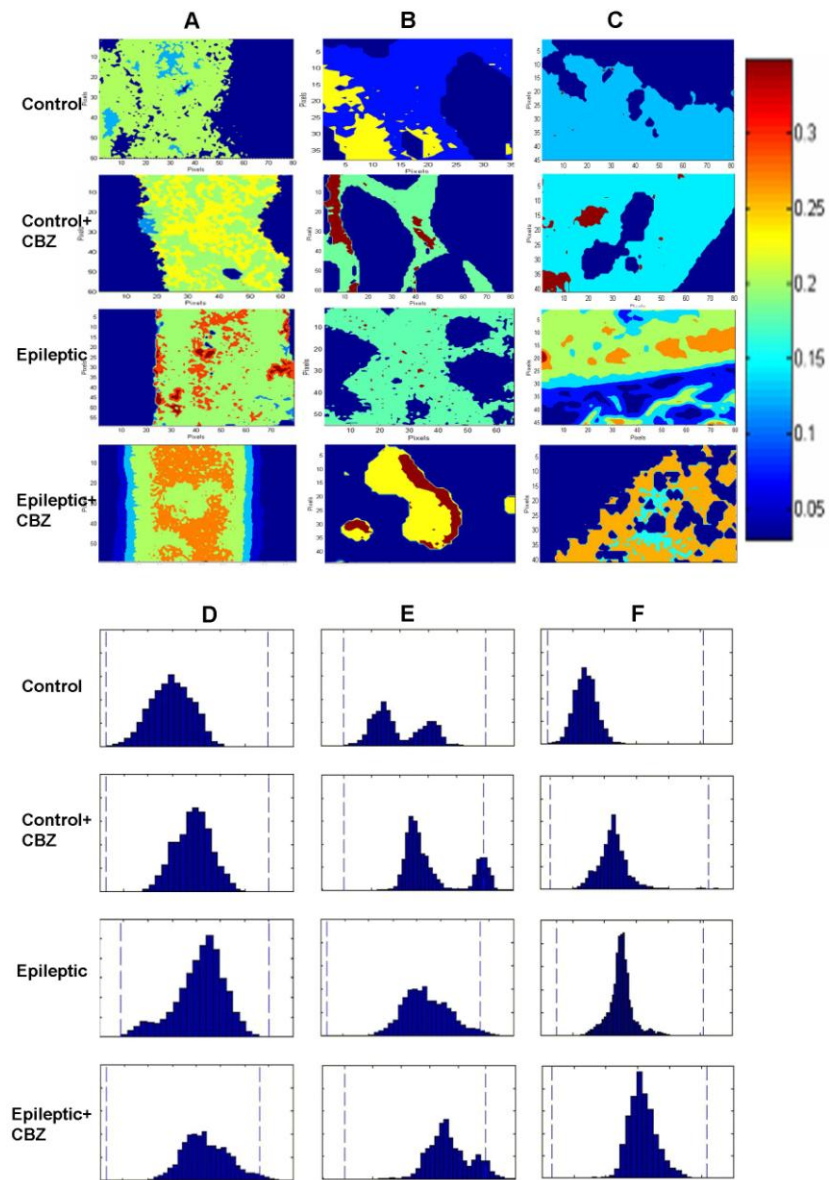


Figure 3.11 Typical FTIR images of crystallinity ratio in cortical (A), trabecular (B) and growth plate (C) sites of tibia bone for control, epileptic and drug-treated groups. The scales of each parameter are represented by color bars. The pixel histograms for these images are shown in (D) cortical, (E) trabecular and (F) growth plate.

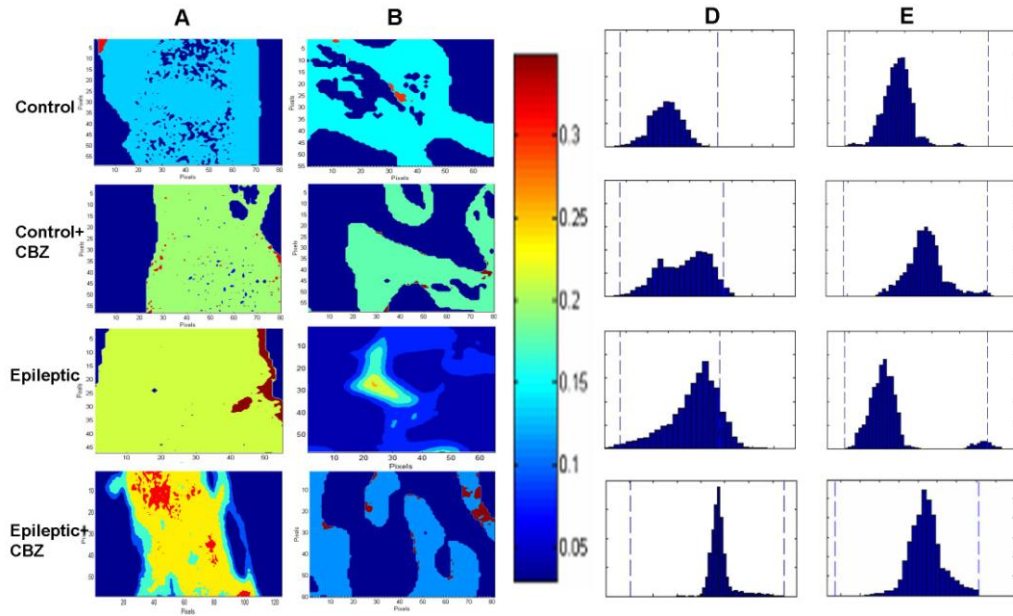


Figure 3.12 Typical FTIR images of crystallinity ratio in cortical (**A**) and trabecular (**B**) sites of tibia bone for control, epileptic and drug-treated groups. The scales of each parameter are represented by color bars. The pixel histograms for these images are shown in (**D**) cortical and (**E**) trabecular.

As a summary, crystallinity value indicating crystal size was found to be increased in epileptic group compared to the healthy control which was due to the effect of epilepsy and epileptic seizures on bones. However, the crystallinity value of carbamazepine-treated bones, mainly drug-treated epileptic bones, were found to be more increased compared to epileptic and healthy groups. Thus, drug administration affected the crystallinity of bone tissues more severely than epileptic seizures.

3.1.1.2 The Effects of Carbamazepine and Epileptic Seizures on Bone Matrix

As mentioned in Section 1.1.1.1, the organic matrix of bone is mainly type I collagen. The triple-helical structure of type I collagen is stabilized by several intermolecular and interfibrillar crosslinks (Viguet-Carrin et al., 2006). An IR parameter called collagen cross-links, corresponds the maturity of the collagen fibrils (Boskey and Mendelsohn, 2005; Gourion-Arsiquaud et al., 2012). This parameter was calculated by taking the ratio of the intensities (or areas) of two sub-bands under the Amide I band. The intensity ratio of the sub-bands at 1660 and 1690 cm^{-1} is related to the relative amount of nonreducible (mature) to reducible (immature) cross links (Huang et al., 2003).

A significant decrease in collagen crosslinks in all spine bone parts of carbamazepine-treated groups relative to the epileptic and control ones was observed (Figure 3.14 and Table 3.6). This ratio was also significantly decreased for epileptic group compared to the healthy control in all bone parts. Pixel distribution for the image of collagen crosslink ratio of bone, was commonly sharp (Figure 3.14), showing limited variation in collagen maturity in spine bone parts (Faibish et al., 2006).

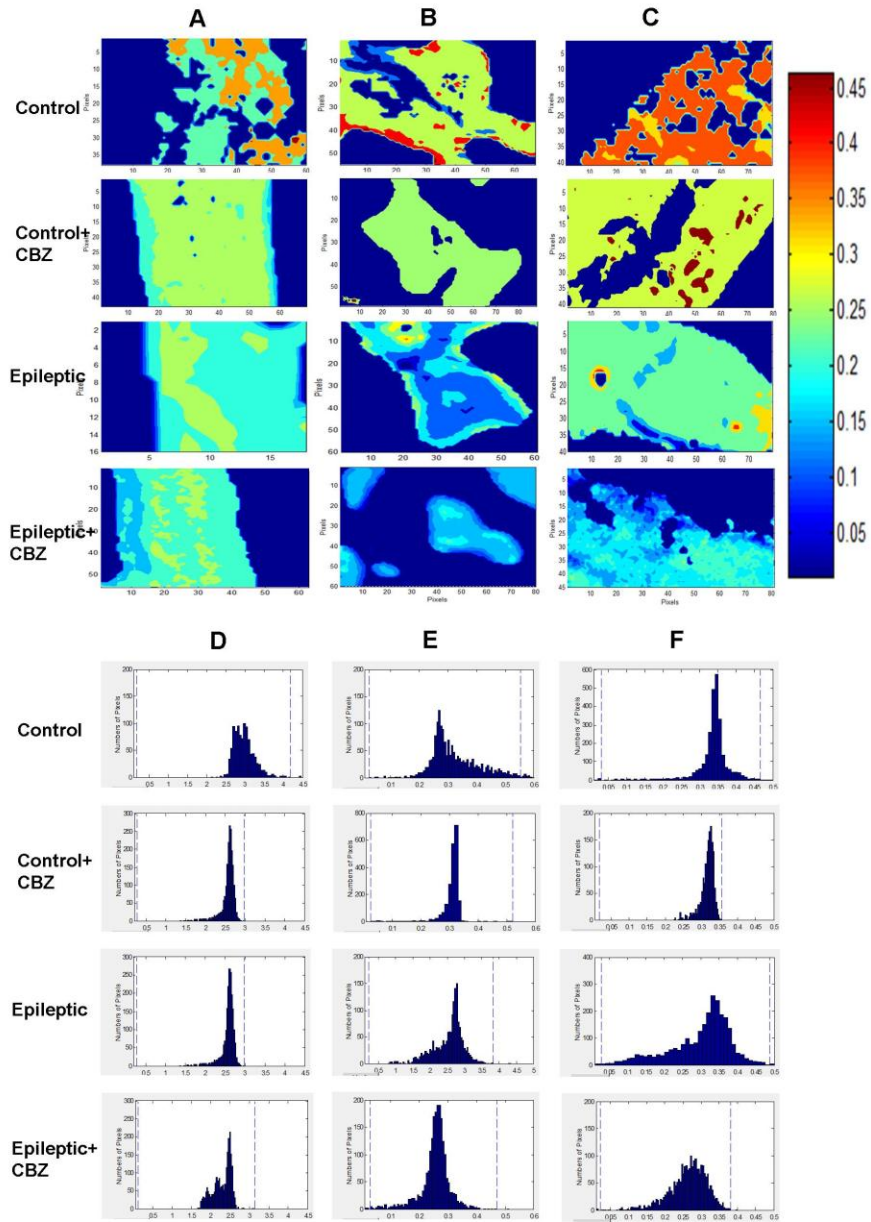


Figure 3.14 Typical FTIR images of collagen crosslinks ratio in cortical (**A**) and trabecular (**B**) and growth plate (**C**) sites of spine bone for control, epileptic and drug-treated groups. The scales of each parameter are represented by color bars. The pixel histograms for these images are shown in (**D**) cortical, (**E**) trabecular and (**F**) growth plate.

Table 3.6 Calculated crosslinks parameter in cortical, trabecular and growth plate parts of bone tissues for control (n=7), control + CBZ (n=7), epileptic (n=7) and epileptic + CBZ groups. (*) represents the significancy compared to control group and (+) represents the significancy compared to epileptic group.

	BONE PART	CONTROL	CONTROL + CBZ	EPILEPTIC	EPILEPTIC + CBZ
Spine	Cortical	0.30 ± 0.03	0.24 ± 0.02*	0.21 ± 0.03**	0.18 ± 0.01***
	Trabecular	0.35 ± 0.03	0.28 ± 0.01**	0.16 ± 0.04***	0.14 ± 0.02***
	Growth Plate	0.39 ± 0.04	0.30 ± 0.02**	0.23 ± 0.02***	0.14 ± 0.03*** +++
Tibia	Cortical	0.28 ± 0.02	0.26 ± 0.01	0.24 ± 0.03	0.23 ± 0.03
	Trabecular	0.25 ± 0.02	0.20 ± 0.02*	0.23 ± 0.01	0.19 ± 0.02* +
	Growth Plate	0.27 ± 0.02	0.24 ± 0.02	0.26 ± 0.03	0.23 ± 0.01
Femur	Cortical	0.33 ± 0.02	0.28 ± 0.02*	0.25 ± 0.01**	0.22 ± 0.01*** +
	Trabecular	0.34 ± 0.01	0.31 ± 0.01*	0.33 ± 0.01	0.25 ± 0.01***+++

In tibia tissues, a significant decrease in collagen crosslinks was obtained in trabecular part of drug-treated bones compared to the epileptic and healthy control bone tissues. Although there was a slight decrease, no significant result was obtained in tibia for collagen crosslinks of epileptic group compared to the healthy control (Figure 3.15, Table 3.6).

In femur tissues, the significant variations for carbamazepine-treated groups compared to the epileptic and healthy controls, showed a similar pattern for all parts as seen in Figure 3.16. In these groups, there was a significant reduction in

collagen crosslinks parameter, while in the epileptic group the variations were only significant in cortical part compared to the control (Figure 3.16, Table 3.6). The severe decrease in the cortical part, could also be seen from the pixel distributions of this value which slid to the left side (to the lower values) of the histogram in drug-treated and epileptic groups.

As a summary, relative amount of nonreducible/reducible cross links, was found to be changed critically in carbamazepine-treated epileptic and healthy groups, indicating an increase in immature crosslinks in the bones of these groups. However, the variation in the ratio of the mature/immature crosslinks, was that much drastic for epileptic group in only spine tissue compared to the healthy control.

In FTIRM studies, according to the degree of variation and significance between the calculated parameter values, the spine tissue was found to be the most affected bone tissue from both epileptic seizures and anti-epileptic drug treatment.

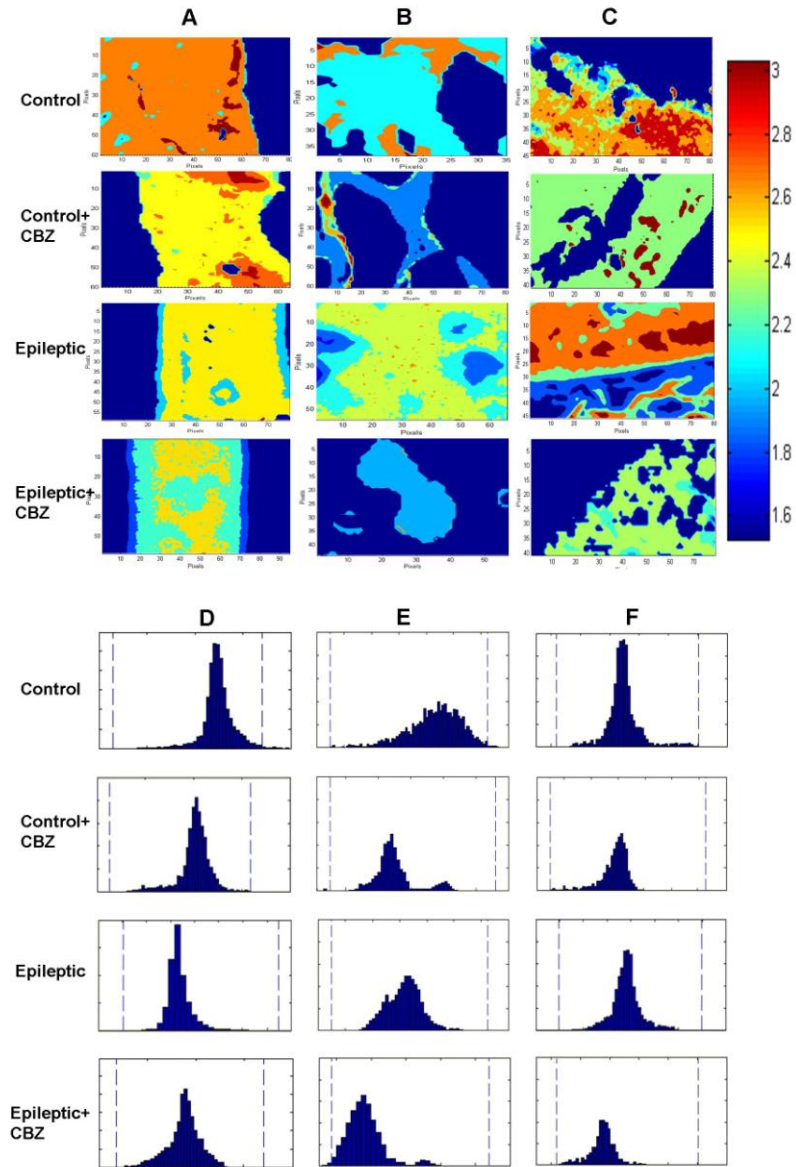


Figure 3.15 Typical FTIR images of collagen crosslinks ratio in cortical (A), trabecular (B) and growth plate (C) sites of tibia bone for control, epileptic and drug-treated groups. The scales of each parameter are represented by color bars. The pixel histograms for these images are shown in (D) cortical, (E) trabecular and (F) growth plate.

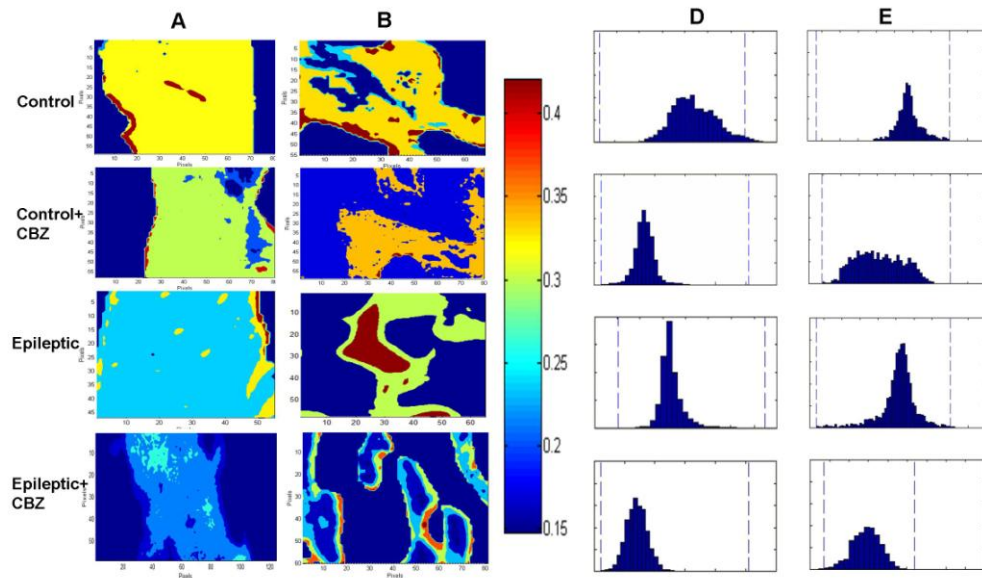


Figure 3.16 Typical FTIR images of collagen crosslinks ratio in cortical (A) and trabecular (B) sites of femur bone for control, epileptic and drug-treated groups. The scales of each parameter are represented by color bars. The pixel histograms for these images are shown in (D) cortical and (E) trabecular.

3.1.2 Hardness Studies

Hardness is used as a parameter to determine the resistance of a material against an indentation (Currey JD, 2003; Ritchie et al., 2005; Oyen ML, 2006). The understanding of bone mechanics can be developed by the hardness tests in different levels (Boivin et al., 2008). For this reason, hardness studies were carried out in both micro- and nano-levels. Microhardness values were determined with Vickers microhardness test in spine, tibia and femur tissues, where nanohardness values were obtained from nano-indentation tests which was applied to spine

tissue as the most affected bone from epileptic seizures and drug treatment according to the FTIRM and microhardness studies.

3.1.2.1 Vickers Microhardness Studies

The results of microhardness measurements for all bone tissues were given in Figure 3.17. As seen from the figure, when the microhardness values of epileptic group were compared with the healthy control, in all three parts of spine tissue, there was a significant decrease in hardness of bones. The most severe decrease in hardness was observed in drug-treated epileptic group compared to the epileptic and healthy groups in cortical, trabecular and growthplate regions of spine bones.

In tibia bone tissues, except the cortical part, epileptic group had significantly decreased hardness values compared to the healthy one. Moreover, hardness values of drug-treated groups, especially the drug-treated epileptic group, were significantly decreased in all bone parts of tibia (Figure 3.17). In femur tissues, the only significant change in hardness was observed in drug-treated epileptic group in cortical bone part.

group. Thus, drug administration affected the hardness of bone tissues more severely than epileptic seizures.

3.1.2.2 Nanohardness Studies

Nanohardness, microhardness, and macrohardness tests may not provide comparable results in high heterogen structures such as bone. The microhardness is affecting a much wider volume thus measuring hardness of a bigger bone areas. The nanoindenter measurement is very localized including a small volume of material and represents the hardness of a particular small bone area. Thus, it enables to measure hardness values across the radial of a bone section from periosteum (outer bone membrane) to endosteum (inner bone membrane). The most affected bone tissue form both epileptic seizures and carbamazepine treatment was found as spine according to the results of FTIRM and microhardness studies. Therefore, nanohardness test was applied to spine tissue with 2 different methods. In the first method, two different maximum loads of 1000 ve 5000 μN were applied to cross section of cortical bone as a grid pattern of totally 98 indents. In the second method, same loads were applied to across the cortical radial section of bone with approximately 300 indents to get information about the effects on different regions of cortical bone.

The hardness (H) and elastic modulus (E) values for spine bone tissues of healthy control, epileptic and carbamazepine-treated groups, in 1000 μN ve 5000 μN loads are shown in Figure 3.18. The hardness values of epileptic group were lower than the hardness values of healthy control rat group. This lower hardness values were only the result of the effects of epilepsy and seizures without interfering with any drug treatment. The administration of carbamazepine to the healthy rats, led to a decrease in bone hardness values of these rats. The same case happened when the drug was given to the epileptic group rats. The hardness values of drug-treated

epileptic group were much more lower than the ones of control epileptic group. There were also dramatic changes for elastic modulus values between animal groups. As in hardness values, elastic modulus of drug-treated groups was also lower than the values of epileptic and healthy control groups. Moreover, elastic modulus values were different between healthy control and epileptic group (Figure 3.18).

Another important observation was that the alteration of H and E values between animal groups increased with the increase of applied load. The alteration between nanomechanic parameter values of different animal groups in 1000 μ N load, was more higher when 5000 μ N load was applied (Figure 3.18).

Figure 3.19 shows the hardness and elastic modulus values of spine tissue of studied animal groups, across the cortical radial sections of each bone. The results were analyzed in three different cortical parts; periosteum to mid-cortical, mid-cortical and mid-cortical to endosteum. As seen from the figure, both the hardness and elastic modulus of drug-treated groups were lower than the epileptic and healthy control groups in all cortical parts. These parameter values were also lower for epileptic group when compared to the healthy control group. Although hardness values of drug-treated healthy rats were also lower than the healthy control group, the most dramatic changes were seen in drug-treated epileptic group compared to epileptic rats. Elastic modulus values of these groups were also lower than the control groups but not as dramatic as the alterations in hardness values (Figure 3.19).

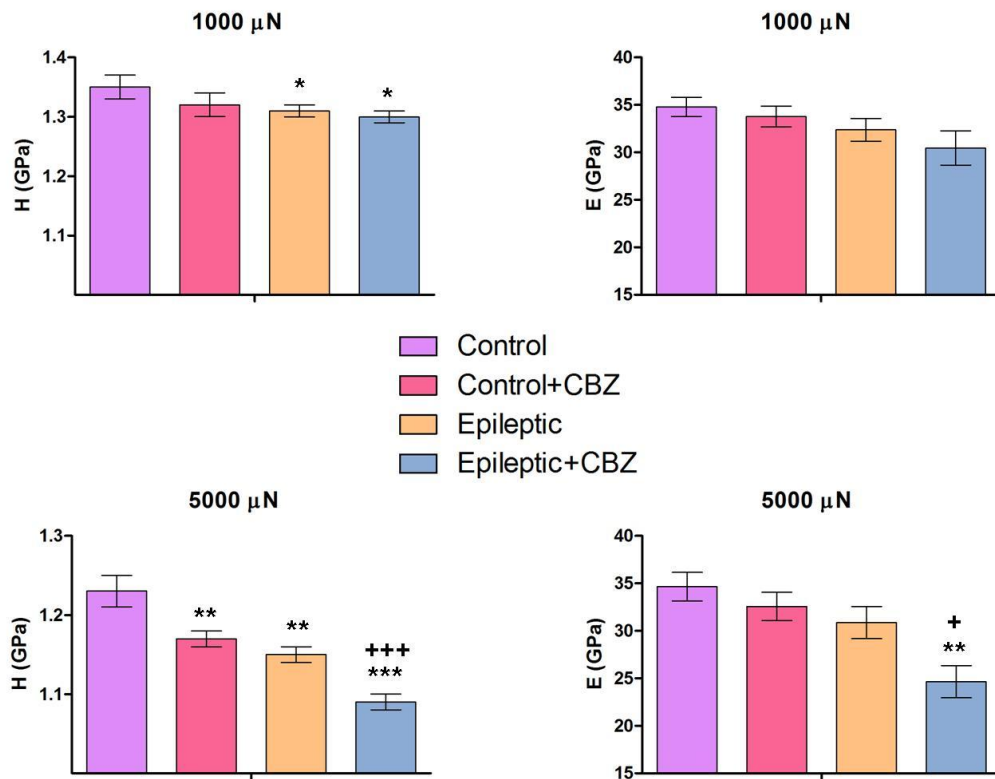


Figure 3.18 Hardness (H) and elastic modulus (E) values obtained from 7x7=49 indents on cortical bone of spine tissues using 1000 μN and 5000 μN loads. (*) represents the significance compared to control group and (+) represents the significance compared to epileptic group (*+p ≤ 0.05; **++p ≤ 0.01; ***+++p ≤ 0.001).

As a summary, the nanohardness values of spine were most affected from carbamazepine treatment in both healthy and epileptic rats. However, the most dramatic changes were seen in drug-treated epileptic group compared to epileptic rats. In elastic modulus changes, there was not that much dramatic reduction as seen in hardness values. Moreover, the most affected cortical regions from both

epileptic seizures and drug treatment, were mid-cortical and close to endosteum parts (inner cortical membrane).

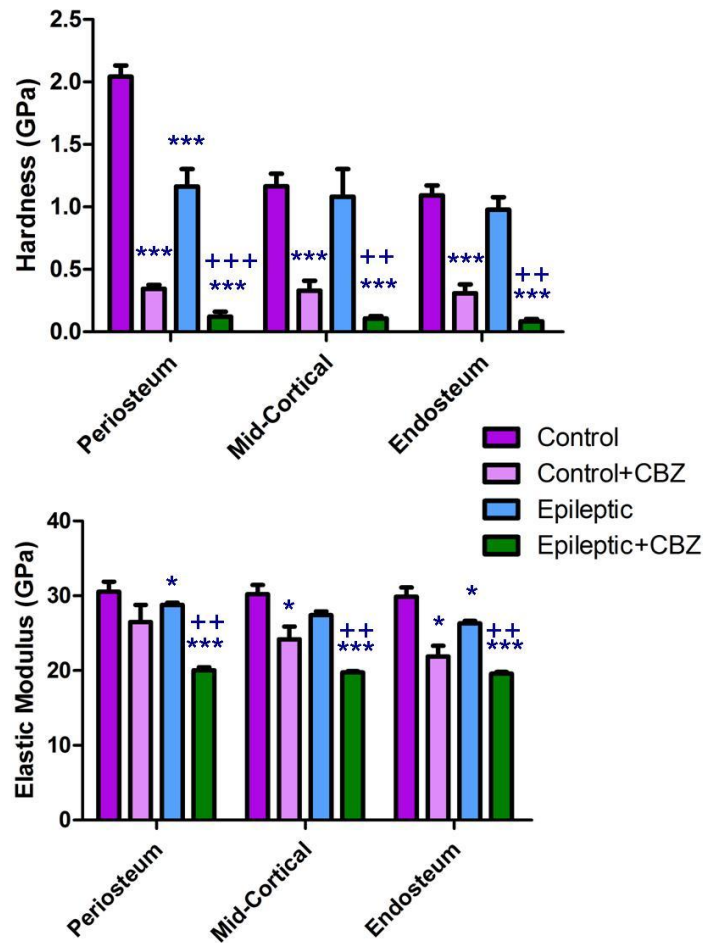


Figure 3.19 Hardness (H) and elastic modulus (E) values from 30x1=30 indents across the cortical radial of spine tissues using 5000 μ N load. (*) represents the significance compared to control group and (+) represents the significance compared to epileptic group (*,+p \leq 0.05; **,++p \leq 0.01; ***,+++p \leq 0.001).

3.1.3 SR-FTIR Microspectroscopy Studies

The further investigated was done for the changes in mineral and matrix parts of drug-treated and epileptic bones with SR-FTIR microspectroscopy because of two important advantages of this technique. Firstly, global FTIRM can only collect data between 4000-700 cm^{-1} , since the 700-400 cm^{-1} frequency region is below the cutoff of the detectors used in commercial infrared microscopes. An advantage of SR-FTIRM for bone research is enabling the collection of data in also between 700-400 cm^{-1} infrared range. In this range, the $\nu_4 \text{PO}_4^{3-}$ band (500-650 cm^{-1}) gives more accurate data for mineral properties including crystallinity, since this band is affected from other absorptions less than the $\nu_1, \nu_3 \text{PO}_4^{3-}$ band (1200-900 cm^{-1}). Another advantage of SR-FTIRM is its 1000 times higher signal/noise ratio than the thermal source for spatial resolutions, enabling us to monitor the small IR bands at better and high spatial resolutions. The latter advantage also provides to study intra-bone variations by enabling investigation of the changes in the small and/or heterogeneous parts of bone tissues more accurately.

Intra-bone variations are important to determine the disease- and/or drug-related bone disorders. Different locations of bone are regarded as being in the early mineralization, bone remodeling and bone formation stages (Kavukcuoglu et al., 2009). Changes in these locations can give valuable results about the cause of the disorder on bone. The changes in biomechanic features of different cortical regions were mentioned in the previous section (3.1.2.2) and these nanoindentation studies showed that mid-cortical and the region between the mid-cortical and endosteum parts (close to inner membrane) were the most affected parts from epileptic seizures and drug-treatment. For further investigation, the structural changes in periosteum, mid-cortical and endosteum parts of spine cortical were studied detailly with SR-FTIR microspectroscopy.

Representative SR-FTIRM images of mineral/matrix, carbonate/mineral, crosslink ratio and crystallinity parameters for three different spine cortical regions were shown in Figure 3.20, Figure 3.21, Figure 3.22, and Figure 3.23, respectively. The decreased mineral content, carbonate substitution, collagen crosslinks and increased crystallinity in epileptic and drug-treated groups compared to the healthy controls, supported the previous FTIRM results in this study (Figure 3.20, Table 3.7). According to the calculated parameters, the most affected cortical regions from epileptic seizures and carbamazepine treatment, were mid-cortical and close to endosteum parts (inner cortical membrane). This result may point to an alteration in the osteoclastic endosteal bone resorption (Kavukcuoglu et al., 2009) due to epilepsy and drug treatment.

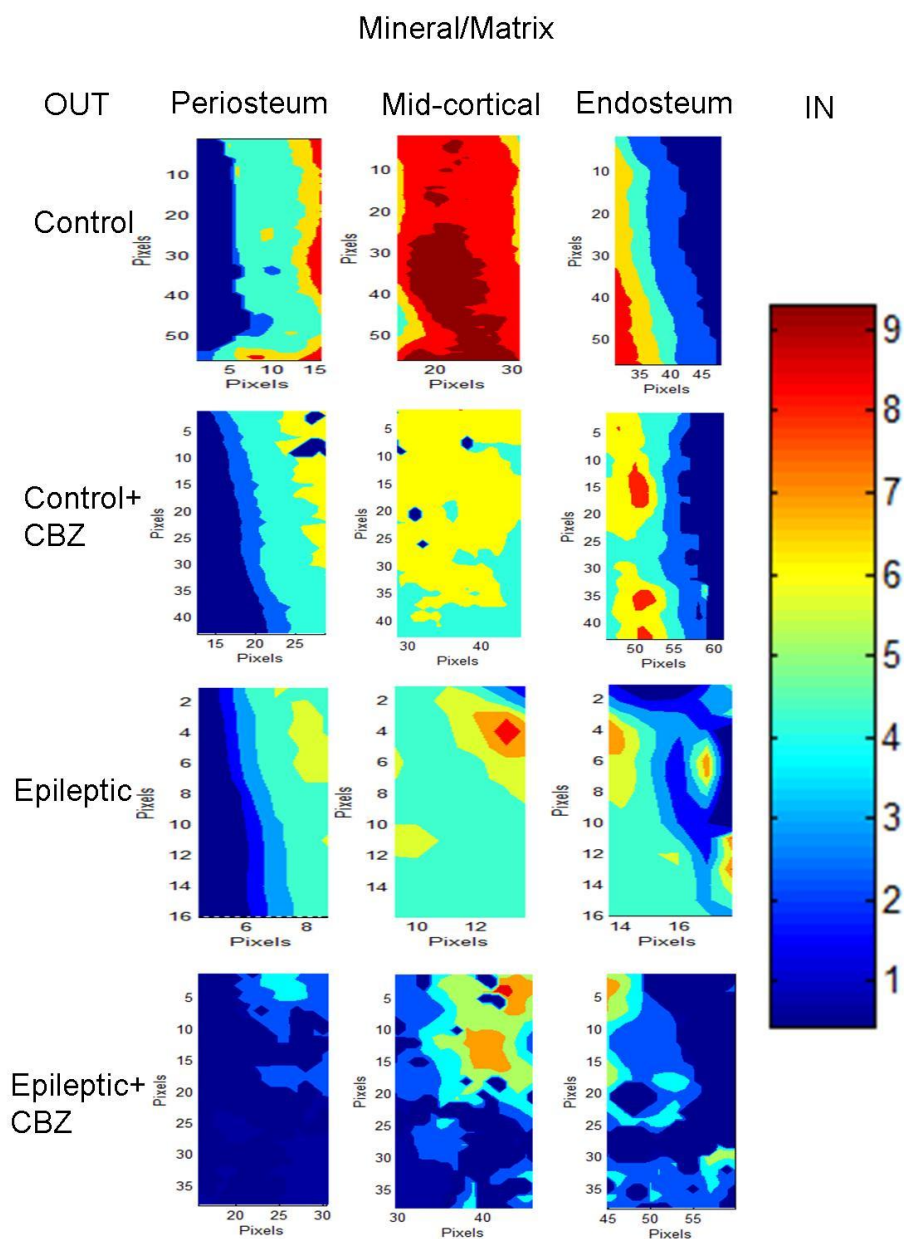


Figure 3.20 Typical FTIR images of mineral/matrix ratio in periosteum, mid-cortical and endosteum parts of spine cortical for control, epileptic and drug-treated groups. The scales of each parameter are represented by color bars. Axes are in pixels (one pixel is 1.0 μm).

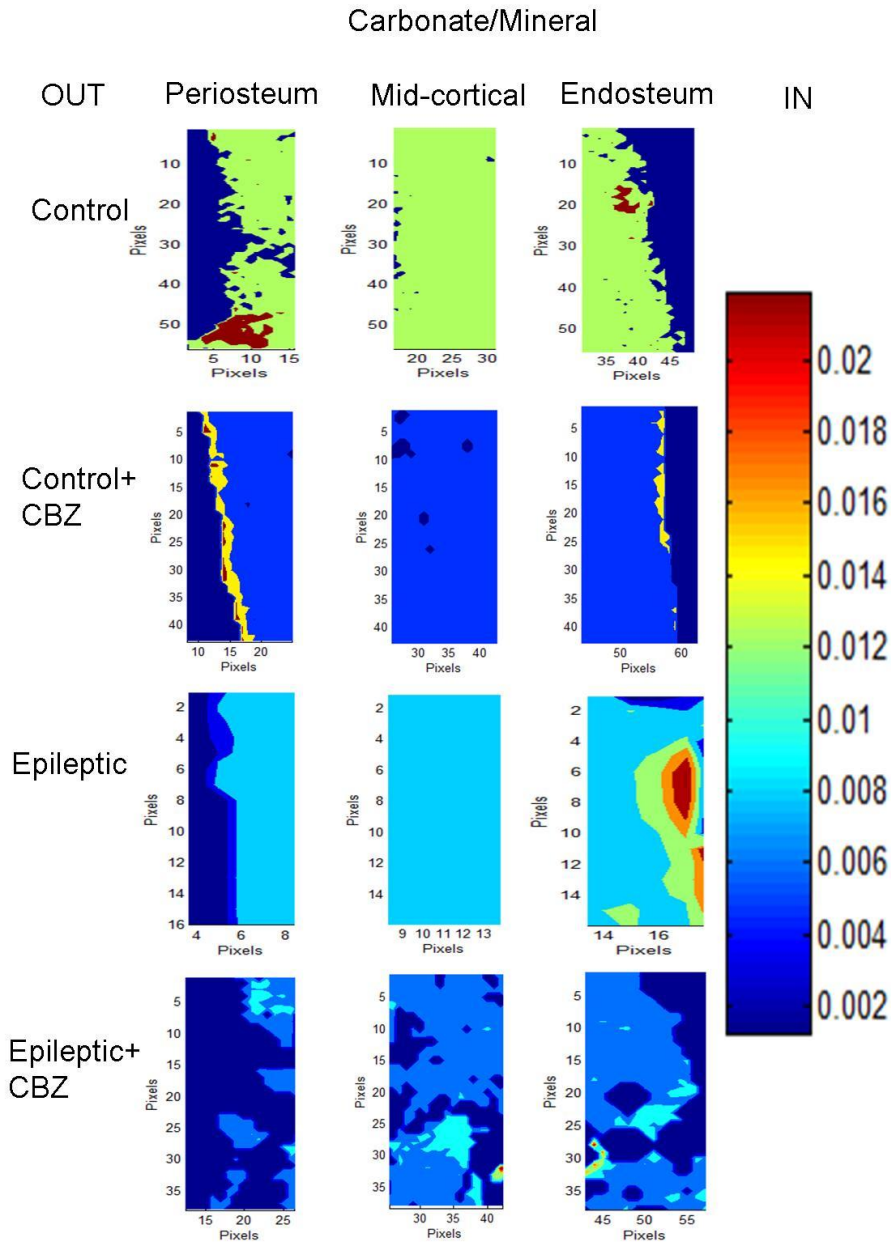


Figure 3.21 Typical FTIR images of carbonate/mineral ratio in periosteum, mid-cortical and endosteum parts of spine cortical for control, epileptic and drug-treated groups. The scales of each parameter are represented by color bars. Axes are in pixels (one pixel is 1.0 μm).

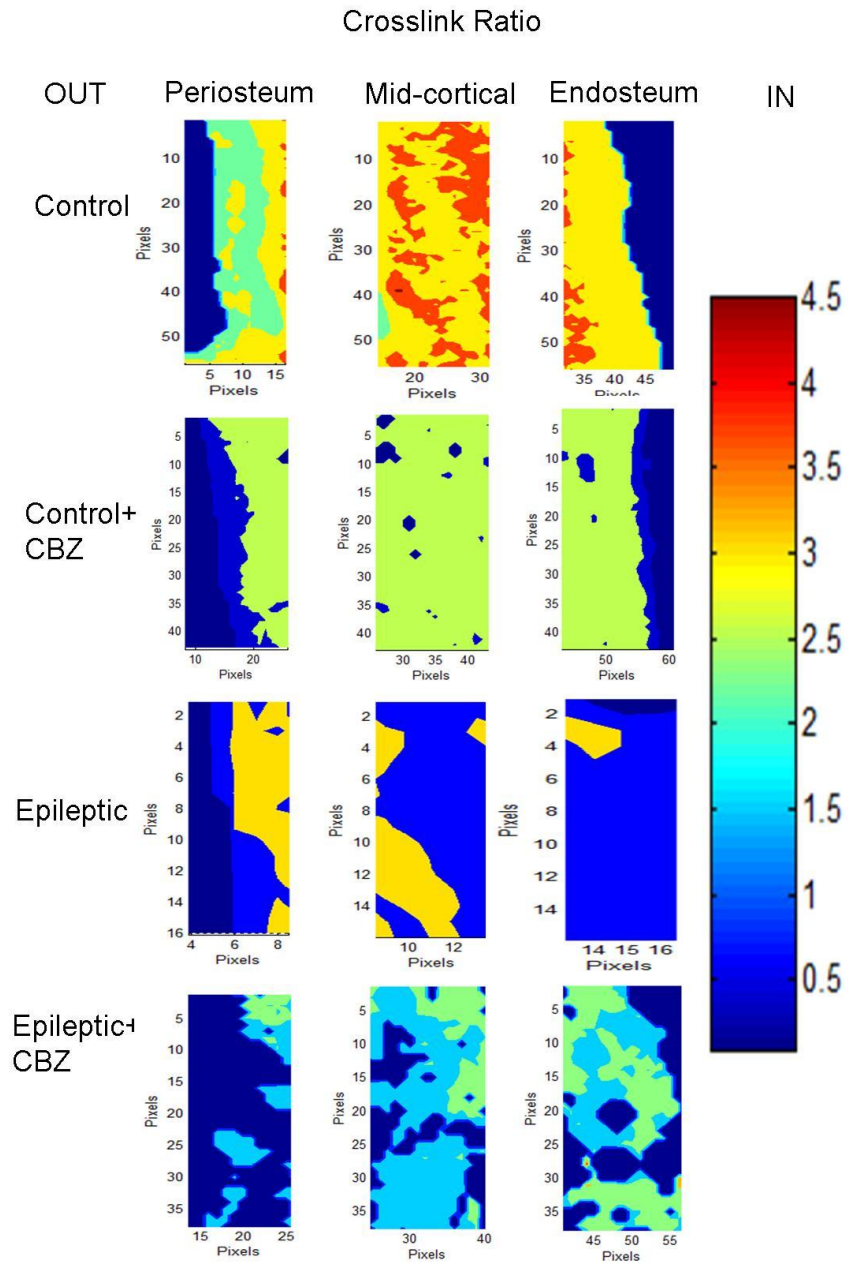


Figure 3.22 Typical FTIR images of crosslink ratio in periosteum, mid-cortical and endosteum parts of spine cortical for control, epileptic and drug-treated groups. The scales of each parameter are represented by color bars. Axes are in pixels (one pixel is 1.0 μm).

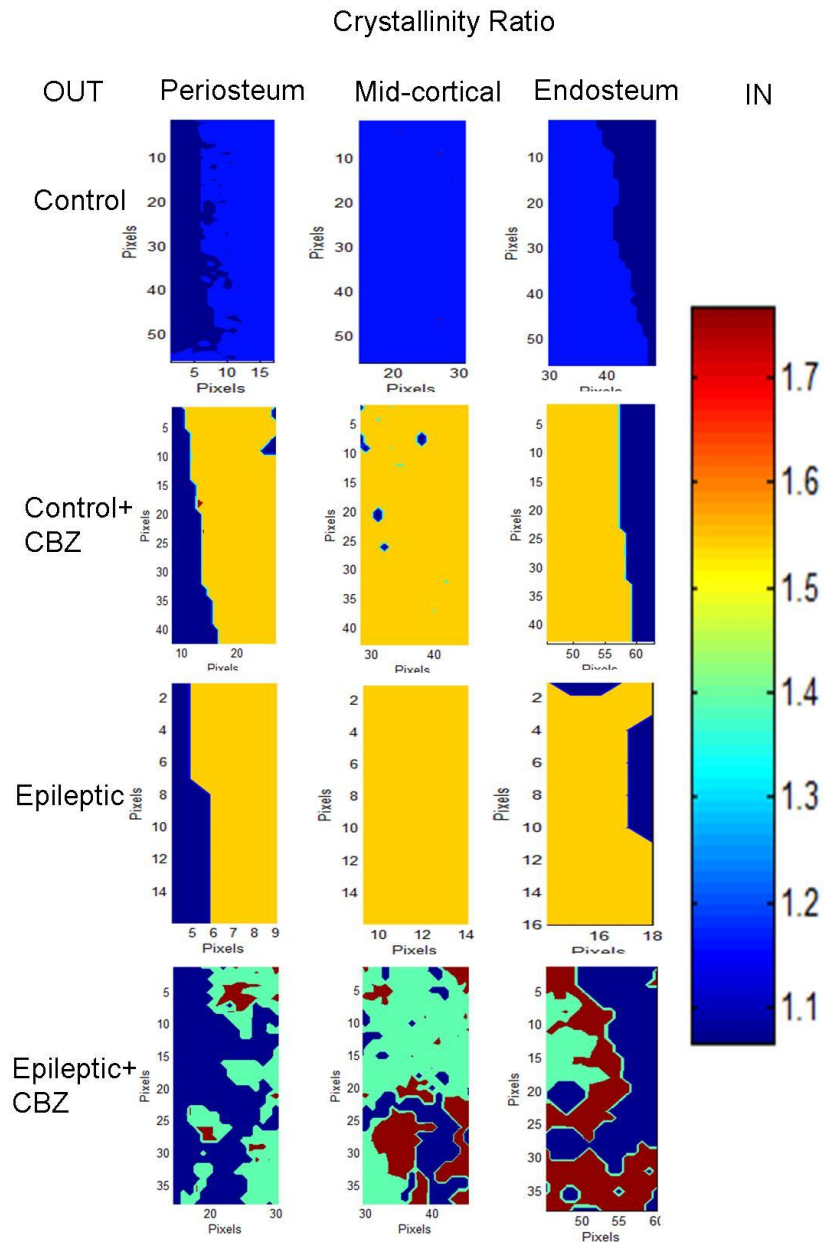


Figure 3.23 Typical FTIR images of crystallinity ratio in periosteum, mid-cortical and endosteum parts of spine cortical for control, epileptic and drug-treated groups. The scales of each parameter are represented by color bars. Axes are in pixels (one pixel is 1.0 μm).

Table 3.7 Calculated SR-FTIR parameters in periosteum, mid-cortical and endosteum parts of spine cortical for control (n=7), control + CBZ (n=7), epileptic (n=7) and epileptic + CBZ groups. (*) represents the significance compared to control group and (+) represents the significance compared to epileptic group.

RATIO	CONTROL			CONTROL+CBZ			EPILEPTIC			EPILEPTIC+CBZ		
	P	M	E	P	M	E	P	M	E	P	M	E
<u>Min/Matrix</u>	5.5±0.2	8.5±0.3	5.7±0.1	5.0±0.1 *	5.5±0.1 ***	5.6±0.1	4.8±0.2 *	5.0±0.1 ***	4.9±0.2 **	3.0±0.2 **++	4.7±0.1 ***+	3.5±0.2 ***+++
<u>Carb/Phosp</u>	0.013± 0.001	0.012± 0.003	0.013± 0.001	0.007± 0.001 ***	0.005± 0.001 ***	0.006± 0.002 ***	0.009± 0.002 **	0.010± 0.001	0.011± 0.001	0.006± 0.002 ***	0.006± 0.001 ***+	0.006± 0.001 ***++
<u>Crosslinks</u>	3.0±0.1	3.5±0.1	3.3±0.2	2.4±0.1 **	2.5±0.1 ***	2.4±0.2* *	2.6±0.1 *	2.6±0.1 ***	2.4±0.1 ***	2.0±0.2 **+	2.1±0.1 ***+	2.2±0.1 ***
<u>Crystallinity</u>	1.2±0.1	1.2±0.1	1.2±0.1	1.5±0.1 *	1.5±0.1 *	1.5±0.1 *	1.5±0.1 *	1.5±0.1 *	1.5±0.1 *	1.5±0.1 *	1.6±0.1 **	1.7±0.1 ***

3.1.4 Atomic Force Microscopy Studies

Figure 3.24 shows the $3 \mu\text{m}^2$ AFM height and phase images of spine bone tissues of healthy, epileptic and carbamazepine-treated animal groups. As seen from the figure, images of drug-treated groups had lower distribution of light color which implied that distribution of minerals were lower in these groups when compared to the control groups.

Table 3.8 shows the root mean square (RMS) and arithmetic average height (Ra) which were measured from $3 \mu\text{m}^2$ AFM images of spine bones of studied animal groups. The roughness value of epileptic group was lower than healthy control group. This lower roughness value was only the result of the effects of epileptic seizures without interfering with any drug treatment. The roughness values of drug-treated healthy and epileptic groups were also lower than the values of epileptic and healthy control groups in spine bones. It was shown that the most affected group from drug treatment was epileptic rat group (Figure 3.24, Table 3.8).

Table 3.8 The root mean square (RMS) and arithmetic average height (Ra) values obtained from 3 μm^2 AFM images of spine tissue for control (n=7), control + CBZ (n=7), epileptic (n=7) and epileptic + CBZ groups. (*) represents the significance compared to control group and (+) represents the significance compared to epileptic group.

	3x3 μm^2 Scan Area	
GROUP	RMS (nm)	Ra (nm)
Control	204.0±25.0	168.0±24.2
Control+CBZ	110.0±21.5***	79.2±24.5***
Epileptic	121±28.2**	91.0±25.1**
Epileptic+CBZ	68.5±20.3*** ++	41.6±13.5*** +

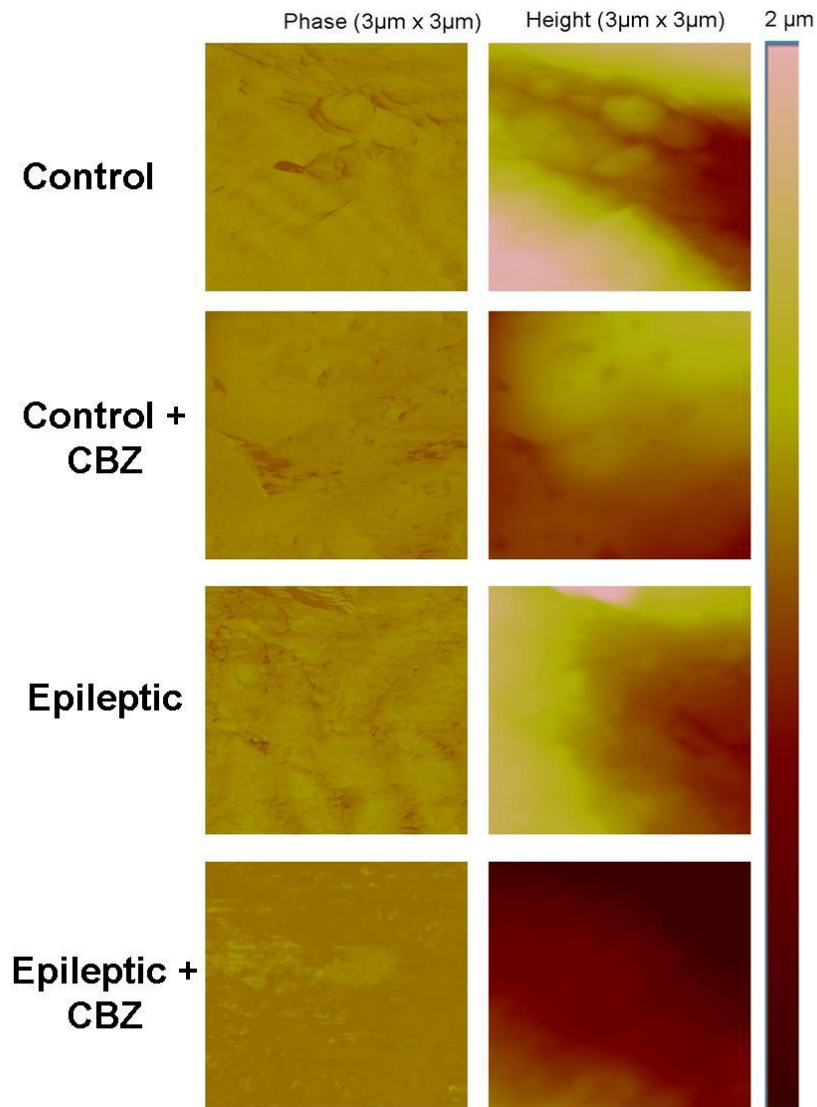


Figure 3.24 $3 \mu\text{m}^2$ AFM height and phase images of spine bone tissues of control, epileptic and drug-treated groups.

As a summary, It was reported that there is a linear correlation between bone hardness and surface roughness (Zhao et al., 2010). Therefore, lower surface

roughness values of epileptic group compared to healthy one and carbamazepine-treated groups compared to epileptic and healthy groups, were supported the lower micro- and nano-hardness values in these groups. As also reported in hardness studies, epileptic rats were observed to be affected most dramatically from carbamazepine treatment in AFM studies.

3.1.5 Biochemical Studies

Measurement of molecular markers that are known as reflecting bone formation and/or bone resorption enables the diagnosis of bone disorders and determine the effects of different factors on bone. In the present study, the serum levels of bone formation markers (BAP, OC) and bone resorption marker (C-telopeptide) and the serum levels of calcium, parathormone, 25-OH and 1,25-OH vitamin D were measured by ELISA. Therefore, measuring these blood parameters can be helpful to understand the mechanism for the adverse effects of carbamazepine and also epileptic seizures on bone structure and mechanics. Moreover, to clarify the action mechanism of anti-epileptic drug and seizures on vitamin D and bone metabolism, the protein levels of vitamin D anabolism and catabolism enzymes were measured by western blot analysis.

3.1.5.1 Measurement of Bone Turnover Markers

Most of the biochemical markers of bone resorption are correspond to collagen breakdown products including collagen telopeptides. However, bone formation markers are products of collagen neosynthesis and/or osteoblast-related proteins including osteocalcin (OC) and bone specific alkaline phosphatase (BAP).

25-hydroxyvitamin D is the only vitamin D metabolite which is used to understand whether there is a vitamin D deficiency, sufficiency or intoxication (Holick M.F.,

2009). 1,25dihydroxy vitamin D affects the classic target organs such as bone, intestine and kidneys and enhances calcium absorption from mentioned organs. The production of 1-alpha-25-dihydroxy vitamin D is stimulated by PTH. While vitamin D deficiency leads to osteoporosis, vitamin D insufficiency (subsequent form of vitamin D deficiency) leads to osteomalacia.

The serum levels of blood parameters and bone turnover markers are shown in Figure 3.25 and Figure 3.26, respectively. As seen from the figure, the serum levels of 25(OH)D and 1,25(OH)D were significantly decreased in both epileptic and carbamazepine-treated groups, compared to the healthy controls. The total serum Ca concentration was significantly decreased in both epileptic and carbamazepine-treated groups while there were elevated levels of PTH and bone turnover markers (OC, BAP, CTX) in drug-treated groups. However, a slight increase was observed in bone turnover markers in epileptic group.

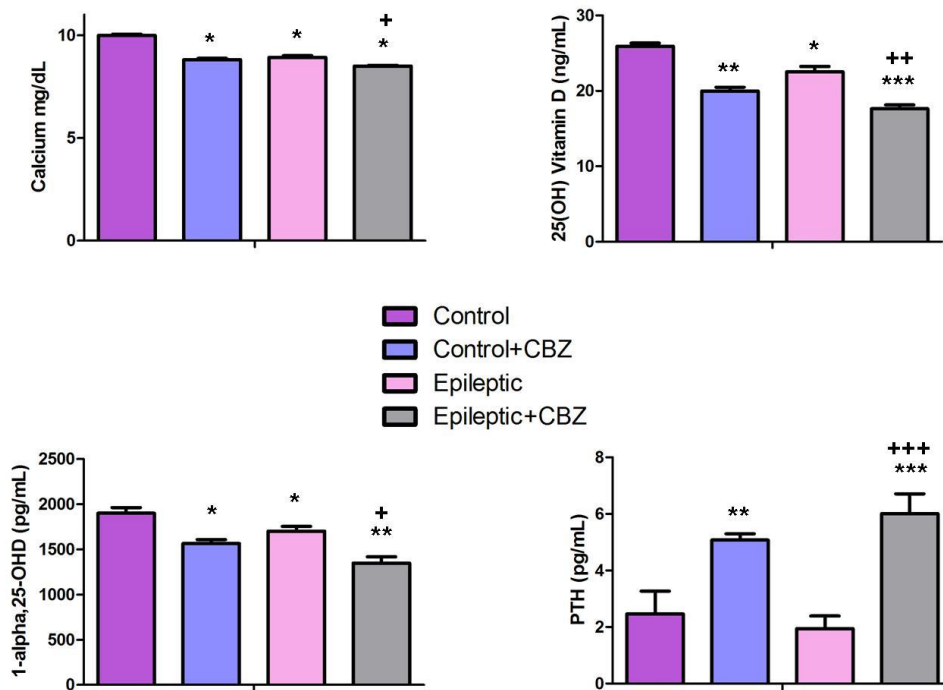


Figure 3.25 Serum calcium, 25(OH)D, 1,25(OH)D and PTH levels of control, epileptic and drug-treated groups. (*) represents the significance compared to control group and (+) represents the significance compared to epileptic group (*,+p ≤ 0.05; **,+,+ p ≤ 0.01; ***,+,+ p ≤ 0.001).

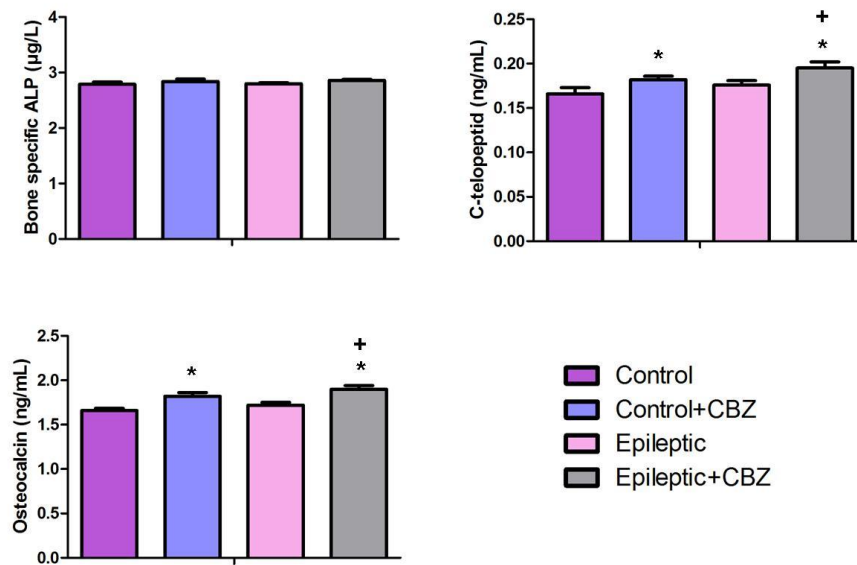


Figure 3.26 Serum bone formation (ALP and osteocalcin) and resorption (C-telopeptide) of control, epileptic and drug-treated groups. (*) represents the significance compared to control group and (+) represents the significance compared to epileptic group (*⁺p ≤ 0.05; **⁺⁺p ≤ 0.01; ***⁺⁺⁺p ≤ 0.001).

3.1.5.2 Protein Level Measurement of Vitamin D Metabolism Enzymes

In the current study, the protein levels of 25-hydroxylase (CYP11A1) in the liver, 1- α -hydroxylase (CYP27B1) and 24-hydroxylase (CYP24) in the kidney were determined by western blot analysis to determine the possible effects of epileptic seizures and carbamazepine treatment on vitamin D metabolism. Western blot analysis results showed that both epileptic seizures and carbamazepine treatment increased the vitamin D catabolism enzyme 24-hydroxylase (CYP24). Moreover, the protein levels of 25-hydroxylase (CYP27A1) was also shown to be increased

in both epileptic and drug-treated groups (Figure 3.27). The drug-treated epileptic group had the highest protein levels of these enzymes.

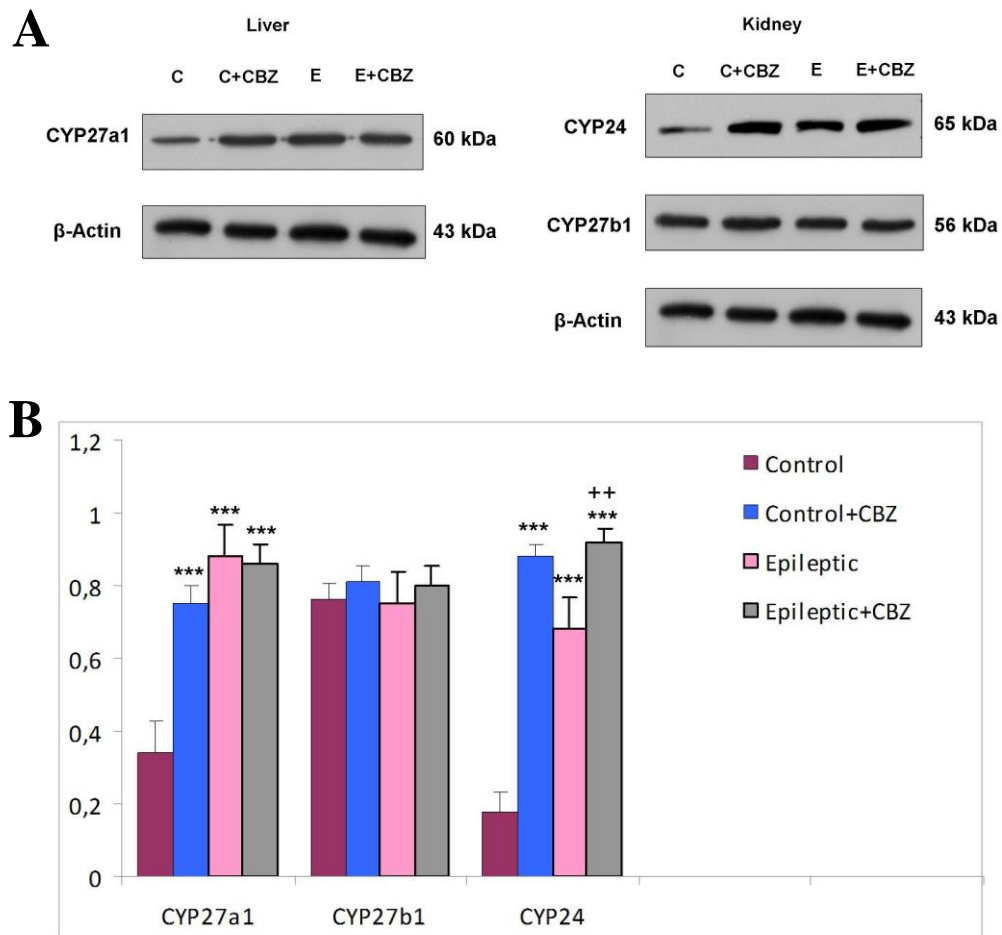


Figure 3.27 Protein levels of CYP27a1, CYP27b1 and CYP24 enzymes in liver and kidney tissues of epileptic and drug-treated groups are shown in representative western blot images (A) and histograms (B). (*) represents the significance compared to control group and (+) represents the significance compared to epileptic group (*⁺p ≤ 0.05; **⁺⁺p ≤ 0.01; ***⁺⁺⁺p ≤ 0.001).

3.2 Study 2: Simvastatin Study

As it was reported in the first study of the current thesis, Carbamazepine which is used for the treatment of neurological diseases, can induce adverse effects on bone tissues. As a comparative study, it was aimed to investigate the possible adverse and/or pleiotropic effects of another commonly used, well-known cholesterol lowering drug; Simvastatin on bone tissues of healthy rats in a dose-dependent manner. Besides the advantages of FTIR microspectroscopy such as enabling the study of different bone parts and intra-bone variations non-destructively with a high spatial resolution, it has a long data acquisition and sample preparation procedures with the need of expensive chemicals for sample embedding. Because of these challenges, another non-destructive and non-invasive, sensitive and high quality vibrational technique; ATR-FTIR spectroscopy, with less cheap and complex experimental procedure and more rapid data acquisition than the FTIR microspectroscopy was preferred. By using ATR-FTIR spectroscopy technique, it would not be able to monitor different parts of the bones and represent them with visual images of bone tissue parts, as it was done in FTIRM studies. However, it would be able to obtain similar information with FTIRM about the structural and conformational changes in bone mineral, matrix, crystallinity and proteins of total bone tissue. Thus, ATR-FTIR spectroscopy provides us sensitive information as FTIRM but not detailed as it. Since it was aimed to investigate the effects of the drug essentially on total bone structure, not on each bone part, this may not introduce a significant problem.

The structural and conformational changes in mineral, matrix, crystallinity, proteins and lipids of bone tissues, were investigated by ATR-FTIR spectroscopy and the possible variations in the secondary structure of bone proteins were determined by Neural Network (NN) analysis. Moreover, cluster analysis was performed to classify the control and high- and low-dose Simvastatin-treated

groups based on the spectral differences. Drug-induced mechanical changes on bone tissues were also clarified by Vickers microhardness tests. Studying with drug-treated healthy Wistar animal group and comparing it with healthy control, enables to determine the effects of the drug without interfering with any disease state.

Clinically relevant simvastatin doses vary depending on the studied animal model. Since rat and mouse models metabolize statins more rapidly than humans, higher doses are required for these animals to access similar effective doses in humans (von Tresckow et al., 2007; Youssef et al., 2007). In the previous studies, it was reported that high therapeutic simvastatin doses in humans correspond to 50–100 mg/kg/day dose in rats (Cartier et al., 2000; Johnson-Anuna et al., 2005; Thelen et al., 2006; Marcoff and Thompson et al., 2007) and 50–202 mg/kg/day dose in mouse (Newman and Hulley 1996; von Tresckow et al., 2007; Golledge et al., 2010). Therefore in the current study, the simvastatin dose used as 50 mg/kg/day for rats is in the lower limit of high dose and corresponds to a clinically relevant dose of simvastatin.

3.2.1 ATR-FTIR Spectroscopy Study

To prove the efficacy of treatment with simvastatin, the total serum cholesterol level of the rats was measured. After 30 days, plasma cholesterol levels were measured as 132.00 ± 22.35 $\mu\text{g/ml}$ ($p < 0.05$) for low dose simvastatin-treated rats and as 122.50 ± 25.04 $\mu\text{g/ml}$ ($p < 0.01$) for high dose simvastatin-treated rats both of which were significantly lower than that of the control group (171.40 ± 16.96 $\mu\text{g/ml}$) (Ozek et al., 2009; Garip et al., 2010a).

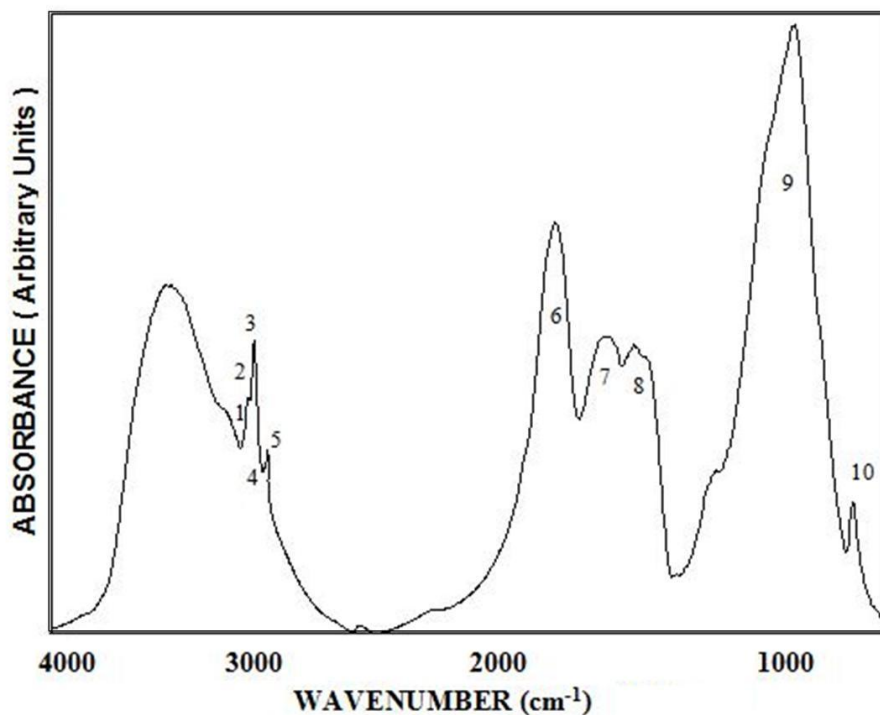


Figure 3.28 A typical FTIR spectrum of a rat tibia in the 4000-750 cm^{-1} region.

Figure 3.28 shows a typical FTIR spectrum of a rat tibia in the 4000–750 cm^{-1} region. This spectrum consists of several bands due to the different functional groups of macromolecules, such as lipids, carbohydrates and proteins. The assignments of these bands are given in Table 3.9. The spectral analyses were performed in two main spectral ranges corresponding to 3030–2840 and 1750–750 cm^{-1} .

Table 3.9 General band assignment of bone tissue between 3030-750 cm^{-1} wavenumber region.

	Wavenumbers (cm^{-1})	Definition of the spectral assignment
1	3012	Olefinic=CH stretch: lipid (mainly unsaturated) (Liu et al., 2002; Cakmak et al., 2012)
2	2959	CH_3 asym. stretch: lipids, protein side chains (Szalontai et al., 2009; Garip et al., 2010a)
3	2927	CH_2 asym. stretch: mainly lipids, with a small contribution from proteins, carbohydrates, nucleic acids (Garip et al., 2010a)
4	2876	CH_3 sym. stretch: mainly proteins, with a small contribution from lipids, carbohydrates, nucleic acids (Ozek et al., 2009)
5	2857	CH_2 sym. stretch: mainly lipids, with a small contribution from proteins, carbohydrates, nucleic acids (Garip et al., 2010a)
6	1657	Amide I (protein C=O stretching) (Krafft et al., 2004; Aksoy et al., 2012)
7	1541	Amide II (protein N-H bend, C-N stretch) (Kneipp et al., 2000)
8	1452	CH_2 Bending: lipids (Toyran et al., 2006; Garip et al., 2010a)
9	1200-900	$\nu_1, \nu_3 \text{PO}_4^{3-}$ stretching: mineral (Boskey et al., 2005)
10	890-850	$\nu_2 \text{CO}_3^{2-}$: mineral (Boskey and Mendelsohn, 2005)

Figure 3.29A shows the spectra of control, 20mg and 50mg simvastatin-treated groups between $3030\text{--}2840\text{cm}^{-1}$ wavenumber region. In this region, the band at 3012cm^{-1} is due to C–H stretching mode of HC=CH groups within the olefinic molecules. This band gives the information about the diverse degrees of unsaturation in lipids (Kneipp et al., 2000; Garip et al., 2010a; Cakmak et al., 2012).

The CH_2 symmetric stretching bands are mainly due to lipids and CH_3 asymmetric band arises from the equal contribution of proteins and lipids. The CH_3 symmetric stretching band is mainly due to proteins (Carmona et al., 2008). The lipid and protein bands in this region result from the organic matrix part of the bone tissue (Daglioglu et al., 2010). Figure 3.29B shows the infrared spectra of control, 20mg simvastatin and 50mg simvastatin-treated groups in $1750\text{--}750\text{cm}^{-1}$ region. There are several bands due to proteins, lipids (organic components of the bone tissue) and carbonate, phosphate (inorganic mineral components of the bone tissues) molecules in this spectral region. (Boyar et al., 2004; Boskey and Mendelsohn, 2005; Daglioglu et al., 2010). The functional groups focused on this region are amide I (1650cm^{-1}), which corresponds to the C=O stretching vibration of proteins (Clarke and Mills, 2006), ν_1 , ν_3 phosphate ($1200\text{--}900\text{cm}^{-1}$) and ν_2 carbonate ($890\text{--}850\text{cm}^{-1}$).

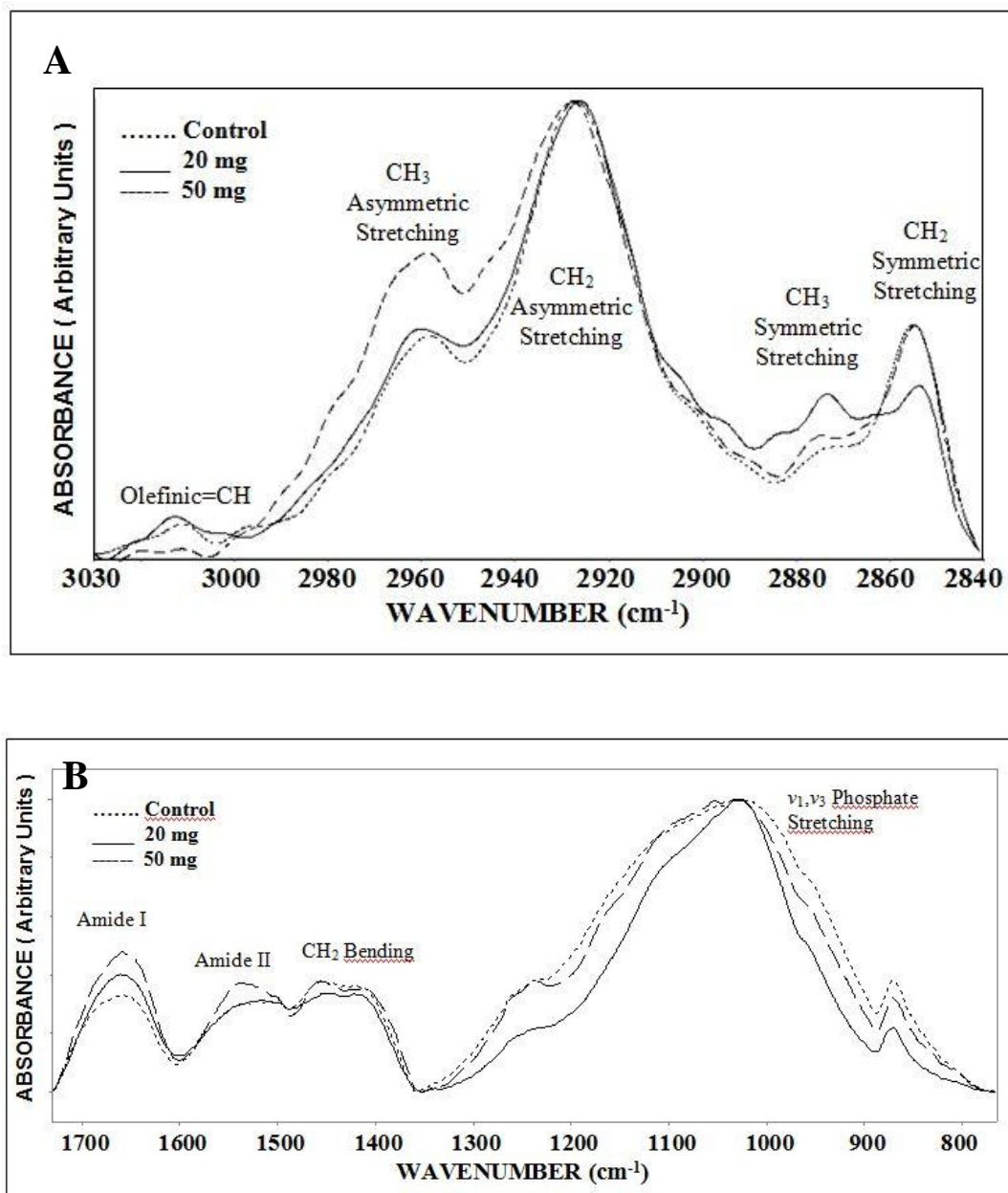


Figure 3.29 The average spectra of control, 20 mg and 50 mg simvastatin-treated groups in (A) 3030-2840 cm⁻¹, (B) 1700-750 cm⁻¹ region (CH₂ asymmetric stretching band was used for normalization process).

3.2.1.1 The Effects of Low and High Dose Simvastatin on Bone Mineral

In FTIR spectroscopy, the concentrations of the functional groups belonging to macromolecules were determined by measuring the band area or intensity of related absorption bands (Garip et al., 2007; Ozek et al., 2009). In the bones of both low and high dose of drug-treated rats, mineral-to-matrix ratio increased significantly respect to the control ($p < 0.001$) (Table 3.10). Moreover, as seen from Table 3.10, the relative carbonate content ($p < 0.05$) and carbonate-to-amide I ratio ($p < 0.001$) significantly decreased for both drug-treated groups respect to the control group. Determination of the variations in the phosphate band is useful for investigating the alterations in the hydroxyapatite crystallinity of bones (Boskey and Mendelsohn, 2005). Therefore, to gain information about crystallinity in the ν_1 , ν_3 phosphate domain, curve-fitting analysis was carried out. Figure 3.30 shows the underlying peaks as obtained by curve-fitting analysis of the ν_1 , ν_3 phosphate region for control and simvastatin-treated groups. For both 20mg and 50mg simvastatin-treated groups, this ratio was significantly higher ($p < 0.001$) than the control (Table 3.10).

As a summary, both 20mg and 50mg simvastatin treatment increased mineral content while the relative carbonate content and crystallinity were decreased. These results implies a more strengthened bone respect to the control group. However, low dose simvastatin therapy was much more affected in increasing bone strength, since the variations were bigger than the high dose simvastatin group when compared to the control.

Table 3.10 The band area ratios of some functional groups in control (n=10), 20mg and 50mg simvastatin-treated groups.

Band Area Ratio	Control (n=10)	20mg (n=10)	P value	50 mg (n=10)	P value
Lipid-to-protein (CH ₂ symmetric stretching/CH ₃ symmetric stretching)	5.85 ±0.80	0.68 ±1.00	<0.001***	10.8 ±0.90	<0.001***
Lipid-to-protein (CH ₂ symmetric stretching/amide I)	0.04 ±0.01	0.01 ±0.01	<0.001***	0.06 ±0.01	<0.001***
Mineral-to-matrix (ν ₁ , ν ₃ phosphate stretching/amide I)	2.58 ±0.05	3.50 ±0.03	<0.001***	3.15 ±0.03	<0.001***
Relative carbonate content (ν ₂ carbonate-to- ν ₁ , ν ₃ phosphate stretch.)	0.07 ±0.01	0.03 ±0.01	<0.05*	0.05 ±0.01	<0.05*
Carbonate-to- amide I (carbonate to amide I)	0.22 ±0.03	0.10 ±0.05	<0.001***	0.15 ±0.02	<0.001***
Crystallinity (1030/1020)	3.49 ±0.50	1.40 ±1.00	<0.001***	1.18 ±1.00	<0.001***

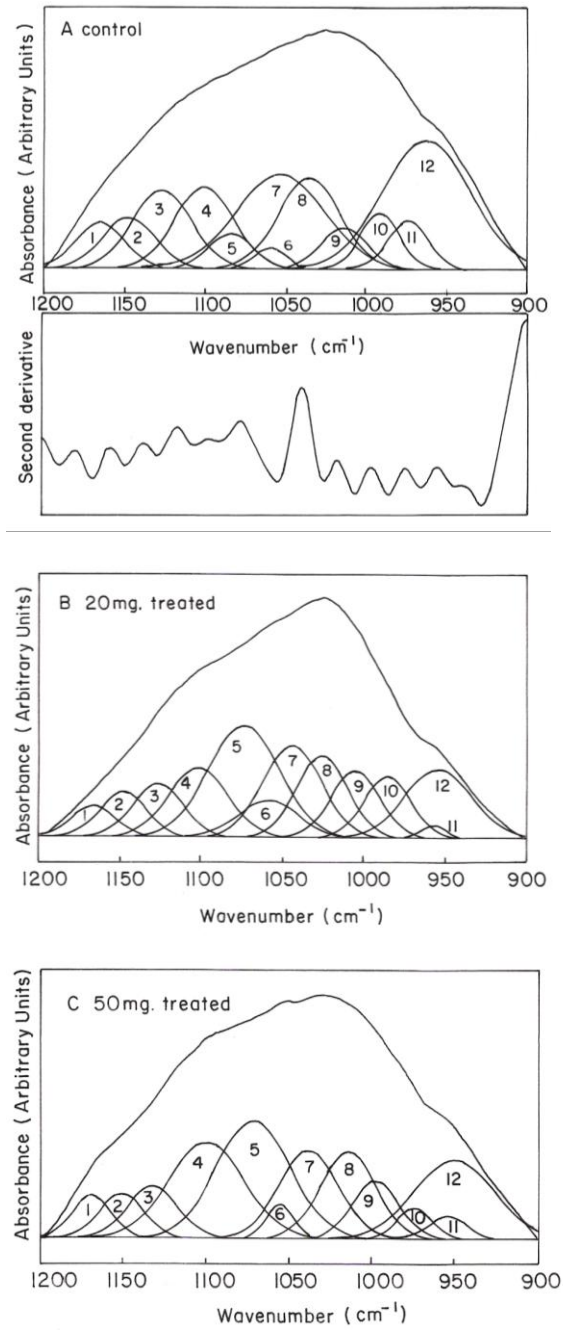


Figure 3.30 Curve-fitting analysis of the ν_1, ν_3 phosphate stretching band (1200-900 cm^{-1}) of **A)** control, **B)** 20 mg simvastatin treated, **C)** 50 mg simvastatin treated groups.

3.2.1.2 The Effects of Low and High Dose Simvastatin on Bone Lipids

The area of the olefinic band at 3012cm^{-1} increased in 20 mg simvastatin-treated group ($p < 0.01$), where in 50 mg treated-group, the olefinic band almost disappeared implying a decrease in the unsaturation level (Figure 3.31 and Table 3.11). The area of the CH_2 symmetric stretching band located at 2853cm^{-1} , which gives information about the lipid content, was lower for the low dose of simvastatin-treated group ($p < 0.01$), while it was higher for high dose-treated group ($p < 0.001$) in comparison to control (Figure 3.31, Table 3.11). This result was further supported by a significant variation ($p < 0.01$) in the area of the CH_2 bending (mainly lipids) at 1452cm^{-1} .

As seen from Figure 3.31, in between $3030\text{--}2840\text{cm}^{-1}$ wavenumber region, the frequency of one of the lipid bands; CH_2 asymmetric stretching shifted to lower values for low dose ($p < 0.001$) and to higher values for high dose ($p < 0.001$) simvastatin treatment when compared to the control (Table 3.11). The alteration in the frequency of this lipid band shows the order/disorder level (flexibility of acyl chains) of the membrane lipids. Thus, the higher values of frequency in high dose treatment implies an more disordered membrane structure via increasing in gauche conformers of fatty acyl chains (Garip et al., 2010a). Moreover the half-bandwidth of this band informs about the fluidity of the membrane (Akkas et al., 2007). The halfbandwidth value of the CH_2 asymm. stretch. band decreased to lower values in 20 mg treated group ($p < 0.001$) implying a lower fluidity of membrane, while the value increased in 50 mg treated group ($p < 0.01$) which implies a higher fluidity of membrane when compared to the control (Table 3.11).

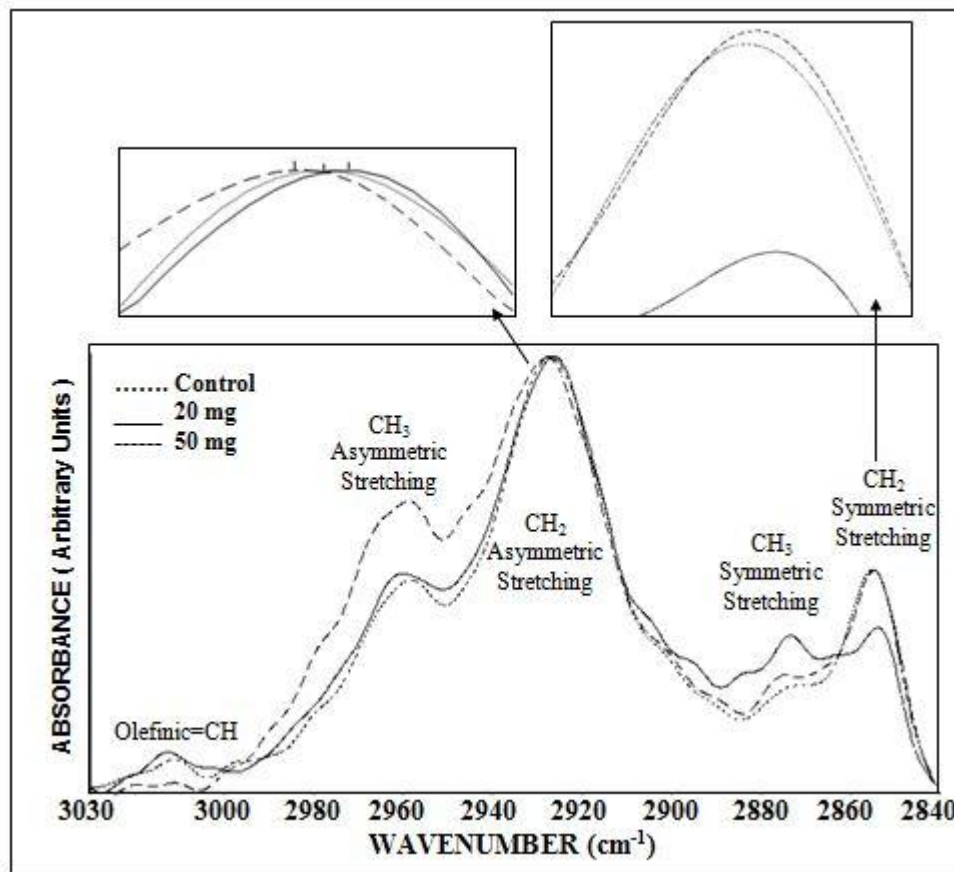


Figure 3.31 The average spectra of control, low dose and high dose simvastatin treated groups between 3030-2840 cm⁻¹ wavenumber region (CH₂ asymm. stretch. band was used for the normalization process). The frequency shift in CH₂ asym. stretch. band and area difference in CH₂ sym. stretch. band were shown in separate windows for better representation.

As a summary, low dose and high dose simvastatin treatment had opposite effects on bone membrane lipid molecules. High dose simvastatin treatment resulted in more disordered membrane structure, while low dose drug treatment enhance more ordered structure in bone membrane. Moreover, in low dose-treated bones,

there was a lower membrane fluidity, while there was a higher membrane fluidity in high dose group, compared to the control.

Table 3.11 The band frequency, area and half-bandwidth values of some functional groups in control, 20mg and 50mg simvastatin-treated groups.

Functional groups	Frequency				
	Control (n=10)	20mg treated (n=10)	P value	50 mg treated (n=6)	P value
CH ₂ asym. stretch.	2927.02 ±0.50	2925.12 ±0.30	<0.001***	2928.34 ±0.30	<0.001***
Amide I	1667.32 ±1.00	1662.75 ±0.50	<0.001***	1659.98 ±0.50	<0.001***
Area					
Olefinic=CH stretch.	0.53 ±0.30	0.90 ±0.20	<0.01**	-	-
CH ₂ sym. stretch.	0.05 ±0.01	0.02 ±0.01	<0.01**	0.08 ±0.01	<0.001***
CH ₃ sym. stretch.	0.41 ±0.30	0.59 ±0.80	<0.001***	0.45 ±0.20	<0.001***
Amide I	11.64 ±0.30	30.87 ±1.00	<0.001***	12.88 ±0.60	<0.05*
Amide II	3.53 ±0.40	7.05 ±1.20	<0.001***	4.61 ±0.50	<0.001***
CH ₂ bending	0.92 ±0.08	0.79 ±0.10	<0.01**	1.69 ±0.1	<0.01**
Half-bandwidth					
CH ₂ asym. stretch.	1.20 ±0.30	0.90 ±0.20	<0.001***	2.00 ±0.40	<0.01**

3.2.1.3 The Effects of Low and High Dose Simvastatin on Bone Proteins

As can be seen from Figure 3.31 and Table 3.11, the area of the CH₃ sym. stretch. band at 2873cm⁻¹, which originates from proteins, increased both in 20mg and 50mg drug-treated groups respect to control (p<0.001). This increase in protein content was further supported by a significant increase (p<0.001) in the area of the Amide I (1667cm⁻¹) and Amide II (1546cm⁻¹) bands, which arise from proteins (Kneipp et al., 2000; Krafft et al., 2004; Aksoy et al., 2012; Garip et al., 2010a). The value of lipid/protein ratio decreased for 20mg simvastatin-treated group (p<0.001), while an increase was observed for 50mg simvastatin-treated group (p<0.001) respect to the control (Table 3.10). This may be due to a decrease in lipid concentration in low dose treatment and an increase in lipid concentration in high dose treatment, since the protein content in both groups increased.

3.2.1.3.1 Protein Secondary Structure

For determination of simvastatin induced variations on protein secondary structure of bone tissues, the protein region, corresponding to absorption values between 1600 and 1700 cm⁻¹ was analysed using NN analysis based on FTIR data. The results are presented in Table 3.12. As seen from the table, simvastatin treatment caused a significant increase in alpha helix structure in both doses. Moreover, significant increase in beta sheet and random coil structures were observed in high dose simvastatin-treated group while there was only a significant decrease in beta-sheet and random coil structures in low dose simvastatin-treated group.

Table 3.12 The results of the neural network predictions based on FTIR data in 1600–1700 cm^{-1} spectral region (Amide I band) for control, 20mg and 50mg simvastatin-treated groups.

Functional Groups	Control (n=10)	20 mg Treated (n=10)	50 mg Treated (n=10)
α-helical structure	13.40±0.63	18.74±1.00*	14.49±1.03
β-sheet structure	49.98±0.98	48.16±0.44*	51.87±0.68*
Turns	24.28±0.8	23.06±0.50*	19.81±0.4*
Random coil structure	12.34±0.74	10.04±0.60***	13.83±1.10*

Since the neural network (NN) analysis gives the amount of total β -sheet structure, further determination of the changes in β -sheet structure was performed with the vector normalization of second derivative spectra of the amide I band in the 1700–1600 cm^{-1} region. Figure 3.32 shows the second derivative spectra of control and simvastatin-treated groups. Since the peak maximum of the amide I band occurs at different frequencies for each secondary structure element, the discrete types of secondary structures in proteins can be identified by the peak maximum of the sub-bands which locate at different frequency values (Ozek et al., 2009; Garip et al., 2010b). The bands at 1655 cm^{-1} and 1637 cm^{-1} are attributable to α -helical and β -sheet structures, respectively. The band located at 1642 cm^{-1} is assigned to random coil structure (Backes and Howard, 2007; Garip et al., 2010a; 2010b). As seen from Table 3.13, the peak intensity values of α -helical structures increased for both low and high dose of simvastatin-treated groups ($p < 0.001$). Moreover, the intensity values of antiparallel beta-sheet structure at 1690 cm^{-1} , aggregated beta-sheet structure at 1629 cm^{-1} showed a significant increase and β -sheet structure at 1638 cm^{-1} showed a significant decrease in high dose of simvastatin treatment, while there was no significant difference in low dose of simvastatin treatment compared to the control treatment. In addition, the intensity of the random coil

band at 1642cm^{-1} decreased in the low dose of drug-treated group while an increase was observed in the high dose of drug-treated group respect to control ($p<0.001$). These results were in agreement with neural network analysis. Increased in the total value of β -sheet structure was observed, since there was an increase in antiparallel and aggregated β -sheet while there was a decrease in β -sheet structure at 1637cm^{-1} .

Table 3.13 The results of the changes in the intensity values of protein secondary structures for control, 20mg and 50mg simvastatin-treated groups

Functional Groups	Control (n=10)	20mg Treated (n=10)	50mg Treated (n=10)
α -helical structure (at 1658cm^{-1})	0.134 \pm 0.012	0.173 \pm 0.010*	0.169 \pm 0.013*
β -sheet structure (at 1638cm^{-1})	0.123 \pm 0.008	0.117 \pm 0.009	0.100 \pm 0.009*
Antiparallel β -sheet structure (at 1690cm^{-1})	0.038 \pm 0.006	0.029 \pm 0.006	0.059 \pm 0.006*
Aggregated β -sheet structure (at 1628cm^{-1})	0.190 \pm 0.009	0.178 \pm 0.009	0.228 \pm 0.009*
Random coil structure (at 1645cm^{-1})	0.293 \pm 0.017	0.226 \pm 0.022***	0.330 \pm 0.022*

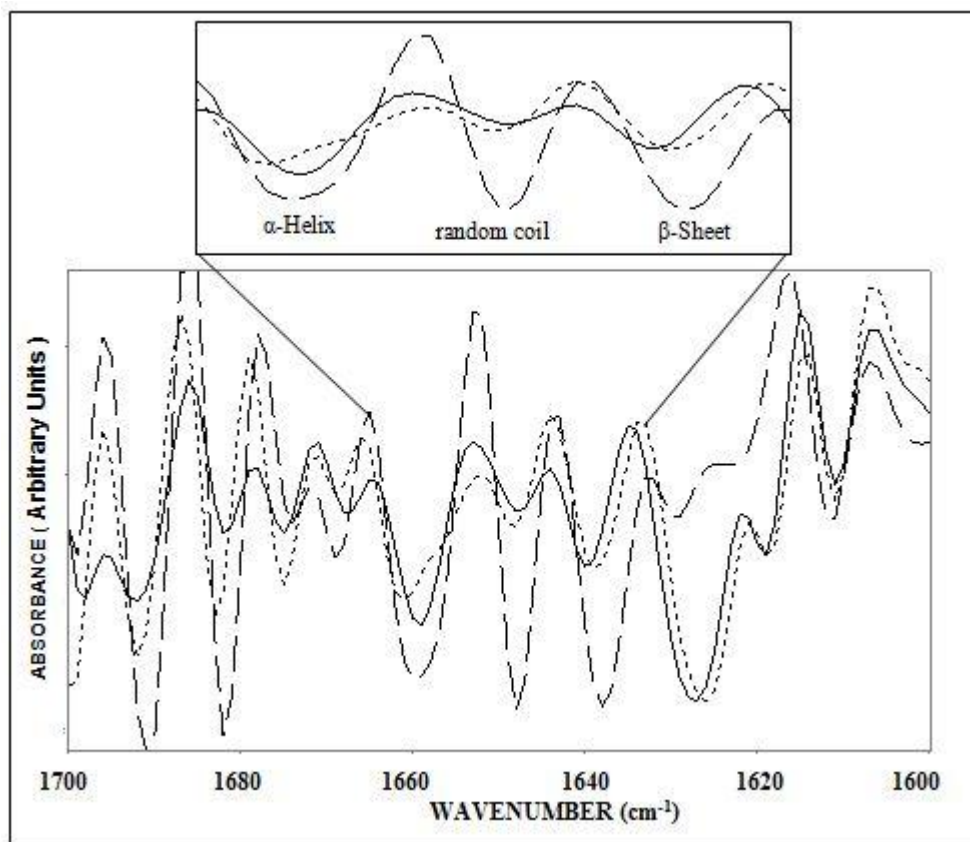


Figure 3.32 The second derivative average spectra of control (dotted spectrum), low dose (solid spectrum) and high dose simvastatin-treated (dashed spectrum) groups between 1700-1600 cm^{-1} wavenumber region.

Finally, based on FTIR data, the three groups were classified via hierarchical cluster method in both the 3050–2800 cm^{-1} and 1800–450 cm^{-1} wavenumber regions with a 100% success (Figure 3.33).

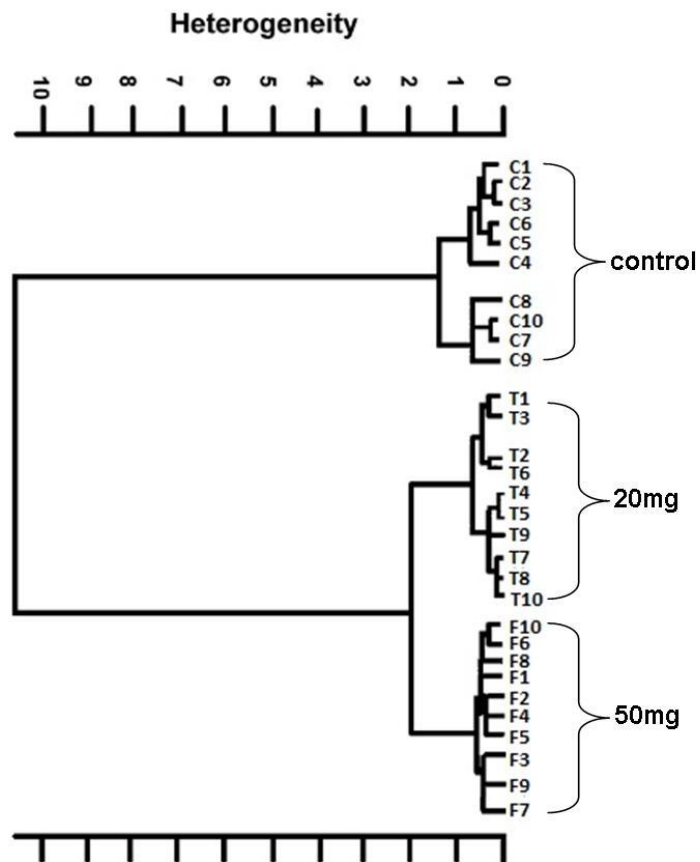
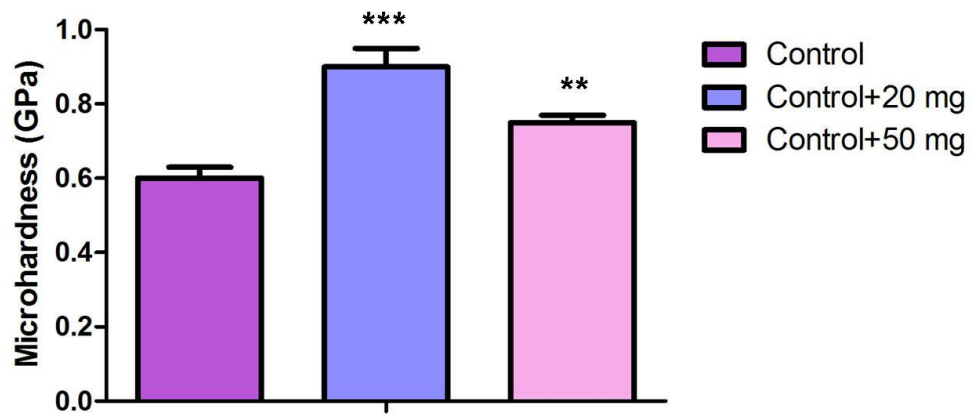


Figure 3.33 The dendrogram of hierarchical clustering with control (C), 20mg simvastatin-treated (T) and 50mg simvastatin-treated (F) groups applied using first derivative spectra and Ward's algorithm. Analysis was performed in the 3050–2800 cm^{-1} and 1800–450 cm^{-1} spectral regions.

3.2.1 Vickers Microhardness Study

The results of microhardness measurements for tibia bone tissues were given in Figure 3.34. As seen from the figure, the microhardness values of both low and high dose simvastatin treated bones were higher than the untreated healthy controls. However, the most severe increase in hardness was observed in low dose drug-treated group compared to the healthy group.



■ ■
Figure 3.34 The hardness values of control, 20 mg and 50 mg simvastatin-treated groups (** $p \leq 0,01$; *** $p \leq 0,001$).

CHAPTER 4

DISCUSSIONS

There are controversial results about the effects of carbamazepine on bone tissues. Moreover, the exact mechanisms for possible effects of this drug on bone, have not been determined yet. Therefore, to contribute resolving these discrepancies, the current thesis investigated the possible side effects of this anti-epileptic drug; Carbamazepine on different bone tissues of healthy and epileptic rats. As a comparative study, the current thesis also investigated the possible adverse and/or pleiotropic effects of another commonly used, well-known cholesterol lowering drug; Simvastatin on bone tissues of healthy rats in a dose-dependent manner.

4.1 Study 1: The Effects of Carbamazepine on Bone Tissues

In the first study, the possible side-effects of Carbamazepine and epileptic seizures on bone tissues of genetically epileptic and healthy rats were investigated to determine the drug- and/or disease-related structural and mechanical changes of bones and to clarify their action mechanism on bone and vitamin D metabolism by FTIR and SR-FTIR microspectroscopy, AFM, micro- and nano-hardness tests, ELISA and western blot analysis. The current study provides the first report of elucidating of the effects of epileptic seizures from the effects of anti-epileptic drug therapy on bone tissues of epileptic and healthy systems. Moreover, it would shed light on the action mechanism of both carbamazepine and epileptic seizures on bone and vitamin D metabolism. In this study we used a genetically epileptic animal model (WAG/Rij rats) which closely resemble the model of genetically

induced absence epilepsy in humans (Coenen et al., 2003; Midzyanovskaya et al., 2004) among the other models. The comparison of epileptic rats with control healthy rats gives information about the effects of epilepsy and epileptic seizures alone. Moreover, since carbamazepine is also used in the treatment of a number of neurological disorders such as bipolar disorder (Colvin et al., 2008), its effect on non epileptic healthy rats was compared with non-treated healthy controls to get information about the effects of the drug in a non-diseased state.

4.1.1 Carbamazepine and Epileptic Seizures Change Bone Mineral and Matrix Composition

The features of bone that determine its mechanical strength are its geometry, composition and its material properties (Bouxsein M.L., 2004) including. mineral content, matrix composition and crystal sizes (Blank et al., 2003; Boskey et al., 2006). These material properties can be investigated by IR microscopy and IR microscopic imaging.

Bone mass is also of great importance in the clinical field, but does not provide information about the quality of bone mineral or bone matrix (Paschalis et al., 1997). Moreover, the study of bone chemistry is complex because different anatomical sites such as cortical and trabecular bones reply differently to diseases and drugs (Jerome et al., 1997; Huang et al., 2003). To study these different responses, traditional biochemical analysis with homogenized bones are not adequate, and microscopic examination of different parts of bone tissue is essential.

The mineral content (mineral/matrix ratio) is important for mechanical strength in bones and the decreased content would make the bones weaker (Ling et al., 2005). In the present study, bone mineral content was calculated by taking the band area

ratio of phosphate band (either ν_1 , ν_3 phosphate or ν_4 phosphate) to Amide I (protein band). The IR parameter called mineral/matrix ratio is correspond to “ash weight,” and provides information about mineralization in the bones (Boskey and Mendelsohn, 2005; Faibish et al., 2005; Gourion-Arsiquaud et al., 2009). In both seizure and Carbamazepine groups, mineral content drastically decreased in all parts of tibia, spine and femur bone tissues. In previous studies, it was reported that the mineral/matrix ratio, i.e. the mineral content, decreased in osteoporotic tissues (Gadaleta et al., 1996; Huang et al., 2003; Leeming et al., 2009). In the study of Bohic et al. (2000) with ovariectomized monkeys, it was noted that decreased mineral/matrix ratio is both a characteristic of immature bone and an indication of osteoporosis. It was reported that the significant decrease in mineral-to-matrix ratio is persistent with the general osteoporotic phenotype which was previously observed by μ -CT analysis (Ueki et al., 2007; Wang et al., 2010). Vitamin D deficiency has been related to the pathogenesis of osteoporosis and fractures (Binkley et al., 2009). Since vitamin D is known to regulate collagen synthesis as well as mineral ion transport, and expression of the vitamin D dependent EMPs, all of these may contribute to the observed decreased mineral content in epileptic and carbamazepine-treated groups.

Biological hydroxyapatite is a poorly crystalline carbonate (Gourion-Arsiquaud et al., 2009). In bone spectra, there are three sub-bands of ν_2 CO_3^{2-} band namely, Type A (878 cm^{-1}), Type B (871 cm^{-1}), and labile (866 cm^{-1}) carbonate (Rey et al., 1991). Type A and Type B carbonates substitute for OH^- and PO_3^{4-} respectively in the hydroxyapatite crystals (Elliot et al., 1995). By curve-fitting the ν_2 CO_3^{2-} infrared band, the carbonate substitution was examined for control, epileptic and drug-treated bone samples. In the current study, the carbonate/phosphate ratio significantly decreased in epileptic and carbamazepine-treated groups. Further analysis of different carbonate types in the bone tissues showed that the B type carbonate which substitutes for phosphate in the mineral crystals increased. On the

other hand, the A type (substitutes for hydroxide in the mineral) and L type (labile) carbonate decreased in both epileptic and drug-treated groups for all bone tissues. This implies that the carbonate substitution in the hydroxyapatites increases. It was previously reported that the carbonate content was higher in the hydroxyapatite crystals in osteoporosis (Faibish et al., 2006), reflecting the accumulation of older tissue. The high concentration of labile carbonate implies the higher level of the unstable carbonate in young bone. "As bone matures and average crystal size increases, the CO_3^{2-} ions settle into the two anionic sites of the apatite structure, where the overall degree of substitution is highly dependent upon many factors, such as bone species, strain, and type" (Gourion-Arsiquaud et al., 2009). The observation that carbonate content is increased in this study suggests that there is either an impaired mineralization due to vitamin D deficiency or excessive bone turnover.

The collagen cross links are necessary for the proper structure and mechanical features of bones. Cross link variations may result in severe disorder in tissues and it has been suggested that the composition of bone collagen is altered in bone disorders (Otsubo et al., 1992; Knott et al., 1995; 1998; Viguet-Carrin et al., 2006; Gourion-Arsiquaud et al., 2009; Leeming et al., 2009). The distinct features of bone (type I) collagen are its cross-linking chemistry and its molecular packing structure (Nagata et al., 2003). Collagen cross links are essential for mineralization and growth of the hydroxyapatite crystals. Collagen matrix is also related with mechanical features including tensile strength and viscoelasticity (Leeming et al., 2009). IR parameter called collagen cross links ratio, gives information about the maturity of cross links in collagen fibrils (Paschalis et al., 2001; 2003). The collagen crosslink ratio results, demonstrate that collagen crosslinks in the bones of epileptic and carbamazepine-treated groups decreased compared to the control group in the current study. In a recent study (Levasseur R., 2009), a condition called homocysteinuria in which homocysteine interferes with collagen crosslink

formation was associated with spontaneous bone insufficiency fractures. In another study (Viguet-Carrin et al., 2006), the formation of collagen crosslinks was chemically inhibited and the bone strength decreased despite “normal mineralization”. Boyar et al. (2004), studied the effects of chronic hypoperfusion on rat bone and reported that 1660/1690 cm^{-1} intensity ratio which reflects the collagen maturation and crosslinks, significantly decreased in hypoperfusion resulting in less mature collagen cross links. Disorders in collagen maturation might affect the mineralization and may result in bone defects (Boyar et al., 2004).

Hydroxyapatite (HA) crystal size provides important information about bone structure. It is well established from the ν_1 , ν_3 PO_4^{3-} ($950\text{-}1200\text{ cm}^{-1}$) that the crystals in newly formed bone mineral is mainly nonstoichiometric with high levels of labile carbonate (CO_3^{2-}) and acid phosphate (HPO_4^{2-}) (Cazalbou et al., 2004; Paschalis et al., 2006). As bone ages or matures, the crystals become more stoichiometric with higher crystal size and perfection (Barry et al., 2002; Farlay et al., 2010). The crystal size (perfection) or crystal maturity can be determined from IR data by taking the ratio of two sub-bands at 1030 and 1020 cm^{-1} . The band at 1030 cm^{-1} , has been assigned to vibrational mode of the PO_4 groups in stoichiometric apatite (Rey et al., 1991; Farlay et al., 2010). The 1020 cm^{-1} band has been associated with non-stoichiometric, miserably crystalline apatite and is present at early mineralization (Termine and Posner, 1966; Boskey and Mendelsohn, 2005).

In the current study, both the epileptic and carbamazepine-treated groups had higher 1030/1020 cm^{-1} ratio, indicating a greater crystal size and perfection in all bone types. Recent studies (Rubin et al., 2003; Benhamou et al., 2007; Gourion-Arsiquaud et al., 2009) suggested that osteoporotic patients also contain larger apatite crystals which negatively affect the mechanical properties of bone tissues. It was reported that increased bone mineral particle size is associated with

increased bone fragility (Gourion-Arsiquaud et al., 2009). Bone hydroxyapatite crystals are very small, allowing a high numbers of electrostatic bonds between mineral and collagen matrix. The ordered orientation of small hydroxyapatite crystals are important for the the rigidity and strength of bone tissues and also provides flexibility without the risk of fracture in the tissue (Landis W.J., 1995; Glimcher, M.G., 1998). The presence of larger crystals cannot provide mechanical strength since the surface area is decreased with collagen fibrils (Chachra et al., 1999; Farlay et al., 2010).

Some x-ray diffraction studies with vitamin D deficient animal models (Donnelly et al., 1993; Said et al., 2008) reported that crystallite size and perfection were increased in osteomalacic bones and rachitic cartilage as compared with healthy controls. Thus in the current study, increases in crystal size of epileptic and drug-treated bones may exist because the younger smaller crystals have been excessively resorbed (osteoporosis) or because formation of new mineral is impaired due to vitamin D deficiency and thus the existing crystals grow rather than forming new ones.

Consequently, variations on bone mineral and matrix composition (decreased mineral content, larger crystals, increased carbonate substitution, decreased collagen crosslinks) in both epileptic and carbamazepine-treated groups, may due to the either excessive bone turnover or impaired mineralization due to vitamin D deficiency. In FTIRM studies, according to the degree of variation and significance between the calculated parameter values, the spine tissue was found to be the most affected bone tissue from both epileptic seizures and anti-epileptic drug treatment.

4.1.2 Carbamazepine and Epileptic Seizures Decrease Bone Hardness and Surface Roughness

Micro- and nano-hardness tests enable the study of the correlation between the bone structure and the mechanical features of the bone at a micro- and nanostructural scale, respectively (Morra et al., 2009). A mineral content which exceeds a limited value makes bones more brittle while the low mineral content makes them unable to bear loads (Zioupos et al., 2000; Currey et al., 2001). The correlation between mineralization, hardness and elastic modulus has been investigated in tissues previously (Zioupos et al., 2000; Currey et al., 2001). Microhardness of bones are depend on mineralization level but but it does not the only important parameter for the alteration in the tissues. In the current study, lower microhardness and nano-hardness values for both the epileptic and carbamazepine-treated groups may indicate a lower mechanical strength in all bone types (Boivin et al., 2008). In a previous study, it was reported that osteoporotic bones have a loss of mechanical strength (Seeman et al., 2006). In osteoporosis, beside the alteration in mineral content, other parameters of bone mineral and organic matrix have roles in the decrease of mechanical strength (Seman et al., 2006; Mulder et al., 2008).

In the current study, the changes in mineral phase of the bones of epileptic and carbamazepine-treated groups, appeared to affect the hardness more than the elasticity. In the current FTIRM studies, it was shown that both epileptic seizures and drug-treatment affected bone matrix by drastically decreasing collagen crosslink ratio. This drastic decrease in epileptic and carbamazepine-treated bones, did not affect the variation of elastic modulus as much as expected. In previous studies, it was shown that hardness and elastic modulus can be affected independently in mouse bones in the presence of osteocalcin deficiency (Ducy et al., 1996; Kavukcuoglu et al., 2009).

The controversial relationship between structural changes in bone matrix and the variation in elastic modulus parameter can be explained by differences in collagen orientation. The elastic properties of bones can be affected from both the mineral and matrix phases of bone. The main considerations are crystallinity and crystal maturity in the mineral phase (Farlay et al., 2010), while in the matrix phase the level of crosslinking determines the ability to absorb energy in bones independently from mineralization (Saito et al., 2006). However, among these parameters, the orientation of the collagens accounts for the alteration between bone mineralization and material features including hardness and elasticity (Zabaze et al., 2011). In an early study (Martin and Ishida, 1989), it was shown that orientation of the collagen fibers were the main determinants for the alteration in elastic modulus. When mechanical features of the tissues are investigated with samples in which the orientation of collagen fibers are the same, the relation between elastic modulus, hardness and mineralization is greater (Currey, J.D., 1984; Gupta et al., 2005; 2006; Zabaze et al., 2011).

As a summary, both the epileptic seizures and carbamazepine treatment reduced hardness and elasticity of bone samples in micro- and nano-level, implying a reduced bone strength. These results supported the decrease in mineral content and increase in crystal size (perfection) of epileptic and drug-treated groups in FTIRM studies. However, the decrease in elastic modulus in nano-indentation studies could not totally reflect the severe decrease in hardness values and collagen crosslink ratio, since the nano-indentation tests were not carried out by taking into account the orientation of collagen fibers. Moreover, another important finding was that the most affected cortical bone parts were the mid-cortical and endosteum sections.

The current AFM results showed a decrease in surface roughness of both epileptic and drug-treated groups. Moreover, the roughness value of epileptic control group

was lower than healthy control group. This lower roughness value was the effect of epilepsy and seizures alone, without interference from any drug treatment. Drug-treated groups had also lower roughness values than the epileptic and control ones. The most effected animal group in the study was drug-treated epileptic group as also seen in nano-indentation and FTIRM studies. Zhao et al. (2010) investigated the process of collagen-mineralization and measured the hardness and roughness values of mineralized collagen fibrils by using nano-indentation and AFM techniques. They showed that there is a linear correlation between bone hardness and surface roughness. The results reported that as the hardness increased, the surface roughness also increased. Previous AFM studies in the literature which investigated the bone surface roughness, reported that surface roughness is related to higher osteoblast-like cell adhesion (Sato et al., 2006; Satoa et al., 2005). It was suggested that pores, fissures and other topographical features might adsorb proteins that mediate osteoblast adhesion (Webster et al., 2000). Thus, an increase in surface roughness might induce the osteoblast adhesion and bone formation on the samples.

4.1.3 Carbamazepine and Epileptic Seizures Affect PTH Levels and Bone Turnover Differently

25-hydroxyvitamin D levels are determined to indicate whether there is a vitamin D deficiency, sufficiency or intoxication (Holick M.F., 2009). 1,25dihydroxy vitamin D is the active form of 25(OH)D. The serum levels of 25-hydroxy vitamin D and 1-alpha-25-dihydroxy vitamin D significantly decreased in both epileptic and carbamazepine-treated groups compared to the healthy controls. The total serum Ca concentration significantly decreased in both epileptic and carbamazepine-treated groups while there was elevated levels of PTH in drug-treated groups but not in the epileptic group.

PTH and $1\alpha,25$ -hydroxy vitamin D_3 together sustains calcium homeostasis in the serum via increased bone resorption, intestine absorptions of calcium and phosphate, reabsorption of calcium and excretion of phosphate from the kidneys. In the drug-treated groups, decreased serum calcium concentration results in the elevated levels of PTH (Fine et al 1993). Furthermore, there is a feedback loop on PTH production by increasing the concentration of calcium in serum (Herfarth et al 1992a). The elevated levels of PTH stimulates the production of $1\alpha,25(OH)_2D_3$. Moreover, $1\alpha,25$ -hydroxy vitamin D_3 inhibits the transcription of the PTH gene, independently (Holick 1994). In the current study, besides the decreased calcium and elevated PTH level in drug-treated groups, there was a reduction in both $25(OH)D$ and $1,12(OH)D$ serum levels. Thus, it was suggested that there was a low vitamin D levels caused by the effects of the drug on vitamin D metabolism. Although, a decrease in serum calcium levels was observed in epileptic group, there was a slight decrease in PTH levels instead of an increase. Thus, it was suggested that an impaired PTH secretion may be taking place in epileptic rats. In a recent study, it was reported that PTH disorder such as impaired secretion can be the reason for primary hypoparathyroidism in low calcium levels (Loupy et al., 2012). As seen in drug-treated groups, low vitamin D levels may be caused by the effects of epileps and epileptic seizures on vitamin D metabolism.

$1\alpha,25$ -hydroxy vitamin D_3 regulates the development and function of osteoblasts (Franceschni et al 1988, Colvard et al 1989). Thus in the presence of reduced $1\alpha,25(OH)_2D_3$ levels as reported in the current study, bone formation may be affected directly through VDR receptors located on osteoblast cells and decreased in both epileptic and drug-treated groups.

PTH was also shown as a factor which increases bone mineral density and improves bone mechanical strength, when administered intermittently (Ejersted et al., 1993). It increases differentiation of skeletal progenitor cells, osteoblast

activity, and osteoblast survival (Schmidt et al., 1995). PTH binding to the PTH/PTHrP receptors on osteoblast cells induces an interaction between receptor and G proteins and the production of cAMP and induction of several kinases (Radeff et al., 2004). This mechanism has been described in detail in Section 1.1.2.2 of the "Introduction" chapter.

Both 1-alpha-25-hydroxy vitamin D and PTH increases the osteoclast number and activity, and thus also increases bone resorption by stimulating the expression of RANKL in osteoblasts, which favors the osteoclast differentiation and bone resorption (Bingham et al 1969). The detailed description of this pathway is given in Section 1.1.2.1 of "Introduction" chapter.

As a summary, changes in PTH and 1-alpha-25-hydroxy vitamin D levels in drug-treated groups may induce bone turnover by increasing and decreasing bone formation and resorption. In the epileptic group, since there was not any significant change in PTH levels, low levels of 1-alpha-25-hydroxy vitamin D may have resulted in low bone formation.

Carboxy terminal collagen crosslinks (CTX), as a marker of bone resorption, is related to collagen breakdown. Osteocalcin (OC) and BAP as bone formation markers, are osteoblast-related proteins. These bone turnover markers showed elevated levels in the drug-treated groups, while a slight increase was observed in bone turnover markers in the epileptic group.

Consequently, carbamazepine drug treatment induces bone turnover in both epileptic and healthy rats, while no significant change was seen in epileptic group compared to the control. Since the only difference between drug-treated and epileptic group according to blood parameter levels (except turnover markers), was the different PTH levels, it may be suggested that elevated PTH play a role in

increasing bone turnover by carbamazepine treatment. High bone turnover explains the conformational changes in bone mineral and matrix composition including decreased mineral content, increased carbonate substitution and higher crystal size in drug-treated groups. However, these compositional changes were also observed in epileptic group compared to the control with a less significance than the drug-treated groups. Thus, in addition to low vitamin D levels, there may be another mechanism by which epilepsy and epileptic seizures affect bone structure and strength. Further studies are essential to make clear this unexplained mechanism.

4.1.4 Carbamazepine and Epileptic Seizures Increase the Protein Levels of Vitamin D Catabolism Enzyme

After absorption or production from precursor, Vitamin D is converted to 25OHD by CYP27B1 in the liver. Then, 25OHD is converted to the active form 1α -25(OH)₂D by CYP27A1 in the kidneys (Horst and Reinhardt 1997). 25OHD is also converted to the biologically inactive form; 24,25(OH)₂D by CYP24 in the kidneys. Vitamin D metabolism was explained in detail in Section 1.4 of "Introduction" chapter.

As mentioned in the previous subsection (4.1.3), both epileptic seizures and carbamazepine treatment decrease serum 25(OH)D and 1,25(OH)D levels. It was hypothesized that carbamazepine causes vitamin D deficiency through the pregnane X receptor (PXR) (Pascucci et al., 2005). DNA binding domain of the vit. D receptor has the sixty percent homology with the domain of pregnane X receptor which is also secreted in intestine, kidneys and liver. Pregnane X receptor was reported to induce the expression of CYP450 enzymes which have roles in the metabolism of drugs. Moreover, pregnane X receptor can be induced by various drugs such as phenytoin, and carbamazepine (Valsamis et al., 2006).

This hypothesized pathway is explained in detail in Section 1.4 of "Introduction" chapter. This hypothesis, however, can not explain the low vitamin D levels in patients administered to VPA therapy which is an inhibitor of CYP450 enzymes and does not activate pregnane X receptor. Thus, If there is another effect of AEDs including carbamazepine on bone and vitamin D metabolism, this point should be clarified.

In the current study, to clarify the action mechanism of carbamazepine on vitamin D metabolism in epileptic and healthy rats and also to determine whether there is an effect of epilepsy and seizures on vitamin D metabolism, the protein levels of vitamin D anabolism (25-hydroxylase and 1- α -hydroxylase) and catabolism (24-hydroxylase) enzymes were calculated by western blot analysis. According to the current results, both epileptic seizures and carbamazepine treatment increase vitamin D catabolism enzyme; 24-hydroxylase (CYP24). Moreover, the protein levels of 25-hydroxylase (CYP27A1) enzyme was also shown to be increased in both epileptic and drug-treated groups.

The increased CYP24 levels induce the catabolism of active vitamin D; 1,25(OH)D to an inactive form 24,25(OH)₂D, thus results in decrease serum levels of 25(OH)D and 1,25(OH)D with vitamin D deficiency in drug-treated groups. This result supports the hypothesis in which carbamazepine causes vitamin D deficiency through the pregnane X receptor (PXR) by increasing the expression of CYP24 (Pascussi et al., 2005). However, an increase in protein levels of CYP27A1 was also observed.

Previous studies showed that PXR mediates induction of the CYP450 enzymes included in the drug metabolism including CYP2C9, CYP2B6 and CYP 3A4 (Li et al., 2007). CYP3A4 is one of the carbamazepine metabolizing enzymes (Kerr et al., 1994). It was reported that 27-hydroxycholesterol (27-HOC) activates LXRA

and induces expression of the cholesterol transporters namely ABCA1 and ABCG1 (Fu et al., 2001; Lund et al., 2003). The steroid and bile acid activated PXR plays a crucial role in regulation of the expression of CYP27A1. This conclusion is supported by two recent reports that ligands for RXR and PPAR γ enhance CYP27A1 expression and 27-HOC production which stimulates LXRA and its target genes, ABCA1 and ABCG1 (Szanto et al., 2004; Quinn et al., 2005). In their study, Li et al., showed that PXR activators induce CYP27A1 gene expression in intestine (Li et al., 2007). In the current study, the increase in protein levels of CYP27A1 can be explained by the activation of PXR receptor by carbamazepine.

Although, there was also an increase in protein levels of CYP27A1 and CYP24 in epileptic animals independent of carbamazepine use, this result can not be explained by the PXR receptor mechanism. There was no known PXR activator in epileptic systems. However, some studies reported a link between PXR polymorphism and drug-resistant human absence epilepsy as discussed below;

Human absence epilepsy is commonly genetical and approximately 1/3 epileptic patients are refractory because of the resistance to AEDs. Previous genetic studies have tried to correlate main genetic variants in the ABCB1 gene to the resistance to AEDs, but the results have been conflicted (Hung et al., 2005; 2007; Seo et al., 2006; Kim et al., 2006; 2009; Lakhan et al., 2009; Shahwan et al., 2007; Kwan et al., 2009; Vahab et al., 2009; Grover et al., 2010; Alpman et al., 2010). It is suggested that "linkage disequilibrium (LD) of the silent C3435T with other ABCB1 variants in a haplotype block may link with resistance to AEDs" (Zimpric et al., 2004).

It was previously shown that ABCB1 gene expression is under the control of PXR. Some studies suggested that PXR gene may be related to response to therapy due

to the essential role of pregnane X receptor in the regulation of ABCB1 gene (Löscher and Potschka, 2005). Thus, PXR polymorphism may play a role in responding AEDs in absence epileptic patients who are resistant to AED treatment. However, this suggestion should be clarified since there is also controversial results about the role of PXR polymorphism in drug response (Haerian et al., 2011).

In the current study, a genetically induced epileptic model; WAG/Rij rats which closely resemble the model of genetically induced absence epilepsy in humans (Luijtelaar and Sitnikova, 2006) among the other models, was used. It is shown that a subgroup of WAG/Rij rats have convulsive audiogenic epileptic seizures besides the non-convulsive epileptic seizures which are called as mixed form of epilepsy (Midzyanovskaya et al., 2004). Mixed epileptic forms are known as commonly resistant to AED treatment. However, in the current study since we used an optimum dose of drug, they responded to the carbamazepine treatment and epileptic drug-treated group did not have convulsive epileptic seizures through the study period (5 weeks). Thus, it was hypothesized that these mixed form epileptic WAG/Rij rats may have ABCB1 polymorphism which results in drug resistance and PXR polymorphism which provides response to AED therapy. This hypothesis may also explain the increased protein levels of CYP27A1 and CYP24 which are PXR induced enzymes, in epileptic rats. There is no study in the literature which reports the ABCB1 and/or PXR polymorphism in WAG/Rij rats.

As a summary, carbamazepine treatment increased the protein levels of both CYP24 and CYP27A1 in kidney by possibly activating the pregnane X receptor (PXR) which regulates expression of the genes involved in the metabolism including CYP24 and CYP27A1. Moreover, epileptic seizures also increased the protein levels of these enzymes. It was hypothesized that WAG/Rij rats which closely resemble the model of genetically induced absence epilepsy in humans,

may have PXR gene polymorphism resulting in the expression of CYP24 and CYP27A1 enzymes. As a result of increased vitamin D catabolism enzyme, serum 25(OH)D and 1,25(OH)D levels were decreased inducing vitamin D deficiency.

Consequently, in the first study of the current thesis, it was found that epilepsy and convulsive seizures caused a decrease in the strength of bone. However, Carbamazepine treatment induce more significant damages than convulsive seizures on epileptic as well as healthy bone tissues. According to the degree of variation and significance between FTIR and biomechanical parameter values, the most affected bone tissue from both convulsive seizures and anti-epileptic drug treatment was the spine tissue. Moreover, the most affected cortical parts in spines, were mid-cortical and endosteum according to SR-FTIR studies. In biochemical studies, a statistically significant elevation was found in PTH and bone turnover markers in the rats receiving carbamazepine treatment, inducing a vitamin D deficiency in drug-treated groups. It was found that Carbamazepin affected vitamin D metabolism by decreasing the levels of the vitamin D catabolism enzyme; 25-hydroxyvitamin D-24-hydroxylase. However, in epileptic group there was no elevated levels of neither PTH nor bone turnover markers. These data suggest that epileptic seizures might alter the skeleton via other mechanisms other than inducing bone turnover. A vitamin D deficiency was also observed in epileptic group. Furthermore, a decrease in the protein levels of 25-hydroxyvitamin D-24-hydroxylase was also found in epileptic group implying a similar effect of epileptic seizures on bone metabolism with the drug.

4.2 Study 2: The Dose-dependent Effects of Simvastatin on Bone Tissues

In the first study of the present thesis, it was reported that Carbamazepine which is used for the treatment of neurological diseases, induced adverse effects on bone tissues. To determine whether the drugs used for the metabolic derangement, have

also adverse effects on bones, another well-known drug; Simvastatin which is commonly used as cholesterol lowering drug, was chosen. As a comparative study, it was aimed to investigate the possible adverse or pleiotropic dose-dependent effects of Simvastatin on bone tissues of healthy rats. Another non-destructive and non-invasive, sensitive and high quality vibrational technique; ATR-FTIR spectroscopy was used for this aim rather than FTIR microspectroscopy, since it provides less cheap and complex experimental procedure and more rapid data acquisition than the FTIRM. By using ATR-FTIR spectroscopy technique, it would not be able to monitor different parts of the bones and to give visual images of bone tissues, as it was done in FTIRM studies. However, it would be able to obtain similar information with FTIRM about the changes in bone mineral and matrix structure of total bone tissue. Thus, ATR-FTIR spectroscopy provides us sensitive information but not as detailed as FTIRM. In the current study, this may not introduce a significant problem since the main point of interest was to investigate the effects of the drug essentially on total bone structure, not on each bone part.

In the second study, the possible dose-dependent effects of Simvastatin on bone tissues were also investigated by micro-hardness tests to determine the drug-related mechanical changes of bones. In the current study, healthy rats were used which are commonly used as animal models to detect only the drug-induced effects without interfering with any disease state (Mucha et al., 2007; Cutuli et al., 2008; Ozek et al., 2009). Low and high dose simvastatin administered to healthy rats to determine the drug-related changes on bone tissue without interfering with any disease state.

4.2.1 Simvastatin Effects Bone Mineral and Matrix Composition

Mineral hydroxyapatite (HA) crystal size provides important information about the bone structure. In both simvastatin-treated groups, the crystal size decreased substantially, implying decreased crystallinity. Recent studies suggested that osteoporotic patients contain larger apatite crystals indicating higher crystallinity value (Durchschlag et al., 2006). The ordered orientation of small hydroxyapatite crystals are important for the the rigidity and strength of bone tissues and also provides flexibility without the risk of fracture in the tissue (Landis W.J., 1995; Glimcher, M.G., 1998). The presence of larger crystals cannot provide mechanical strength since the surface area is decreased with collagen fibrils (Chachra et al., 1999; Farlay et al., 2010). Therefore, decreased crystal size (crystallinity) in simvastatin-treated groups indicates more rigid bone tissues with enough flexibility. Durchschlag et al. (2006) studied bone composite material features of human iliac crest biopsies after 3- and 5-year treatment with an osteoporosis drug (risedronate) by FTIR spectroscopy. In this study, crystallinity value decreased after drug treatment implying an optimal rigidity with flexibility in bone tissues.

The IR parameter called mineral/matrix ratio is correspond to “ash weight,” and provides information about mineralization in the bones (Faibish et al., 2005; Gourion-Arsiquaud et al., 2009). The mineral/matrix ratio was lower for both simvastatin-treated groups. This decreased in mineral/matrix ratio can be the result of the stimulated expression of matrix proteins by simvastatin treatment (Nogaki et al., 2001). Mundy et al. (1999) reported that simvastatin stimulates BMP-2 promoter resulting in the induction of bone formation in an osteoblast cell line. It was hypothesized that "simvastatin may support BMP-induced osteoblast differentiation through antagonizing TNF- α -to-Ras/Rho/MAPK pathway and amplifying BMP-Smad signaling" (Yamashita et al., 2008; 2010; Moon et al.,

2011). The detailed explanation of this pathway is given in Section 1.7.1.1.4 of "Introduction" chapter.

The carbonate substitution and carbonate/amide I ratio decreased in high dose and even more decreased in low dose simvastatin treatment compared to the control. Carbonate can substitute for hydroxyl or phosphate molecules (A-type and B-type carbonate respectively) or it can place on the surface of the crystals (L-type carbonate) in bones (Gourion-Arsiquaud et al., 2009). The low relative carbonate content observed in both low and high dose simvastatin-treated rats, implies that the carbonate substitution in hydroxyapatite crystals is decreasing. It was previously reported that in osteoporosis, the carbonate content was higher in the hydroxyapatite crystals (Faibish et al., 2006), reflecting the accumulation of older tissue. As bone matures and hydroxyapatite crystal size increases, the CO_3^{2-} ions substitute for hydroxyl and phosphate ions in the hydroxyapatite, resulting in an increase in relative carbonate content (Gourion-Arsiquaud et al., 2009).

The decreased carbonate content observed in this study suggests that there is low bone turnover in simvastatin treated groups compared to the healthy controls. While simvastatin stimulates bone formation in a number of ways, it was reported that it also inhibits osteoclast generation in a similar way with some bisphosphonates. Recent studies showed that simvastatin inhibits osteoclast generation by inhibiting the prenylation of certain GTP binding proteins (Rho, Rac, Rab etc.) (Cruz and Gruber, 2002; Jadhav and Jain, 2006) which is explained in detail in Section 1.7.1.1.4 of "Introduction" chapter.

Consequently, both low and high dose simvastatin decrease crystal size and carbonate substitution which results in stronger bones. Moreover, low dose simvastatin decrease these parameters more severely than high dose simvastatin, implying to be more effective in strengthening bones.

4.2.2 High and Low Dose Simvastatin Have Opposite Effects on Bone Lipids and Membrane

Several ion channels including voltage-gated Na⁺, Ca²⁺ and K⁺ channels were shown to present in the osteoblast and osteoclast bone cell membranes. Evidence suggests that bone formation or resorption can be activated by the variations in ion channel activity found on the bone cell membranes (Davidson et al., 1990). Davidson et al. (1990), have also described mechanosensitive ion channels in osteoblast-like cells. Knowledge of the activation of osteoblasts via ion channels is of great importance for identifying new drugs designed to stimulate bone formation (Charras et al., 2004). The ion channels of bone tissues can be affected by the structure and the dynamics of the membrane (Akkas et al., 2007). The changes in the composition of lipids and proteins might also affect the membrane dynamics, which in turn affects membrane potential via ion channel kinetics (Akkas et al., 2007).

The frequency value of the CH₂ asymmetric stretching band of treated groups indicates that membrane structure becomes more ordered in the low dose (20 mg) treated group; the high dose (50 mg) treatment of simvastatin renders the membrane structure into a more disordered state. This disorder might be induced by the increase in lipid peroxidation as reported in the study of McNulty et al. (McNulty et al., 2008). It is also known that the variation in membrane order may alter the function of ion channels (Akkas et al., 2007). Furthermore, decrease of the half-bandwidth value of this band indicates a decrease in membrane fluidity in low dose of simvastatin while the high dose of simvastatin increases it. Broncel et al. (Broncel et al., 2007) also supported these results and found an increase in the fluidity of erythrocyte membrane during high dose of simvastatin treatment. Previously, Ortiz et al. proposed a relation between increased membrane fluidity

and lipid peroxidation in submitochondrial particles of platelets and erythrocyte membranes (Ortiz et al., 2008).

4.2.3 High Dose Simvastatin Induce Lipid Peroxidation

Oxidized lipids have been shown to inhibit osteoblastic differentiation in vitro (Parhami et al., 1999) and in vivo (Parhami et al., 2001). A loss of unsaturation in the high dose simvastatin-treated group was observed. It is well known that the decrease in unsaturation corresponds to an increase in lipid peroxidation (Sills et al., 1994). Lipid peroxidation takes place mainly at the double bonds of polyunsaturated acyl chains resulted in the loss of the olefinic bonds (Sills et al., 1994; Moore et al., 1995). The increase in lipid content calculated from the area of the lipid bands, also supported the lipid peroxidation with a high dose of simvastatin treatment (Newairy et al., 2007). There are contradictory results in the literature about the molecular effects of statins on lipid peroxidation in bone tissues. In the study by Lankin et al. (2003), it was suggested that high dose of pravastatin (40 mg/kg/day) induces an accumulation of LDL lipoperoxides in vivo. Moreover, Mortensen et al. (1997) and Sinzinger et al. (2000) also reported in their studies that low (20 mg/kg/day) and high (40–80 mg/kg/day) dose of lovastatin increases lipid peroxidation. Although the current results are in agreement with these studies (Mortensen et al., 1997; Sinzinger et al., 2000; Lankin et al., 2003) for high dose of simvastatin therapy, a decrease was found in lipid peroxidation for low dose simvastatin therapy, which is in agreement with Broncel et al. (2007) and Koter et al. (2003). High dose treatment of simvastatin may enhance the lipid peroxidation via stimulating the reduction of CoQ10 (Coenzyme Q10) which is a regular protector for free radical oxidation (Mortensen et al., 1997; McNulty et al., 2008).

Early studies reported that the decrease in BMD associated with osteoporosis has been closely related to high lipid levels (Broulik and Kapitola, 1993; Laroche et al., 1994a; 1994b). Several in vitro studies have implicated lipids and lipid oxidation in inhibiting or altering the normal differentiation pathway of osteoblastic progenitor cells (Parhami et al., 1997; 1999). Lipids might accumulate around bone vessels in osteoporotic patients (Rajendran et al., 1995). In each cylindrical unit of bone, the osteon, a central vessel is lined with endothelial cells and a subendothelial matrix. Osteoblast progenitor cells are located immediately outside the matrix. Since the progenitors are located near to the subendothelial matrix, this lipid accumulation might alter the development of the bone-forming osteoblastic progenitor cells (Parhami et al., 2000). In vitro studies, using bone- and marrow-derived preosteoblastic cells, it has been found that treatment with minimally oxidized low-density lipoprotein (MM-LDL) and other bioactive oxidized lipids inhibit various markers of osteoblastic differentiation, including alkaline phosphatase, collagen I, osteocalcin, and finally accumulation of hydroxyapatite minerals (Parhami et al., 1997; 1999). Similarly, preosteoblasts harvested from the bone marrow of mice that were fed a high-fat, high-cholesterol diet, have been shown to have significantly less osteoblastic differentiation, (Parhami et al., 1999) suggesting that high-lipid diet might result in lipid accumulation which might induce alterations in osteoblastic differentiation. In addition to inhibiting osteoblastic differentiation, it is suggested that through recruitment and differentiation of osteoclast precursor cells, (Parhami et al., 2000) oxidized lipids may contribute to increased bone breakdown.

4.2.4 The effects of Simvastatin on Protein Secondary Structure

As reported previously, membrane proteins show sensitivity to the order and fluidity of the lipid environment (Lee, A. G., 2003). Therefore, any change in this

lipid environment, lipid composition and consequently lipid–protein interactions, alters the redistribution of protein components and affects the structure and function of channel proteins (Lee, A. G., 2003; Akkas et al., 2007). An increase in protein content was deduced from the significant increase in the area of CH₃ symmetric stretching (2873cm⁻¹), amide I (1667cm⁻¹) and amide II (1546cm⁻¹) bands. It has been reported that, simvastatin induces type I collagen production in bone tissues(Nogaki et al., 2001). This may be the reason of increase observed in protein content in response to both doses. Type I collagen can be differentiated from other types of collagen by the higher amounts of alpha-helix and triple helix (Petibois et al., 2006). According to the current vector normalization and neural network analysis results, the absorbance values of the peak corresponding to α -helical structure increased for both simvastatin-treated groups due to the increase of collagen I production (Petibois et al., 2006). Moreover, the increase in the intensity values of the peak corresponding to antiparallel β -sheet and aggregated β -sheet and random coil structure band for the 50mg simvastatin-treated group indicates protein denaturation due to oxidative modification (Hamilton et al., 2008).

As a summary, it was shown that both simvastatin doses increased the rigidity of healthy bone tissues with enough flexibility to protect them from fracture. However, low dose of simvastatin treatment is much more effective in reducing the carbonate substitution and crystal size in the mineral crystal which implies more strengthened bones. Moreover, high dose may enhance lipid peroxidation and resulted in an increased disorder and fluidity of the membrane. Moreover, it alters the composition and concentration of the lipids which changes ion channels and receptors by affecting the asymmetry and thickness of the membrane. The current study clearly showed that low dose simvastatin therapy is much more safer and effective for bone health than the high dose therapy.

CHAPTER 5

CONCLUSION

A number of drugs may have metabolic effects on the skeletal system, and may result in either bone loss or increased bone strength. Among these drugs, anti-epileptic drug; Carbamazepine and a cholesterol lowering drug; Simvastatin were used to determine their possible effects on bone tissues in the current thesis. These studies will provide new strategies to prevent the side-effects of drugs on bone metabolism and to support new treatments against bone disorders.

The reported results about carbamazepine's side-effects on bones are contradictory. Moreover, there is no study in the literature, investigating the independent effect of epileptic seizures on bone tissues. Thus, the side-effects of anti-epileptic drug; Carbamazepine therapy on bone tissues could not be differentiated from the effects of the epileptic seizures. The exact mechanisms for possible adverse bone effects of Carbamazepine have not been determined yet. Thus, to contribute resolving these discrepancies, the current thesis mainly aimed to clarify and elucidate the effects of Carbamazepine and epileptic seizures on bone tissues and clarify the action mechanism of anti-epileptic drug and seizures on vitamin D and bone metabolism.

As a comparative study, one of the common and well-known cholesterol reducing drug; Simvastatin was used to determine its possible dose dependent effects on healthy bone tissues. In recent years, among the pleiotropic effects, there has been a growing interest in the effect of simvastatin on bone tissue and osteoporosis.

However, the relationship between the use of simvastatin and improvement of bone quality reported in the literature is still controversial. Moreover, It was reported that high and low dose simvastatin treatment may cause lipid peroxidation in soft tissues. There is not any report about the effects of simvastatin on bone lipids. Thus, considering an urgent need for the more effective drugs that are able to induce new bone formation with less negative side effect, the current study aimed to investigate dose-dependent effects of simvastatin treatment on bone tissues and to clarify whether it causes lipid peroxidation on bones.

When the effects of these drugs on bone tissues were compared in general;

- Carbamazepine and simvastatin treatment affected the bone mineral and matrix adversely. Carbamazepine caused a decrease in bone mineral content, carbonate substitution and collagen crosslinks where simvastatin induced an increase in these parameters. Moreover, the crystallinity value increased in carbamazepine-treated healthy bones while this value decreased in simvastatin-treated bones. All the results of these parameters implies a less strengthened bone in carbamazepine treatment, where a more strengthened bone due to simvastatin treatment in healthy rats.
- Low microhardness values for carbamazepine-treated bones and high microhardness values for simvastatin-treated ones, were also in agreement with spectroscopic studies. Thus, carbamazepine treatment caused a decrease in the strength of healthy bone tissues. However, simvastatin treatment induced more strength bone tissues on healthy system.

Other important findings in carbamazepine study;

- Epilepsy and epileptic seizures had also adverse effects on bone tissues as drug treatment. A decrease in bone mineral content, carbonate substitution and collagen crosslinks and an increase in crystallinity value obtained from microspectroscopic studies, low micro- and nanohardness and surface roughness values obtained from biomechanical and AFM studies, respectively, implies a less strengthened bone in epileptic rats. However, the drug treatment was found to cause more severe damage on bone tissues than the epileptic seizures.
- Both carbamazepine and epileptic seizures induced vitamin D deficiency but had different effects on serum PTH levels and bone turnover markers. Carbamazepine treatment induced elevated serum PTH and bone turnover marker levels, while epileptic seizures causes a slight decrease in PTH level without significant change in markers, implying that seizures induce adverse effects on bone with a different mechanism rather than inducing bone turnover.
- Both carbamazepine and epileptic seizures induced vitamin D deficiency through increasing the protein levels of vitamin D catabolism enzyme (CYP24) in kidney tissues. In drug treated groups, it may be because of the activation of PXR receptor by carbamazepine, which causes an increase in CYP24 and CYP27a1 enzymes. Moreover, in epileptic group this mechanism may also take place but not with the activation of PXR receptor by a drug but with a possible PXR polymorphism in WAG/Rij mixed form of epileptic rats.

Other important findings in simvastatin study;

- Although both low and high dose simvastatin caused an increase in mineral content and a decrease in carbonate substitution and crystallinity, implying a more strengthened bone compared to the non-treated healthy controls, low dose simvastatin was more effective in changing these parameters than high-dose simvastatin.
- The increased microhardness values which reports more strengthened bones, were also in agreement with the current spectroscopic results.
- High dose simvastatin therapy may enhance lipid peroxidation and denaturation of proteins while it also favors higher disorder and flexibility of the membranes.
- The current study also clearly showed that low dose simvastatin therapy is much more safer and effective for bone health than the high dose therapy.

As future directions of this thesis study, it can be suggested that in carbamazepine study, further studies may be performed to investigate the possible effects of new generation anti-epileptic drugs, especially the non-enzyme inducing drugs such as Levetiracetam, on bone tissues which provides a new strategy on both the treatment of epilepsy and the prevention of bone disorders. Further molecular studies may be performed to investigate the possible PXR polymorphism in WAG/Rij rats to clarify the detailed mechanism of the effects of epilepsy and seizures on bone metabolism. In simvastatin study, further studies may be performed with Simvastatin to identify the reasons that lie beneath the observed structural alterations in bone mineral and matrix. Possible reasons of these alterations can be either an elevated protein levels of vitamin D activating enzymes, or the induced expression of bone formation-related proteins. Therefore, future studies can be conducted to determine the protein levels and mRNA expressions of vitamin D

enzymes and bone formation-related proteins. Moreover, further structural and compositional analyses can be performed by FTIR and SR-FTIR microspectroscopy studies to clarify the site-specific effects of simvastatin and intra-bone variation due to drug treatment.

REFERENCES

- Akin R, Okutan V, Sarici U, Altunbas A, Gokcay E (1998) Evaluation of bone mineral density in children receiving antiepileptic drugs. *Pediatric neurology* 19: 129-131
- Akkas SB, Inci S, Zorlu F, Severcan F (2007) Melatonin affects the order, dynamics and hydration of brain membrane lipids. *Journal of molecular structure* 834: 207-215
- Alahouhala M, Korpela R, Koivikko M, Koskinen T, Koskinen M, Koivula T (1986) Long-Term Anticonvulsant Therapy and Vitamin-D Metabolism in Ambulatory Pubertal Children. *Neuropediatrics* 17: 212-216
- Alpman A, Ozkinay F, Tekgul H, Gokben S, Pehlivan S, Schalling M, Ozkinay C (2010) Multidrug resistance 1 (MDR1) gene polymorphisms in childhood drug-resistant epilepsy. *Journal of child neurology* 25: 1485-1490
- Altay EE, Serdaroglu A, Tumer L, Gucuyener K, Hasanoglu A (2000) Evaluation of bone mineral metabolism in children receiving carbamazepine and valproic acid. *Journal of pediatric endocrinology and metabolism* 13: 933-939
- Anbinder AL, Prado Fde A, Prado Mde A, Balducci I, Rocha RF (2007) The influence of ovariectomy, simvastatin and sodium alendronate on alveolar bone in rats. *Brazilian oral research* 21: 247-252
- Andress DL, Ozuna J, Tirschwell D, Grande L, Johnson M, Jacobson AF, Spain W (2002) Antiepileptic drug-induced bone loss in young male patients who have seizures. *Archives of neurology-Chicago* 59: 781-786
- Arabi A, Baddoura R, El-Rassi R, El-Hajj Fuleihan G (2012) PTH level but not 25 (OH) vitamin D level predicts bone loss rates in the elderly. *Osteoporosis international* 23: 971-980
- Aziz H, Guvener A, Akhtar SW, Hasan KZ (1997) Comparative epidemiology of epilepsy in Pakistan and Turkey: population-based studies using identical protocols. *Epilepsia* 38: 716-722

Banse X, Devogelaer JP, Lafosse A, Sims TJ, Grynpas M, Bailey AJ (2002) Cross-link profile of bone collagen correlates with structural organization of trabeculae. *Bone* 31: 70-76

Baronas-Lowell D, Lauer-Fields JL, Fields GB (2003) Defining the roles of collagen and collagen-like proteins within the proteome. *Journal of liquid chromatography & related technologies* 26: 2225-2254

Barry AB, Baig AA, Miller SC, Higuchi WI (2002) Effect of age on rat bone solubility and crystallinity. *Calcified tissue international* 71: 167-171

Bauer DC, Mundy GR, Jamal SA, Black DM, Cauley JA, Ensrud KE, van der Klift M, Pols HA (2004) Use of statins and fracture: results of 4 prospective studies and cumulative meta-analysis of observational studies and controlled trials. *Archives of internal medicine* 164: 146-152

Bauer DC, Mundy GR, Jamal SA, Black DM, Cauley JA, Ensrud KE, van der Klift M, Pols HAP (2004) Use of statins and fracture - Results of 4 prospective studies and cumulative meta-analysis of observational studies and controlled trials. *Archives of internal medicine* 164: 146-152

Bazin D, Chappard C, Combes C, Carpentier X, Rouziere S, Andre G, Matzen G, Allix M, Thiaudiere D, Reguer S, Jungers P, Daudon M (2009) Diffraction techniques and vibrational spectroscopy opportunities to characterise bones. *Osteoporosis international* : 20: 1065-1075

Beerhorst K, Schouwenaars FM, Tan IY, Aldenkamp AP (2012) Epilepsy: fractures and the role of cumulative antiepileptic drug load. *Acta neurologica scandinavica* 125: 54-59

Bhan A, Rao AD, Rao DS (2012) Osteomalacia as a result of vitamin D deficiency. *Rheumatic diseases clinics of North America* 38: 81-91, viii-ix

Blank RD, Baldini TH, Kaufman M, Bailey S, Gupta R, Yershov Y, Boskey AL, Coppersmith SN, Demant P, Paschalis EP (2003) Spectroscopically determined collagen Pyr/deH-DHLNL cross-link ratio and crystallinity indices differ markedly in recombinant congenic mice with divergent calculated bone tissue strength. *Connective tissue research* 44: 134-142

Boivin G, Bala Y, Doublier A, Farlay D, Ste-Marie LG, Meunier PJ, Delmas PD (2008) The role of mineralization and organic matrix in the microhardness of bone tissue from controls and osteoporotic patients. *Bone* 43: 532-538

- Bonetti PO, Lerman LO, Napoli C, Lerman A (2003) Statin effects beyond lipid lowering--are they clinically relevant? *European heart journal* 24: 225-248
- Boskey A, Frank A, Fujimoto Y, Spevak L, Verdelis K, Ellis B, Troiano N, Philbrick W, Carpenter T (2009) The PHEX transgene corrects mineralization defects in 9-month-old hypophosphatemic mice. *Calcified tissue international* 84: 126-137
- Boskey A, Pleshko Camacho N (2007) FT-IR imaging of native and tissue-engineered bone and cartilage. *Biomaterials* 28: 2465-2478
- Boskey AL (2007) Mineralization of bones and teeth. *Elements* 3: 385-391
- Boskey AL, Gelb BD, Pourmand E, Kudrashov V, Doty SB, Spevak L, Schaffler MB (2009) Ablation of cathepsin k activity in the young mouse causes hypermineralization of long bone and growth plates. *Calcified tissue international* 84: 229-239
- Boskey AL, Mendelsohn R (2005) Infrared spectroscopic characterization of mineralized tissues. *Vibrational Spectroscopy* 38: 107-114
- Boskey AL, Spevak L, Weinstein RS (2009) Spectroscopic markers of bone quality in alendronate-treated postmenopausal women. *Osteoporosis international* 20: 793-800
- Bouxsein ML (2004) Non-invasive measurements of bone strength: promise and peril. *Journal of musculoskeletal & neuronal interactions* 4: 404-405
- Boyar H, Zorlu F, Mut M, Severcan F (2004) The effects of chronic hypoperfusion on rat cranial bone mineral and organic matrix. A Fourier transform infrared spectroscopy study. *Analytical and bioanalytical chemistry* 379: 433-438
- Brighton CT, Hunt RM (1986) Histochemical localization of calcium in the fracture callus with potassium pyroantimonate. Possible role of chondrocyte mitochondrial calcium in callus calcification. *The Journal of bone and joint surgery American volume* 68: 703-715
- Broncel M, Bala A, Koter-Michalak M, Duchnowicz P, Wojsznis W, Chojnowska-Jeziarska J (2007) Physicochemical modifications induced by statins therapy on human erythrocytes membranes. *Wiadomosci lekarskie* 60: 321-328

Broulik PD, Kapitola J (1993) Interrelations between body weight, cigarette smoking and spine mineral density in osteoporotic Czech women. *Endocrine regulations* 27: 57-60

Cakmak G, Miller LM, Zorlu F, Severcan F (2012) Amifostine, a radioprotectant agent, protects rat brain tissue lipids against ionizing radiation induced damage: an FTIR microspectroscopic imaging study. *Archives of biochemistry and biophysics* 520: 67-73

Calton EF, Macleay J, Boskey AL (2011) Fourier transform infrared imaging analysis of cancellous bone in alendronate- and raloxifene-treated osteopenic sheep. *Cells, tissues, organs* 194: 302-306

Cartier N, Guidoux S, Rocchiccioli F, Aubourg P (2000) Simvastatin does not normalize very long chain fatty acids in adrenoleukodystrophy mice. *FEBS letters* 478: 205-208

Cazalbou S, Combes C, Eichert D, Rey C, Glimcher MJ (2004) Poorly crystalline apatites: evolution and maturation in vitro and in vivo. *Journal of bone and mineral metabolism* 22: 310-317

Chachra D, Turner CH, Dunipace AJ, Grynepas MD (1999) The effect of fluoride treatment on bone mineral in rabbits. *Calcified tissue international* 64: 345-351

Chan MH, Mak TW, Chiu RW, Chow CC, Chan IH, Lam CW (2001) Simvastatin increases serum osteocalcin concentration in patients treated for hypercholesterolaemia. *The Journal of clinical endocrinology and metabolism* 86: 4556-4559

Chan MHM, Mak TWL, Chiu RWK, Chow CC, Chan IHS, Lam CWK (2001) Simvastatin increases serum osteocalcin concentration in patients treated for hypercholesterolaemia. *The Journal of Clinical Endocrinology and Metabolism* 86: 4556-4559

Charras GT, Williams BA, Sims SM, Horton MA (2004) Estimating the sensitivity of mechanosensitive ion channels to membrane strain and tension. *Biophysical journal* 87: 2870-2884

Chen PY, Sun JS, Tsuang YH, Chen MH, Weng PW, Lin FH (2010) Simvastatin promotes osteoblast viability and differentiation via Ras/Smad/Erk/BMP-2 signaling pathway. *Nutrition research* 30: 191-199

Clarke BL, Khosla S (2010) Physiology of bone loss. *Radiologic clinics of North America* 48: 483-495

Cocciardi RA, Ismail AA, Sedman J (2005) Investigation of the potential utility of single-bounce attenuated total reflectance Fourier transform infrared spectroscopy in the analysis of distilled liquors and wines. *Journal of agricultural and food chemistry* 53: 2803-2809

Coenen AM, Drinkenburg WH, Inoue M, van Luijtelaar EL (1992) Genetic models of absence epilepsy, with emphasis on the WAG/Rij strain of rats. *Epilepsy research* 12: 75-86

Coenen AM, Van Luijtelaar EL (2003) Genetic animal models for absence epilepsy: a review of the WAG/Rij strain of rats. *Behavior genetics* 33: 635-655

Colina M, La Corte R, De Leonardis F, Trotta F (2008) Paget's disease of bone: a review. *Rheumatology international* 28: 1069-1075

Compston J (2010) Osteoporosis: social and economic impact. *Radiologic clinics of North America* 48: 477-482

Currey JD (1984) Effects of differences in mineralization on the mechanical properties of bone. *Philosophical transactions of the Royal Society of London Series B, Biological sciences* 304: 509-518

Cutuli D, Foti F, Mandolesi L, De Bartolo P, Gelfo F, Federico F, Petrosini L (2008) Cognitive performance of healthy young rats following chronic donepezil administration. *Psychopharmacology* 197: 661-673

Dam M (1996) Epilepsy surgery. *Acta neurologica Scandinavica* 94: 81-87

Davidson RM, Tatakis DW, Auerbach AL (1990) Multiple forms of mechanosensitive ion channels in osteoblast-like cells. *Pflugers Archiv : European journal of physiology* 416: 646-651

Davignon J (2004) Beneficial cardiovascular pleiotropic effects of statins. *Circulation* 109: III39-43

de Sousa DP, Goncalves JC, Quintans-Junior L, Cruz JS, Araujo DA, de Almeida RN (2006) Study of anticonvulsant effect of citronellol, a monoterpene alcohol, in rodents. *Neuroscience letters* 401: 231-235

- Delorenzo RJ, Sun DA, Deshpande LS (2005) Cellular mechanisms underlying acquired epilepsy: the calcium hypothesis of the induction and maintenance of epilepsy. *Pharmacology & therapeutics* 105: 229-266
- Diem M, Boydston-White S, Chiriboga L (1999) Infrared spectroscopy of cells and tissues: Shining light onto a novel subject. *Applied spectroscopy* 53: 148a-161a
- Dogan A, Siyakus G, Severcan F (2007) FTIR spectroscopic characterization of irradiated hazelnut (*Corylus avellana* L.). *Food Chemistry* 100: 1106-1114
- Dooley KA, McCormack J, Fyhrie DP, Morris MD (2009) Stress mapping of undamaged, strained, and failed regions of bone using Raman spectroscopy. *Journal of biomedical optics* 14: 044018
- Dreifuss FE (1990) The Epilepsies - Clinical Implications of the International Classification. *Epilepsia* 31: S3-S10
- Du Z, Chen J, Yan F, Doan N, Ivanovski S, Xiao Y (2011) Serum bone formation marker correlation with improved osseointegration in osteoporotic rats treated with simvastatin. *Clinical oral implants research*. Doi:10.1111/j.1600-0501.2011.02341.x. [Epub ahead of print]
- Durchschlag E, Paschalis EP, Zoehrer R, Roschger P, Fratzl P, Recker R, Phipps R, Klaushofer K (2006) Bone material properties in trabecular bone from human iliac crest biopsies after 3- and 5-year treatment with risedronate. *Journal of bone and mineral research* 1581-1590
- Ecevit CG, Aydogan A, Kavakli T, Altinoz S (2004) Effect of carbamazepine and valproate on bone mineral density. *Pediatric neurology* 31: 279-282
- Ejersted C, Andreassen TT, Oxlund H, Jorgensen PH, Bak B, Haggblad J, Topping O, Nilsson MH (1993) Human parathyroid hormone (1-34) and (1-84) increase the mechanical strength and thickness of cortical bone in rats. *Journal of bone and mineral research* 8: 1097-1101
- Elliott JC, Holcomb DW, Young RA (1985) Infrared determination of the degree of substitution of hydroxyl by carbonate ions in human dental enamel. *Calcified tissue international* 37: 372-375
- Ellis DI, Goodacre R (2006) Metabolic fingerprinting in disease diagnosis: biomedical applications of infrared and Raman spectroscopy. *The Analyst* 131: 875-885

Faibish D, Gomes A, Boivin G, Binderman I, Boskey A (2005) Infrared imaging of calcified tissue in bone biopsies from adults with osteomalacia. *Bone* 36: 6-12

Faibish D, Ott SM, Boskey AL (2006) Mineral changes in osteoporosis - A review. *Clinical Orthopaedics and Related Research*: 28-38

Fantner GE, Birkedal H, Kindt JH, Hassenkam T, Weaver JC, Cutroni JA, Bosma BL, Bawazer L, Finch MM, Cidade GAG, Morse DE, Stucky GD, Hansma PK (2004) Influence of the degradation of the organic matrix on the microscopic fracture behavior of trabecular bone. *Bone* 35: 1013-1022

Farhat G, Yamout B, Mikati MA, Demirjian S, Sawaya R, Fuleihan GEH (2002) Effect of antiepileptic drugs on bone density in ambulatory patients. *Neurology* 58: 1348-1353

Farlay D, Panczer G, Rey C, Delmas PD, Boivin G (2010) Mineral maturity and crystallinity index are distinct characteristics of bone mineral. *Journal of bone and mineral metabolism* 28: 433-445

Feldkamp J, Becker A, Witte OW, Scharff D, Scherbaum WA (2000) Long-term anticonvulsant therapy leads to low bone mineral density - evidence for direct drug effects of phenytoin and carbamazepine on human osteoblast-like cells. *Experimental and Clinical Endocrinology & Diabetes* 108: 37-43

Fu X, Menke JG, Chen Y, Zhou G, MacNaul KL, Wright SD, Sparrow CP, Lund EG (2001) 27-hydroxycholesterol is an endogenous ligand for liver X receptor in cholesterol-loaded cells. *The Journal of biological chemistry* 276: 38378-38387

Fukui T, Ii M, Shoji T, Matsumoto T, Mifune Y, Kawakami Y, Akimaru H, Kawamoto A, Kuroda T, Saito T, Tabata Y, Kuroda R, Kurosaka M, Asahara T (2012) Therapeutic effect of local administration of low-dose simvastatin-conjugated gelatin hydrogel for fracture healing. *Journal of bone and mineral research* 27: 1118-1131

Futatsugi Y, Riviello JJ (1998) Mechanisms of generalized absence epilepsy. *Brain & development* 20: 75-79

Garip S, Severcan F (2010a) Determination of simvastatin-induced changes in bone composition and structure by Fourier transform infrared spectroscopy in rat animal model. *Journal of pharmaceutical and biomedical analysis* 52: 580-588

Garip S, Yapici E, Ozek NS, Severcan M, Severcan F (2010b) Evaluation and discrimination of simvastatin-induced structural alterations in proteins of different

rat tissues by FTIR spectroscopy and neural network analysis. *The Analyst* 135: 3233-3241

Garrett IR, Mundy GR (2002) The role of statins as potential targets for bone formation. *Arthritis research* 4: 237-240

Gissel T, Poulsen CS, Vestergaard P (2007) Adverse effects of antiepileptic drugs on bone mineral density in children. *Expert Opin Drug Saf* 6: 267-278

Gniatkowska-Nowakowska A (2010) Fractures in epilepsy children. *Seizure* 19: 324-325

Golledge J, Cullen B, Moran C, Rush C (2010) Efficacy of simvastatin in reducing aortic dilatation in mouse models of abdominal aortic aneurysm. *Cardiovascular drugs and therapy* 24: 373-378

Gough H, Goggin T, Bissessar A, Baker M, Crowley M, Callaghan N (1986) A Comparative-Study of the Relative Influence of Different Anticonvulsant Drugs, Uv Exposure and Diet on Vitamin-D and Calcium-Metabolism in out-Patients with Epilepsy. *Q J Med* 59: 569-577

Gourion-Arsiquaud S, Burket JC, Havill LM, DiCarlo E, Doty SB, Mendelsohn R, van der Meulen MC, Boskey AL (2009) Spatial variation in osteonal bone properties relative to tissue and animal age. *Journal of bone and mineral research* 24: 1271-1281

Gourion-Arsiquaud S, Lukashova L, Power J, Loveridge N, Reeve J, Boskey AL (2012) Fourier transformed infra-red imaging of femoral neck bone: Reduced heterogeneity of mineral-to-matrix and carbonate-to-phosphate and more variable crystallinity in treatment-naive fracture cases compared to fracture-free controls. *Journal of bone and mineral research* 23: 124-134

Grover S, Bala K, Sharma S, Gourie-Devi M, Baghel R, Kaur H, Gupta M, Talwar P, Kukreti R (2010) Absence of a general association between ABCB1 genetic variants and response to antiepileptic drugs in epilepsy patients. *Biochimie* 92: 1207-1212

Guo CY, Ronen GM, Atkinson SA (2001) Long-term valproate and lamotrigine treatment may be a marker for reduced growth and bone mass in children with epilepsy. *Epilepsia* 42: 1141-1147

Gupta HS, Schratte S, Tesch W, Roschger P, Berzlanovich A, Schoeberl T, Klaushofer K, Fratzl P (2005) Two different correlations between nanoindentation

modulus and mineral content in the bone-cartilage interface. *Journal of structural biology* 149: 138-148

Gupta HS, Seto J, Wagermaier W, Zaslansky P, Boesecke P, Fratzl P (2006) Cooperative deformation of mineral and collagen in bone at the nanoscale. *Proceedings of the National Academy of Sciences of the United States of America* 103: 17741-17746

Haerian BS, Lim KS, Mohamed EH, Tan HJ, Tan CT, Raymond AA, Wong CP, Wong SW, Mohamed Z (2011) Lack of association of ABCB1 and PXR polymorphisms with response to treatment in epilepsy. *Seizure* 20: 387-394

Hamilton RT, Asatryan L, Nilsen JT, Isas JM, Gallaher TK, Sawamura T, Hsiai TK (2008) LDL protein nitration: implication for LDL protein unfolding. *Archives of biochemistry and biophysics* 479: 1-14

Hamilton RT, Asatryan L, Nilsen OT, Isas JM, Gallaher TK, Sawamura T, Hsiai TK (2008) LDL protein nitration: Implication for LDL protein unfolding. *Archives of biochemistry and biophysics* 479: 1-14

Han X, Yang N, Cui Y, Xu Y, Dang G, Song C (2012) Simvastatin mobilizes bone marrow stromal cells migrating to injured areas and promotes functional recovery after spinal cord injury in the rat. *Neuroscience letters* 521: 136-141

Haris PI, Severcan F (1999) FTIR spectroscopic characterization of protein structure in aqueous and non-aqueous media. *Journal of Molecular Catalysis B: Enzymatic* 7: 207-221

Hassenkam T, Fantner GE, Cutroni JA, Weaver JC, Morse DE, Hansma PK (2004) High-resolution AFM imaging of intact and fractured trabecular bone. *Bone* 35: 4-10

Hassenkam T, Jorgensen HL, Pedersen MB, Kourakis AH, Simonsen L, Lauritzen JB (2005) Atomic force microscopy on human trabecular bone from an old woman with osteoporotic fractures. *Micron* 36: 681-687

Hauge EM, Qvesel D, Eriksen EF, Mosekilde L, Melsen F (2001) Cancellous bone remodeling occurs in specialized compartments lined by cells expressing osteoblastic markers. *Journal of bone and mineral research* 16: 1575-1582

Hauser WA (1997) Sudden unexpected death in patients with epilepsy: Issues for further study. *Epilepsia* 38: S26-S29

Hauser WA, Annegers JF, Rocca WA (1996) Descriptive epidemiology of epilepsy: Contributions of population-based studies from Rochester, Minnesota. *Mayo Clin Proc* 71: 576-586

Hazenberg JG, Freeley M, Foran E, Lee TC, Taylor D (2006) Microdamage: a cell transducing mechanism based on ruptured osteocyte processes. *Journal of biomechanics* 39: 2096-2103

Henriksen K, Gram J, Schaller S, Dahl BH, Dziegiel MH, Bollerslev J, Karsdal MA (2004) Characterization of osteoclasts from patients harboring a G215R mutation in *CLC-7* causing autosomal dominant osteopetrosis type II. *American Journal of Pathology* 164: 1537-1545

Hoc T, Henry L, Verdier M, Aubry D, Sedel L, Meunier A (2006) Effect of microstructure on the mechanical properties of Haversian cortical bone. *Bone* 38: 466-474

Hsia J, Morse M, Levin V (2002) Effect of simvastatin on bone markers in osteopenic women: a placebo-controlled, dose-ranging trial [ISRCTN85429598]. *BMC musculoskeletal disorders* 3

Huang RY, Miller LM, Carlson CS, Chance MR (2003) In situ chemistry of osteoporosis revealed by synchrotron infrared microspectroscopy. *Bone* 33: 514-521

Hung CC, Jen Tai J, Kao PJ, Lin MS, Liou HH (2007) Association of polymorphisms in *NR1H2* and *ABCB1* genes with epilepsy treatment responses. *Pharmacogenomics* 8: 1151-1158

Hung CC, Tai JJ, Lin CJ, Lee MJ, Liou HH (2005) Complex haplotypic effects of the *ABCB1* gene on epilepsy treatment response. *Pharmacogenomics* 6: 411-417

Jadhav SB, Jain GK (2006) Statins and osteoporosis: new role for old drugs. *Journal of Pharmacy and Pharmacology* 58: 3-18

Jayo MJ, Register TC, Hughes CL, Blas-Machado U, Sulistiawati E, Borgerink H, Johnson CS (2000) Effects of an oral contraceptive combination with or without androgen on mammary tissues: A study in rats. *Journal of the Society for Gynecologic Investigation* 7: 257-265

Jerome CP, Carlson CS, Register TC, Bain FT, Jayo MJ, Weaver DS, Adams MR (1994) Bone functional changes in intact, ovariectomized, and ovariectomized,

hormone-supplemented adult cynomolgus monkeys (*Macaca fascicularis*) evaluated by serum markers and dynamic histomorphometry. *Journal of bone and mineral research* 9: 527-540

Johnson WM, Rapoff AJ (2007) Microindentation in bone: hardness variation with five independent variables. *Journal of materials science Materials in medicine* 18: 591-597

Johnson-Anuna LN, Eckert GP, Keller JH, Igbavboa U, Franke C, Fechner T, Schubert-Zsilavec M, Karas M, Muller WE, Wood WG (2005) Chronic administration of statins alters multiple gene expression patterns in mouse cerebral cortex. *The Journal of pharmacology and experimental therapeutics* 312: 786-793

Jouishomme H, Whitfield JF, Gagnon L, Maclean S, Isaacs R, Chakravarthy B, Durkin J, Neugebauer W, Willick G, Rixon RH (1994) Further definition of the protein kinase C activation domain of the parathyroid hormone. *Journal of bone and mineral research* 9: 943-949

Karsdal MA, Henriksen K, Sorensen MG, Gram J, Schaller S, Dziegiel MH, Heegaard AM, Christophersen P, Martin TJ, Christiansen C, Bollerslev J (2005) Acidification of the osteoclastic resorption compartment provides insight into the coupling of bone formation to bone resorption. *American Journal of Pathology* 166: 467-476

Kerr BM, Thummel KE, Wurden CJ, Klein SM, Kroetz DL, Gonzalez FJ, Levy RH (1994) Human liver carbamazepine metabolism: Role of CYP3A4 and CYP2C8 in 10,11-epoxide formation. *Biochemical Pharmacology* 47(11): 1969–1979

Kim DW, Lee SK, Chu K, Jang IJ, Yu KS, Cho JY, Kim SJ (2009) Lack of association between ABCB1, ABCG2, and ABCC2 genetic polymorphisms and multidrug resistance in partial epilepsy. *Epilepsy research* 84: 86-90

Kim SH, Lee JW, Choi KG, Chung HW, Lee HW (2007) A 6-month longitudinal study of bone mineral density with antiepileptic drug monotherapy. *Epilepsy & Behavior* 10: 291-295

Kim YO, Kim MK, Woo YJ, Lee MC, Kim JH, Park KW, Kim EY, Roh YI, Kim CJ (2006) Single nucleotide polymorphisms in the multidrug resistance 1 gene in Korean epileptics. *Seizure* 15: 67-72

- Kneipp J, Beekes M, Lasch P, Naumann D (2002) Molecular changes of preclinical scrapie can be detected by infrared spectroscopy. *Journal of Neuroscience* 22: 2989-2997
- Knott L, Bailey AJ (1998) Collagen cross-links in mineralizing tissues: a review of their chemistry, function, and clinical relevance. *Bone* 22: 181-187
- Kocsis GF, Pipis J, Fekete V, Kovacs-Simon A, Odendaal L, Molnar E, Giricz Z, Janaky T, van Rooyen J, Csont T, Ferdinandy P (2008) Lovastatin interferes with the infarct size-limiting effect of ischemic preconditioning and postconditioning in rat hearts. *American Journal of Physiology - Heart and Circulatory Physiology* 294: H2406-H2409
- Koter M, Franiak I, Broncel M, Chojnowska-Jezierska J (2003) Effects of simvastatin and pravastatin on peroxidation of erythrocyte plasma membrane lipids in patients with type 2 hypercholesterolemia. *Canadian journal of physiology and pharmacology* 81: 485-492
- Kumandas S, Koklu E, Gumus H, Koklu S, Kurtoglu S, Karakukcu M, Keskin M (2006) Effect of carbamazepine and valproic acid on bone mineral density, IGF-I and IGFBP-3. *Journal of Pediatric Endocrinology and Metabolism* 19: 529-534
- Kwan P, Wong V, Ng PW, Lui CH, Sin NC, Poon WS, Ng HK, Wong KS, Baum L (2009) Gene-wide tagging study of association between ABCB1 polymorphisms and multidrug resistance in epilepsy in Han Chinese. *Pharmacogenomics* 10: 723-732
- Laemmli UK (1970) Cleavage of structural proteins during the assembly of the head of bacteriophage T4. *Nature* 227: 680-685
- Lakhan R, Misra UK, Kalita J, Pradhan S, Gogtay NJ, Singh MK, Mittal B (2009) No association of ABCB1 polymorphisms with drug-refractory epilepsy in a north Indian population. *Epilepsy & behavior* : E&B 14: 78-82
- Lamba J, Lamba V, Schuetz E (2005) Genetic variants of PXR (NR1I2) and CAR (NR1I3) and their implications in drug metabolism and pharmacogenetics. *Current drug metabolism* 6: 369-383
- Landis WJ (1995) The strength of a calcified tissue depends in part on the molecular structure and organization of its constituent mineral crystals in their organic matrix. *Bone* 16: 533-544

- Lankin VZ, Tikhaze AK, Kukharchuk VV, Konovalova GG, Pisarenko OI, Kamynnyi AI, Shumaev KB, Belenkov YN (2003) Antioxidants decreases the intensification of low density lipoprotein in vivo peroxidation during therapy with statins. *Molecular and cellular biochemistry* 249: 129-140
- Laroche M, Moulinier L, Bon E, Cantagrel A, Mazieres B (1994) Renal tubular disorders and arteriopathy of the lower limbs: risk factors for osteoporosis in men? *Osteoporosis international* 4: 309-313
- Laroche M, Pouilles JM, Ribot C, Bendayan P, Bernard J, Boccalon H, Mazieres B (1994) Comparison of the bone mineral content of the lower limbs in men with ischaemic atherosclerotic disease. *Clinical rheumatology* 13: 611-614
- Lee AG (1991) Lipids and Their Effects on Membrane-Proteins - Evidence against a Role for Fluidity. *Progress in Lipid Research* 30: 323-348
- Lee AG (2003) Lipid-protein interactions in biological membranes: a structural perspective. *Biochimica et Biophysica Acta (BBA) - Biomembranes* 1612: 1-40
- Lee Y, Schmid MJ, Marx DB, Beatty MW, Cullen DM, Collins ME, Reinhardt RA (2008) The effect of local simvastatin delivery strategies on mandibular bone formation in vivo. *Biomaterials* 29: 1940-1949
- Lee YJ, Schmid MJ, Marx DB, Beatty MW, Cullen DM, Collins ME, Reinhardt RA (2008) The effect of local simvastatin delivery strategies on mandibular bone formation in vivo. *Biomaterials* 29: 1940-1949
- Lewis EN, Treado PJ, Reeder RC, Story GM, Dowrey AE, Marcott C, Levin IW (1995) Fourier transform spectroscopic imaging using an infrared focal-plane array detector. *Analytical chemistry* 67: 3377-3381
- Li T, Chen W, Chiang JY (2007) PXR induces CYP27A1 and regulates cholesterol metabolism in the intestine. *Journal of lipid research* 48: 373-384
- Li X, Song QS, Wang JY, Leng HJ, Chen ZQ, Liu ZJ, Dang GT, Song CL (2011) Simvastatin induces estrogen receptor-alpha expression in bone, restores bone loss, and decreases ERalpha expression and uterine wet weight in ovariectomized rats. *Journal of bone and mineral metabolism* 29: 396-403
- Li ZY, Lam WM, Yang C, Xu B, Ni GX, Abbah SA, Cheung KMC, Luk KDK, Lu WW (2007) Chemical composition, crystal size and lattice structural changes after incorporation of strontium into biomimetic apatite. *Biomaterials* 28: 1452-1460

- Liao JK, Laufs U (2005) Pleiotropic effects of statins. *Annual review of pharmacology and toxicology* 45: 89-118
- Liu KZ, Jackson M, Sowa MG, Ju HS, Dixon IMC, Mantsch HH (1996) Modification of the extracellular matrix following myocardial infarction monitored by FTIR spectroscopy. *Biochimica et Biophysica Acta (BBA) - Molecular Basis of Disease* 1315: 73-77
- Liu S, Bertl K, Sun H, Liu ZH, Andrukhov O, Rausch-Fan X (2012) Effect of simvastatin on the osteogenetic behavior of alveolar osteoblasts and periodontal ligament cells. *Human cell* 25: 29-35
- Loupy A, Ramakrishnan SK, Wootla B, Chambrey R, de la Faille R, Bourgeois S, Bruneval P, Mandet C, Christensen EI, Faure H, Cheval L, Laghmani K, Collet C, Eladari D, Dodd RH, Ruat M, Houillier P (2012) PTH-independent regulation of blood calcium concentration by the calcium-sensing receptor. *The Journal of clinical investigation* 122: 3355-3367
- Löshner W, Potschka H (2005) Drug resistance in brain diseases and the role of drug efflux transporters. *Nature Reviews Neuroscience* 6: 591-602.
- Lund EG, Menke JG, Sparrow CP (2003) Liver X receptor agonists as potential therapeutic agents for dyslipidemia and atherosclerosis. *Arteriosclerosis, thrombosis, and vascular biology* 23: 1169-1177
- Lupattelli G, Scarponi AM, Vaudo G, Siepi D, Roscini AR, Gemelli F, Pirro M, Latini RA, Sinzinger H, Marchesi S, Mannarino E (2004) Simvastatin increases bone mineral density in hypercholesterolemic postmenopausal women. *Metabolism: clinical and experimental* 53: 744-748
- Ma B, Clarke SA, Brooks RA, Rushton N (2008) The effect of simvastatin on bone formation and ceramic resorption in a peri-implant defect model. *Acta Biomater* 4: 149-155
- Maeda T, Matsunuma A, Kawane T, Horiuchi N (2001) Simvastatin promotes osteoblast differentiation and mineralization in MC3T3-E1 cells. *Biochemical and biophysical research communications* 280: 874-877
- Marcelli A, Cricenti A, Kwiatek WM, Petibois C (2012) Biological applications of synchrotron radiation infrared spectromicroscopy. *Biotechnology advances*.

Marcoff L, Thompson PD (2007) The role of coenzyme Q10 in statin-associated myopathy: a systematic review. *Journal of the American College of Cardiology* 49: 2231-2237

Marcott C, Reeder RC, Paschalis EP, Tatakis DN, Boskey AL, Mendelsohn R (1998) Infrared microspectroscopic imaging of biomineralized tissues using a mercury-cadmium-telluride focal-plane array detector. *Cellular and molecular biology* 44: 109-115

Maritz FJ, Conradie MM, Hulley PA, Gopal R, Hough S (2001) Effect of statins on bone mineral density and bone histomorphometry in rodents. *Arteriosclerosis Thrombosis and Vascular Biology* 21: 1636-1641

Martin RB, Ishida J (1989) The relative effects of collagen fiber orientation, porosity, density, and mineralization on bone strength. *Journal of biomechanics* 22: 419-426

Martin TJ, Sims NA (2005) Osteoclast-derived activity in the coupling of bone formation to resorption. *Trends in molecular medicine* 11: 76-81

Matsuda I, Higashi A, Inotsume N (1989) Physiologic and Metabolic Aspects of Anticonvulsants. *Pediatric Clinics of North America* 36: 1099-1111

McFarlane SI, Muniyappa R, Francisco R, Sowers JR (2002) Clinical review 145 - Pleiotropic effects of statins: Lipid reduction and beyond. *The Journal of Clinical Endocrinology and Metabolism* 87: 1451-1458

McHugh JC, Delanty N (2008) Epidemiology and classification of epilepsy: Gender comparisons. *Epilepsy in Women: The Scientific Basis for Clinical Management* 83: 11-26

McNamara JO (1994) Cellular and molecular basis of epilepsy. *The Journal of neuroscience* 14: 3413-3425

Mcnamara JO (1994) Cellular and Molecular-Basis of Epilepsy. *Journal of Neuroscience* 14: 3413-3425

McNamara JO (1999) Emerging insights into the genesis of epilepsy. *Nature* 399: A15-A22

McNulty H, Jacob RF, Mason RP (2008) Biologic activity of carotenoids related to distinct membrane physicochemical interactions. *The American journal of cardiology* 101: 20D-29D

- Megli FM, Sabatini K (2003) EPR studies of phospholipid bilayers after lipoperoxidation 1. Inner molecular order and fluidity gradient. *Chemistry and Physics of Lipids* 125: 161-172
- Melin AM, Perromat A, Deleris G (2000) Pharmacologic application of Fourier transform IR spectroscopy: In vivo toxicity of carbon tetrachloride on rat liver. *Biopolymers* 57: 160-168
- Menon B, Harinarayan CV (2010) The effect of anti epileptic drug therapy on serum 25-hydroxyvitamin D and parameters of calcium and bone metabolism--a longitudinal study. *Seizure* 19: 153-158
- Midy V, Plouet J (1994) Vasculotropin Vascular Endothelial Growth-Factor Induces Differentiation in Cultured Osteoblasts. *Biochemical and biophysical research communications* 199: 380-386
- Midzyanovskaya IS, Kuznetsova GD, Vinogradova LV, Shatskova AB, Coenen AM, van Luijtelaaar G (2004) Mixed forms of epilepsy in a subpopulation of WAG/Rij rats. *Epilepsy & behavior* : E&B 5: 655-661
- Miller LM, Vairavamurthy V, Chance MR, Mendelsohn R, Paschalis EP, Betts F, Boskey AL (2001) In situ analysis of mineral content and crystallinity in bone using infrared micro-spectroscopy of the nu(4) PO(4)(3-) vibration. *Biochimica et biophysica acta* 1527: 11-19
- Mintzer S (2010) Metabolic consequences of antiepileptic drugs. *Current opinion in neurology* 23: 164-169
- Misof BM, Roschger P, Baldini T, Raggio CL, Zraick V, Root L, Boskey AL, Klaushofer K, Fratzl P, Camacho NP (2005) Differential effects of alendronate treatment on bone from growing osteogenesis imperfecta and wild-type mouse. *Bone* 36: 150-158
- Misra A, Aggarwal A, Singh O, Sharma S (2010) Effect of carbamazepine therapy on vitamin D and parathormone in epileptic children. *Pediatric neurology* 43: 320-324
- Miura M, Satoh S, Inoue K, Kagaya H, Saito M, Inoue T, Habuchi T, Suzuki T (2008) Influence of CYP3A5, ABCB1 and NR1I2 polymorphisms on prednisolone pharmacokinetics in renal transplant recipients. *Steroids* 73: 1052-1059
- Montagnani A, Gonnelli S, Cepollaro C, Pacini S, Campagna MS, Franci MB, Lucani B, Gennari C (2003) Effect of simvastatin treatment on bone mineral

density and bone turnover in hypercholesterolemic postmenopausal women: a 1-year longitudinal study. *Bone* 32: 427-433

Moon HJ, Kim SE, Yun YP, Hwang YS, Bang JB, Park JH, Kwon IK (2011) Simvastatin inhibits osteoclast differentiation by scavenging reactive oxygen species. *Experimental & molecular medicine* 43: 605-612

Mortensen SA, Leth A, Agner E, Rohde M (1997) Dose-related decrease of serum coenzyme Q10 during treatment with HMG-CoA reductase inhibitors. *Molecular aspects of medicine* 18 Suppl: S137-144

Mourant JR, Yamada YR, Carpenter S, Dominique LR, Freyer JP (2003) FTIR spectroscopy demonstrates biochemical differences in mammalian cell cultures at different growth stages. *Biophysical journal* 85: 1938-1947

Mucha K, Foronczewicz B, Koziak K, Czarkowska-Paczek B, Paczek L (2007) The effects of indomethacin on angiogenic factors mRNA expression in renal cortex of healthy rats. *Journal of physiology and pharmacology : an official journal of the Polish Physiological Society* 58: 165-178

Mundy G, Garrett R, Harris S, Chan J, Chen D, Rossini G, Boyce B, Zhao M, Gutierrez G (1999) Stimulation of bone formation in vitro and in rodents by statins. *Science* 286: 1946-1949

Myllyharju J, Kivirikko KI (2004) Collagens, modifying enzymes and their mutations in humans, flies and worms. *Trends in genetics* : TIG 20: 33-43

Nakahara K, Yada T, Kuriyama M, Osame M (1994) Cytosolic Ca²⁺ Increase and Cell-Damage in L6 Rat Myoblasts by Hmg-Coa Reductase Inhibitors. *Biochemical and biophysical research communications* 202: 1579-1585

Newairy AA, El-Sharaky AS, Badreldeen MM, Eweda SM, Sheweita SA (2007) The hepatoprotective effects of selenium against cadmium toxicity in rats. *Toxicology* 242: 23-30

Newman TB, Hulley SB (1996) Carcinogenicity of lipid-lowering drugs. *JAMA : the journal of the American Medical Association* 275: 55-60

Nissen-Meyer LS, Svalheim S, Tauboll E, Gjerstad L, Reinholt FP, Jemtland R (2008) How can antiepileptic drugs affect bone mass, structure and metabolism? Lessons from animal studies. *Seizure* 17: 187-191

Nogaki F, Muso E, Yashiro M, Kasuno K, Kamata T, Ono T, Sasayama S (1999) Direct inhibitory effects of simvastatin on matrix accumulation in cultured murine mesangial cells. *Kidney international Supplement* 71: S198-201

Nowinska B, Folwarczna J, Dusilo A, Pytlik M, Sliwinski L, Cegiela U, Kaczmarczyk-Sedlak I, Pietryka W, Hanke T, Trzeciak HI (2012) Effects of vigabatrin on the skeletal system of young rats. *Acta poloniae pharmaceutica* 69: 327-334

Onodera K, Takahashi A, Mayanagi H, Wakabayashi H, Kamei J, Shinoda H (2001) Phenytoin-induced bone loss and its prevention with alfacalcidol or calcitriol in growing rats. *Calcified tissue international* 69: 109-116

Ortiz GG, Pacheco-Moises F, El Hafidi M, Jimenez-Delgado A, Macias-Islas MA, Corral SAR, de la Rosa AC, Sanchez-Gonzalez VJ, Arias-Merino ED, Velazquez-Brizuela IE (2008) Detection of membrane fluidity in submitochondrial particles of platelets and erythrocyte membranes from Mexican patients with Alzheimer disease by intramolecular excimer formation of 1,3 dipyranylpropane. *Disease markers* 24: 151-156

Ortiz GG, Pacheco-Moises F, El Hafidi M, Jimenez-Delgado A, Macias-Islas MA, Rosales Corral SA, de la Rosa AC, Sanchez-Gonzalez VJ, Arias-Merino ED, Velazquez-Brizuela IE (2008) Detection of membrane fluidity in submitochondrial particles of platelets and erythrocyte membranes from Mexican patients with Alzheimer disease by intramolecular excimer formation of 1,3 dipyranylpropane. *Disease markers* 24: 151-156

Otsubo K, Katz EP, Mechanic GL, Yamauchi M (1992) Cross-linking connectivity in bone collagen fibrils: the COOH-terminal locus of free aldehyde. *Biochemistry* 31: 396-402

Pack AM, Morrell MJ (2004) Epilepsy and bone health in adults. *Epilepsy & behavior* : E&B 5 Suppl 2: S24-29

Pack AM, Morrell MJ, McMahon DJ, Shane E (2011) Normal vitamin D and low free estradiol levels in women on enzyme-inducing antiepileptic drugs. *Epilepsy & behavior* : E&B 21: 453-458

Paiva H, Thelen KM, Van Coster R, Smet J, De Paepe B, Mattila KM, Laakso J, Lehtimaki T, von Bergmann K, Lutjohann D, Laaksonen R (2005) High-dose statins and skeletal muscle metabolism in humans: A randomized, controlled trial. *Clin Pharmacol Ther* 78: 60-68

Palomaki A, Malminiemi K, Solakivi T, Malminiemi O (1998) Ubiquinone supplementation during lovastatin treatment: effect on LDL oxidation ex vivo. *Journal of lipid research* 39: 1430-1437

Parfitt AM (2001) The bone remodeling compartment: a circulatory function for bone lining cells. *Journal of bone and mineral research* 16: 1583-1585

Parfitt AM (2002) Targeted and nontargeted bone remodeling: relationship to basic multicellular unit origination and progression. *Bone* 30: 5-7

Parhami F, Garfinkel A, Demer LL (2000) Role of lipids in osteoporosis. *Arteriosclerosis, thrombosis, and vascular biology* 20: 2346-2348

Parhami F, Jackson SM, Tintut Y, Le V, Balucan JP, Territo M, Demer LL (1999) Atherogenic diet and minimally oxidized low density lipoprotein inhibit osteogenic and promote adipogenic differentiation of marrow stromal cells. *Journal of bone and mineral research* 14: 2067-2078

Parhami F, Morrow AD, Balucan J, Leitinger N, Watson AD, Tintut Y, Berliner JA, Demer LL (1997) Lipid oxidation products have opposite effects on calcifying vascular cell and bone cell differentiation. A possible explanation for the paradox of arterial calcification in osteoporotic patients. *Arteriosclerosis, thrombosis, and vascular biology* 17: 680-687

Parhami F, Tintut Y, Beamer WG, Gharavi N, Goodman W, Demer LL (2001) Atherogenic high-fat diet reduces bone mineralization in mice. *Journal of bone and mineral research* 16: 182-188

Paschalis EP, Betts F, DiCarlo E, Mendelsohn R, Boskey AL (1997) FTIR microspectroscopic analysis of human iliac crest biopsies from untreated osteoporotic bone. *Calcified tissue international* 61: 487-492

Paschalis EP, DiCarlo E, Betts F, Sherman P, Mendelsohn R, Boskey AL (1996) FTIR microspectroscopic analysis of human osteonal bone. *Calcified tissue international* 59: 480-487

Paschalis EP, Recker R, DiCarlo E, Doty SB, Atti E, Boskey AL (2003) Distribution of collagen cross-links in normal human trabecular bone. *Journal of bone and mineral research* 18: 1942-1946

Paschalis EP, Verdelis K, Doty SB, Boskey AL, Mendelsohn R, Yamauchi M (2001) Spectroscopic characterization of collagen cross-links in bone. *Journal of bone and mineral research* 16: 1821-1828

Pascussi JM, Robert A, Nguyen M, Wairant-Debray O, Garabedian M, Martin P, Pineau T, Saric J, Navarro F, Maurel P, Vilarem MJ (2005) Possible involvement of pregnane X receptor-enhanced CYP24 expression in drug-induced osteomalacia. *Journal of Clinical Investigation* 115: 177-186

Petibois C, Gouspillou G, Wehbe K, Delage JP, Deleris G (2006) Analysis of type I and IV collagens by FT-IR spectroscopy and imaging for a molecular investigation of skeletal muscle connective tissue. *Analytical and bioanalytical chemistry* 386: 1961-1966

Pleshko N, Boskey A, Mendelsohn R (1991) Novel Infrared Spectroscopic Method for the Determination of Crystallinity of Hydroxyapatite Minerals. *Biophysical journal* 60: 786-793

Quinn CM, Jessup W, Wong J, Kritharides L, Brown AJ (2005) Expression and regulation of sterol 27-hydroxylase (CYP27A1) in human macrophages: a role for RXR and PPARgamma ligands. *The Biochemical journal* 385: 823-830

Radeff JM, Nagy Z, Stern PH (2004) Rho and Rho kinase are involved in parathyroid hormone-stimulated protein kinase C alpha translocation and IL-6 promoter activity in osteoblastic cells. *Journal of bone and mineral research* 19: 1882-1891

Raisz LG (2005) Pathogenesis of osteoporosis: concepts, conflicts, and prospects. *The Journal of clinical investigation* 115: 3318-3325

Rajendran KG, Chen SY, Sood A, Spielvogel BF, Hall IH (1995) The anti-osteoporotic activity of amine-carboxyboranes in rodents. *Biomedicine & pharmacotherapy = Biomedecine & pharmacotherapie* 49: 131-140

Ralston SH, Uitterlinden AG (2010) Genetics of osteoporosis. *Endocrine reviews* 31: 629-662

Rawadi G, Vayssiere B, Dunn F, Baron R, Roman-Roman S (2003) BMP-2 controls alkaline phosphatase expression and osteoblast mineralization by a Wnt autocrine loop. *Journal of Bone and Mineral Research* 18: 1842-1853

Rejnmark L, Vestergaard P, Heickendorff L, Mosekilde L (2010) Simvastatin does not affect vitamin d status, but low vitamin d levels are associated with dyslipidemia: results from a randomised, controlled trial. *International journal of endocrinology* 2010: 957174

Rey C, Renugopalakrishnan V, Collins B, Glimcher MJ (1991) Fourier transform infrared spectroscopic study of the carbonate ions in bone mineral during aging. *Calcified tissue international* 49: 251-258

Rey C, Shimizu M, Collins B, Glimcher MJ (1990) Resolution-enhanced Fourier transform infrared spectroscopy study of the environment of phosphate ions in the early deposits of a solid phase of calcium-phosphate in bone and enamel, and their evolution with age. I: Investigations in the ν_4 PO₄ domain. *Calcified tissue international* 46: 384-394

Rey C, Shimizu M, Collins B, Glimcher MJ (1991) Resolution-enhanced Fourier transform infrared spectroscopy study of the environment of phosphate ion in the early deposits of a solid phase of calcium phosphate in bone and enamel and their evolution with age: 2. Investigations in the ν_3 PO₄ domain. *Calcified tissue international* 49: 383-388

Rieppo J, Hyttinen MM, Halmesmaki E, Ruotsalainen H, Vasara A, Kiviranta I, Jurvelin JS, Helminen HJ (2009) Changes in spatial collagen content and collagen network architecture in porcine articular cartilage during growth and maturation. *Osteoarthritis and cartilage / OARS* 17: 448-455

Rodriguez-Casado A, Alvarez I, Toledano A, de Miguel E, Carmona P (2007) Amphetamine effects on brain protein structure and oxidative stress as revealed by FTIR microspectroscopy. *Biopolymers* 86: 437-446

Rosenson RS, Tangney CC, Langman CB, Parker TS, Levine DM, Gordon BR (2005) Short-term reduction in bone markers with high-dose simvastatin. *Osteoporosis international* 16: 1272-1276

Russell DW (2003) The enzymes, regulation, and genetics of bile acid synthesis. *Annual review of biochemistry* 72: 137-174

Saito M, Fujii K, Mori Y, Marumo K (2006) Role of collagen enzymatic and glycation induced cross-links as a determinant of bone quality in spontaneously diabetic WBN/Kob rats. *Osteoporosis international* 17: 1514-1523

Sato Y, Kondo I, Ishida S, Motooka H, Takayama K, Tomita Y, Maeda H, Satoh K (2001) Decreased bone mass and increased bone turnover with valproate therapy in adults with epilepsy. *Neurology* 57: 445-449

Scaramuzza L, Messuti L, Manicone PF, Raffaelli L, Rossi B, Gallenzi P, Berardi D, Maccauro G (2009) Clinical and histological modifications in osteopetrotic bone: a review. *Journal of biological regulators and homeostatic agents* 23: 59-63

Schaller S, Henriksen K, Sveigaard C, Heegaard AM, Helix N, Stahlhut M, Ovejero MC, Johansen JV, Solbjerg H, Andersen TL, Hougaard D, Berryman M, Shiodt CB, Sorensen BH, Lichtenberg J, Christophersen P, Foged NT, Delaisse JM, Engsig MT, Karsdal MA (2004) The chloride channel inhibitor NS3736 prevents bone resorption in ovariectomized rats without changing bone formation (vol 19, pg 1144, 2004). *Journal of Bone and Mineral Research* 19: 1378-1378

Schmidt IU, Dobnig H, Turner RT (1995) Intermittent parathyroid hormone treatment increases osteoblast number, steady state messenger ribonucleic acid levels for osteocalcin, and bone formation in tibial metaphysis of hypophysectomized female rats. *Endocrinology* 136: 5127-5134

Seeman E (2009) Bone modeling and remodeling. *Critical reviews in eukaryotic gene expression* 19: 219-233

Seeman E, Delmas PD (2006) Bone quality--the material and structural basis of bone strength and fragility. *The New England journal of medicine* 354: 2250-2261

Seo T, Ishitsu T, Ueda N, Nakada N, Yurube K, Ueda K, Nakagawa K (2006) ABCB1 polymorphisms influence the response to antiepileptic drugs in Japanese epilepsy patients. *Pharmacogenomics* 7: 551-561

Severcan F, Bozkurt O, Gurbanov R, Gorgulu G (2010) FT-IR spectroscopy in diagnosis of diabetes in rat animal model. *Journal of biophotonics* 3: 621-631

Severcan F, Gokduman K, Dogan A, Bolay S, Gokalp S (2008) Effects of in-office and at-home bleaching on human enamel and dentin: an in vitro application of Fourier transform infrared study. *Applied spectroscopy* 62: 1274-1279

Shaama FA (2005) An in vitro comparison of implant materials cell attachment, cytokine and osteocalcin production. *West Indian Medical Journal* 54: 250-256

Shahwan A, Murphy K, Doherty C, Cavalleri GL, Muckian C, Dicker P, McCarthy M, Kinirons P, Goldstein D, Delanty N (2007) The controversial association of ABCB1 polymorphisms in refractory epilepsy: an analysis of multiple SNPs in an Irish population. *Epilepsy research* 73: 192-198

Shellhaas RA, Joshi SM (2010) Vitamin D and bone health among children with epilepsy. *Pediatric neurology* 42: 385-393

Sheth RD, Wesolowski CA, Jacob JC, Penney S, Hobbs GR, Riggs JE, Bodensteiner JB (1995) Effect of Carbamazepine and Valproate on Bone-Mineral Density. *Journal of Pediatrics* 127: 256-262

- Shitara Y, Sugiyama Y (2006) Pharmacokinetic and pharmacodynamic alterations of 3-hydroxy-3-methylglutaryl coenzyme A (HMG-CoA) reductase inhibitors: drug-drug interactions and interindividual differences in transporter and metabolic enzyme functions. *Pharmacology & therapeutics* 112: 71-105
- Shui CX, Scutt A (2001) Mild heat shock induces proliferation, alkaline phosphatase activity, and mineralization in human bone marrow stromal cells and Mg-63 cells in vitro. *Journal of Bone and Mineral Research* 16: 731-741
- Sills RH, Moore DJ, Mendelsohn R (1994) Erythrocyte Peroxidation - Quantitation by Fourier-Transform Infrared-Spectroscopy. *Analytical biochemistry* 218: 118-123
- Sills RH, Moore DJ, Mendelsohn R (1994) Erythrocyte peroxidation: quantitation by Fourier transform infrared spectroscopy. *Analytical biochemistry* 218: 118-123
- Simsek Ozek N, Sara Y, Onur R, Severcan F (2010) Low dose simvastatin induces compositional, structural and dynamic changes in rat skeletal extensor digitorum longus muscle tissue. *Bioscience reports* 30: 41-50
- Sinzinger H, Lupattelli G, Chehne F (2000) Increased lipid peroxidation in a patient with CK-elevation and muscle pain during statin therapy. *Atherosclerosis* 153: 255-256
- Slosarczyk A, Bialoskorski J (1998) Hardness and fracture toughness of dense calcium-phosphate-based materials. *Journal of Materials Science Materials in Medicine* 9: 103-108
- Soares CN, Taylor V (2007) Effects and management of the menopausal transition in women with depression and bipolar disorder. *Journal of Clinical Psychiatry* 68: 16-21
- Stark Z, Savarirayan R (2009) *Osteopetrosis* Orphanet journal of rare diseases 4: 5
- Stein EA, Farnier M, Waldstreicher J, Mercuri M, Simvastatin/Atorvastatin Study G (2001) Effects of statins on biomarkers of bone metabolism: a randomised trial. *Nutrition, metabolism, and cardiovascular diseases* 11: 84-87
- Stein SH, Dean IN, Rawal SY, Tipton DA (2011) Statins regulate interleukin-1beta-induced RANKL and osteoprotegerin production by human gingival fibroblasts. *Journal of periodontal research* 46: 483-490

Suda T, Nakamura I, Jimi E, Takahashi N (1997) Regulation of osteoclast function. *Journal of bone and mineral research* 12: 869-879

Suzuki R, Domon T, Wakita M (2000) Some osteocytes released from their lacunae are embedded again in the bone and not engulfed by osteoclasts during bone remodeling. *Anatomy and embryology* 202: 119-128

Swarthout JT, D'Alonzo RC, Selvamurugan N, Partridge NC (2002) Parathyroid hormone-dependent signaling pathways regulating genes in bone cells. *Gene* 282: 1-17

Szanto A, Benko S, Szatmari I, Balint BL, Furtos I, Ruhl R, Molnar S, Csiba L, Garuti R, Calandra S, Larsson H, Diczfalusy U, Nagy L (2004) Transcriptional regulation of human CYP27 integrates retinoid, peroxisome proliferator-activated receptor, and liver X receptor signaling in macrophages. *Molecular and cellular biology* 24: 8154-8166

Tarnowski CP, Ignelzi MA, Jr., Wang W, Taboas JM, Goldstein SA, Morris MD (2004) Earliest mineral and matrix changes in force-induced musculoskeletal disease as revealed by Raman microspectroscopic imaging. *Journal of bone and mineral research* 19: 64-71

Tekgul H, Serdaroglu G, Huseyinov A, Gokben S (2006) Bone mineral status in pediatric outpatients on antiepileptic drug monotherapy. *Journal of child neurology* 21: 411-414

Termine JD, Posner AS (1966) Infra-red determination of the percentage of crystallinity in apatitic calcium phosphates. *Nature* 211: 268-270

Thelen KM, Rentsch KM, Gutteck U, Heverin M, Olin M, Andersson U, von Eckardstein A, Bjorkhem I, Lutjohann D (2006) Brain cholesterol synthesis in mice is affected by high dose of simvastatin but not of pravastatin. *The Journal of pharmacology and experimental therapeutics* 316: 1146-1152

Tian Y, Xu Y, Fu Q, He M (2011) Parathyroid hormone regulates osteoblast differentiation in a Wnt/beta-catenin-dependent manner. *Molecular and cellular biochemistry* 355: 211-216

Tiribilli B, Bani D, Quercioli F, Ghirelli A, Vassalli M (2005) Atomic force microscopy of histological sections using a chemical etching method. *Ultramicroscopy* 102: 227-232

Toyran N, Zorlu F, Donmez G, Oge K, Severcan F (2004) Chronic hypoperfusion alters the content and structure of proteins and lipids of rat brain homogenates: a Fourier transform infrared spectroscopy study. *European Biophysics Journal* 33: 549-554

Tsuchiya M, Hosaka M, Moriguchi T, Zhang S, Suda M, Yokota-Hashimoto H, Shinozuka K, Takeuchi T (2010) Cholesterol biosynthesis pathway intermediates and inhibitors regulate glucose-stimulated insulin secretion and secretory granule formation in pancreatic beta-cells. *Endocrinology* 151: 4705-4716

Tsukahara H, Kimura K, Todoroki Y, Ohshima Y, Hiraoka M, Shigematsu Y, Tsukahara Y, Miura M, Mayumi M (2002) Bone mineral status in ambulatory pediatric patients on long-term anti-epileptic drug therapy. *Pediatrics International* 44: 247-253

Turner CH (2002) Biomechanics of bone: determinants of skeletal fragility and bone quality. *Osteoporosis international* 13: 97-104

Ueki Y, Lin CY, Senoo M, Ebihara T, Agata N, Onji M, Saheki Y, Kawai T, Mukherjee PM, Reichenberger E, Olsen BR (2007) Increased myeloid cell responses to M-CSF and RANKL cause bone loss and inflammation in SH3BP2 "cherubism" mice. *Cell* 128: 71-83

Vaananen K (2005) Mechanism of osteoclast mediated bone resorption--rationale for the design of new therapeutics. *Advanced drug delivery reviews* 57: 959-971

Vahab SA, Sen S, Ravindran N, Mony S, Mathew A, Vijayan N, Nayak G, Bhaskaranand N, Banerjee M, Satyamoorthy K (2009) Analysis of genotype and haplotype effects of ABCB1 (MDR1) polymorphisms in the risk of medically refractory epilepsy in an Indian population. *Drug metabolism and pharmacokinetics* 24: 255-260

Valimaki MJ, Tiihonen M, Laitinen K, Tahtela R, Karkkainen M, Lambergallardt C, Makela P, Tunninen R (1994) Bone-Mineral Density Measured by Dual-Energy X-Ray Absorptiometry and Novel Markers of Bone-Formation and Resorption in Patients on Antiepileptic Drugs. *Journal of Bone and Mineral Research* 9: 631-637

van der Rest M, Garrone R (1991) Collagen family of proteins. *FASEB journal* 5: 2814-2823

van Luijckelaaar G, Sitnikova E (2006) Global and focal aspects of absence epilepsy: the contribution of genetic models. *Neuroscience and biobehavioral reviews* 30: 983-1003

van Staa TP, Wegman S, de Vries F, Leufkens B, Cooper C (2001) Use of statins and risk of fractures. *JAMA* 285: 1850-1855

van Staa TP, Wegman S, deVries F, Leufkens B, Cooper C (2001) Use of statins and risk of fractures *JAMA* 286: 674-674

Verborgt O, Gibson GJ, Schaffler MB (2000) Loss of osteocyte integrity in association with microdamage and bone remodeling after fatigue in vivo. *Journal of bone and mineral research* 15: 60-67

Verrotti A, Greco R, Latini T, Morgese T, Chiarelli F (2002) Increased bone turnover in prepubertal, pubertal, and postpubertal patients receiving carbamazepine. *Epilepsia* 43: 1488-1492

Verrotti A, Greco R, Morgese G, Chiarelli F (2000) Increased bone turnover in epileptic patients treated with carbamazepine. *Annals of Neurology* 47: 385-388

Vestergaard P, Rejnmark L, Mosekilde L (2004) Fracture risk associated with use of antiepileptic drugs. *Epilepsia* 45: 1330-1337

Viguet-Carrin S, Roux JP, Arlot ME, Merabet Z, Leeming DJ, Byrjalsen I, Delmas PD, Buxsein ML (2006) Contribution of the advanced glycation end product pentosidine and of maturation of type I collagen to compressive biomechanical properties of human lumbar vertebrae. *Bone* 39: 1073-1079

Vogiatzi MG, Tsay J, Verdelis K, Rivella S, Grady RW, Doty S, Giardina PJ, Boskey AL (2010) Changes in bone microarchitecture and biomechanical properties in the th3 thalassemia mouse are associated with decreased bone turnover and occur during the period of bone accrual. *Calcified tissue international* 86: 484-494

von Tresckow B, von Strandmann EP, Sasse S, Tawadros S, Engert A, Hansen HP (2007) Simvastatin-dependent apoptosis in Hodgkin's lymphoma cells and growth impairment of human Hodgkin's tumors in vivo. *Haematologica* 92: 682-685

Wadagaki R, Mizuno D, Yamawaki-Ogata A, Satake M, Kaneko H, Hagiwara S, Yamamoto N, Narita Y, Hibi H, Ueda M (2011) Osteogenic induction of bone marrow-derived stromal cells on simvastatin-releasing, biodegradable, nano- to microscale fiber scaffolds. *Annals of biomedical engineering* 39: 1872-1881

Weinstein RS, Bryce GF, Sappington LJ, King DW, Gallagher BB (1984) Decreased Serum Ionized Calcium and Normal Vitamin-D Metabolite Levels with Anticonvulsant Drug-Treatment. *The Journal of Clinical Endocrinology and Metabolism* 58: 1003-1009

Wetzel DL, Slatkin DN, Levine SM (1998) FT-IR microspectroscopic detection of metabolically deuterated compounds in the rat cerebellum: A novel approach for the study of brain metabolism. *Cellular and molecular biology* 44: 15-27

Whyte MP, McAlister WH, Novack DV, Clements KL, Schoenecker PL, Wenkert D (2008) Bisphosphonate-induced osteopetrosis: novel bone modeling defects, metaphyseal osteopenia, and osteosclerosis fractures after drug exposure ceases. *Journal of bone and mineral research* 23: 1698-1707

Wong RW, Rabie AB (2005) Early healing pattern of statin-induced osteogenesis. *The British journal of oral & maxillofacial surgery* 43: 46-50

Wong RWK, Rabie ABM (2005) Early healing pattern of statin-induced osteogenesis. *British Journal of Oral and Maxillofacial Surgery* 43: 46-50

Yamashita M, Otsuka F, Mukai T, Otani H, Inagaki K, Miyoshi T, Goto J, Yamamura M, Makino H (2008) Simvastatin antagonizes tumor necrosis factor- α inhibition of bone morphogenetic proteins-2-induced osteoblast differentiation by regulating Smad signaling and Ras/Rho-mitogen-activated protein kinase pathway. *The Journal of endocrinology* 196: 601-613

Yamashita M, Otsuka F, Mukai T, Yamanaka R, Otani H, Matsumoto Y, Nakamura E, Takano M, Sada KE, Makino H (2010) Simvastatin inhibits osteoclast differentiation induced by bone morphogenetic protein-2 and RANKL through regulating MAPK, AKT and Src signaling. *Regulatory peptides* 162: 99-108

Yang G, Song L, Guo C, Zhao S, Liu L, He F (2012) Bone responses to simvastatin-loaded porous implant surfaces in an ovariectomized model. *The International journal of oral & maxillofacial implants* 27: 369-374

Yano K, Ohoshima S, Shimizu Y, Moriguchi T, Katayama H (1996) Evaluation of glycogen level in human lung carcinoma tissues by an infrared spectroscopic method. *Cancer Letters* 110: 29-34

Yao W, Farmer R, Cooper R, Chmielewski PA, Tian XY, Setterberg RB, Jee WS, Lundy MW (2006) Simvastatin did not prevent nor restore ovariectomy-induced

bone loss in adult rats. *Journal of musculoskeletal & neuronal interactions* 6: 277-283

Yao W, Li CY, Farmer RW, Chen JL, Mo A, Cooper R, Chmielewski P, Setterberg RB, Lee WSS, Lundy MW (2001) Simvastatin did not prevent bone loss in ovariectomized rats. *Journal of Bone and Mineral Research* 16: S294-S294

Youn JI, Milner TE (2008) Evaluation of photothermal effects in cartilage using FT-IR spectroscopy. *Lasers in medical science* 23: 229-235

Zebaze RM, Jones AC, Pandy MG, Knackstedt MA, Seeman E (2011) Differences in the degree of bone tissue mineralization account for little of the differences in tissue elastic properties. *Bone* 48: 1246-1251

Zeiser R, Maas K, Youssef S, Durr C, Steinman L, Negrin RS (2009) Regulation of different inflammatory diseases by impacting the mevalonate pathway. *Immunology* 127: 18-25

Zimprich F, Sunder-Plassmann R, Stogmann E, Gleiss A, Dal-Bianco A, Zimprich A, Plumer S, Baumgartner C, Mannhalter C (2004) Association of an ABCB1 gene haplotype with pharmacoresistance in temporal lobe epilepsy. *Neurology* 63: 1087-1089

APPENDIX A

CHEMICALS

Ethanol	Sigma
Methanol	Sigma
2-propanol	Sigma
Xylene	Sigma
Methylmethacrylate	Applichem
Buthylmethacrylate	Applichem
Methylbenzoate	Applichem
Polyethylene glycol 200	Applichem
Benzoyl peroxide	Applichem
N,N-dimethyl-p-toluidine	Applichem
Tris	Sigma
SDS	Sigma
N,N,N',N'-tetramethylethylenediamine (TEMED)	Sigma
Glycine	Sigma
Carbamazepine	Sigma
Simvastatin	Merck

CURRICULUM VITAE

PERSONEL INFORMATION

Surname, Name: Garip, Şebnem
Nationality: Turkish (TC)
Date and Place of Birth: 17 October 1980, İstanbul
Marital Status: Single
Phone: +90 312 210 51 57
E-mail: sbnm_grp@yahoo.com
Foreign Languages: English

EDUCATION

Degree	Institution	Graduation	C.GPA
Ph.D.	METU Biochemistry Dept.	2012	3.64/4
M.Sc.	METU Biology Dept.	2005	3.48/4
B.Sc.	İstanbul Univ. Biology Dept.	2000	68/100

WORK EXPERIENCE

Year	Place	Enrollment
September,2011-March,2012	Brookhaven National Laboratory, NY, USA	Visiting Scientist
March-September,2011	The State University of New Jersey (Rutgers University),NJ, USA	Visiting Scientist
November,2007-February,2008	Hospital for Special Surgery, Mineralized Tissue Laboratory, NY, USA	Visiting Scientist

AWARDS and SCHOLARSHIPS

Research Abroad Scholarship from Scientific and Technological Research Council of Turkey (TÜBİTAK), 2010 (For 12 months after March 2011).

Poster Second Prize Award "2nd International Biophysics Congress and Biotechnology at GAP & 21st National Biophysics Congress", Diyarbakır, TURKEY, 2009.

Scholarship from Republic of Turkey Prime Ministry during my B.Sc.

PUBLICATIONS

A) Book Chapters

Garip S., Boskey AL., 'Diagnosis of bone and cartilage diseases' in Vibrational Spectroscopy in Diagnosis and Screening, Ed. Haris I. Parvez and Feride Severcan, IOS Press, (2012) [ISBN: 978-1-61499-058-1].

B) Articles in refereed Journals (SCI)

1. **Garip S.,** Evis Z., Ilbay G., Boskey AL., Severcan F., Effects on bone of anti-seizure therapy in a rat model of epilepsy: An FTIR imaging study, Bone (Submitted to Epilepsia).
2. **Garip S.,** Yapici E., Ozek NS., Severcan M., Severcan F., Evaluation and discrimination of Simvastatin-induced structural alterations in proteins of different rat tissues by FTIR spectroscopy and neural network analysis, Analyst, 2010, 135 (12), 3233-41.
3. **Garip S.,** Severcan F., Determination of Simvastatin-induced changes in bone composition and structure by Fourier transform infrared spectroscopy in rat animal model, Journal of Pharmaceutical and Biomedical Analysis, 2010, 52(4), 580-8.
4. **Garip S.,** Bozoglu F., Severcan F., Differentiation of mesophilic and thermophilic bacteria with Fourier transform infrared spectroscopy, Applied Spectroscopy, 2007, 61(2), 186-192.
5. **Garip S.,** Cetin Gozen A., Severcan F., Use of Fourier transform infrared spectroscopy for rapid comparative analysis of *Bacillus* and *Micrococcus* isolates, Food Chemistry, 2009, 113(4), 1301-1307.

C) Articles in preparation:

1. **Garip S.**, Sahin D., Mann A.B., Miller L., Severcan F., Epilepsy-induced structural and functional changes in rat spine bone tissues: SR-FTIRM and AFM imaging, biomechanical and biochemical studies (Research Article).
2. **Garip S.**, Sahin D., Mann A.B., Miller L., Severcan F., Various effects of anti-epileptic drug; Carbamazepine on bone microarchitecture, mechanical properties and Vitamin-D metabolism of healthy and epileptic rats (Research Article).
3. Bozkurt O., **Garip S.**, Severcan M., Severcan F., Diagnosis of bone disorders by FTIR microspectroscopy together with chemometric methods: A case study on epileptic and diabetic rat models (Research Article).

D) Articles in the Refereed Journals (Not covered by SCI), International Conference Proceeding and in Books

1. Bozkurt Ö., Çakmak G., **Garip Ş.**, Severcan F., “FTIR Microspectroscopic Imaging of Soft and Hard Tissues”, 14. National Meeting of Biomedical Engineering, BİYOMUT 2009, 20-24 May 2009, İzmir, Turkey, 6B2, 118.

E) Abstracts in refereed journals (SCI)

1. **Garip S.**, Severcan F. ‘The effects of high and low dose Simvastatin on rat tibia: A Fourier Transform Infrared Spectroscopy’ *Cells Tissues Organs* (2009); 189:298.

F) Presentations in International Meetings:

1. **Garip S.**, Evis Z., Ilbay G., Boskey AL., Severcan F., The side-effects of convulsive epileptic seizures and carbamazepine therapy on bone tissues of genetically-induced epileptic rats: an FTIR imaging and biomechanical study, *Experimental Biology* (2011), 9-13 April, Washington, DC, USA.
2. **Garip S.**, Ilbay G., Boskey A., Severcan F. ‘The side-effects of convulsive seizures on epileptic rat bone tissues’ (2009), 2nd International Biophysics Congress and Biotechnology at GAP & 21st National Biophysics Congress, Diyarbakır, TURKEY.
3. Bozkurt O, Çakmak G, **Garip S**, Severcan F, “Implications of FTIR Microspectroscopy in Pathological Conditions”, Sözlü sunum,

International Workshop on Molecular Approaches to Obesity with New Implications, 12 June 2009, METU, Ankara.

4. **Garip S.**, Severcan F. ‘The effects of high and low dose Simvastatin on rat tibia: A Fourier Transform Infrared Spectroscopy’, (2007), 9th International Conference on the Chemistry and Biology of Mineralized Tissues, Austin/Texas, ABD, Abstract Book pp: 49.
5. **Garip S.**, Bozoglu F., Severcan F. ‘The characterization of mesophilic and thermophilic bacteria with Fourier transform infrared spectroscopy’, (2006), Shedding light on disease: Optical diagnosis for the new millenium, Heidelberg, Germany, Abstract Book pp: 155.

F) Presentations in National Meetings:

1. Bozkurt O., Cakmak G., **Garip S.**, Severcan F. ‘Imaging of soft and hard tissues with FTIR Microspectroscopy’ (2009), 14th National Meeting of Biomedical Engineering, May 20th-24th, Izmir, TURKEY.
2. **Garip S.**, Sahin D., Boskey A., Severcan F. ‘The side-effects of convulsive seizures and long term Carbamazepine treatment on mix form epileptic rat bone tissues’ (2009) 8. National Neuroscience Congress, Bolu, TURKEY.
3. **Garip S.**, Severcan F. ‘The molecular effects of high and low dose Simvastatin therapy on rat bone tissues’ (2008); XX. National Biophysics Congress, Mersin, TURKEY (Oral presentation).
4. **Garip S.**, Bozoglu F., Severcan F. ‘The characterization of bacteria with Fourier transform infrared spectroscopy’, (2005), XVII. National Biophysics Congress, Izmir, TURKEY (Oral presentation).